DYNAMIC CENTRIFUGE TESTING

OF CANTILEVER RETAINING WALLS

Thesis by

L. Alexander Ortiz

In Partial Fulfillment of the Requirements

for the Degree of

Doctor of Philosophy

California Institute of Technology

Pasadena, California

1982

(Submitted May 24, 1982)

ABSTRACT

An investigation was made into the behavior of flexible cantilever walls retaining a cohesionless soil backfill and subjected to earthquake-type dynamic excitations using the centrifuge modelling technique. The study was motivated by the abundant observations of earth retaining structure damage and failures documented in earthquake damage reports.

The "prototype" typical walls were designed using the traditional Mononobe-Okabe dynamic lateral earth pressure theory, were properly scaled for use in the centrifuge at 50 g's, and were subjected to lateral earthquake-like motions which were considered to be of realistic levels. The walls were amply instrumented with pressure and displacement transducers, accelerometers, and strain gages. Moment, pressure, shear, and displacement distributions (static, dynamic, and residual) were obtained.

From the test data, some empirical curves for relating the upper bound responses of the retaining walls to the strong motion characteristics of the applied earthquakes were obtained.

ACKNOWLEDGMENTS

The author wishes to express his appreciation and gratitude to his research advisor, Professor Ronald F. Scott for, first of all, suggesting the research topic, and then providing guidance and suggestions during the course of the investigation. Additional thanks are owed to other faculty members and postgraduate fellows at Caltech, especially Professor Paul C. Jennings, Dr. John F. Hall and Dr. John M-M. Ting, for helpful discussions of some of the problems which were encountered.

In addition, the aid provided by Mr. John R. Lee in designing, building, and maintaining the experimental equipment is gratefully acknowledged and appreciated. Special gratitude is also owed to Mr. Raul Relles for his help in maintaining the digitizer in working order when it was most needed.

Finally the author wishes to thank Mrs. Sharon Beckenbach, Mrs. Gloria Jackson and Mrs. Beth McGrath for the expert typing of this work.

TABLE OF CONTENTS

TABLE OF CONTENTS (CONCLUDED)

CHAPTER I

INTRODUCTION

In this study, an investigation was made into the behavior of cantilever retaining walls, with a cohesionless soil backfill, subjected to earthquake-type dynamic excitations.

Interest in this problem arose from the fact that in virtually every earthquake damage report there is documentation of damage or failure of bridge abutments, sea walls, quay walls, canals, dikes, retaining walls, etc.; in other words, earth retaining structures. This is further enhanced by the fact that in most seismically active areas, there are absolutely no code provisions for some aseismic design of retaining structures. Where seismic considerations are taken into account, a design with the 60 year old pseudo-static Mononobe-Okabe theory with reduced design accelerations is usually accomplished.

Even though many experimental (model) and analytical studies have been done on the subject in the last 60 years, many have been improperly formulated, oversimplified, or simply inadequate. To this day there seems to be no general agreement as to what seismic method of design should be used or even if one should be used at all.

In recent years, the centrifuge has become a more accepted and useful tool in the modelling of soil mechanics problems. It was therefore decided to use this device in order to try to develop some empirical-type design guidelines for at least one type of retaining structure, namely cantilever retaining walls. In order to do this an

"earthquake generating" mechanism, simple and light enough not to take up a substantial portion of the centrifuge payload, was developed in order to provide properly scaled earthquake-type excitations to the properly scaled and designed wall-soil system.

A series of fourteen tests was performed on two properly scaled retaining walls which were designed according to the traditional seismic theory. Since these walls are bending beams, bending moments were measured directly. This appears to be unprecedented since model studies have generally been done only on rigid walls. In addition, earth pressures behind the walls were measured and these results integrated to determine the shear forces. With the aid of accelerometers and displacement transducers, deflection shapes were also determined.

Although model tests were performed, they provided the response of a real (not idealized) retaining structure system subjected to a real earthquake excitation. This was afforded by using the artificial gravity field provided by the centrifuge.

1.1. Mononobe-Okabe Method

During the 1920's, N. Mononobe and N. Matsuo [31], and S. Okabe [39], developed an approximate method for determining the dynamic lateral earth pressure on a retaining structure. The method was based on the traditional Coulomb lateral earth pressure theory where inertial forces of the soil due to the earthquake were treated as additional static forces, through the use of horizontal and vertical accelerations. The observed failure mechanisms of gravity walls which had displaced

under lateral acceleration provided a physical basis for this approach. The method, therefore, does not incorporate a calculation of the pressures which may develop between wall and soil prior to wall failure.

The Mononobe-Okabe method set a standard with which most future research in the field would be compared. Ensuing research has been concerned with refinement of the method or tests of its validity by model studies. Only a few countries have building codes that specify earthquake provisions for wall structures [17,55], but in general, when specified, these provisions are based on the Mononobe-Okabe method. Even in localities where no specific code requirements exist, it appears that the Mononobe-Okabe method is used in design when a dynamic analysis is desired.

Details of the Mononobe-Okabe method and suggestions regarding its application to design problems are given by Seed and Whitman [55].

1. The wall is assumed to displace laterally a sufficient amount to generate minimum active pressure.

2. The soil is assumed to satisfy the Mohr-Coulomb failure criterion.

3. Failure in the soil is assumed to occur along a plane surface through the toe of the wall and inclined at some angle to the horizontal.

4. The wedge of soil between the wall and the failure plane is assumed to be in equilibrium at the point of incipient failure, under gravity, earthquake, and the boundary forces along the
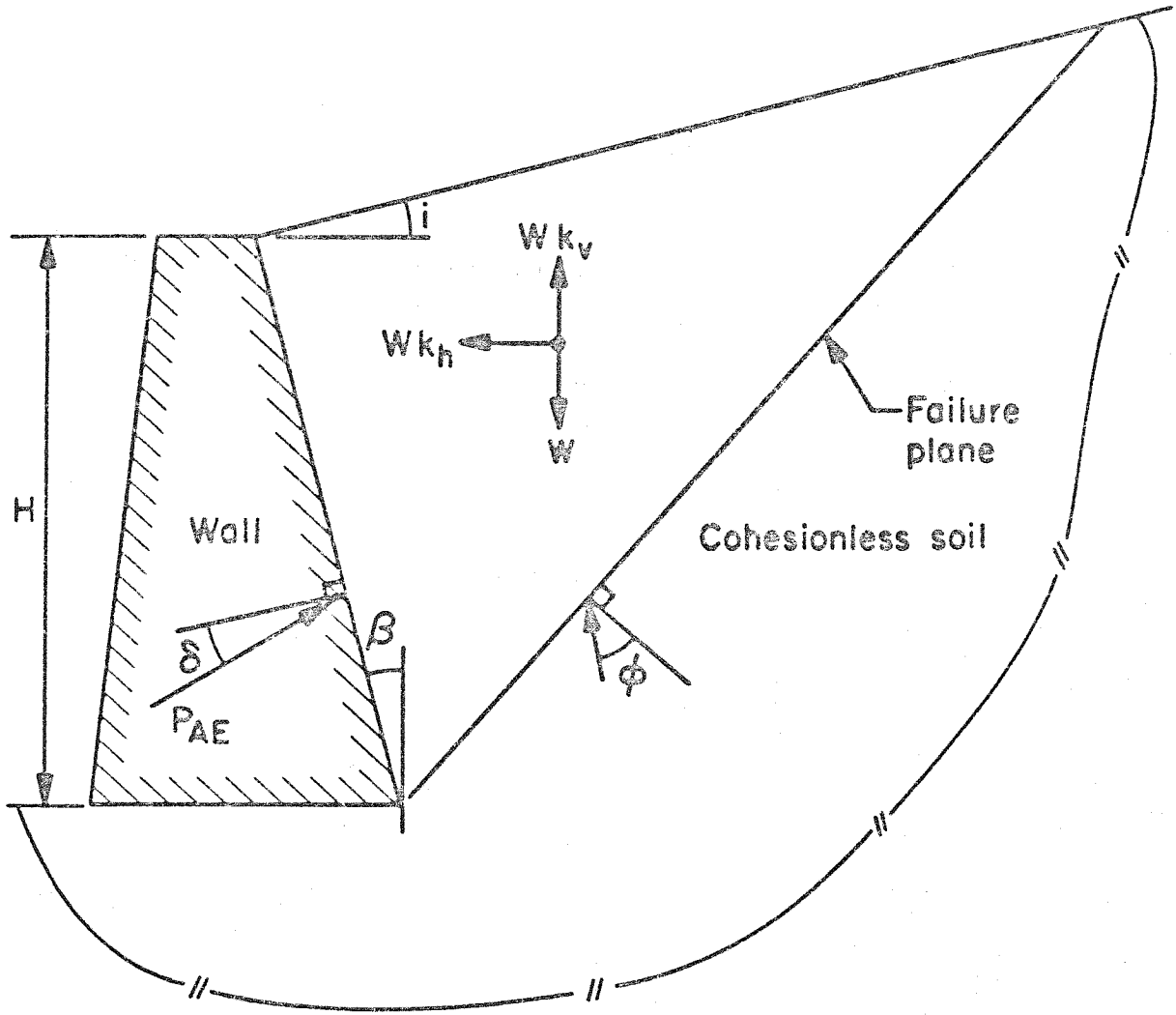
MONONOBE-OKABE ANALYSIS

FIGURE 1.1

wall and failure surface. The forces acting on the soil wedge of weight W are shown in Figure 1.1 for the case of a cohesionless soil.

5. Equivalent static horizontal and vertical forces $k_h W$ and $k_v W$, applied to the center of gravity of the wedge, represent the earthquake effect. The parameters k_h and k_v are the horizontal and vertical earthquake coefficients expressed as fractions of g, the gravitational acceleration.

6. The method gives the magnitude of the total acting force on the wall, but does not give the point of application or the pressure distribution. The method apparently was developed with the assumption that the total force acted 1/3H above the base of the wall of height H. Based on more recent refinements to the method, as well as model test results, Seed and Whitman [55] recommended that the dynamic force should be assumed to act 0.6H above the base. The total active wall force, due to gravity and earthquake, is determined by a force and moment equilibrium analysis of the soil wedge behind the wall (Figure 1.1).

As in a Coulomb analysis, the angle of the failure plane is varied to give a maximum value of the wall force per unit width P_{AE}, and under the critical condition it can be shown that

$$P_{AE} = 1/2\gamma H^2 (1-k_v) K_{AE} \qquad (1.1)$$

in which:

$$K_{AE} = \frac{\cos^2(\phi-\theta-\beta)}{\cos\theta \cos^2\beta \cos(\delta+\beta+\theta)} \left[1 + \left(\frac{\sin(\phi+\delta)\sin(\phi-\theta-i)}{\cos(\delta+\beta+\theta)\cos(i-\beta)}\right)^{1/2}\right]^{-2} \quad (1.2)$$

(coefficient of lateral earth pressure)

$$\theta = \tan^{-1} \frac{k_h}{1 - k_v}$$

γ = unit weight of soil

ϕ = angle of internal friction of soil

δ = angle of wall-soil friction

i = angle of backfill slope

β = angle of wall slope

k_h = horizontal earthquake coefficient (fraction of g)

k_v = vertical earthquake coefficient (fraction of g)

Figure 1.2 illustrates the variation of K_{AE} with k_h with changes in the various soil/wall/lateral acceleration parameters. The Mononobe-Okabe method can be readily extended to encompass cohesive soils by considering the equilibrium of cohesive forces acting along the wall boundary and the failure surface.

Some limitations on the method are given by Wood [67]. A brief summary follows:

1. For full active pressure (full plastic state) to develop in the soil behind the wall, it is necessary for the top of the wall to deflect laterally about 0.5% of the wall height. This
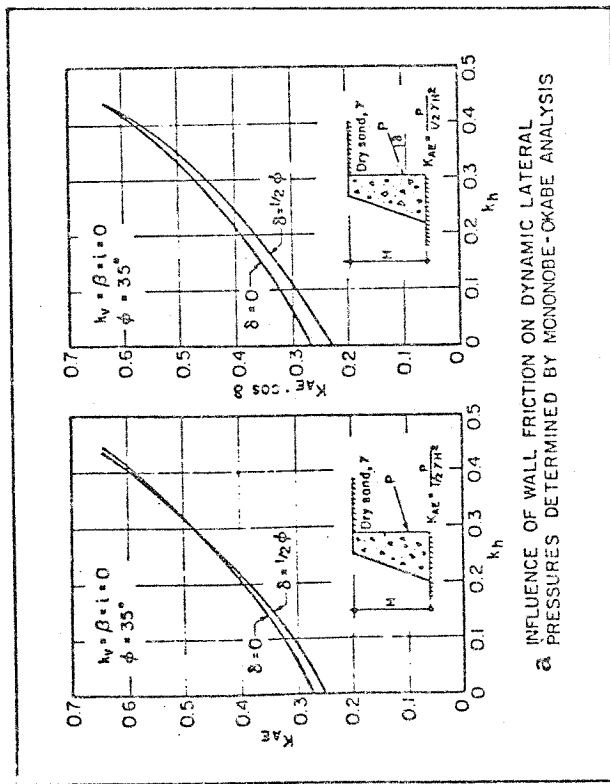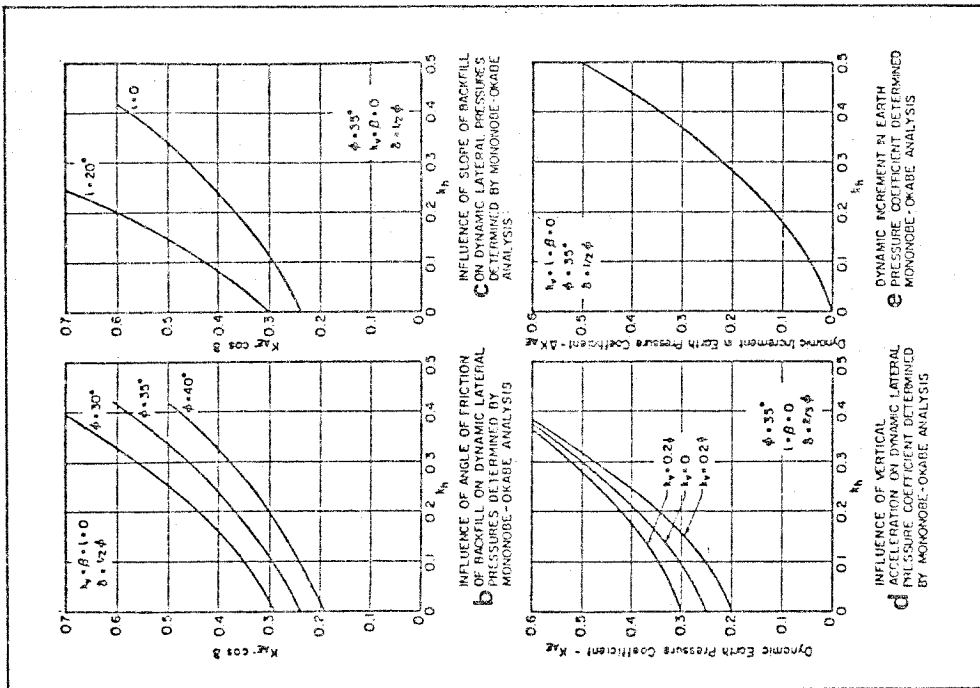
FIGURE I.2 – FROM (55)

condition probably occurs readily in gravity and cantilever walls, but may not always occur in channel sections or anchored sheet-pile walls. It was shown by Wood that for a rigid wall on a rigid foundation the earthquake force component computed by elastic theory was likely to be greater than twice the force computed by the Mononobe-Okabe method. This result was based on a static solution of identical horizontal earthquake coefficients for each case. Thus failure of a rigid structure designed using the Mononobe-Okabe criterion is a great possibility.

Unlike design procedures which allow yielding of structural members of building frames during strong earthquakes, it is generally undesirable to allow excessive yielding in retaining structures. This is because yielding of the structure generally tends to occur in only one direction away from the backfill. Unidirectional yielding may lead to excessive wall displacements with severe cracking to both wall and backfill. It is thus considered desirable to prevent yielding of the retaining structure during an earthquake.

2. Although the assumption of a plane failure surface appears reasonable, its validity has been based on a very limited number of test and field observations.

3. The Mononobe-Okabe Method is a pseudo-static method. Inertia forces are included by use of the earthquake coefficients k_h and k_v. These are generally chosen without any uniform basis

and are generally well below the values for expected peak accelerations. This is basically due to the assumption that some permanent movement of the wall due to shaking can be tolerated.

4. In the Mononobe-Okabe method no account is taken of resonance effects or the amplification of earthquake motions that might occur as a result of the propagation of the motion through the relatively soft soil behind the wall.

5. The Mononobe-Okabe method neglects the influence of the dynamic behavior of the wall structure itself on the earth pressures. Richards and Elms [43] (see section 1.3) have performed a study taking wall parameters into consideration.

1.2. Experimental Studies

In order to verify the Mononobe-Okabe theory, experiments on small-scale laboratory models subjected to sinusoidal excitation on shaking tables have been performed by a number of researchers: Mononobe and Matsuo, 1929 [31]; Jacobsen, 1939 [19]; Ishii, Arai, and Tsuchida, 1960 [18]; Matsuo and Ohara, 1960, [28]; Murphy, 1960 [33]; Niwa, 1960 [36]; Ohara, 1960 [38].

Mononobe and Matsuo used a 4 ft high, 4 ft wide, and 9 ft long sandbox which was subjected to horizontal excitations with vibration periods of 0.42 to 0.48 seconds. The end-walls of the box were hinged at the base and restrained by pressure measuring devices at the top. Total end-wall forces were measured and were found to be in reasonable

agreement to those given by the Mononobe-Okabe method. Although no details were given, the wall was presumably allowed to displace sufficiently to allow full active pressure to develop.

Jacobsen performed tests on a sandbox using a shaking table and a 3 ft high layer of sand. Although no other details as to size of the box, flexibility of the wall, or type of excitation are given, it was concluded that the tests were in reasonable agreement with the Mononobe-Okabe method, and that the dynamic component of the force acted at about two thirds of the height of the sand layer above the base.

Ishii, Arai and Tsuchida performed tests with which they concluded that, in general, their results were in agreement with the Mononobe-Okabe analysis. They conducted tests on a sandbox with fixed and movable end-walls. Model gravity walls were also used in the box. A 2.3 ft depth of sand was used behind the walls. The entire box was subjected to sinusoidal excitations of approximately 3 Hz and 0.1g to 0.7g amplitude. Observations on wall displacement, sand settlement, residual earth pressures, and phase relationships between the earth pressures and base motion were made.

Matsuo and Ohara performed tests on dry and saturated sands in a shaking box 3.28 ft x 1.97 ft x 1.31 ft high. Conditions were similar to the tests of Ishii, et al. The box was subjected to 3 Hz sinusoidal excitations with an amplitude of 0.1g to 0.4g. Tests were conducted for both a fixed end-wall (essentially rigid) and a movable end-wall that was permitted to rotate about its base. Shaking was allowed to vary during the tests. For the rigid case the earth pressures were

significantly higher than predicted by Mononobe-Okabe. The earth pressure distributions were also found to deviate considerably from linear.

Based on elasticity theory, Matsuo and Ohara also derived analytical expressions for pressure distributions for the fixed and rotating wall. The experimental pressures were significantly less for the rigid wall than those predicted by their theory. They attribute the discrepancies to influences of the side walls of the box and to the elasticity of the pressure cells used.

Murphy conducted tests to determine the mode of failure of wall-soil systems. A 1/64 scale wall model was placed in a shaking sand box and subjected to a 5.4 Hz excitation with a maximum acceleration of 0.25g. No pressures or displacements were recorded. It was found that failure occurred by outward rotation of the wall about the toe with a failure surface in the soil inclined at 35° to the horizontal. The results were considered consistent with the failure plane in the Mononobe-Okabe method.

Niwa performed tests on a large-scale gravity-type quay wall model. The wall was 9.8 ft high and 13.1 ft wide with a 16.4 ft long sand backfill. In addition, a 6.6 ft X 6.6 ft X 13.1 ft surcharge of sand was placed right behind the wall. A large vibration generator was used. It was capable of delivering frequencies of 3 Hz to 6 Hz with a lateral force of 35 tons @ 6 Hz and a lateral acceleration of 0.3g @ 6 Hz. The generator was placed 34.8 ft behind the wall. A sizeable number of transducers were used to instrument the wall. These included pressure cells, as well as displacement, velocity and acceleration transducers.

Unfortunately, results were very sketchy. Pressures recorded were zero at the top and increased fairly linearly towards the bottom. No comparison with the Mononobe-Okabe method was given.

Ohara conducted experiments on a 12 in deep, 22 in wide and 39 in long sandbox which was harmonically forced with accelerations of up to 0.4g. The end wall was given controlled displacements and the results were found to be consistent with those predicted by the Mononobe-Okabe method.

From the shaking table experiments it is generally concluded that the Mononobe-Okabe method gives the total resultant force reasonably well, but not the pressure distribution, and hence, does not predict the point of application of the force or the magnitude of the overturning moment correctly. Overall, the results of the shaking table experiments are questionable. The tests were performed under fairly unreal conditions. They generally had externally controlled restricted displacements and rotations of the wall. The tests were performed in the laboratory at earth gravity, using scaled harmonic forcing, which was not random as seismic forcing is and may not adequately represent transient earthquake stresses. The rationale for these tests is based on the following argument (Wood[67]). A similarity condition for an elastic soil and a rigid wall under the assumption that both the model and prototype have the same Poisson's ratio is given by the dimensionless equation for the frequency of a vibrating elastic system:

$$\frac{f_p^2 \rho_p \ H_p^2}{G_p} = \frac{f_m^2 \rho_m \ H_m^2}{G_m} \tag{1.3}$$

where:

$f_{m,p}$ = frequency of vibration of model and prototype respectively.

$\rho_{m,p}$ = soil mass density

$H_{m,p}$ = height

$G_{m,p}$ = shear modulus

and both model and prototype tests are performed at the same gravitational acceleration.

The equation is usually employed to determine the frequency at which the model is to be vibrated to simulate the full-scale behavior. If the ratio of length scale in prototype to model is denoted as N, the equation can be rearranged in terms of frequency to give

$$\frac{f_m}{f_p} = \left[\left(\frac{H_p}{H_m} \right)^2 \left(\frac{G_m}{G_p} \right) \left(\frac{\rho_p}{\rho_m} \right) \right]^{1/2} \tag{1.4}$$

However, H_p/H_m = N, and, since the same soil is generally used in model and prototype, ρ_p/ρ_m is close to unity so that

$$\frac{f_m}{f_p} = N \left(\frac{G_m}{G_p} \right)^{1/2} \tag{1.5}$$

In a clay, a laboratory model can be prepared with G_m essentially any desired value, from a low level, appropriate in some way to the model dimension, to a value the same as the prototype. In sands, the shear modulus G varies with the effective stress, which depends directly

on the gravitational field. As a consequence G_m in a model sand is considerably smaller over the wall depth than G_p in the full-scale domain. The choice of f_m therefore, depends on the relationship adopted between G and the effective stress in the sand. If G is taken to vary linearly with effective stress, then f_m is approximately equal to $N^{1/2} f_p$. Alternative if G is taken to vary as some power of effective stress, say 1/2 (Seed and Idriss [54]), f_m would be given as $N^{3/4} f_p$.

Given this uncertainty about the variation of G with effective stress, no clear approach is indicated, nor do the experiments clarify the effect on the dynamic pressure distributions obtained by the use of different model exciting frequencies. It can be concluded that it is difficult or impossible to achieve a pressure distribution in a (one g) model on a shaking table similar to that found in the full-scale field situation. Therefore, true modelling of the prototype soil cannot be attained in a (one g) shaking table experiment.

1.3. Analytical Studies

In addition to the experimental research, analytical models have been proposed to describe the dynamic earth pressures acting on walls: Tajimi, 1969-73 [59-61]; Prakash and Basavanna, 1969 [42]; Scott, 1973 [50]; Wood, 1973 [67]; Richards and Elms, 1977 [43]; Chang and Chen, 1981 [6,7].
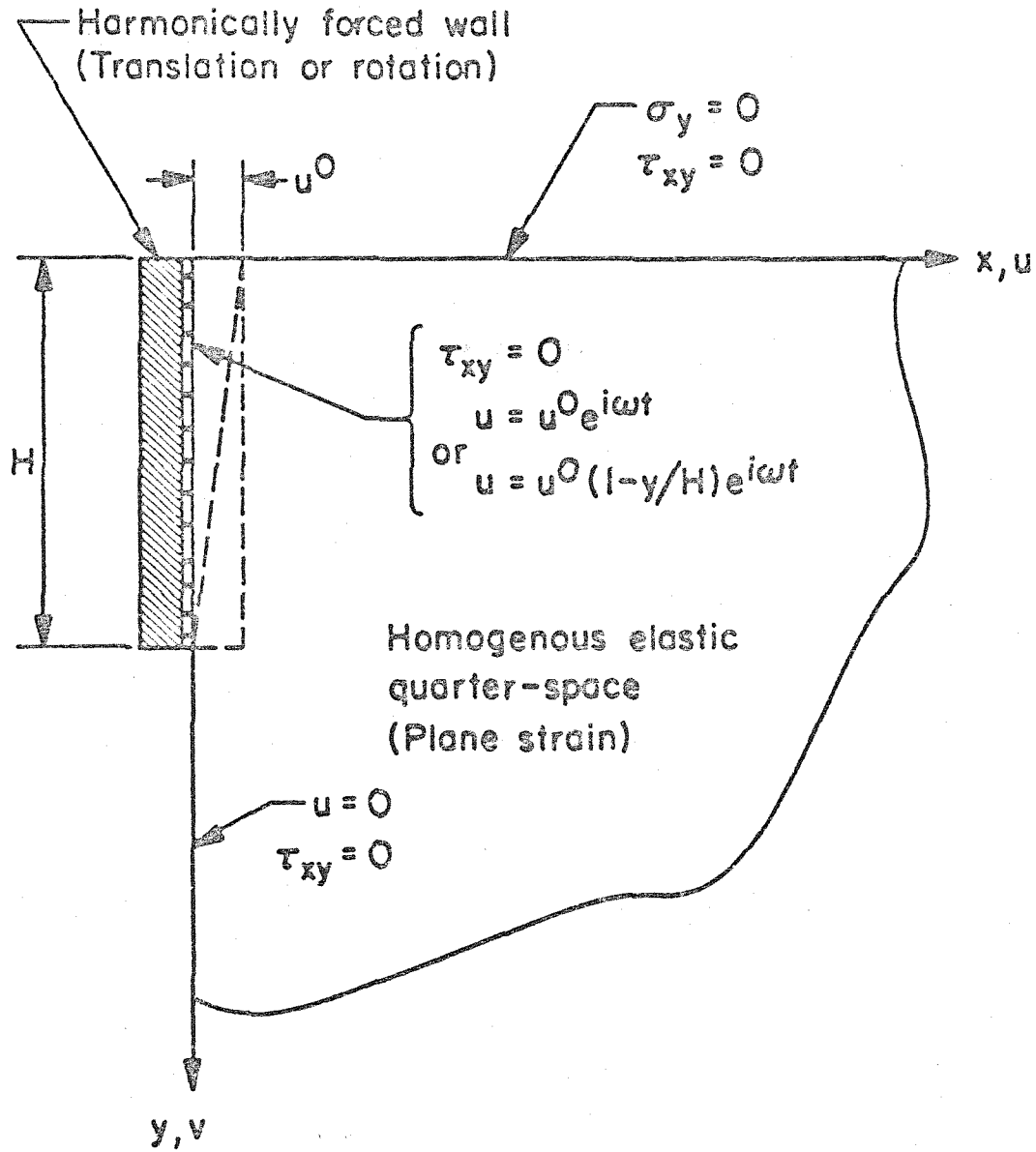
Tajimi obtained the solution for earthquake-induced soil pressures on a cylindrical structure embedded in an elastic soil. He also obtained the solution for a harmonically forced rigid wall of finite height at the corner of a quarter-infinite elastic medium (Figure 1.3). The analysis was based on elastic wave propagation theory. Although the boundary conditions are not very realistic, the solution can be used as an approximation for some dynamic problems.

Prakash and Basavanna computed an approximate wall pressure distribution on a wall under similar assumptions to those of the Mononobe-Okabe method. It was determined that the pressure distribution was essentially parabolic although the resultant was virtually of the same magnitude as give by Mononobe-Okabe. The resultant, however, acts at a height above the base H_a given by:

$$H_a = C_a H/3 \tag{1.6}$$

where C_a is a very complicated expression dependent on all the Mononobe-Okabe wall-soil parameters. H is the height of the wall. C_a is greater than one. For $k_h = 0.3$, H_a is approximately midheight and continues to rise with higher lateral acceleration.

Scott performed an analysis on a simple yet useful model (Figure 1.4). It basically consists of a rigid wall with the soil modelled as a simple shear beam on a Winkler foundation. He also performed an analysis where a wall flexibility was included. Closed form solutions were obtained for various cases that include variations of the elastic constants with depth and certain types of wall

Harmonically forced wall
(Translation or rotation)

$\sigma_y = 0$
$\tau_{xy} = 0$

u^0

x, u

$\begin{cases} \tau_{xy} = 0 \\ \quad u = u^0 e^{i\omega t} \\ \text{or} \\ \quad u = u^0 (1 - y/H) e^{i\omega t} \end{cases}$

H

Homogenous elastic
quarter-space
(Plane strain)

$u = 0$
$\tau_{xy} = 0$

y, v

TAJIMI'S PROBLEM

FIGURE 1.3
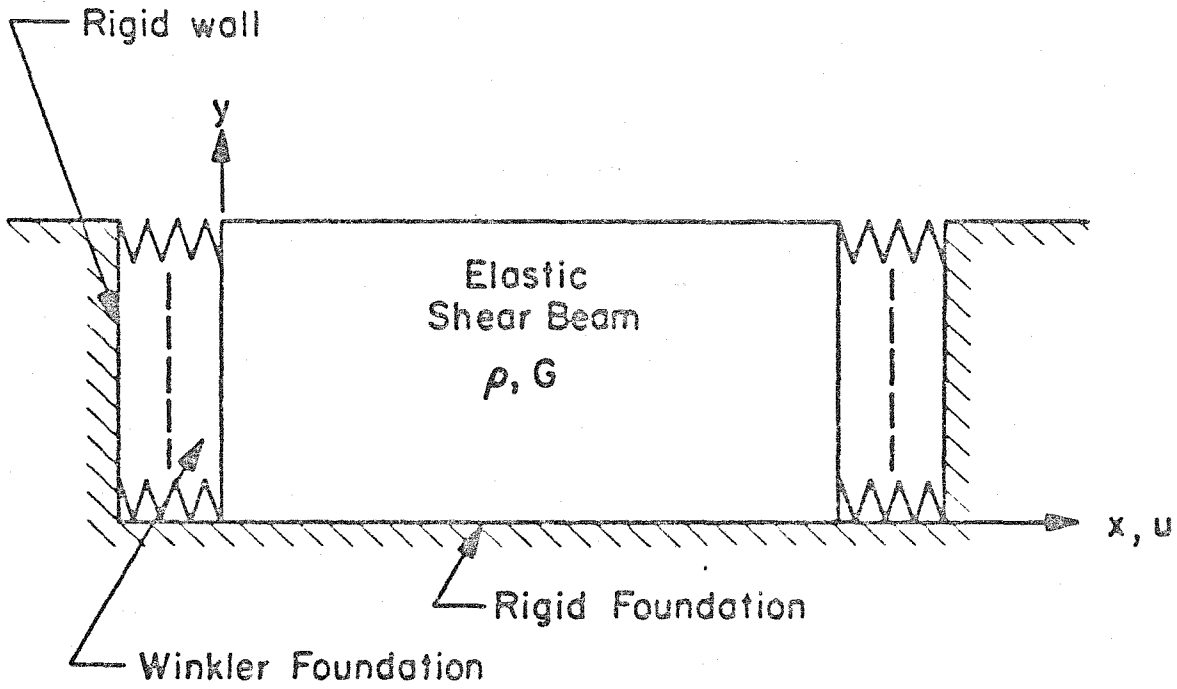
SCOTT'S MODEL

FIGURE 1.4

deformations. Because of simplicity the solutions are quite useful in preliminary design applications. Scott concluded that what happens in an earthquake to a wall designed by the Mononobe-Okabe method is that "elastic", transient forces much higher than those predicted by Mononobe-Okabe act on the wall, causing it to displace and rotate. When the wall reaches a displacement of 1/2% or so of the height, the soil reaches failure. The wall continues to displace and rotate due to inertia and when it stops what is observed is the failure (Mononobe-Okabe) mechanism – not the stresses that caused failure. This is why all the experiments involving failure end up by concluding that Mononobe-Okabe is the right analysis. If the earthquake force only reached Mononobe-Okabe levels of stress, then the wall designed to M-O should not fail.

Wood, using elastic and elastic wave propagation theories developed solutions for an elastic soil stratum of finite or infinite length and finite depth on a rigid base with a rigid wall under various and forcing conditions. For a perfectly rigid wall (Figure 1.5), supporting a relatively long layer of soil, he determined that the earthquake force component computed was likely to be greater than twice that estimated by the Mononobe-Okabe method (Figure 1.6). Identical horizontal earthquake coefficients k_n were used in the comparison. It was thus recommended that for a rigid wall embedded in rock or very firm soil, restrained by piles or deeply buried, an elastic analysis should be used in lieu of the Mononobe-Okabe method.
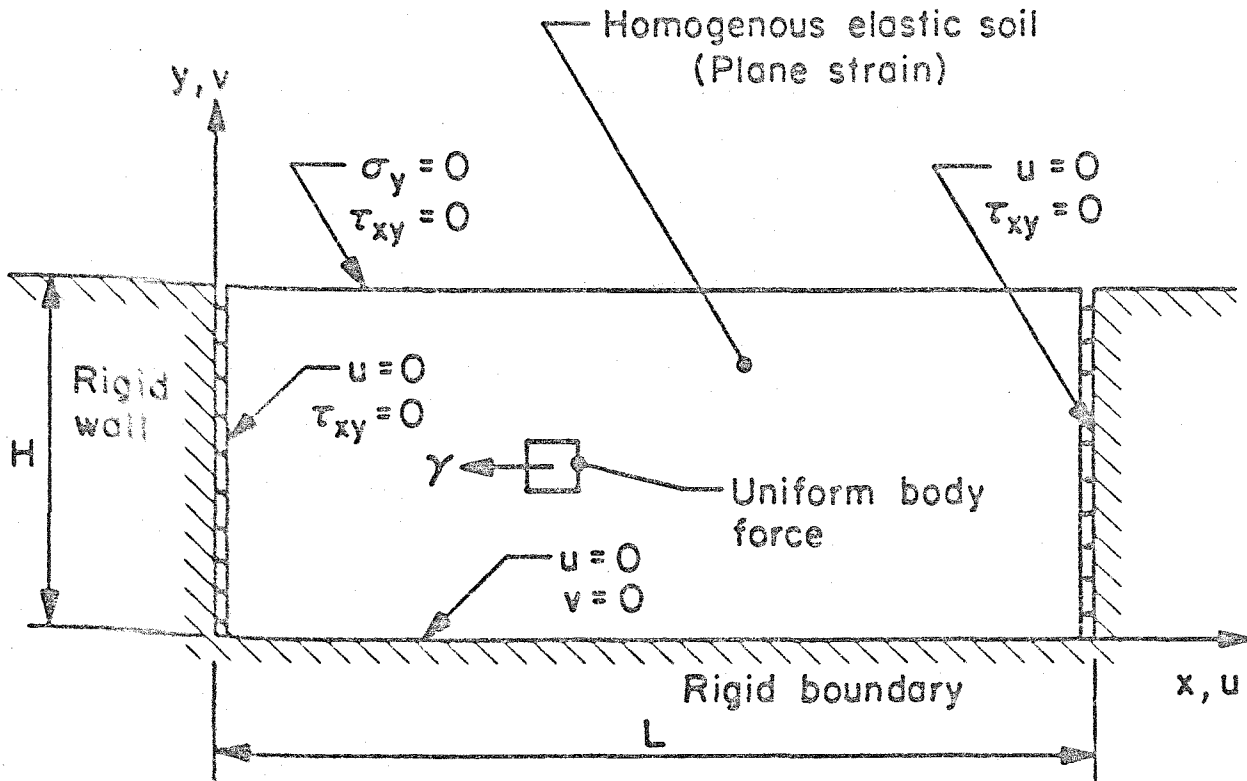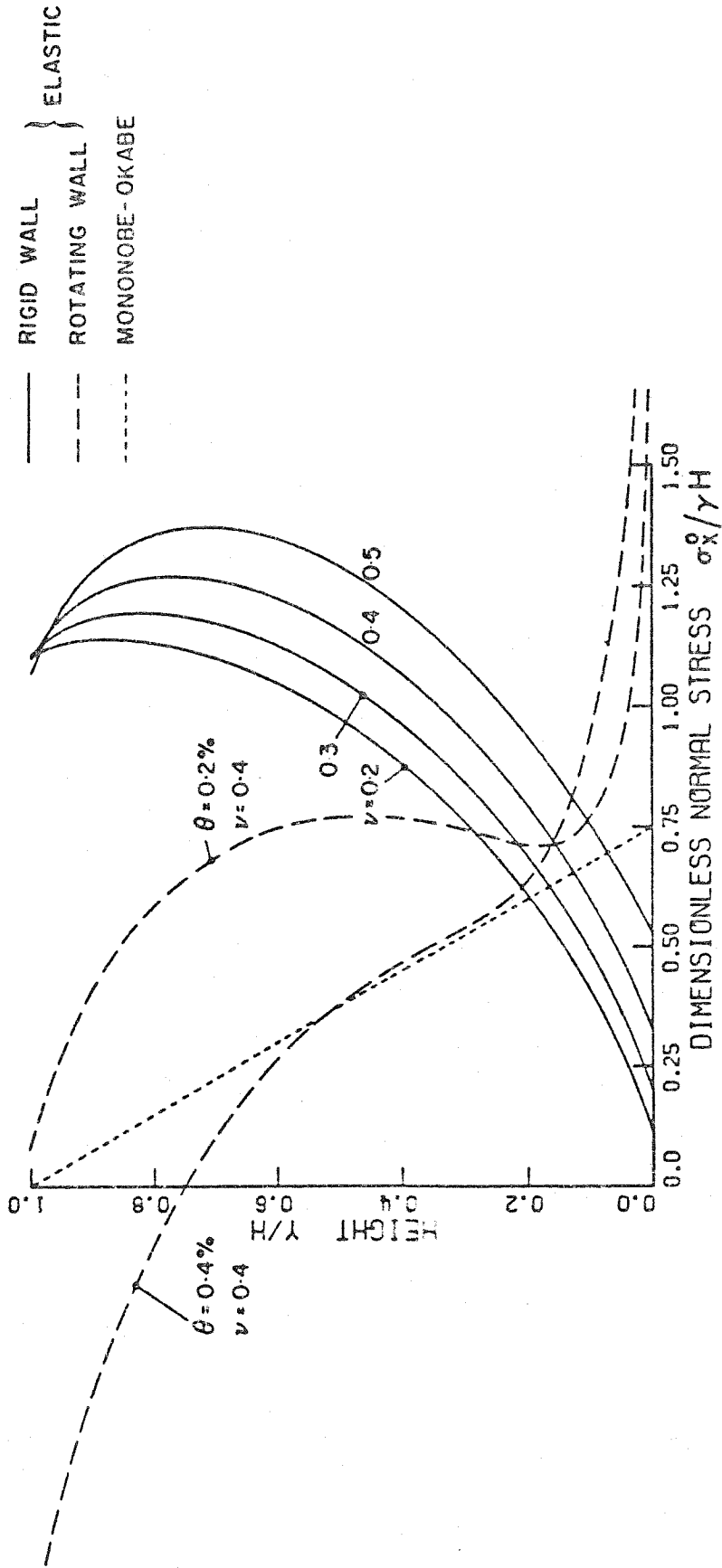
WOOD'S RIGID WALL PROBLEM

FIGURE 1.5

LENGTH/HEIGHT = 10.0

Pressure distributions for one-g static horizontal
body force.   Comparison between elastic theory
and Mononobe-Okabe method.
FIGURE 1.6 – FROM (67)

Richards and Elms extended the Mononobe-Okabe method to include the influence of the dynamic behavior of the wall structure itself (Figure 1.7). It was concluded that for gravity retaining walls the Mononobe-Okabe analysis is satisfactory provided that the inertia of the wall is taken into consideration. In addition, Richards and Elms give a description of the significance of each of the Mononobe-Okabe parameters which is useful in a further understanding of the method.

Chang and Chen developed an upper bound technique of limit analysis and then applied it the earthquake problem. It is basically an approach similar to Mononobe-Okabe with the main difference being that more refined failure surfaces (Figure 1.8) are used. The seismic coefficient of active earth pressure K_{AE} was found to be practically the same as that obtained by a Mononobe-Okabe analysis.

1.4. Earthquake Damage to Retaining Structures

Failures in retaining structures due to earthquakes occur very frequently. These are documented in virtually every earthquake-damage report. It should be noted that in most reports, unless failures are dramatic, retaining-structure damage is given secondary importance. This is generally due to the fact that failure of these structures does not entail severe loss of life and limb. The damage done by the earthquake can, however, be very costly in terms of repair and replacement as well as economic setbacks to a community. A few examples of damage to retaining structures follow.
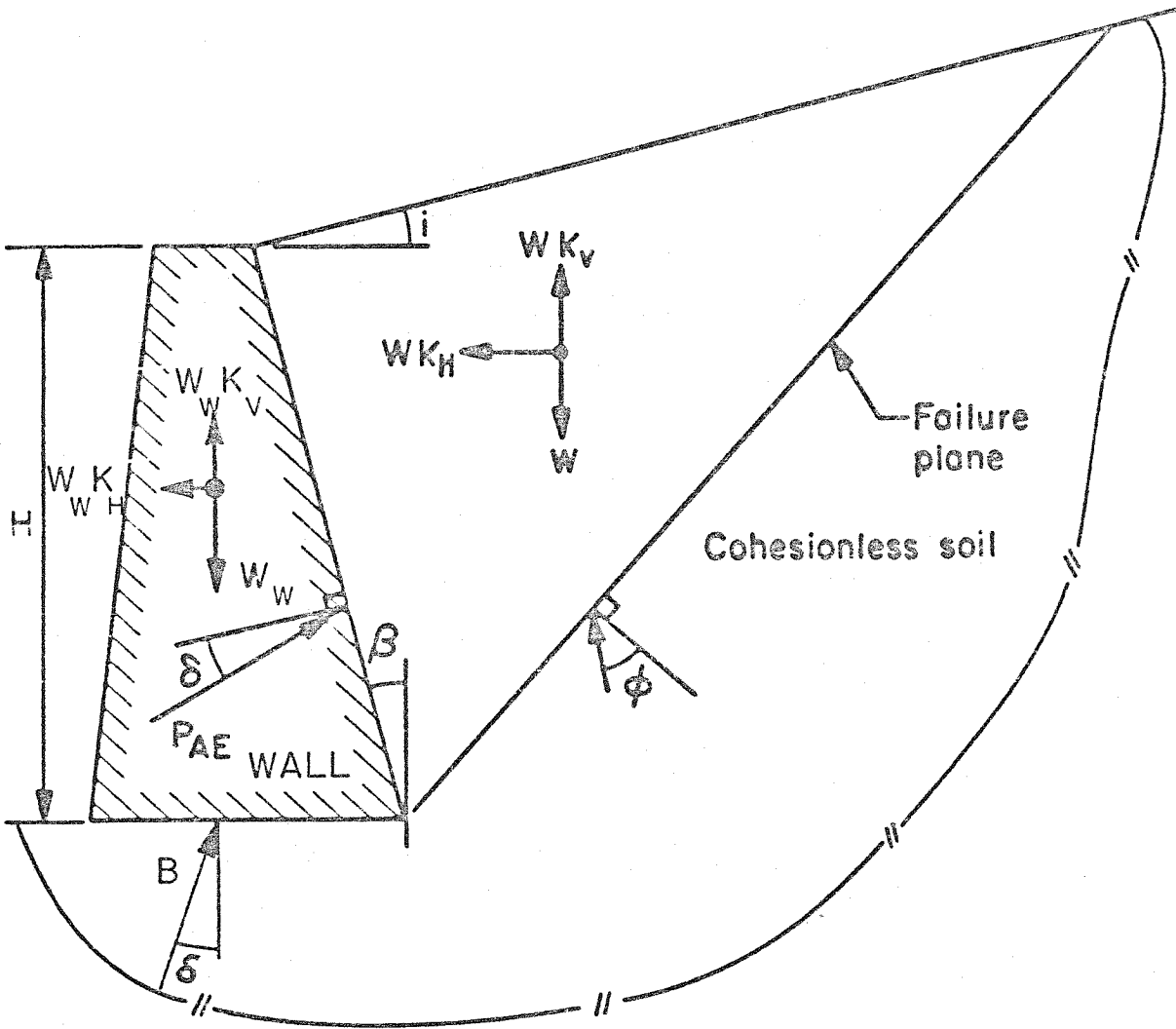
RICHARDS & ELMS ANALYSIS

FIGURE 1.7
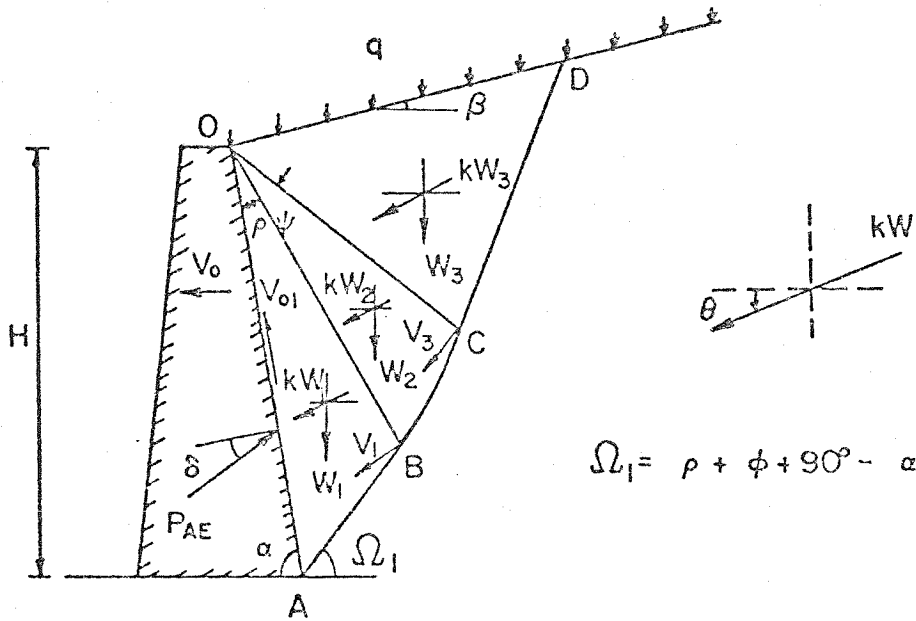
FIGURE 1.8 – FROM (7) Log–Sandwich Failure Mechanism for Seismic Active Earth Pressure Analysis

$$\Omega_1 = \rho + \phi + 90° - \alpha$$

1.4.1. Chile

Duke and Leeds [11] provide an extensive account of damage to retaining structures in the 1960 Chilean Earthquakes, the most severe of which had a Richter magnitude of 8.5. At Puerto Montt (Figure 1.9), the Modified Mercalli Intensity (MMI) was estimated to be between VIII and IX. There was essentially total failure of the harbor gravity-type quay walls (Figs. 1.10, 1.11, 1.12, 1.13). Both walls completely overturned. Sheet pile sea walls (Figs. 1.11, 1.14) were severely damaged. The piles had approximately 5" x 15" hat-shaped cross-sections with 5/16" thick webs and were made in Germany. Since the walls were about 30 years old at the time of the earthquake, failure principally occurred when the corroded rods broke due to the added tension resulting from the added soil pressure.

Most of the above-mentioned structures were founded on fill consisting of gravel, sand, silt, some masonry fragments, and organic matter. In general, it was placed by dumping although some was placed hydrodynamically by dredging from the harbor bottom. The disastrous damage to structures retaining this material was largely due to liquefaction as a result of earthquake motion.

Figure 1.15 shows distortion of the Isla Teja bridge in Valdivia (MMI X) due to the added soil pressure on the abutment whose excessive movement caused damage to the bridge superstructure. Unlike the Puerto Montt failures, damage to this structure was not due to liquefaction, but solely to the added inertia from the shaking.
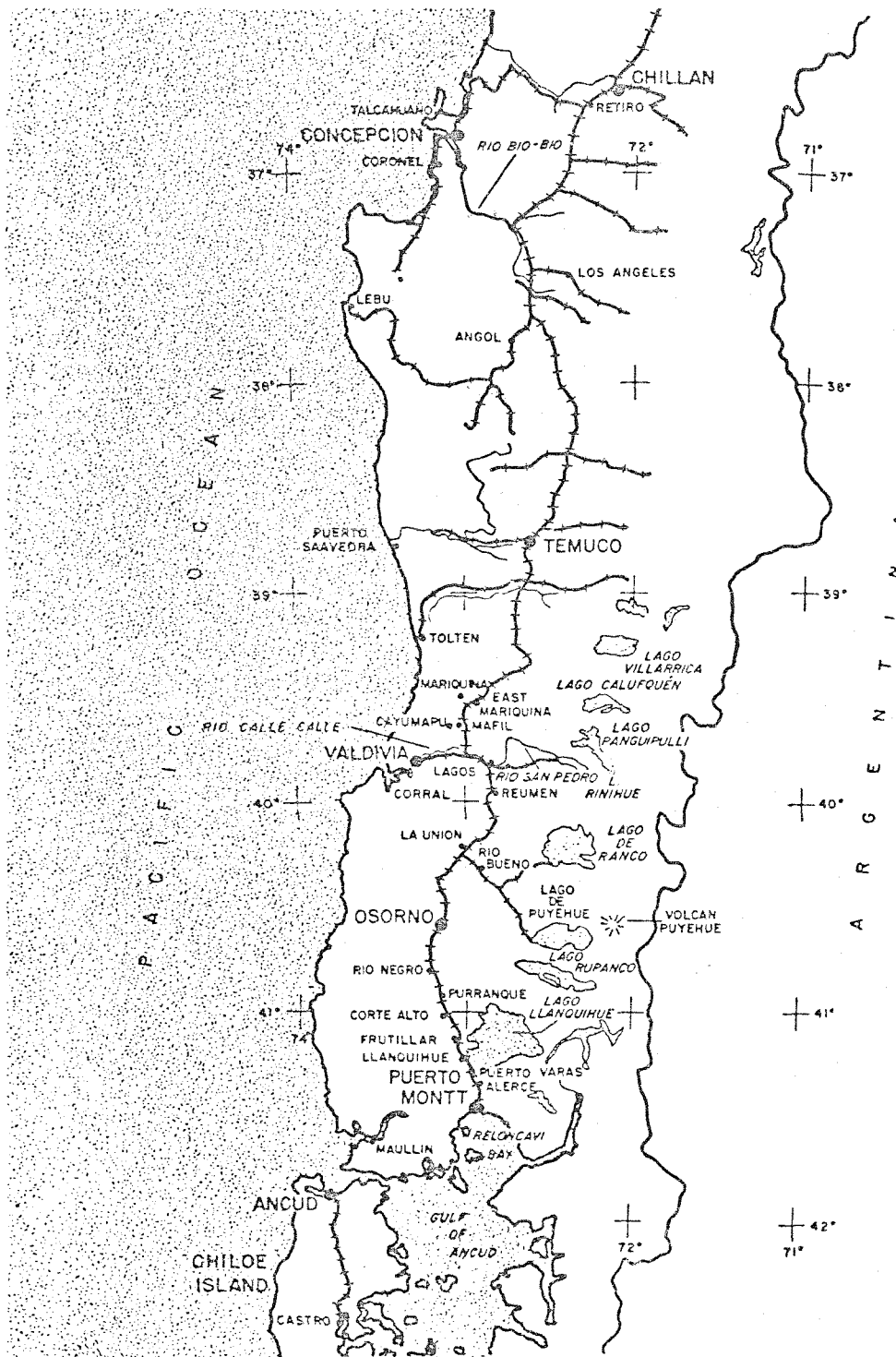
Region affected by the Chile Earthquakes of May 1960.

FIGURE 1.9 – FROM (11)
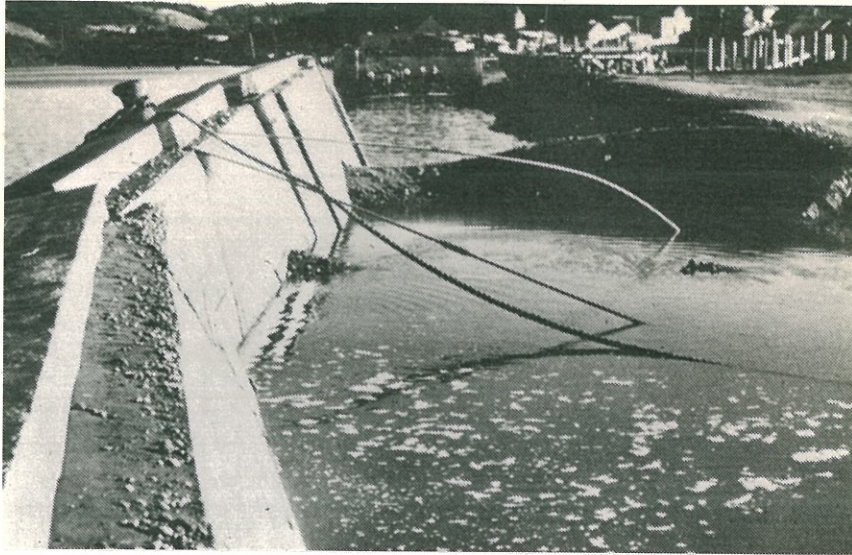
FIGURE 1.10 — FAILURE OF QUAY WALL AT PUERTO MONTT — FROM (55)

15.5 METER QUAY WALL
(after Chile Dept. of Ports)

18.5 METER QUAY WALL
(after Chile Dept. of Ports)

STEEL SHEET PILE SEA WALL
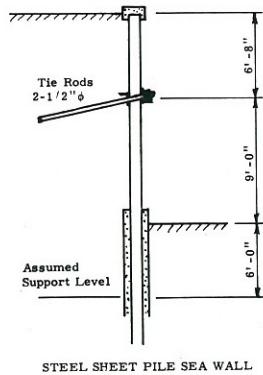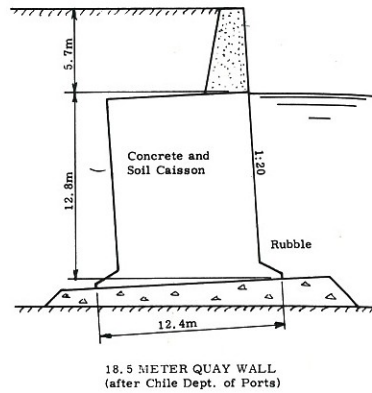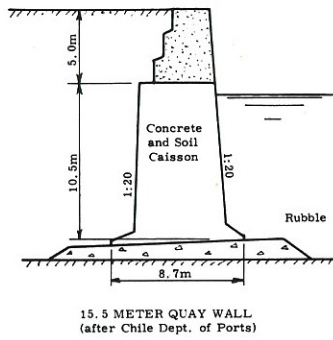
FIGURE 1.11 — PUERTO MONTT, WATERFRONT WALLS, DESIGN FEATURES — FROM (11)

FIGURE 1.12 — FAILURE OF GRAVITY WALL AT PUERTO MONTT — FROM (11)

FIGURE 1.13 — PUERTO MONTT, GRAVITY WALL FAILURE — FROM (11)

FIGURE 1.14 - FAILURE OF SHEET-PILE SEA WALL AT PUERTO MONTT - FROM (11)
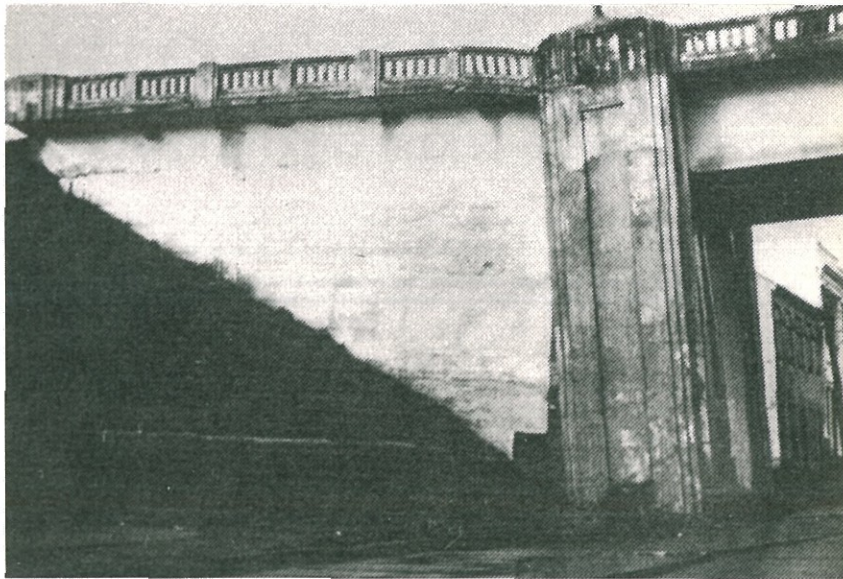
FIGURE 1.15 - DISTORTION OF ISLA TEJA BRIDGE DUE TO
SOIL PRESSURE ON ABUTMENT - FROM (55)

Seed and Whitman [55] also report on a gravity retaining wall
failure at Frutillar (MMI VIII) where dry material was encountered
(Fig. 1.16).

1.4.2. Alaska

Ross, Seed, and Migliaccio [45] report on extensive bridge damage
due to the 8.4 magnitude Alaska earthquake of 1964. Most of the bridges
which suffered damage were 50 to 80 miles away from the cone of major
energy release. The most severe damage occurred on the Seward,
Sterling, and Copper River Highways (Fig. 1.17). Table 1.1 gives a
foundation damage classification reduced from reports of the Alaska
Department of Highways.

Most of the bridges were founded on alluvial deposits composed of
granular materials which ranged anywhere from coarse gravels to fine
sands and silts depending on location. The deposits ranged in depth
from 50 to 150 ft and were generally underlain by clays or bedrock. A
few bridges were founded on bedrock.

Damage was due completely or in part to the lateral displacement of
the bridge abutments toward the channels causing tilting of piers and
buckling of superstructures (Figs. 1.18, 1.19, 1.20). There was also
spreading and settlement of abutment fills. The greatest concentrations
of severe damage occurred in regions characterized by thick deposits of
saturated cohesionless soils. There was ample evidence of liquefaction
of these materials during the earthquake. This phenomenon probably
played a major role in the development of foundation displacements and

FIGURE 1.16 — FRUTILLAR, RETAINING WALL FAILURE — FROM (55)

TABLE 1.1

Classification of Damage to Highway Bridge Foundations
During the Alaska Earthquake (from Ross et al. [45])

114 Bridges Classified

Classification	Description	Percentage
Severe	Abutments moved streamward and/or markedly subsided; piers shifted, tilted, or settled; substructure rendered unsalvageable	28
Moderate	Distinct and measurable net displacements as in previous category, but to a lesser degree, so that substructure could perhaps be repaired and used to support a new superstructure	22
Minor	Evidence of foundation movements (such as cracked backwalls, split piles, closed expansion devices), but net displacements small and substructure serviceable.	18
Nil	No evidence of foundation displacements	32

bridge damage. Even where damage was moderate or minor, there was evidence of bridge joints closing indicating lateral displacement of the abutments.

It should be noted that where bridges were founded completely on bedrock there was virtually no damage. However, severe to moderate displacements were reported for bridges founded partly on bedrock and partly in soils.
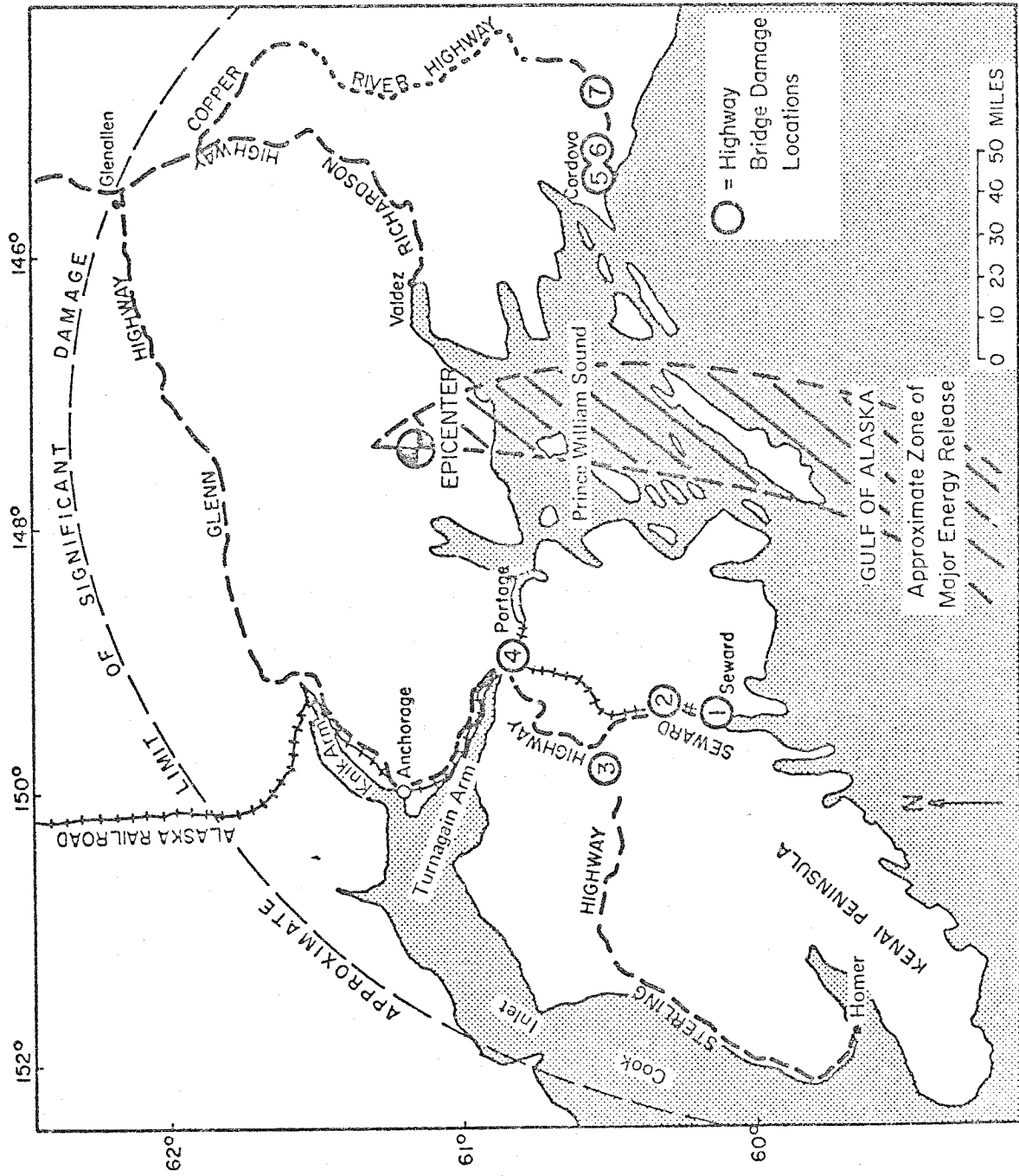
Highway routes of seven main bridge-damage locations in earthquake-damaged region, south central Alaska.

FIGURE 1.17 – FROM (45)
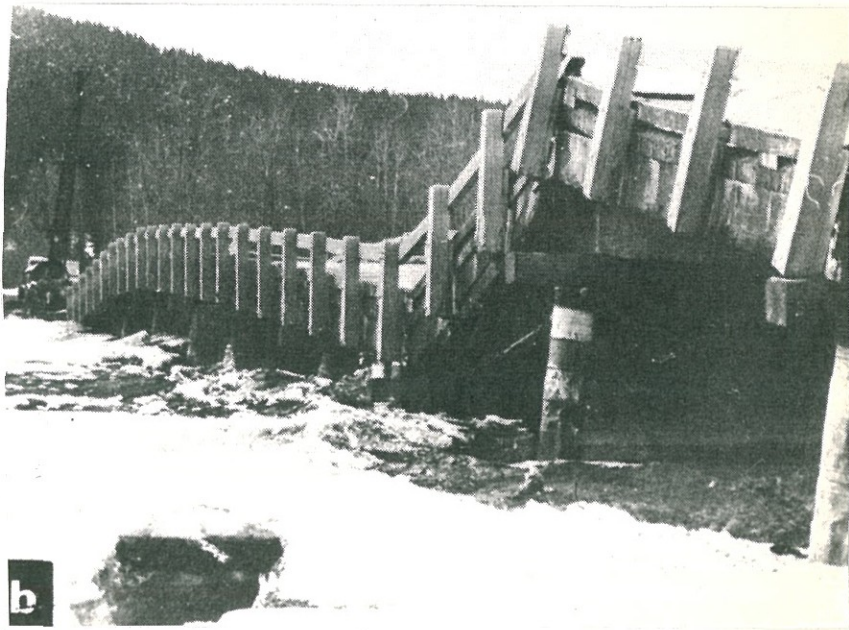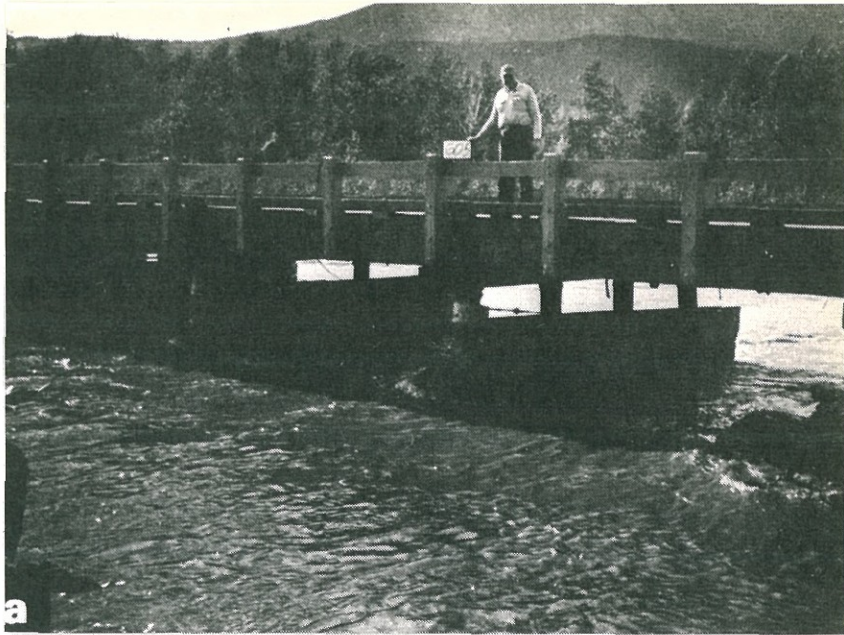
FIGURE 1.18 – SUPERSTRUCTURE BUCKLING OF SNOW RIVER BRIDGE 605 – FROM (45)

FIGURE 1.19 – SUPERSTRUCTURE BUCKLING OF SNOW RIVER BRIDGE 604 – FROM (45)

FIGURE 1.20 – SUPERSTRUCTURE DRIVEN THROUGH ABUTMENT

BACKWALL, COPPER RIVER BRIDGE 345 – FROM (45)

1.4.3. Niigata, Japan

The 7.5 magnitude, 1964 Niigata, Japan earthquake caused severe damage to waterfront structures and virtually paralyzed operations at the port of Niigata, one of Japan's most important. Accounts of the damage are given by Hayashi, Kubo, and Nakase [14], and by Kawasumi [22].

The total length of waterfront structures including jetties and dikes at the port of Niigata was 10.25 miles. About 76% of this length was composed of earth retaining structures. Sixty-nine percent of these were steel sheetpile bulkheads, 8% were concrete sheetpile walls and 6% were concrete gravity walls. The severity of damage to harbor structures is outlined in Table 1.2.

TABLE 1.2

(from Hayashi, et al. [14])

Grade of Damage	Description	Total Length* (mi.)	Proportion to the Overall Length* (%)
4	Complete failure of whole structure	5.43 (4.43)	52.8 (57.1)
3	Failure in main part of structure	2.32 (2.32)	22.6 (30.0)
2	Appreciable Deformation to main part of structure	0.07 (0.02)	0.7 (0.3)
1	Failure in sub-part of structure	3.98 (0.39)	14.5 (5.0)
0	No damage	0.97 (0.59)	9.4 (7.6)

*Figures in parentheses refer to earth retaining structures only.

It should be noted that due to the failure of earth retaining structures, 61 warehouses and sheds, 676, 600 ft^2 in total area, fell down completely, and 92, 691, 500 ft^2, were seriously damaged (Figs. 1.21, 1.22).

Most of the sheet pile structures in Niigata Harbor underwent damage and a large number were completely destroyed or submerged. A common feature of the damage was a swelling of the backfill and inclination of the wall toward the sea. This type of damage was typically observed in bulkheads with poor anchor resistance. Tie rods were severed in some cases. In others there was a shear failure in the concrete anchor blocks due to the stress concentration created by the tie rods. The sheetpile bulkheads were designed employing a Mononobe-Okabe Analysis and a seismic coefficient of 0.10. Actual horizontal ground accelerations were around 0.2g amplitude.

The brand new Yamanoshita wharf (completed 1963) which had been Mononobe-Okabe designed with a seismic coefficient of 0.12 suffered no appreciable damage, except for local sinking of the fill behind the anchor plate.

Concrete sheetpile walls, which formed a small part of the waterfront, were completely destroyed by the earthquake.

The gravity retaining walls were generally composed of several concrete blocks stacked up on top of each other and then assumed to act as a monolithic structure. A seismic coefficient of 0.10 was used in design, but it was later found that when the seismic coefficient reaches
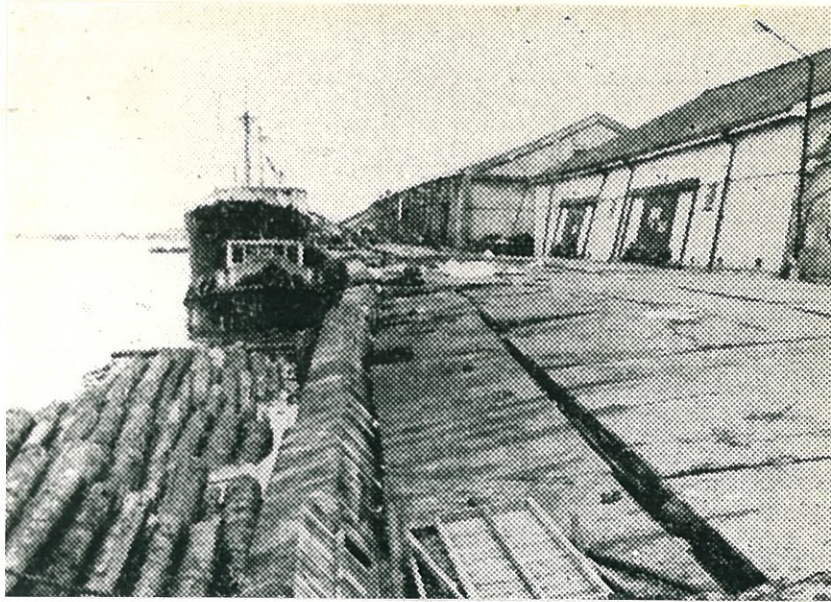
FIGURE 1.21 – SHEET-PILE BULKHEAD FAILURE, NIIGATA – FROM (14)
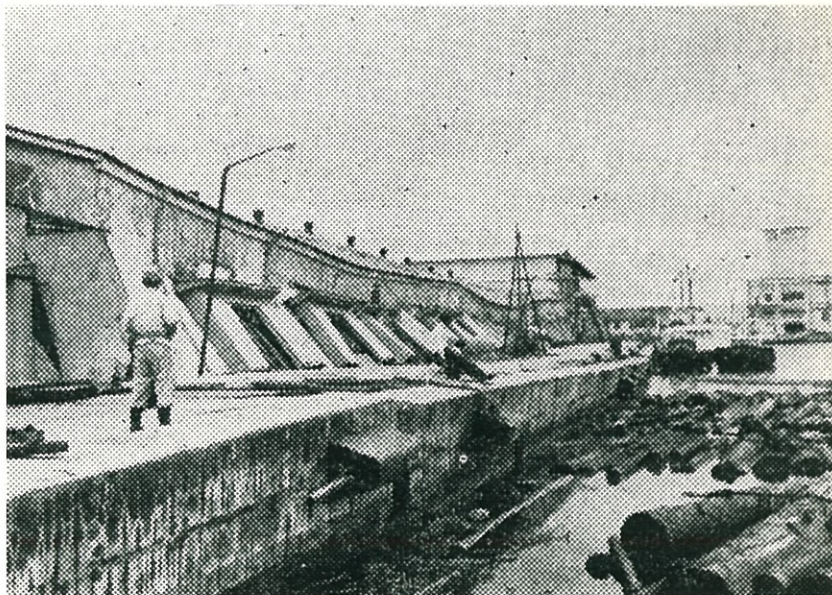
FIGURE 1.22 – WAREHOUSE COLLAPSE DUE TO SHEET-PILE
BULKHEAD FAILURE, NIIGATA – FROM (14)

0.12 or 0.13 the structure cannot any longer be assumed to act monolithically. As a result, damage was characterized by blocks falling forward, slippage, and sinking of blocks, and general inclination and sliding of the structures. Damage was severe.

The general soil profile of the Niigata area consists of a layer of sand about 130 ft deep underlain by clays and containing pockets of fine silty soil in the top 60 ft. The soil was generally saturated and much of the damage was due to the occurrence of liquefaction. Before the earthquake the top 30 ft of soil was characterized by an average blowcount of from 4 to 8 using the Standard Penetration Test. Between 30 and 60 feet, it varied linearly from about 8 at 30 ft to about 30 at 60 ft. These figures were reduced by one third after the earthquake. In general, the deeper the structure was embedded in the soil the less severe the damage.

Based on the damage caused by the 1964 earthquakes, replacement structures have been designed and built based on a seismic coefficient of 0.2.

1.4.4. San Fernando, California

The 1971 San Fernando, California, earthquake, which had a magnitude of 6.2, severely damaged, in some cases, earth retaining structures including flood control channels, bridge abutments, and underground water storage tanks and tunnels.

Murphy [32], Scott in Reference [21], Lew, Leyendecker and Dickers [24], and Wood [67] provide descriptions of damage to the Wilson Canyon

and Mansfield Street Flood Control Channels and to the Lopez Canyon

Diversion Channel which were located in an area where transient lateral

accelerations may have been as high as 50%g.

The Wilson Canyon Channel is partially an open, rectangular,

reinforced concrete channel, with a width of about 15 feet and wall

heights which vary from 9 to 11.5 feet (Figure 1.23) and partially a

covered, rectangular, box section with widths varying from 15 to 22 feet

and wall heights ranging from 105 to 16 feet; it is about 3 miles long.

The Lopez Canyon Diversion Channel is an open, rectangular

reinforced concrete channel about 1.8 miles long, with widths varying

from 12 to 16 feet and wall heights ranging from 7 to 12 feet.

All the above-mentioned structures were built in the early 1960's

by the Corps of Engineers in accordance with the Chief of Engineers'

design criteria with no seismic consideration. Allowable design

stresses were $f_c' = 1.05$ ksi for concrete and $f_s = 20$ ksi for steel.

The channels were designed as L-type retaining walls where the wall

heights were less than half the channel width, and as U-type channel

sections otherwise.

No significant ground displacements seem to have occurred in the

vicinity of the damaged sections of the Wilson Canyon and Mansfield

Street Channels so the damage can be attributed to an increase in the

lateral earth pressure due to ground shaking. There were some inward

displacements in the open sections which measured up to 6 inches at the

top of the walls (Figs. 1.24, 1.25). Damage to the underground box sec-

tions varied from hairline cracks to major shear and moment failures in

10" 7'-0"

℄

#4 at 12"
alternate
bars stop
2'-0" from
top

2-1/2"cl

2"cl

10'-0"

Soil Properties at
Olive View Hospital:
Coarse Sand & Gravel
ϕ = 38°
Cohesion = 0
γ = 113 lb/ft^3

#4 at 2'-0"

3'-3"

#4 at 12"

12"

#6 at 12"
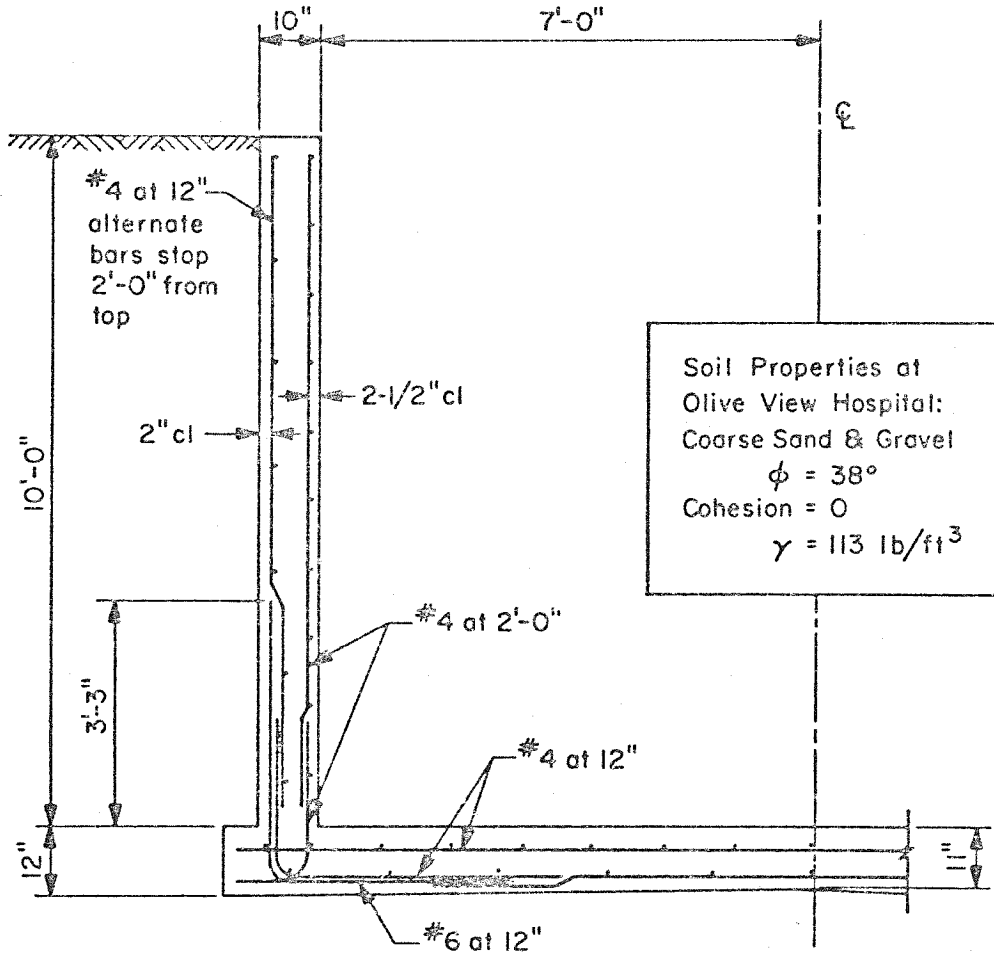
WILSON CANYON CHANNEL
Section 65' Upstream & Downstream of ℄ Olive Ave. Bridge

FIGURE 1.23 - FROM (67)
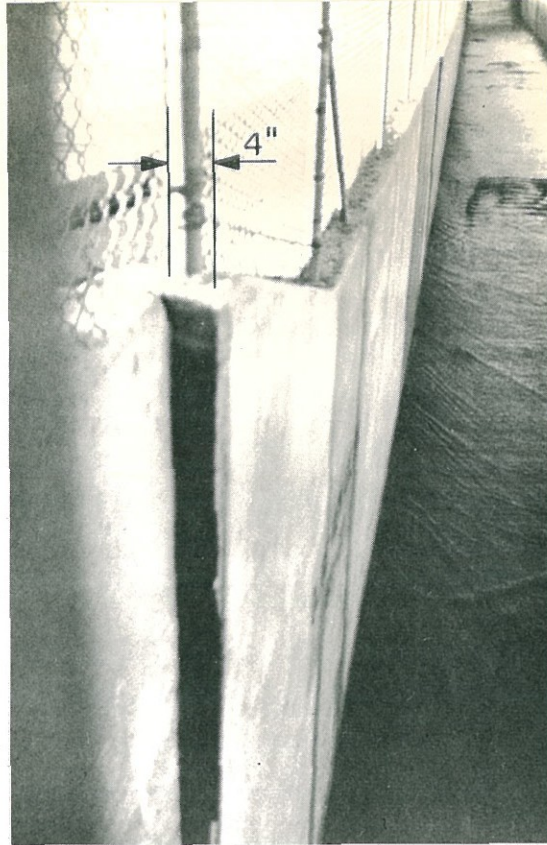
FIGURE I.24 — WILSON CANYON CHANNEL: WALL TOP DISPLACED 4" WITH RESPECT TO THE BRIDGE ABUTMENT AT LEFT — FROM (67)

FIGURE I.25 — WILSON CANYON CHANNEL: CRACKING IN SOIL AS A RESULT OF WALL DISPLACEMENT — FROM (67)

walls. Inward deflections of up to 12 inches at midheight were measured at the most severely damaged sections.

Complete failure occurred in sections of the Lopez Canyon Channel, but the failed sections were close to a surface expression of the faulting associated with the earthquake and probably permanent ground displacements contributed significantly to the damage.

It should be noted that the failure of the flood control structures did not create any danger to human life and since in the Los Angeles area these carry only infrequent flood flows, a need for seismic consideration in design and construction might not be economically warranted except for replacement costs.

1.4.5. Friuli, Italy

Similar in magnitude to the San Fernando Earthquake were the 1976 Friuli, Italy earthquakes. The May main shock had a magnitude of about 6.5 while two September aftershocks had magnitudes around 6.0. There was some damage to earth retaining structures [10,57].

Along the Ledra River a retaining wall was considerably damaged during the May shock (Figs. 1.26, 1.27). There were reports of water and sand gushing and evidence of severe cracking in the backfill indicating that liquefaction had occurred. After the September shocks water and sand gushing occurred again in lines parallel to the river course, and the damaged wall completely collapsed.

After the May event damage to the Udine-Carnia-Tarvisio highway due to movement by the retaining structures below it was observed

FIGURE 1.26 – WEIR ON THE LEDRA RIVER:DAMAGED RETAINING WALL – FROM (10)

FIGURE 1.27 – WEIR ON THE LEDRA RIVER:DAMAGED RETAINING WALL – FROM (10)

(Figs. 1.28, 1.29). This is where the highway runs between a canal and a mountainside. On the canal side the embankment is retained by a 33 ft high wall built on piles. Figure 1.30 illustrating a normal section of the road axis shows the relative positions of the canal, the retaining wall, and road embankment, with a rough representation of the supporting soil profile.

Perhaps the fact that the entire embankment was underlain by an inclined rock formation contributed to the slipping of the retaining wall towards the canal and probably to the failure of the foundation piles. Vertical displacements along the 660 yards of retaining wall ranged from 1.6 to 9.5 inches while horizontal movements were between 9.1 and 19.3 inches.

As a consequence of the September aftershocks the damage described above increased.

In addition, there was also some severe damage of several auto-strada (freeway) bridges in the area, but these were due mainly to impact from the moving bridge superstructures as opposed to failure due to increase in lateral earth pressure.

1.4.6. Tangshan, China

Yuxian [70] reports bridge failure during the 1976 Tangshan (People's Republic of China) earthquake which had a Richter magnitude of 7.8. The failure came from falling of superstructures to the river, or more usually, from sliding and tilting of the abutments. Lateral movement of abutments is blamed for buckling in bridge decks which would
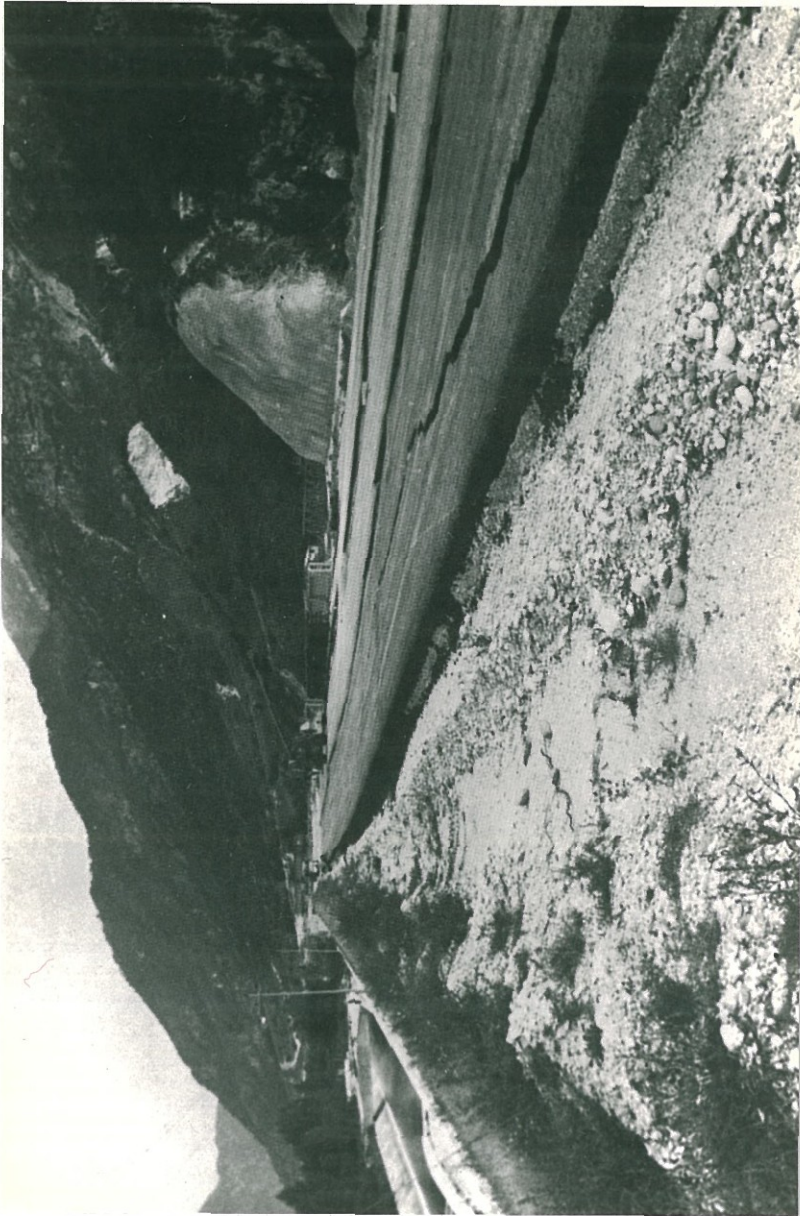
FIGURE I.28 — UDINE—CARNIA—TARVISIO HIGHWAY, ROAD CRACKING DUE TO EMBANKMENT WALL DAMAGE — FROM (IO)

FIGURE 1.29 — DAMAGE TO EMBANKMENT RETAINING WALL AND
CANAL, UDINE—CARNIA—TARVISIO HIGHWAY — FROM (I·C)

PALI ⌀ 120
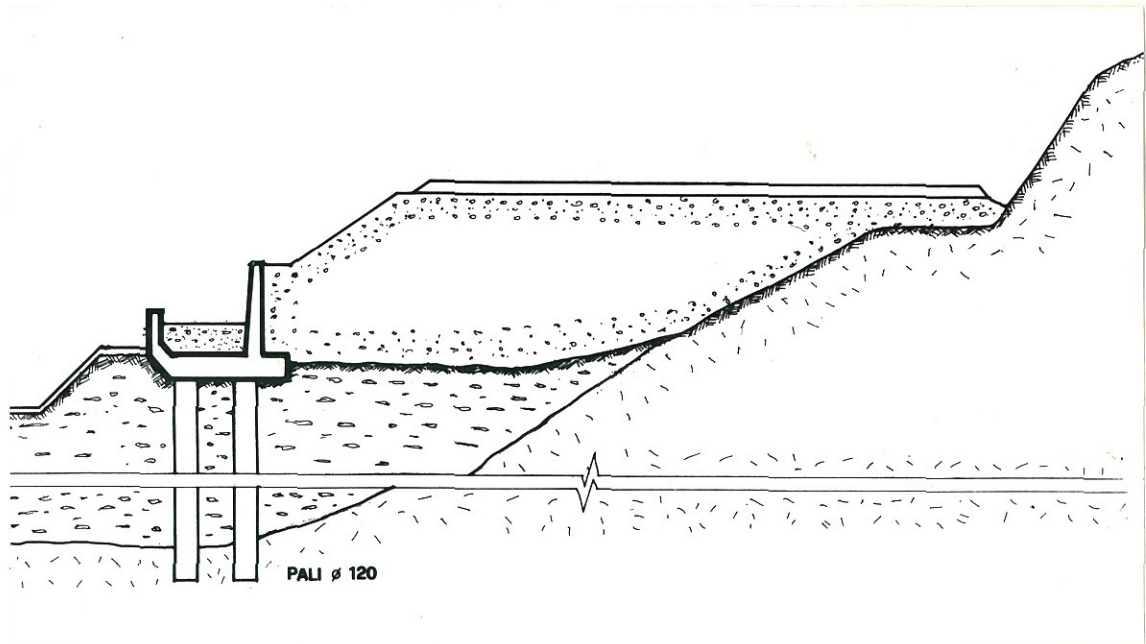
FIGURE 1.30 — UDINE—CARNIA—TARVISIO HIGHWAY, SECTION THROUGH EMBANKMENT
RETAINING STRUCTURE ADJACENT TO CANAL —FROM (10)

have otherwise remained standing. No details were given on design
criteria or construction methods.

1.4.7. Miyagi-Ken-Oki, Japan

The 7.4 magnitude Miyagi-Ken-Oki, Japan earthquake of 1978 caused
failures in several sites where earth retaining structures were in place
due mainly to soil liquefaction (Yanev [6] and Ellingwood [12]). A dike
along the Natori River was contained by a concrete retaining wall.
A section of wall several hundred yards long moved about one foot toward
the river (Figure 1.31). Longitudinal fissures opened in the dike
behind the wall and in some concrete pavement along part of the dike.
The dike also settled as much as one foot. The site, which is at the
mouth of the river, is underlain by at least 65 feet of sand.

In the port of Ishinomaki, a fine-sand fill liquefied, causing
severe damage to anchored sheet-pile bulkheads. The fill material had
been dredged from the seafloor and placed hydraulically with no compac-
tion. It was placed next to old beach deposits, and the boundary of the
liquefaction damage followed the contact very closely; the beach
deposits were not involved in the liquefaction.

In addition, there were reports of cracking and settlements of
bridge abutments. A comparison was made between the Japanese and
American criteria for bridge design under earthquake conditions.
According to the 1971 Japan Road Association (JRA) bridge design code a
provision is made for the inclusion of a design force for lateral
seismic earth pressure, whereas the 1977 American Association of State
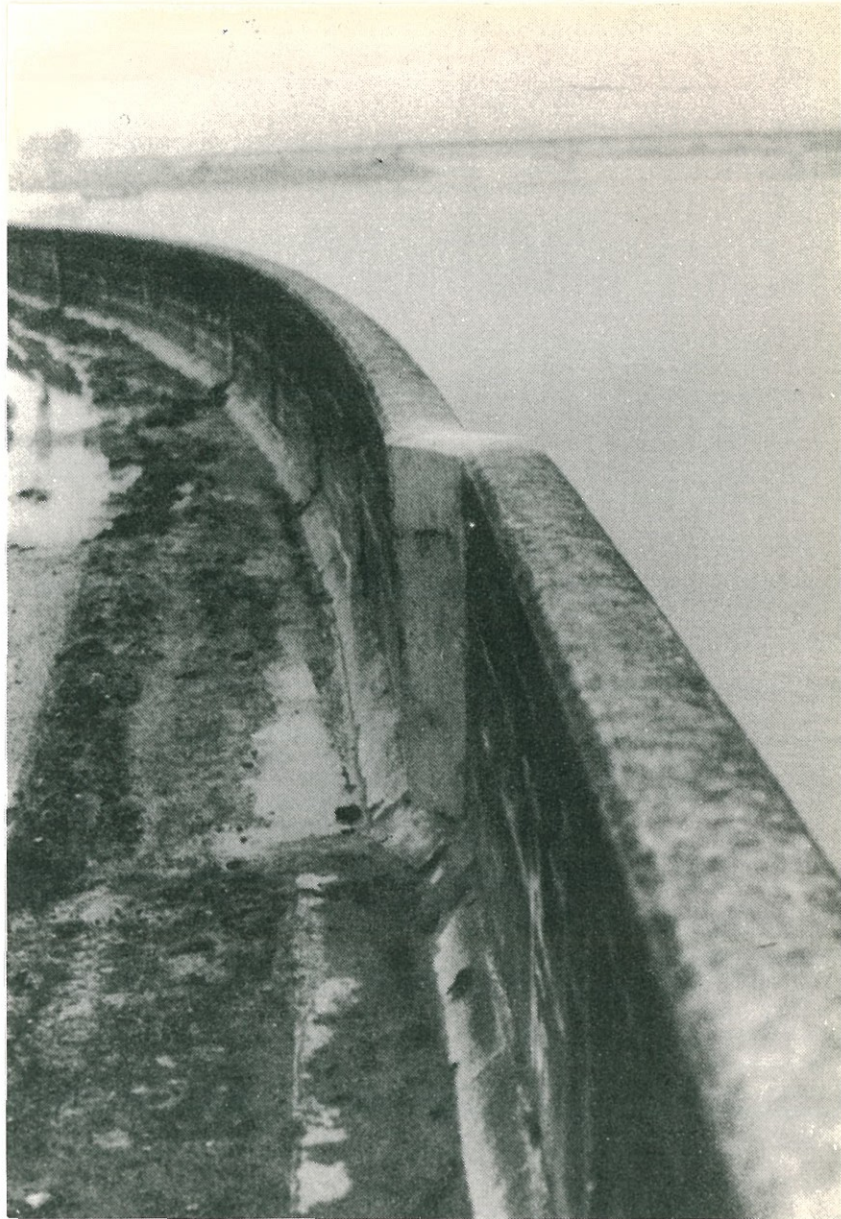
FIGURE 1.31 - REPAIRED PORTION OF DIKE, NATORI RIVER - FROM (12)

Highway and Transportation Officials (AASHTO) criteria, which is an adaptation of the criteria developed by the California Department of Transportation in 1973, does not. From the earthquake damage descriptions above, it seems clear that even the seismic design criteria for earth retaining structures are inadequate. No country, whether wealthy or poor, where there is seismic activity seems to be immune from this type of damage.

CHAPTER II

CENTRIFUGE MODEL TESTING

In recent years, the centrifuge has become a more accepted and useful tool in the modelling of soil mechanics problems. Most soil properties are generally dependent on continuum stresses which are generally gravity-induced. Thus, it is very difficult and inconvenient, if not impossible, to find a model material which will exhibit correctly scaled properties if a test is to be performed at the same gravitational acceleration as the prototype. It would be convenient to use prototype material, but as demonstrated in Chapter I, it would obviously not behave in an appropriate manner at the reduced confining stresses in the model. In such a model, in order to develop the same stresses as in the prototype, it is necessary to increase the gravitational acceleration by the lineal scale factor. Thus, if a 1/50th scale model, made of the same material as the prototype is subjected to a gravitational acceleration 50 times that of the prototype, the confining stresses, and thus the properties and behavior of the model are the same as in the prototype (an analytical description of scaling relations is found in Appendix A). A centrifuge is a machine that can provide model gravity as desired.

It must be realized that the model structure must be properly scaled to provide accurate results. The ratio of the accelerations in model and prototype structures is inversely proportional to the ratio of their lineal dimensions. If the ratio of linear prototype dimensions to

those of the centrifuge model is N, then the ratio of area is N^2 and

volumes N^3. The scaling relations indicate that the forces in the

prototype are N^2 times those in the model and moments N^3 times while the

stresses (force per unit area) are unchanged. Deformation in the

prototype is N times larger than in the model, but strains (deformation

per unit length) are the same. Thus, the pressure of the same material

in both prototype and model results in identical stresses and strains at

homologous points.

In the experiments, it was necessary to model the reinforced

concrete walls by means of aluminum due to the difficulty in properly

scaling down both the reinforcement bars and concrete to a small scale

(see Chapter 3). Therefore, the model wall was designed to a similar

stiffness per unit width, EI with the stiffness in the prototype being

N^3 times that in the model.

Where dynamic problems are involved, it turns out that the

prototype time scale is N times that in the model. As a consequence,

model frequencies are higher by the factor N. Table 2.1 lists the rela-

tions between prototype and model (centrifuge) parameters when the

centrifuge is employed [15,46].

In the experiments described here, N was chosen to be 50, so that

the model was 1/50 of the prototype linear dimension, and the model

acceleration employed was 50 times normal terrestrial gravity. It was

also considered desirable to subject the retaining wall and associated

TABLE 2.1

Scaling Relations

Parameter	Full Scale (Prototype)	Centrifugal Model at Ng's
Acceleration	1	N
Velocity	1	1
Linear Dimension	1	$1/N$
Area	1	$1/N^2$
Volume	1	$1/N^3$
Stress	1	1
Strain	1	1
Force	1	$1/N^2$
Mass	1	$1/N^3$
Mass Density	1	1
Weight Density (Unit Weight)	1	N
Time (dynamic)	1	$1/N$
Time (consolidation)	1	$1/N^2$
Frequency	1	N
Unit stiffness, EI	1	$1/N^3$

soil mass as a passive system to essentially random, earthquake-like excitations at levels equivalent to strong earthquake motions.

As previously described by Scott [52], the attractiveness of the centrifugal method is that the stresses and strains in the model are identical to those in the prototype so that it avoids problems associated with testing, at earth gravity, small soil models involving

material with strongly nonlinear behavior. The disadvantages are
associated with performing the tests on models which are rotating at
rates of 100 to 500 rpm in a centrifuge. Power and signals have to be
passed in and out through electric and hydraulic sliprings. There are
problems associated with the addition of electrical noise in recording
transducer output. The noise comes from ambient sources, the electric
motor driving the centrifuge, as well as mundane sources such as local
radio stations. Most noise can be effectively taken care of by proper
amplification and filtering of output signals as well as numerical
smoothing of the digitized data.

In initiating a program of centrifuge testing several questions
must be asked concerning the proof or the accuracy of the technique.
How well does a model test predict a prototype behavior? Do the scaling
relations tell the whole story? In addition, particularly when models
of particularly small dimensions such as retaining walls are considered
for testing, there is a problem in deciding at what soil grain scale the
applicability of continuum constitutive laws to both model and prototype
soils breaks down. For very fine grained soils, such as clays, there
will be many particles per unit width in both model and prototype
retaining wall; on the other hand, in a coarse sand, with grains one
twentieth of an inch or so in diameter, there will be relatively few
grains per model retaining wall unit width. It is likely that gravity
scaling will apply to the constitutive laws, but not to the grain dimen-
sions in the first example. In the second example, it seems possible
that the stress-strain relations of model and prototype may not be the

relevant factors, but that the individual grains in the model represent the behavior of boulders in the prototype. Thus, a model retaining wall in coarse sand may not represent the behavior of a prototype retaining wall in the same coarse sand, but that of a retaining wall with a backfill composed of boulders.

The use of the centrifuge in geomechanics dates back to the early 1930's when Bucky [4] first used one in the study of some simple mining problems. The use of a soil mechanics centrifuge was also reported in the Soviet Union around the same time [52]. The use of the centrifuge technique, however, has not been extensively practiced since then, although in the past 15 or 20 years it has been gaining in popularity.

At present, a number of centrifuges have been built and used for soil testing. There are three in the United Kingdom, two at Cambridge and one at Manchester, with radii up to 16 ft and acceleration capabilities up to 200g. It has been reported that "several dozen" centrifuges for soil testing purposes are in use in the Soviet Union [41]. In addition, centrifuges are currently used for geotechnical research in Sweden, Denmark, France, and Japan. Surprisingly, in the United States, where the technique originated, there are only a handful of small centrifuges currently in use. There is one at Princeton, one at Colorado, and one is being developed at the Ames Research Center by the University of California at Davis, in addition to the one at Caltech. The reasons for their limited usage have not been determined.

A compilation of references on centrifugal testing, worldwide, extends to more than 150 papers and a number of books.

With the number of centrifuges built and operational, and the number of tests performed, it might well be thought that the questions above would have been satisfactorily answered by this time; that many comparisons would have been made between models and prototypes. Study of the accessible literature does not show this to be the case in the quantitative sense, although a fair number of studies show qualitatively similar behavior and mechanisms. The particular type of testing involved in this case, the dynamic centrifuge testing of flexible retaining walls, however, has, as far as known, no precedent.

CHAPTER III

EQUIPMENT AND INSTRUMENTATION

3.1. The Centrifuge

The centrifuge (Figure 3.1) used is a Model A1030 Genisco G-accelerator", which consists of an 80-inch diameter aluminum-alloy arm which rotates in the horizontal plane and is rated at 10,000 g-pounds payload capacity. At each end of the arm is located an 18 X 22 inch magnesium mounting frame (Figure 3.2) capable of carrying a 200-pound payload to 50g or 60 pounds to 175g. The acceleration range at the approximately 40-inch radius of the basket is from 1 to 175g.

The machine is driven by means of a Sabina Electric and Engineering Type RG 2600 Single phase Full Wave Regenerative Static D.C. Drive with a 5 HP, 1725 rpm, 230v, 3-phase, constant torque, double-ended electric drive motor. For accurate determination of the rotational speed, there is located on the main drive shaft a 600 tooth gear wheel, which via a magnetic pickoff produces 600 pulses per revolution. The pulses are read by an electronic counter which converts them to an LED display of RPM accurate to 0.1 rpm. The drift and wow of the system at any given setting is 0.05%. The acceleration arm is housed in an extruded aluminum enclosure, with all the controls and instrumentation, in the interests of safety, located remotely.

CENTRIFUGE
SIDE VIEW

HYDRAULIC SLIPRINGS

CLOSED CIRCUIT TV CAMERA

BASKET ASSEMBLY

HYDRAULIC CYLINDER

ARM

DRIVE SHAFT

TRANSMISSION ASSEMBLY

MAGNETIC PICKUP & GEAR

ELECTRICAL SLIPRINGS

MOTOR

SPEED CONTROL
ARM

1 FT.
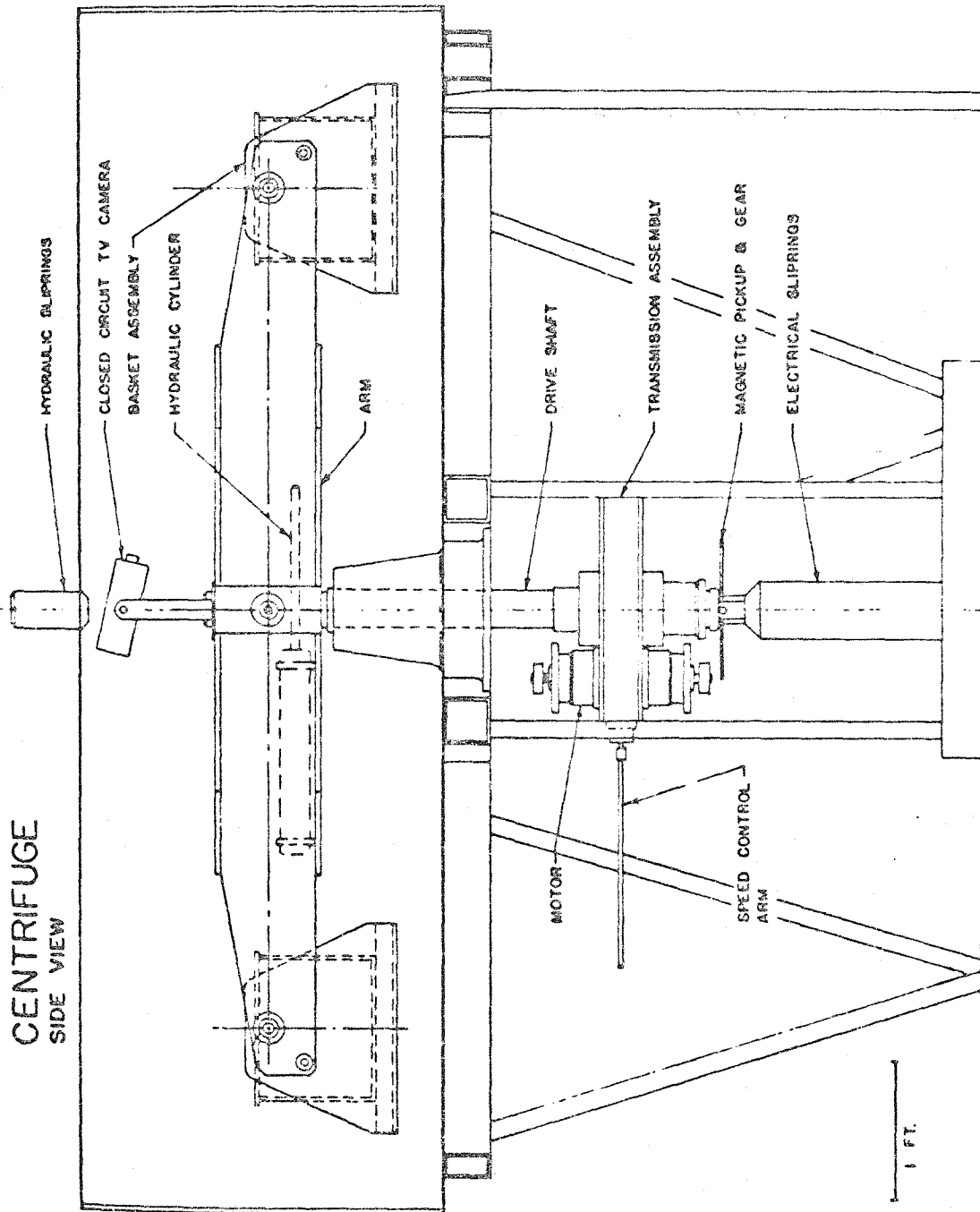
FIGURE 3.1 — SIDE VIEW OF CALTECH CENTRIFUGE AT REST
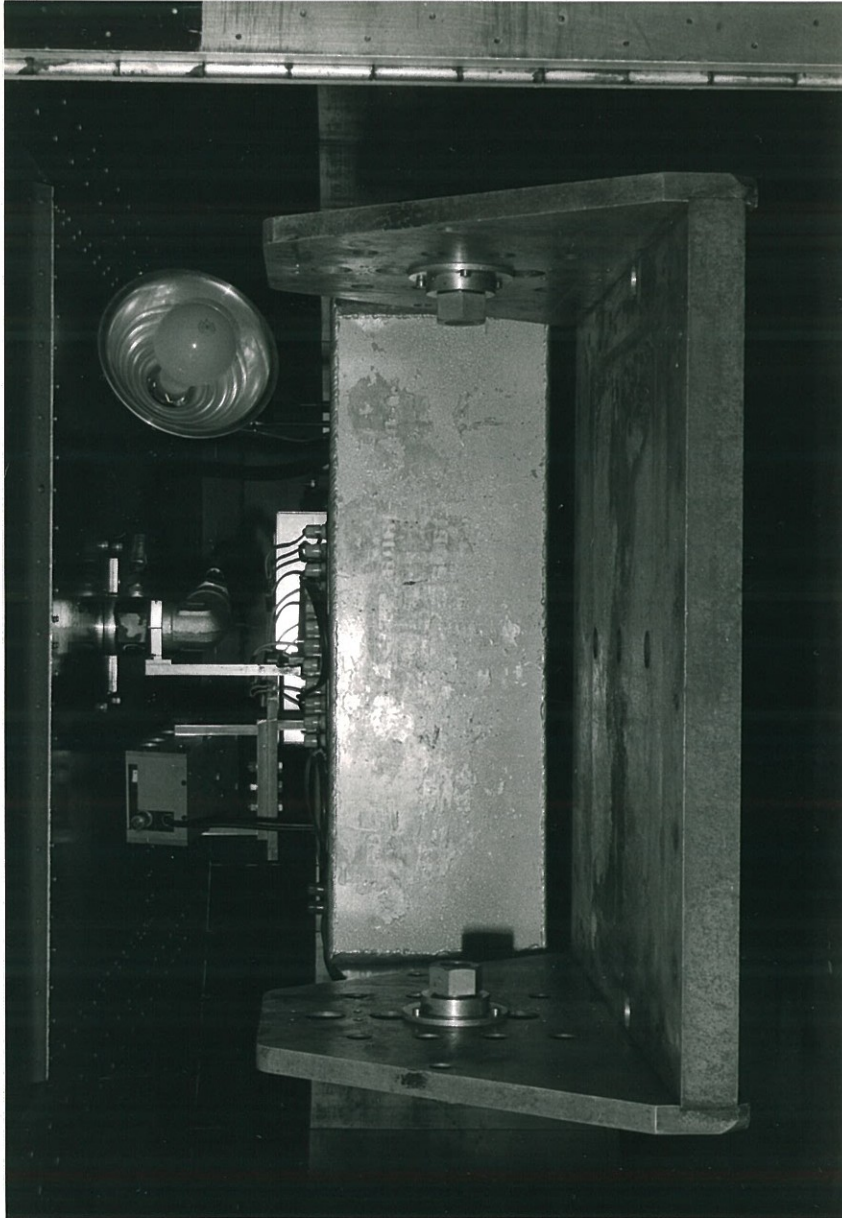
FIGURE 3.2 – CENTRIFUGE FRAME

Electrical power and signals to and from the rotating arm or frame are conducted through 44 sliprings of various capacities in the 10 to 30 amp range. Hydraulic pressure is externally generated with a Haskell Engineering and Supply Co. Model DEN.PR51 pump unit with a line capacity of 3000 psi and is transmitted through either two or four lines by means of rotary unions (hydraulic sliprings). Operations on the centrifuge can be observed by means of a television camera mounted on the arm close to the axis; its signal is conveyed either through the rings mentioned above or through coaxial cable and related, separate sliprings to a monitor TV in the instrumentation room.

3.2. The "Earthquake Generating" Mechanism

As mentioned previously the centrifuge is rated at 10,000 g-pounds payload capacity. The load ("payload") of model structure, soil, and containment that it can sustain is limited to 200 lbs (taken up to 50g). Consequently, the need for a method of creating an earthquake-like motion in the centrifuge without taking up a substantial amount of the payload was imperative and was developed with the aid of John Lee.

The "earthquake-generating" mechanism (Figures 3.3, 3.4) consists of a 14.6" X 11.6"X 10" reinforced aluminum container mounted on a bed of ball bearings which lie in horizontal parallel grooves in a steel plate attached to the swinging magnesium centrifuge frame. The bearings were separated with a perforated teflon sheet which allowed equal spacing between them and thus an even pressure distribution throughout (Figure 3.5). At one end, between the bucket and the frame is a spring
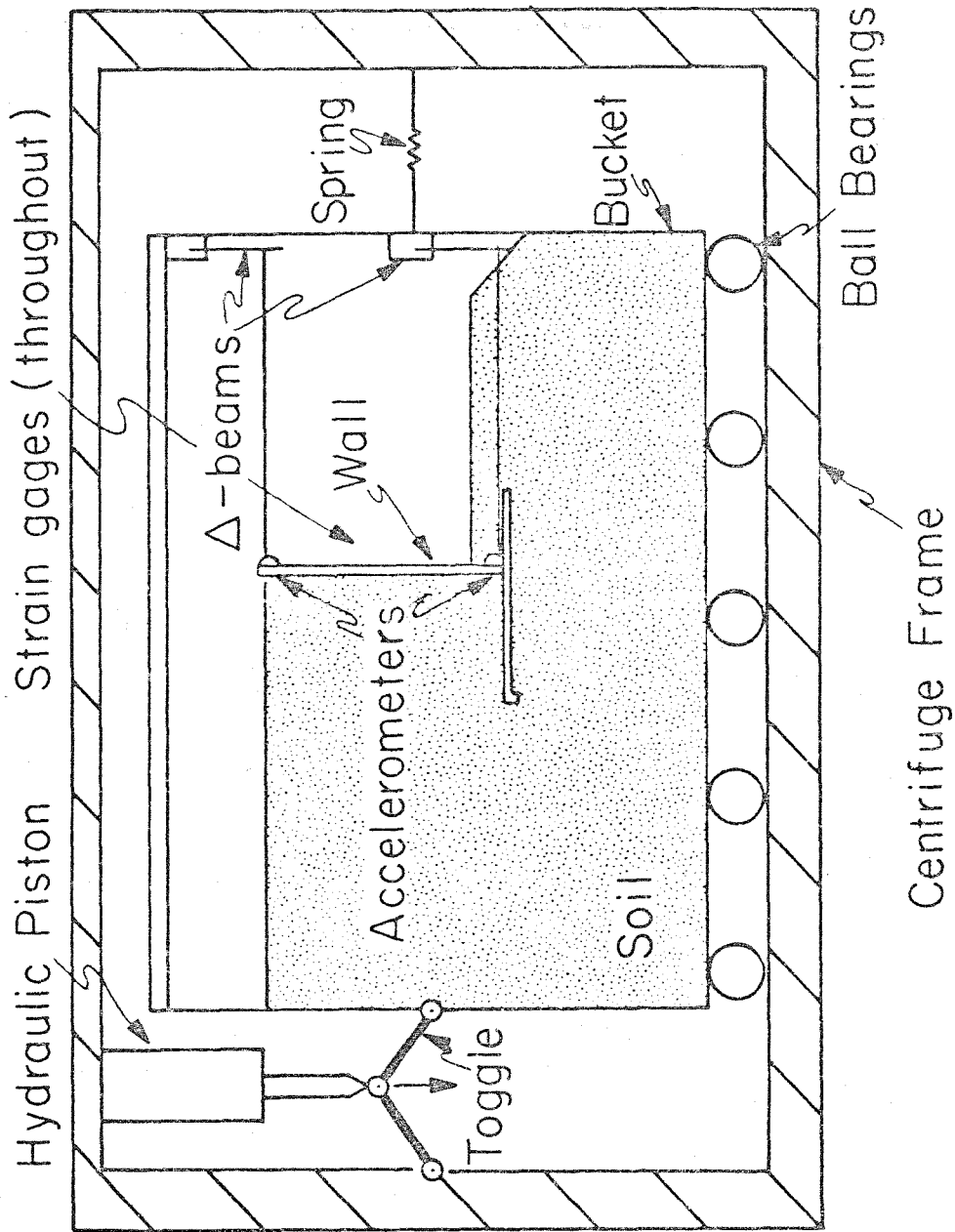
FIGURE 3.3 – SCHEMATIC OF EXPERIMENT
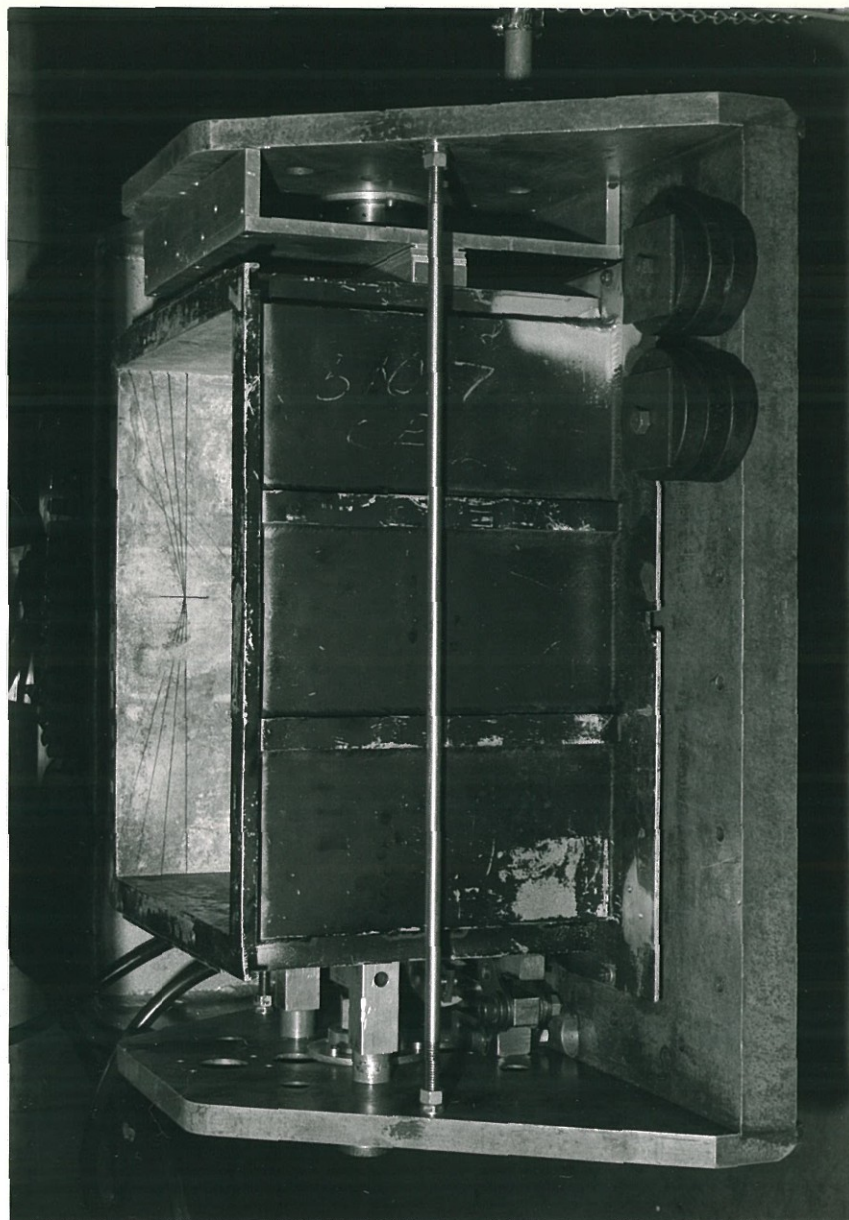
FIGURE 3.4 — EARTHQUAKE GENERATING MECHANISM
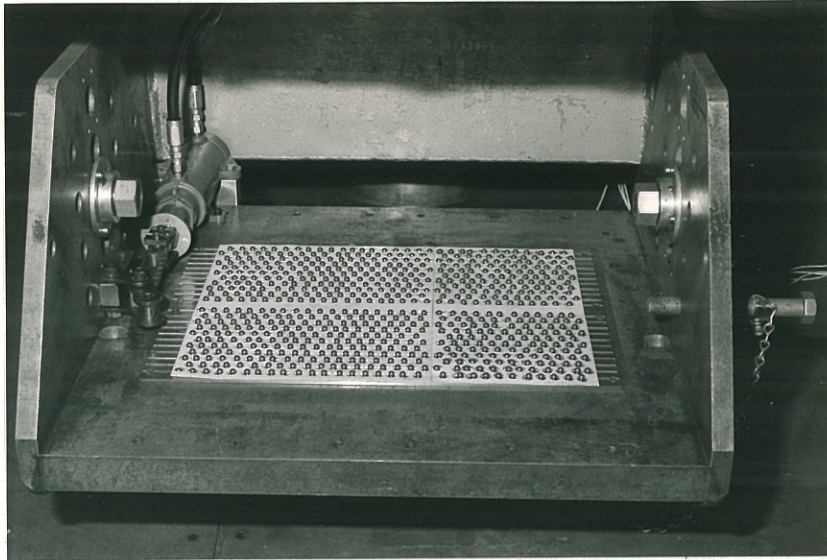
FIGURE 3.5 – BALL BEARINGS SEPARATED BY TEFLON SHEET
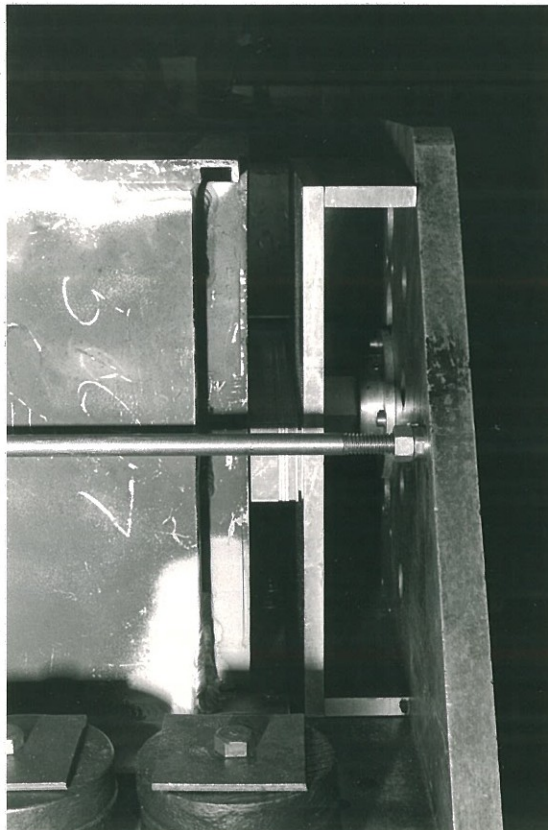
FIGURE 3.6 – REACTION SPRING

(spring constant = 75 kips/in) (Figure 3.6). At the other end is a toggle mechanism connected to a hydraulic piston (Figures 3.7,3.8). Under control the piston displaces the center of the toggle, spreading the ends, and thus forcing the bucket to move, deforming the spring at the other end. When the toggle goes over center, it snaps through, driven by the sudden energy release of the spring, and the soil container snaps back until it hits, stops and rebounds. This happens a number of times for one model "earthquake" event. The bucket thus moves back and forth for a couple of tenths of a second in a relatively random motion which resembles that of a short but intense earthquake. The comparison of the model earthquakes with that of one component of a record of the 1966 Parkfield, California earthquake is done in Section 5.2. Because of the simplicity of the "earthquake generating" mechanism, the motion attained resembles that which would occur near a short fault rupture. The production of prolonged earthquake motions typical of sites at intermediate distances from a long fault rupture (a "great" earthquake) would require another (probably more complicated and thus heavier) mechanism.

3.3. Model Retaining Walls

Ideally, a model retaining wall made of (properly scaled) reinforced concrete similar to one described in the design example of Section 12.7 of Wang and Salmon's Reinforced Concrete Design [64] would be desirable for centrifuge testing, but as can be seen from the design sketch (Figure 3.9) of a prototype, it would be very difficult to scale
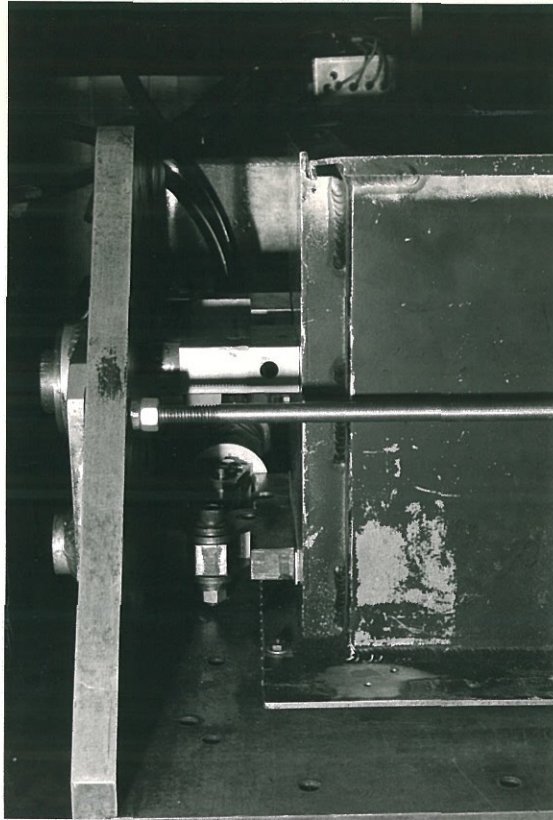
FIGURE 3.7 — PISTON, TOGGLE, AND BUMPER (FRONT VIEW)
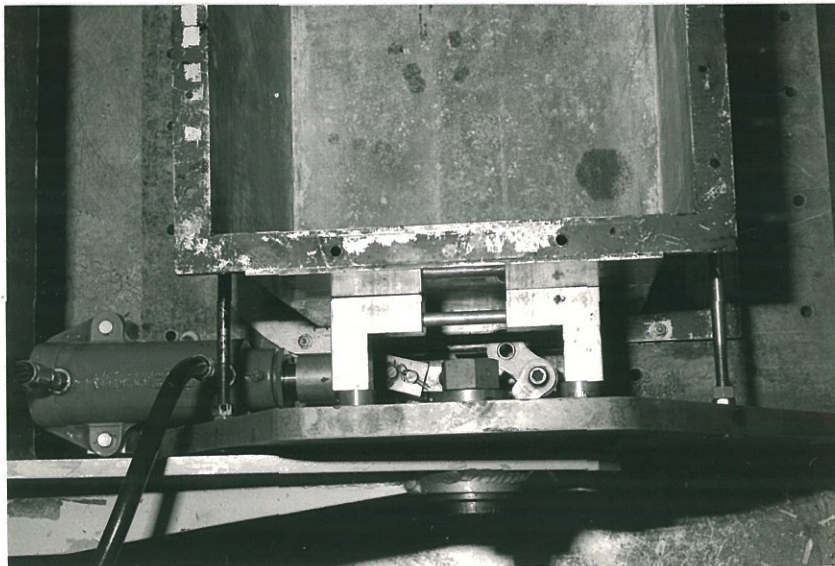
FIGURE 3.8 — PISTON, TOGGLE, AND BUMPER (TOP VIEW)
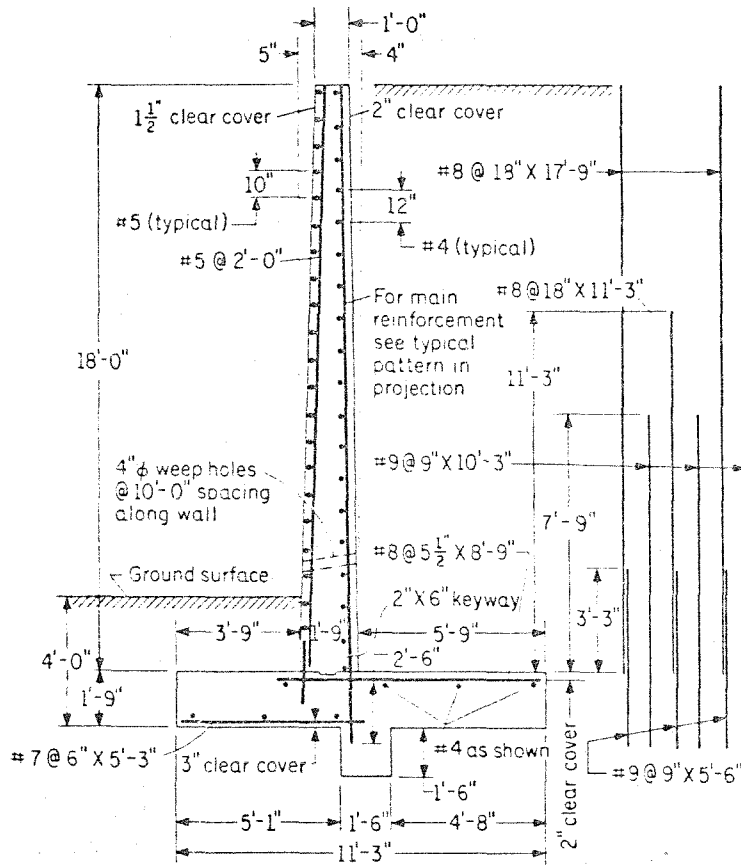
Design sketch for cantilever retaining wall.

FIGURE 3.9 — FROM (64)

down all the components of the wall to 1/50th the size shown. Because
of the ease of modelling, it was decided to design a retaining wall made
of aluminum instead, and then scale it down. The procedure is similar
to the procedure used in the design of a regular reinforced concrete
cantilever retaining wall.

3.3.1. Design of the Retaining Walls

It is required to design a prototype, aluminum cantilever retain-
ing wall to support a backfill of earth 16 ft high above the final level
of earth at the toe of the wall. The backfill is to be level. A
lateral earthquake acceleration of 0.25g is expected for design purposes
(in actuality, it doesn't occur though). The following data is given
for design:

soil density γ = 92 pcf   (Nevada 120 sand @ medium density)

Elastic Strength of 6061-T6 Aluminum f_A = 48,000 psi

Elastic Modulus E_A = 10×10^6 psi

First of all, it is necessary for the wall-soil system to be in a
state of equilibrium. A Mononobe-Okabe analysis (see Section 1.1) with
k_H = 0.25 will be used.

The Mononobe-Okabe parameters are:

$$\theta = \tan^{-1}(0.25) = 14^o \qquad \delta = 0^o$$

$$\gamma = 0.092 kcf \qquad\qquad i = 0^o$$

$$\phi = 35^o \qquad\qquad\qquad \beta = 0^o$$

Therefore:

$$K_{AE} = 0.43$$

and the total force P_{AE} is thus

$$P_{AE} = 1/2\gamma h^2(1-k_v)K_{AE} \qquad (3.1)$$

or

$$P_{AE} = (1/2)(0.092)(18.3)^2(0.43) = 6.6\text{kips/ft.}$$

This is the total lateral force acting on the wall. As recommended by Seed and Whitman [55], the force increment on the wall, ΔP_{AE}, due to the earthquake load should be assumed to act 0.6 h or so above the base. Thus, it is necessary to find the static force P_A and place the forces on the wall as shown in Figure 3.10.

From the Rankine static lateral earth pressure theory P_A is given by:

$$P_A = 1/2\gamma h^2 K_A \qquad (3.2)$$

where:

$$K_A = \frac{1-\sin\phi}{1+\sin\phi} \qquad (3.3)$$

For the soil involved $K_A = 0.27$ so:

$$P_A = (1/2)(0.092)(18.3)^2(0.27) = 4.2\text{kips/ft.}$$
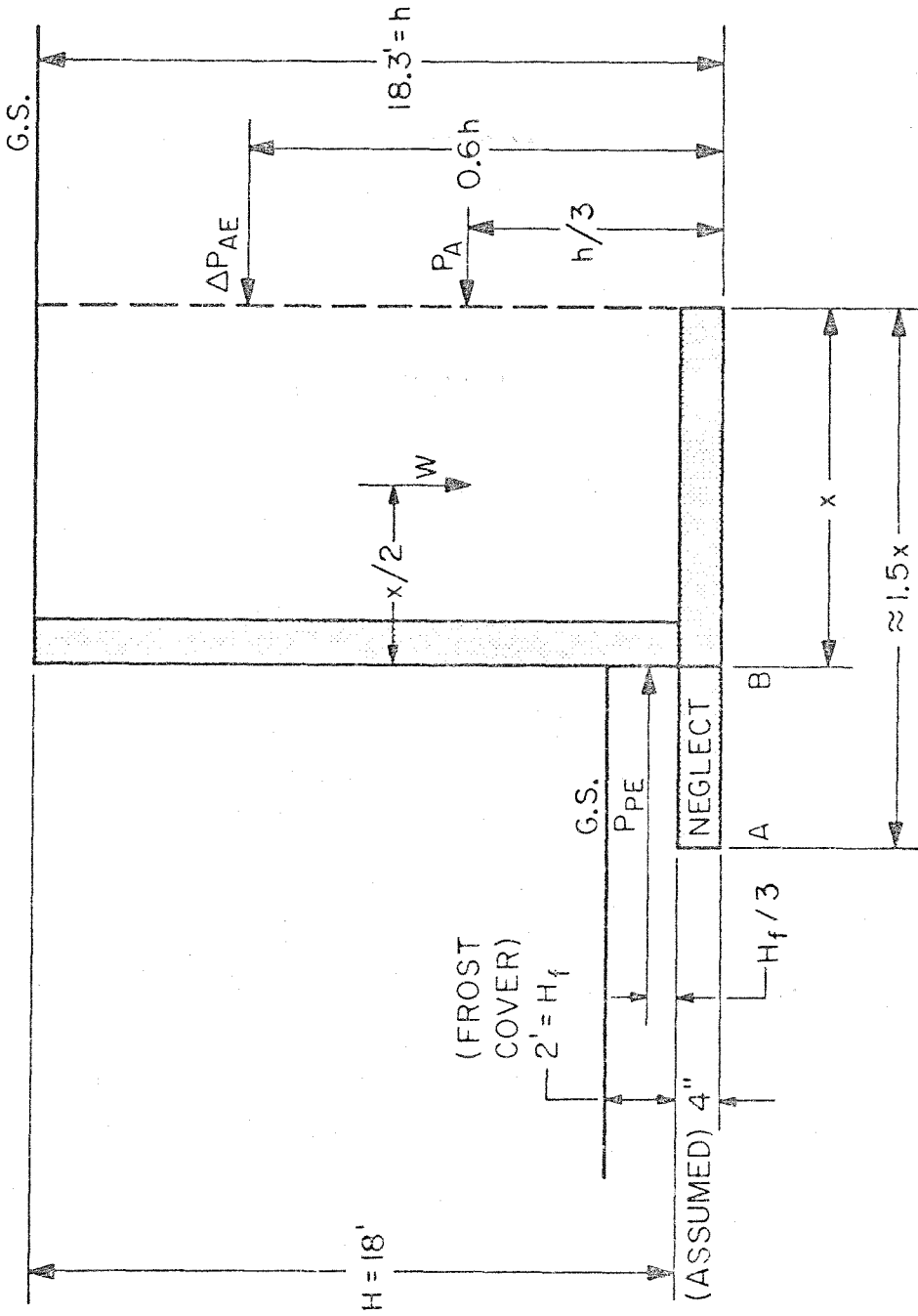
FIGURE 3.10 – PRELIMINARY PROPORTIONING OF PROTOTYPE CANTILEVER RETAINING WALL

which acts at h/3 above the base of the wall. Thus:

$$\Delta P_{AE} \;=\; P_{AE} - P_A \;=\; 6.6-4.2 \;=\; 2.4 \text{kips/ft}$$

which acts at 0.6 h above the base.

The weight of the backfill, W, is:

$$W \;=\; \gamma H x \;=\; (0.092)(18)X \;=\; 1.6 x \text{kips/ft.}$$

Summing moments about point B. $\left(\sum M_b = 0 \right)$

$$\frac{Wx}{2} \;=\; \frac{P_A h}{3} + 0.6 \Delta P_{AE} h \;=\; h(1/3 P_A + 0.6\,\Delta P_{AE})$$

Consequently:

$$\frac{1.6 x^2}{2} \;=\; (18.3)[(1/3)(4.2) + (0.6)(2.4)]$$

Therefore:

$$x \;=\; \left[\frac{(2)(18.3)[(1/3)(4.2) + (0.6)(2.4)]}{1.6} \right]^{1/2} \;=\; 8.1 \text{ ft.}$$

The entire base length is recommended by Wang and Salmon to be approximately:

$$\text{Base length} \;\approx\; 1.5x \;=\; (1.5)(8.1) \;=\; 12.2 \text{ft.}$$

The base length was thus decided upon to be 15.25 feet long (3.66 in long in the 1/50 scale model) which gives about an extra 25% or so of

length for safety. A check must now be made for safety against over-turning. Recalling that the design base length is 15.25 ft, the design x (Figure 3.10) is thus 2/3 of this or 10.2 ft. (10 ft,2 in). Thus the weight W of the backfill is, from above:

$$W = 1.6x = (1.6)(10.2) = 16.3 \text{kips/ft.}$$

Taking moments about point A of the base and neglecting the weight of the wall, the resisting moment is:

$$M_R = (10.2)(16.3) = 166.3 \text{ ft k/ft}$$

The overturning moment is:

$$M_o = h(1/3P_A + 0.6\Delta P_{AE})$$

Thus:

$$M_o = (18.3)[(1/3)(4.2) + (0.6)(2.4)] = 52.0 \text{ft-k/ft}$$

Therefore, the factor of safety against overturning is:

$$F.S. = \frac{M_R}{M_o} = \frac{166.3}{52.0} = 3.2$$

which is greater than the traditional value of 2.0. This factor of safety does not even include the weight of the wall itself which would provide additional resistance to overturning.

The stem of the wall must now be designed to resist the bending moment M given by:

$$M = H(1/3P_A + 0.6\Delta P_{AE}) - 1/3P_{PE}H_f$$

where P_{PE} is the resultant of the passive force provided by the frost cover of depth H_f (Figure 3.10).

The coefficient of passive earth pressure, K_{PE}, for a Mononobe-Okabe analysis is given by

$$K_{PE} = \frac{\cos^2(\phi-\theta+\beta)}{\cos\theta\cos^2\beta\cos(\beta-\delta-\theta)\left(1 - \sqrt{\frac{\sin(\phi+\delta)\sin(\phi-\theta+i)}{\cos(\beta-\delta-\theta)\cos(\beta-i)}}\right)^2} \quad (3.4)$$

and:

$$P_{PE} = 1/2\gamma H_f^2(1-k_v)K_{PE} \quad (3.5)$$

Therefore:

$$K_{PE} = 3.18$$

Therefore:

$$P_{PE} = (1/2)(0.092)(4)(3.18) = 0.6 \text{ kips}$$

Thus:

$$M = 18[(1/3)(4.2) + (0.6)(2.4)] - (1/3)(0.6)(2) = 50.7 \text{ ft k/ft}$$

With a bending factor of safety of 1.7, the design moment is:

$$M_D = 86.1 \text{ ft k/ft}$$

The thickness of the stem is determined by the use of the bending formula for a beam:

$$\sigma = M/S \qquad (3.6)$$

Where:

σ = stress of the material

S = unit section modulus of cross section

For a rectangular cross section, the unit section modulus is:

$$S = \frac{d^2}{6} \qquad (3.7)$$

Where d is the thickness of the section. Taking the elastic strength of the aluminum f_A as σ, the stem thickness is determined:

$$d = \left(\frac{6M}{\sigma}\right)^{1/2} = \left(\frac{6M_o}{f_A}\right)^{1/2} = \left[\frac{(6)(86.1)}{48}\right]^{1/2} = 3.28 \text{ in.}$$

This corresponds to a thickness of 0.065 inches in the model wall, at 1/50 scale.

Two models of the 16 ft high cantilever retaining wall were built (Figure 3.11). They were made of two aluminum 6061-T6 plates dip-brazed together by Precision Dipbraze, Inc. of Van Nuys, CA. The base of both walls is made of 0.063 inch plate while the stems are 0.063 inches thick in wall No. 1 and 0.050 in wall No. 2. The thicknesses stated are standard aluminum plate sizes. The 0.063 inch thickness of wall No. 1 is approximately the correct size for the design conditions imposed with the appropriate safety factors. Wall No. 2 has no safety factor (F.S. = 1.0) at all. (Its prototype wall would have a moment capacity of 50.0 ft-k/ft versus the calculated acting moment of 52.0 ft-k/ft).
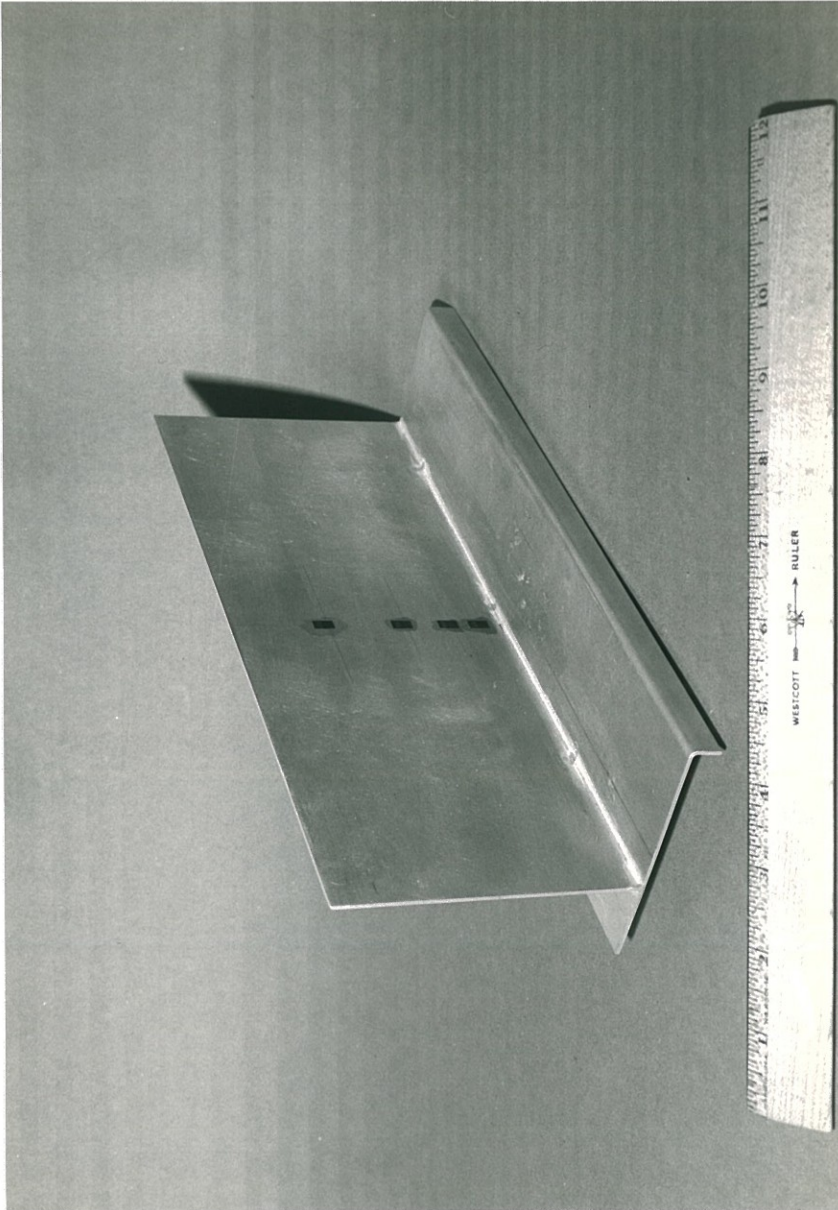
FIGURE 3.11 — MODEL RETAINING WALL

It should be noted that it is generally agreed upon in practice that the Mononabe-Okabe method gives a conservative design (i.e., calls for larger walls than "necessary"), and in most cases is not even used (nor is any other method) when a seismic design is in order.

3.3.2. Determination of Actual EI of Walls

In order to determine the true stiffness (EI) of the retaining walls, the Young's Modulus E of the aluminum used had to be measured. To do this a rectangular piece of the same 0.063" thick plate used to make the walls 6.555" long and 1.493" wide was cut. The piece was then clamped and held horizontal so that it formed a cantilever beam 5.026" long. Weights of 0, 0.220, 0.441, 0.661 and 0.772 lbs (0, 100, 200, 300, and 350 grams) were then hung from the free end. The end deflection was measured with a Federal dial gage accurate to 0.0001 inches. Recalling that the end (maximum) deflection y_{MAX} of a cantilever beam with an end point load is:

$$y_{MAX} = \frac{Pl^3}{3EI} \tag{3.8}$$

where P is the load, l the beam length, and I the bending moment of inertia it follows that:

$$E = \frac{Pl^3}{3Iy_{MAX}} \tag{3.9}$$

The average E then determined from the measurements was found to be 9.699×10^6 psi.

Recalling that the moment of inertia per unit width I of a rectangular cross section is $\frac{h^3}{12}$, where h is the section depth, for retaining wall No. 1 (RW1) the EI was determined as 202.1 lb in^2/in and for (RW2) as 101.0 lb in^2/in.

3.3.3. Determination of the Fundamental Frequency of the Wall-Soil System

The fundamental frequency of the wall-soil system was determined by an examination of the Fourier Amplitude Spectra of the accelerograms recorded at the top and bottom of the wall (in prototype scale) from tests 1CN0001,[*] 1CN0002, and 1CN1003 for RW1, and from test 2CN0011 for RW2 using the FORTRAN program IVMAIN described in Section 4.2. The accelerograms at the top of the wall indicate the output response of the system while those at the bottom are a measure of the input excitation to the system. Taking the corresponding pairs of Fourier Spectra for each test and finding where the ratio of output (top) to input (bottom) amplitude is a maximum provides an accurate determination of the system's natural frequencies.

Upon examination of the Fourier spectra (Figures 3.12 through 3.19), it was determined that the fundamental frequencies were 2.3 Hz for 1CN0001, 2.7 Hz for 1CN0002, and 2.7 Hz for 1CN1003. There was

---

[*] The following nomenclature was chosen for test numbering:

$$\text{Test } \underset{1}{\underline{a}} \ \underset{C}{\underline{b}} \ \underset{N}{\underline{c}} \ \underset{00}{\underline{d}} \ \underset{01}{\underline{e}}$$

a = wall number; b = type of wall; c = type of sand; d = backfill angle (in degrees); e = test number; C = cantilever; N = Nevada 120.

FOURIER AMPLITUDE SPECTRUM OF ACCELERATION
TEST 1CN0001   CENTRIFUGE EARTHQUAKE   11-12-80
1VX0100   80.001.0   SOIL MECHANICS CENTRIFUGE -- TOP OF WALL ACCELEROMETER   COMP HOR
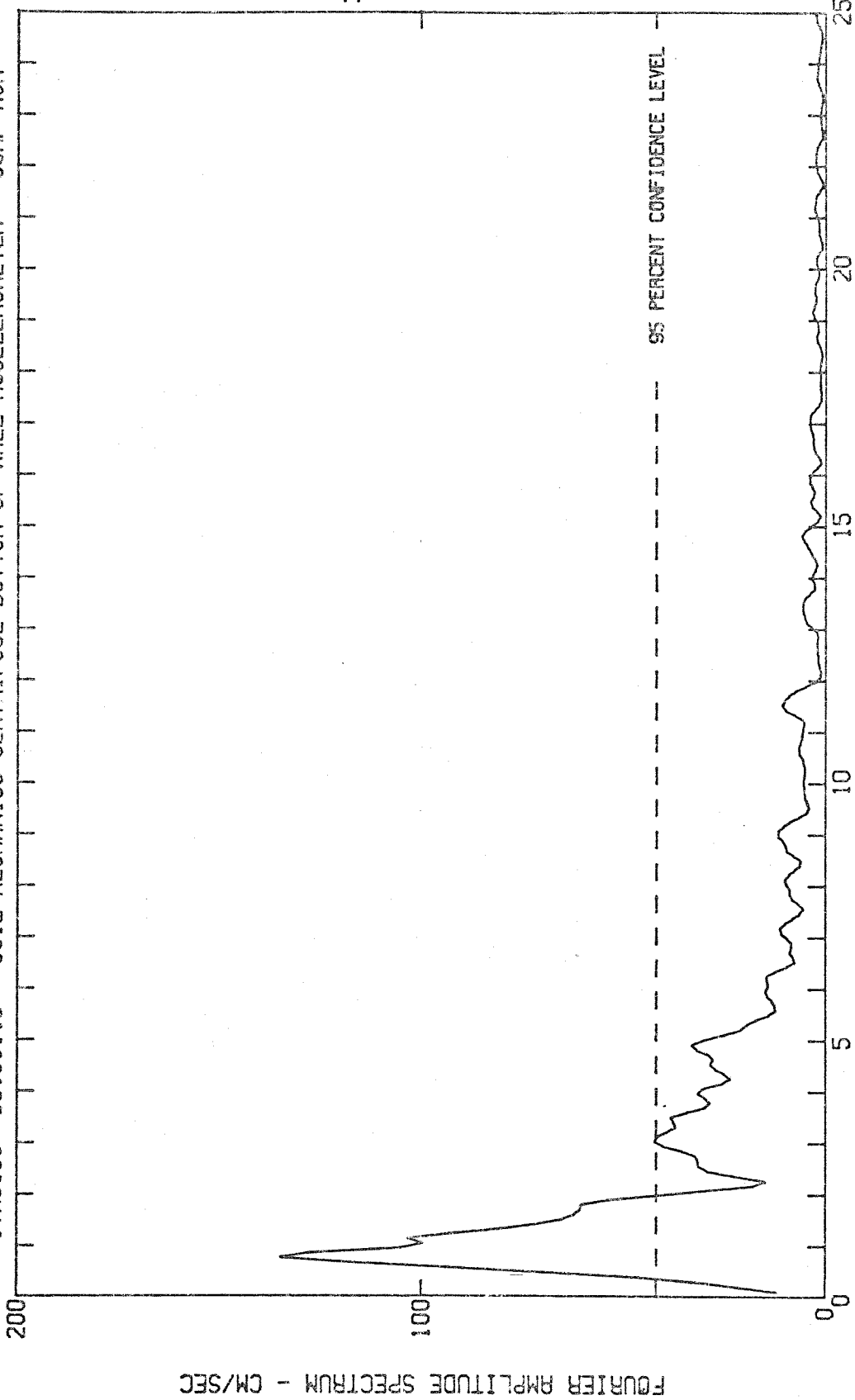
95 PERCENT CONFIDENCE LEVEL

FREQUENCY - CPS

FOURIER AMPLITUDE SPECTRUM - CM/SEC

FIGURE 3.12

FOURIER AMPLITUDE SPECTRUM OF ACCELERATION
TEST 1CN0001   CENTRIFUGE EARTHQUAKE   11-12-80
SOIL MECHANICS CENTRIFUGE-BOTTOM OF WALL ACCELEROMETER   COMP HOR

IVX0100   80.001.0

FOURIER AMPLITUDE SPECTRUM - CM/SEC

FREQUENCY - CPS

95 PERCENT CONFIDENCE LEVEL

FIGURE 3.13

FOURIER AMPLITUDE SPECTRUM OF ACCELERATION
TEST 1CN0002   CENTRIFUGE EARTHQUAKE   3- 4-81
IVX0200   81.002.0   SOIL MECHANICS CENTRIFUGE -- TOP OF WALL ACCELEROMETER   COMP HOR

FIGURE 3.14

FOURIER AMPLITUDE SPECTRUM OF ACCELERATION
TEST 1CN0002   CENTRIFUGE EARTHQUAKE   3- 4-81   COMP HOR
IVX0200   81.002.0   SOIL MECHANICS CENTRIFUGE-BOTTOM OF WALL ACCELEROMETER

FIGURE 3.15

FOURIER AMPLITUDE SPECTRUM OF ACCELERATION
TEST 1CN1003   CENTRIFUGE EARTHQUAKE   3- 9-81
IVX0300 81.003.0   SOIL MECHANICS CENTRIFUGE -- TOP OF WALL ACCELEROMETER   COMP HOR

95 PERCENT CONFIDENCE LEVEL

FREQUENCY - CPS

FOURIER AMPLITUDE SPECTRUM - CM/SEC
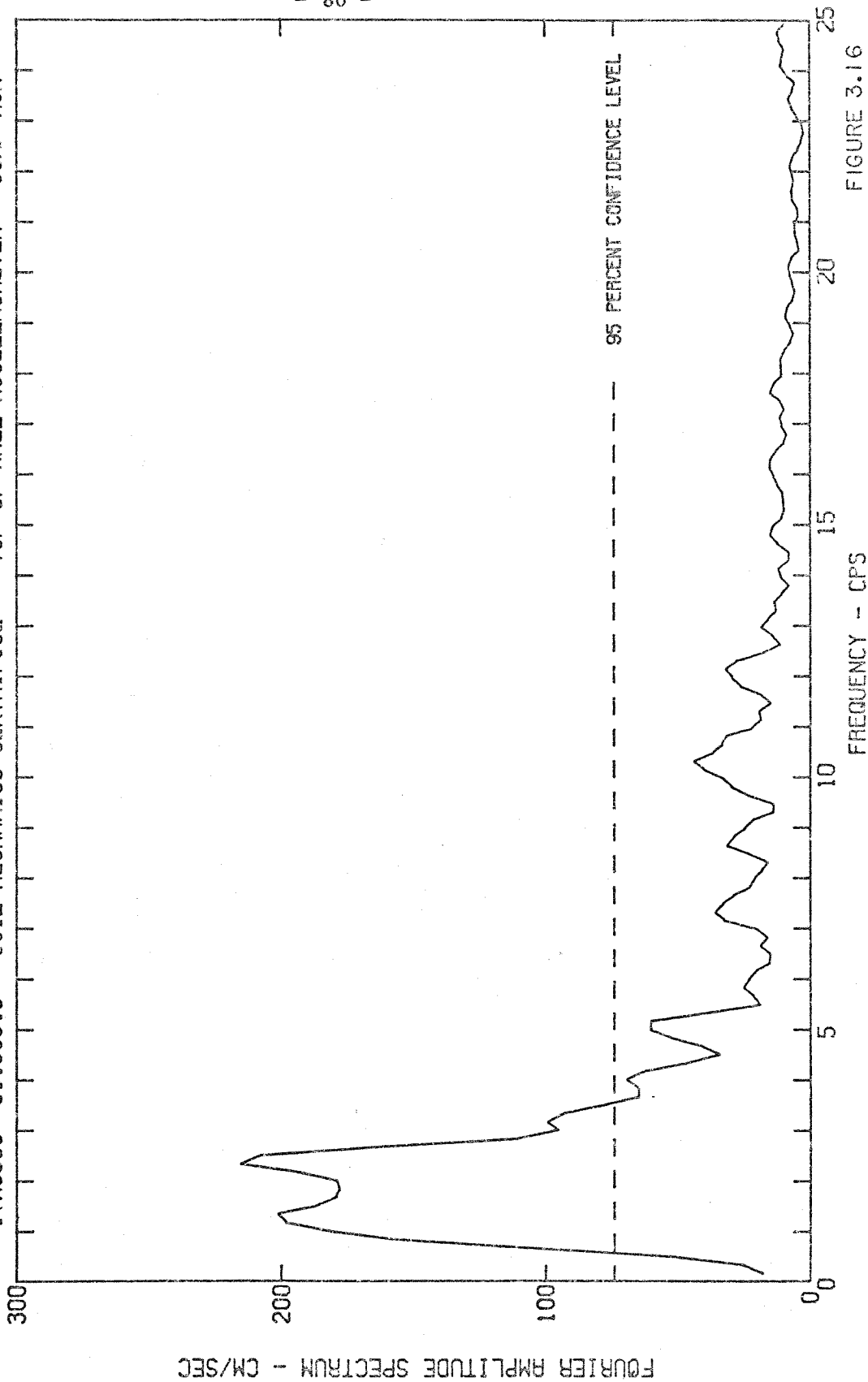
FIGURE 3.16

FOURIER AMPLITUDE SPECTRUM OF ACCELERATION
TEST ICN1003   CENTRIFUGE EARTHQUAKE   3- 9-81   COMP HOR

IVX0300   81.003.0   SOIL MECHANICS CENTRIFUGE-BOTTOM OF WALL ACCELEROMETER

95 PERCENT CONFIDENCE LEVEL

FREQUENCY - CPS

FOURIER AMPLITUDE SPECTRUM - CM/SEC
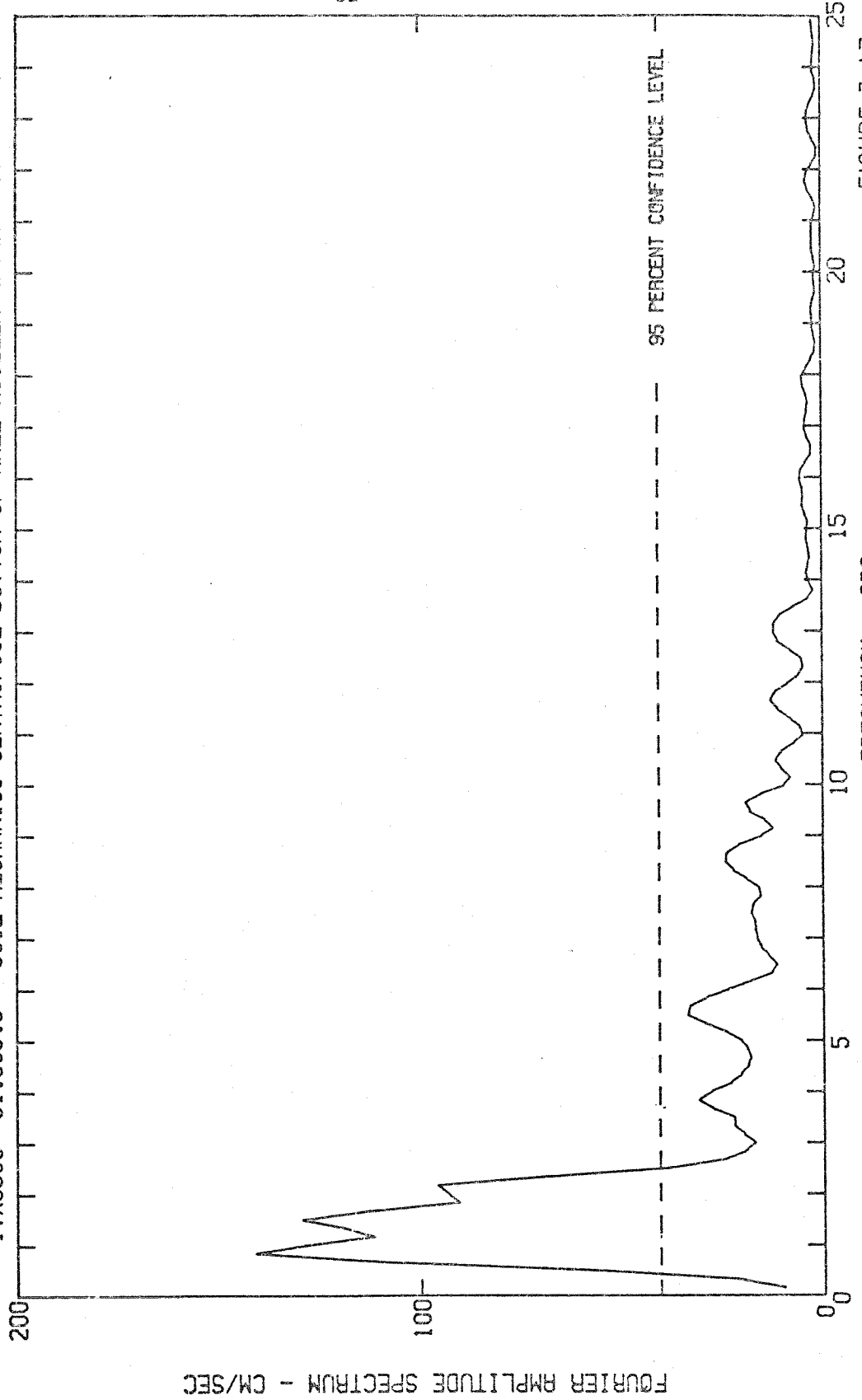
FIGURE 3.17

FOURIER AMPLITUDE SPECTRUM OF ACCELERATION
TEST 2CN0011   CENTRIFUGE EARTHQUAKE   2-25-82
IVX0100   82.011.0   SOIL MECHANICS CENTRIFUGE -- TOP OF WALL ACCELEROMETER   COMP HOR

95 PERCENT CONFIDENCE LEVEL

FOURIER AMPLITUDE SPECTRUM - CM/SEC

FREQUENCY - CPS
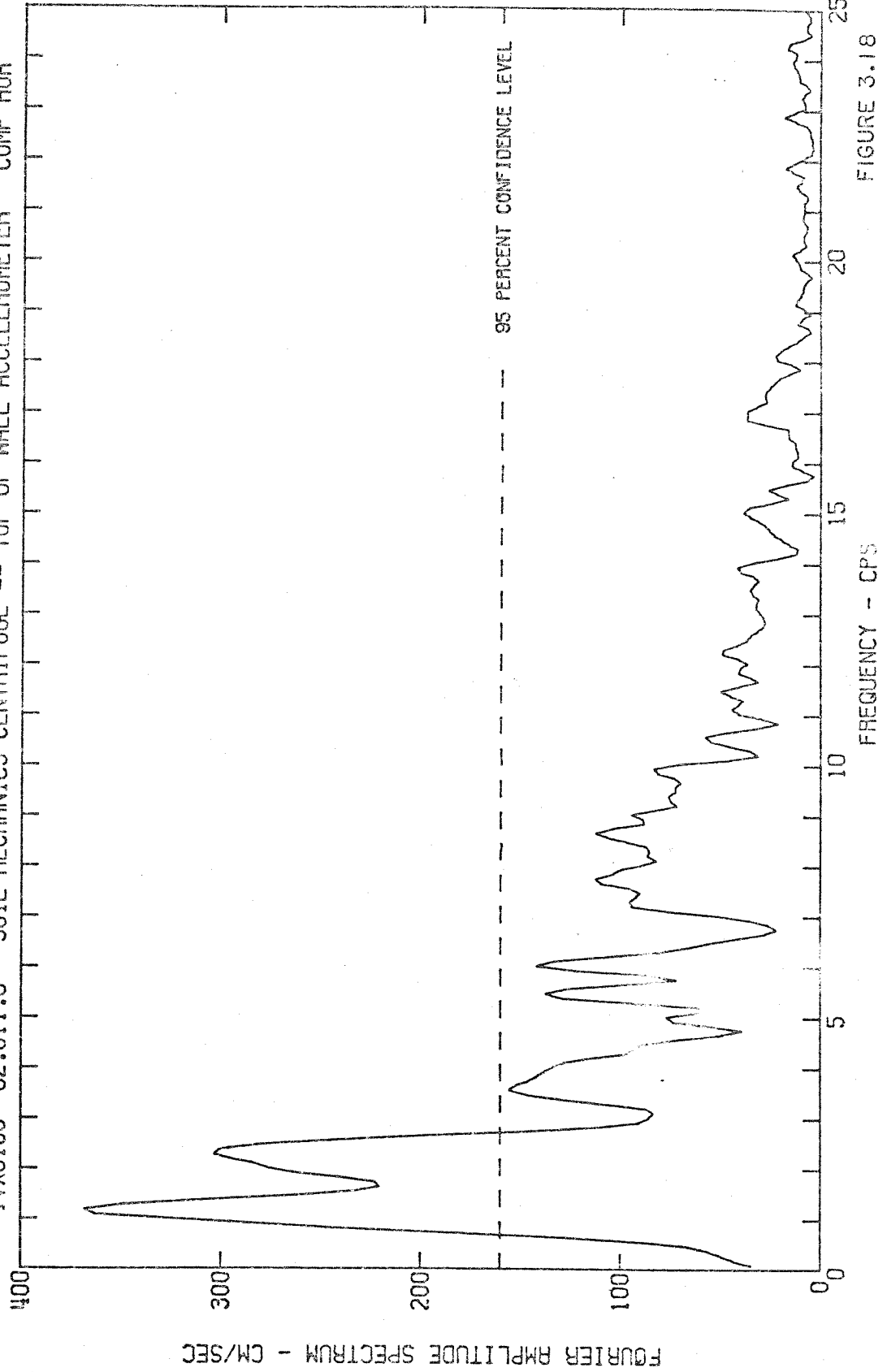
FIGURE 3.18

FOURIER AMPLITUDE SPECTRUM OF ACCELERATION
TEST 2CN0011   CENTRIFUGE EARTHQUAKE   2-25-82
IVX0100   82.011.0   SOIL MECHANICS CENTRIFUGE-BOTTOM OF WALL ACCELEROMETER   COMP HOR

95 PERCENT CONFIDENCE LEVEL

FREQUENCY - CPS

FOURIER AMPLITUDE SPECTRUM - CM/SEC
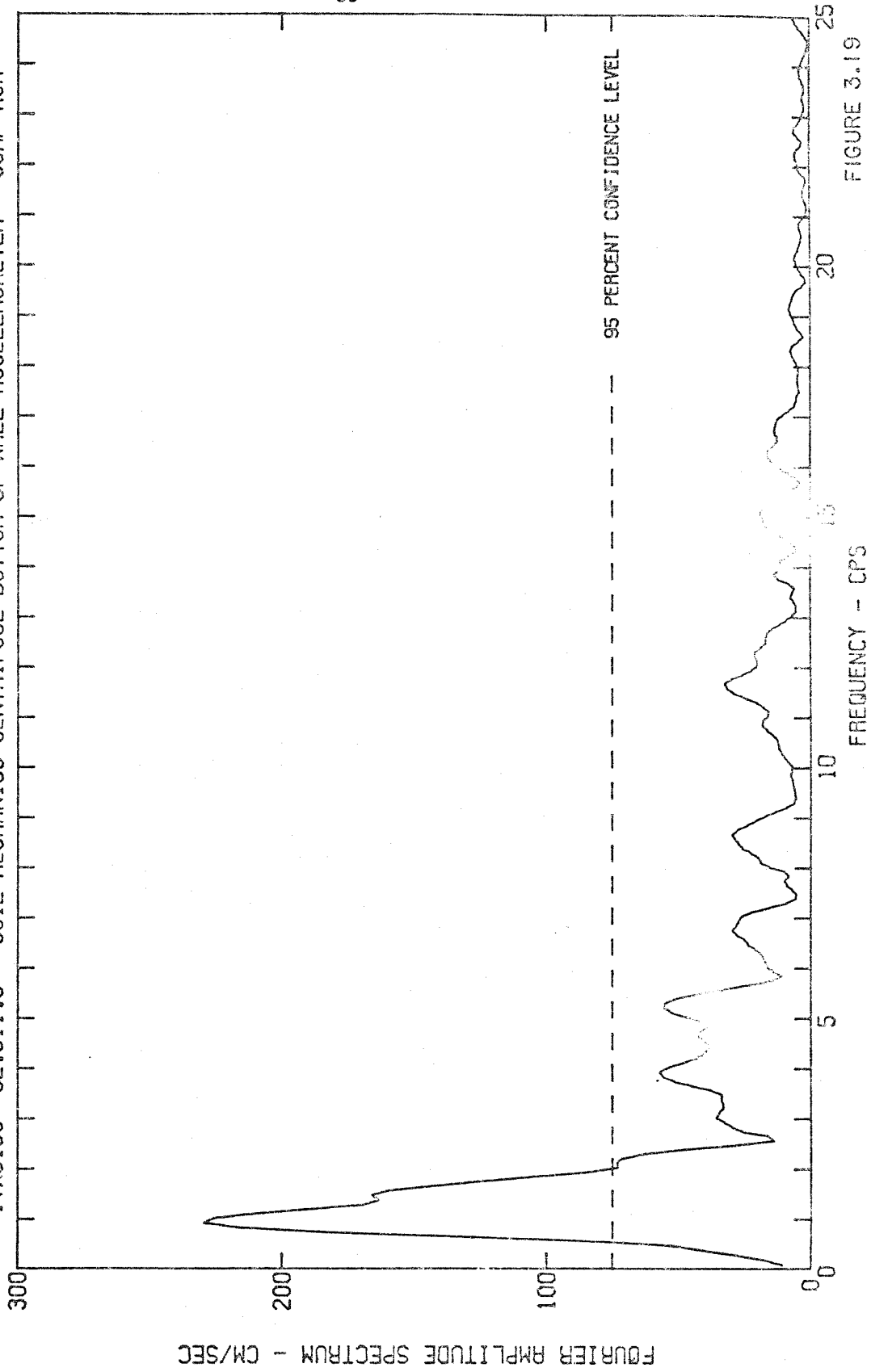
FIGURE 3.19

very little relative difference between the frequencies determined from these tests, leading to the conclusion that there is little sensitivity in the system with regard to backfill slope or soil density differences for RW1. The fundamental frequency of the tests where RW1 was used was then taken to be the average of these tests, 2.6 Hz (129 Hz model). Similarly from the spectra for 2CN0011, the fundamental frequency of RW2 was taken to be 2.5 Hz (123 Hz model). This is also very close to the frequencies of tests using RW1, so there is little variation of frequency with regard to wall stiffness as well.

From examination of the Fourier spectra it can also be seen that there is only a significant contribution to the response of the systems by only one frequency, the fundamental. This is confirmed upon examination of the displacement curves presented in Chapter 5.

As will be explained in section 5.1, the fundamental frequencies of the systems are used to create dimensionless time parameters since they are a characteristic of each system.

3.4. Soil

The type of soil used was Nevada 120 Silica. This sand is a uniformly-graded, fine grained soil. A grain size distribution is shown in Figure 3.20. The soil was dry in all of the tests. It has a density range of from about 85 pcf in its loosest state to 99 pcf in its most dense. For the tests the density ranged from 91 to 99 pcf. For the medium density soil, the angle of internal friction ϕ is about 35°.
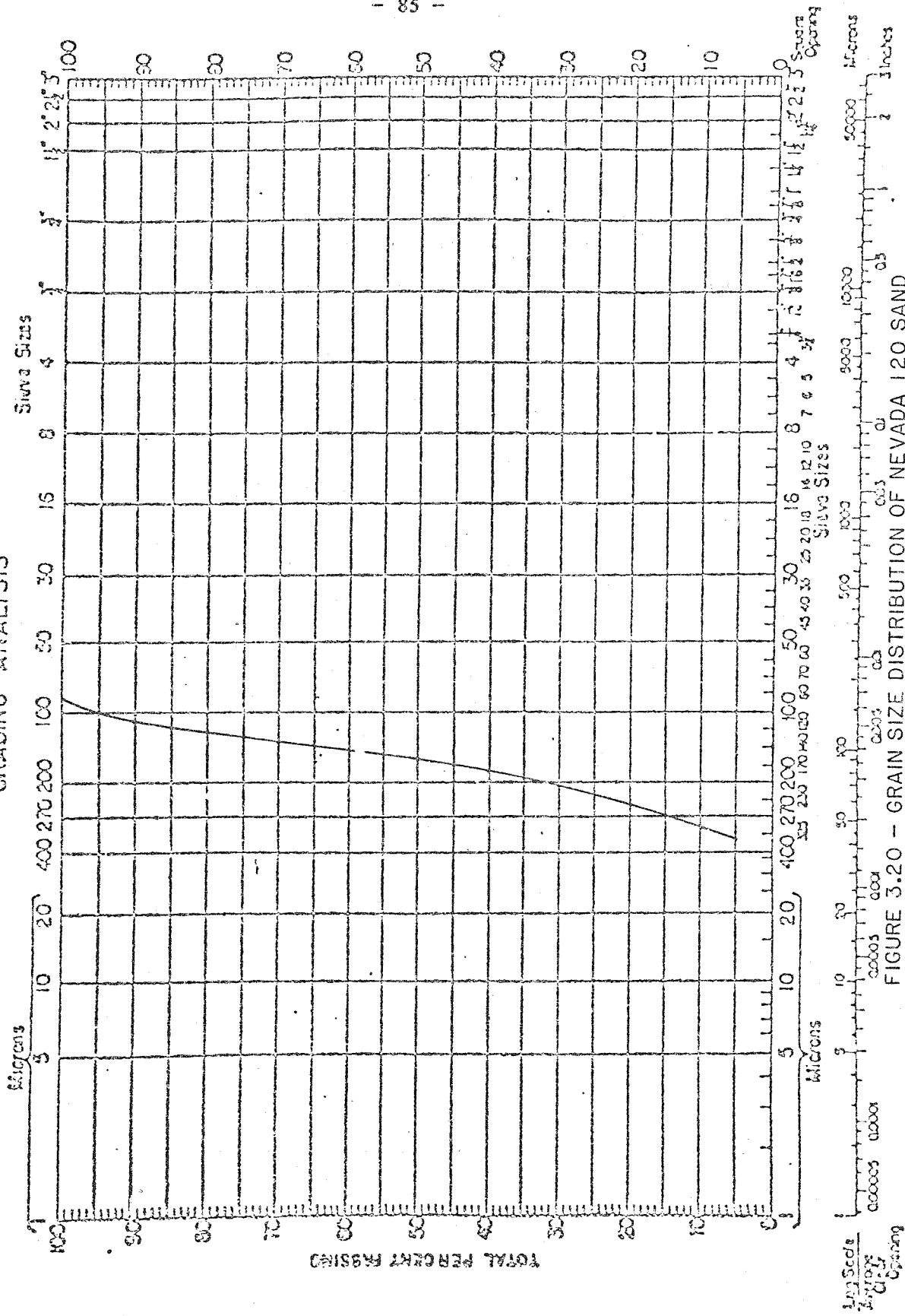
FIGURE 3.20 — GRAIN SIZE DISTRIBUTION OF NEVADA 120 SAND

The soil was chosen because of its fine grained size which is desirable when doing centrifuge work, as already mentioned in Chapter 2.

3.5. Instrumentation

A cross section of the retaining walls indicating the location of all the transducers which will be described below is shown in Figure 3.21.

3.5.1. Strain Gages

Moments on the retaining walls are measured directly by the use of strain gages which in reality measure the curvature, M/EI.

Retaining wall No. 1 (RW1) is instrumented with seven pairs of Micromeasurements Model CEA-13-062UW-350 strain gages located at distances 1.50", 2.25", 275", 3.15", 3.50", 3.75" and 4.00" from the top of the wall, and down the centerline, one strain gage of each pair on the front and one on the back at each location. Retaining wall No. 2 (RW2) is likewise instrumented with four pairs at distances from the top of 1.50", 2.75", 3.50" and 4.00" (Figure 3.22). The type of strain gage used is a universal general-purpose strain gage. These gages are polymide-encapsulated Constantan ('A' Alloy) gages featuring large, integral, copper-coated terminals. This construction provides optimum capability for direct leadwire attachment. The gage is extremely thin and flexible (0.0022"). The gage length is 0.062" and the grid width is 0.062". The resistance is 350 ± 0.3% Ω with a strain range of ± 3%.

Ground Level

0.063" IN RW1

0.050" IN RW2

1 (1.50)

(VARIES)   X 1

2 (2.75)

(VARIES)   X 2

3 (3.50)

(VARIES)   X 3

4 (4.00)

(VARIES)   X 4

3.84"

Ground Level

0.48"

0.40"

0.063"

1.22"

3.66"
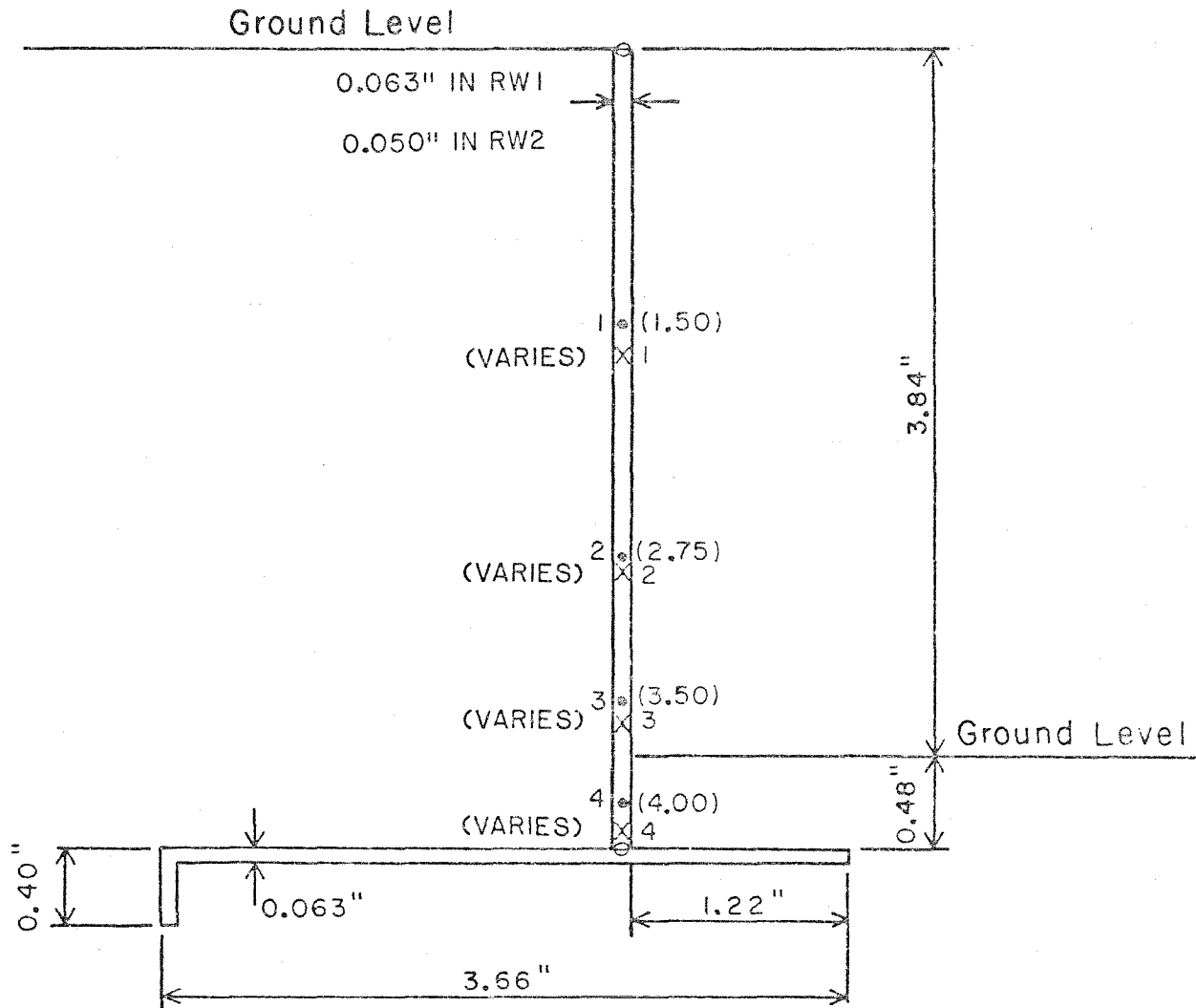
o Accelerometer and △- beam locations

● Strain gage locations

X Pressure transducer locations

(Parentheses indicate distance of
  transducer from top of wall in inches)

FIGURE 3.21 – MODEL WALL CROSS SECTION
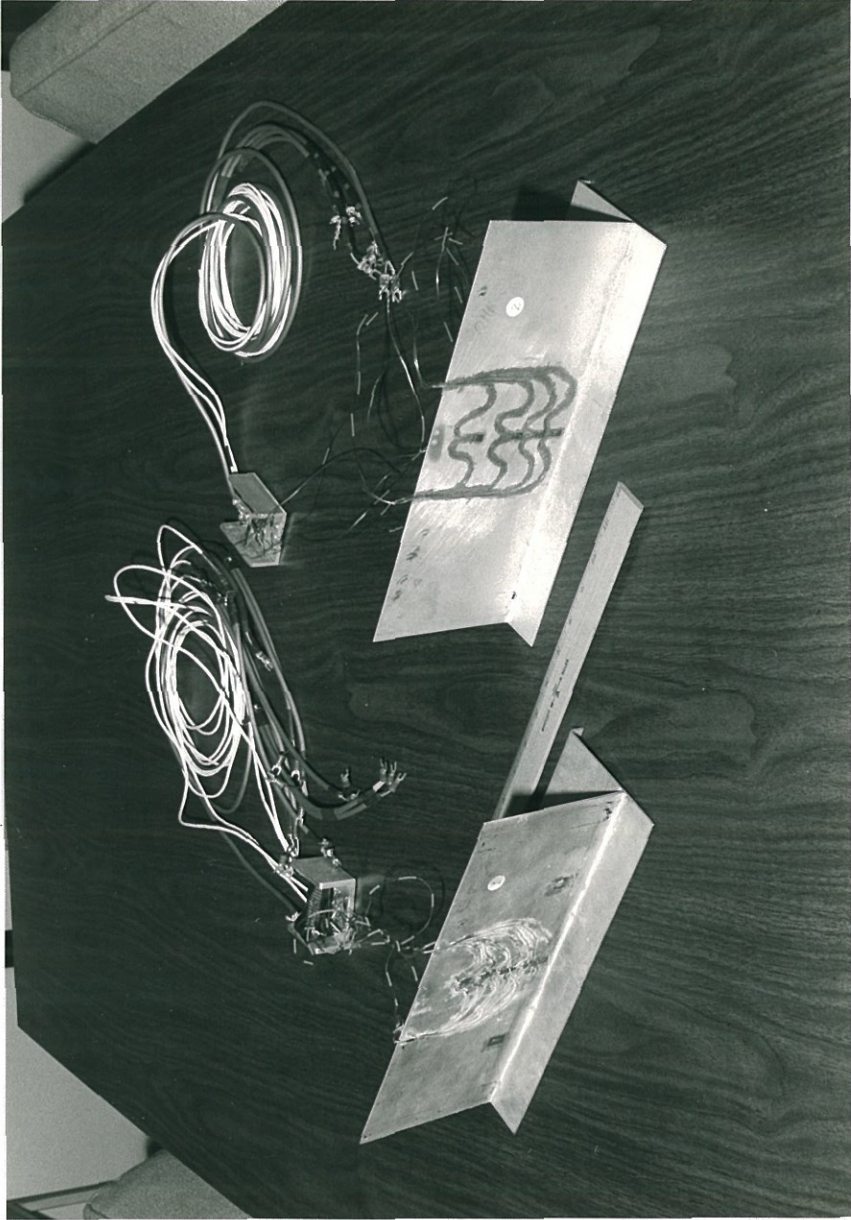
FIGURE 3.22 - MODEL RETAINING WALLS (RW1,LEFT:RW2,RIGHT)   STRAIN GAGE BRIDGES IN BACKGROUND

The gages are bonded to the wall surface according to M-Line Accessories Instruction Bulletin B-130-6 (8/77) with M-Bond 600 epoxy resin adhesive. Soldered to each gage are two lengths of Belden AWG32 magnet wire. The leads were laid on the faces of the wall and coated with a flexible, impermeable protective coating (BLH Barrier J).

The strain gage circuit is arranged as a Chevron Wheatstone bridge circuit as shown in Figure 3.23. This configuration minimizes the number of balancing resistors used as well as the number of sliprings taken up since all the pairs of strain gages have but one common ground. The excitation voltage is 5V DC.

The location of the Soil Mechanics Centrifuge at Caltech is on the roof of Thomas Laboratory in close proximity to air conditioning units and elevator drive motors which make for a very noisy electrical environment. In order to minimize this noise, the signals from the strain gage bridge are amplified with one LF352 amplifier (Figure 3.24) for each pair of strain gages. This is done inside the centrifuge itself as the amplifiers are loaded on the centrifuge arm. The gain is set at 50. The amplified signals then pass through the sliprings to the control room where they are recorded on a Honeywell Model 1858 CRT Visicorder which allows inertialess recording from DC to 5 kHz. The analog signals are recorded on Kodak Type UV 1920-80330Y Visicorder Recording Paper at an amplitude of 200 mV/division (1 division = 2.5 cm). In the dynamic portions of the test, the recording takes
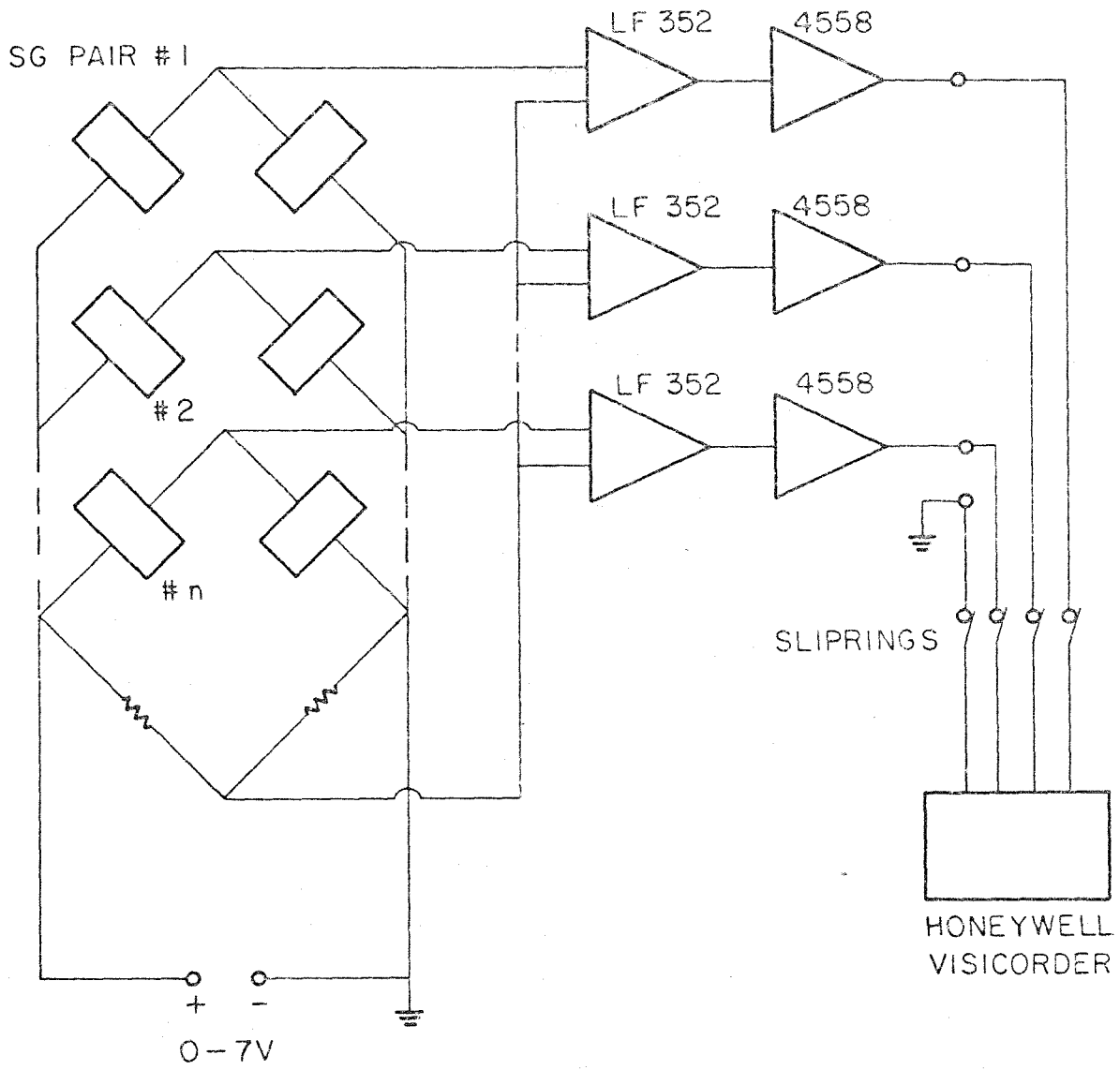
FIGURE 3.23 — STRAIN GAGE CIRCUIT
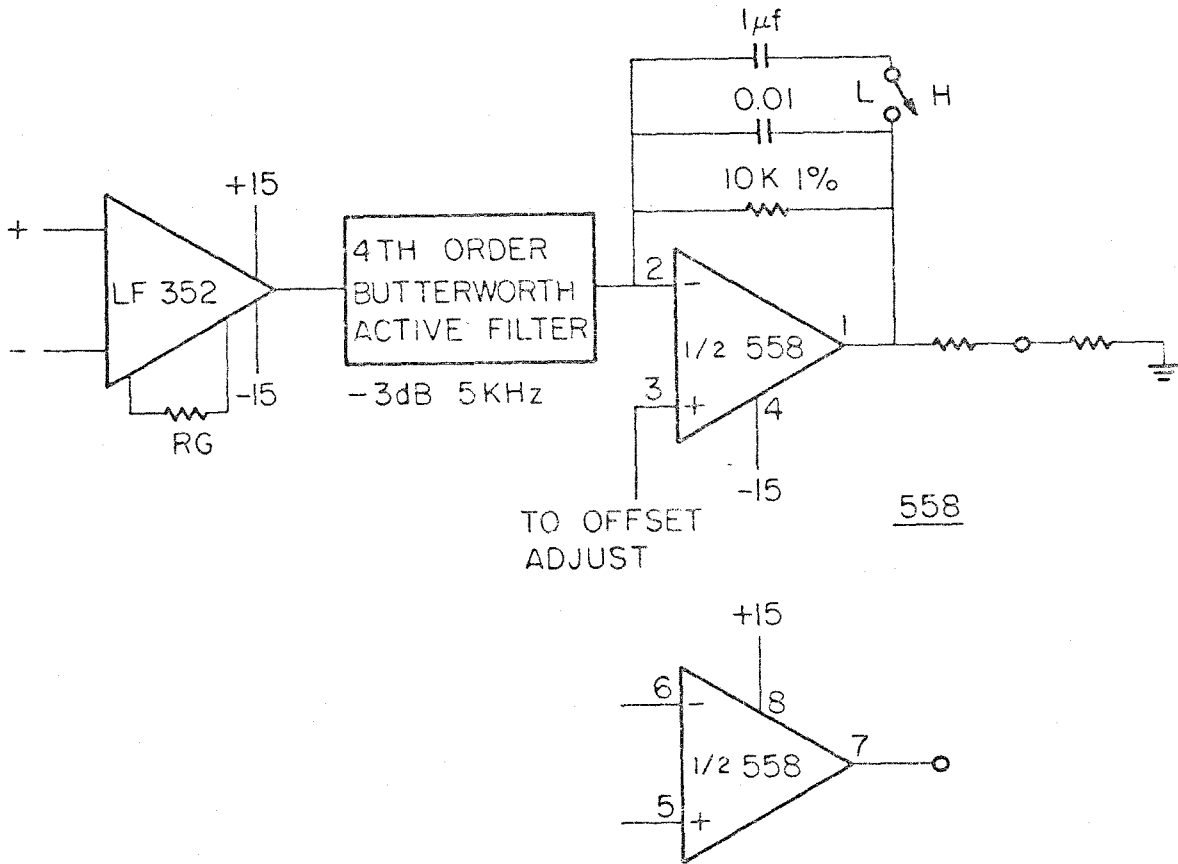
FIGURE 3.24 — AMPLIFIERS FOR STRAIN GAGES AND ACCELEROMETERS
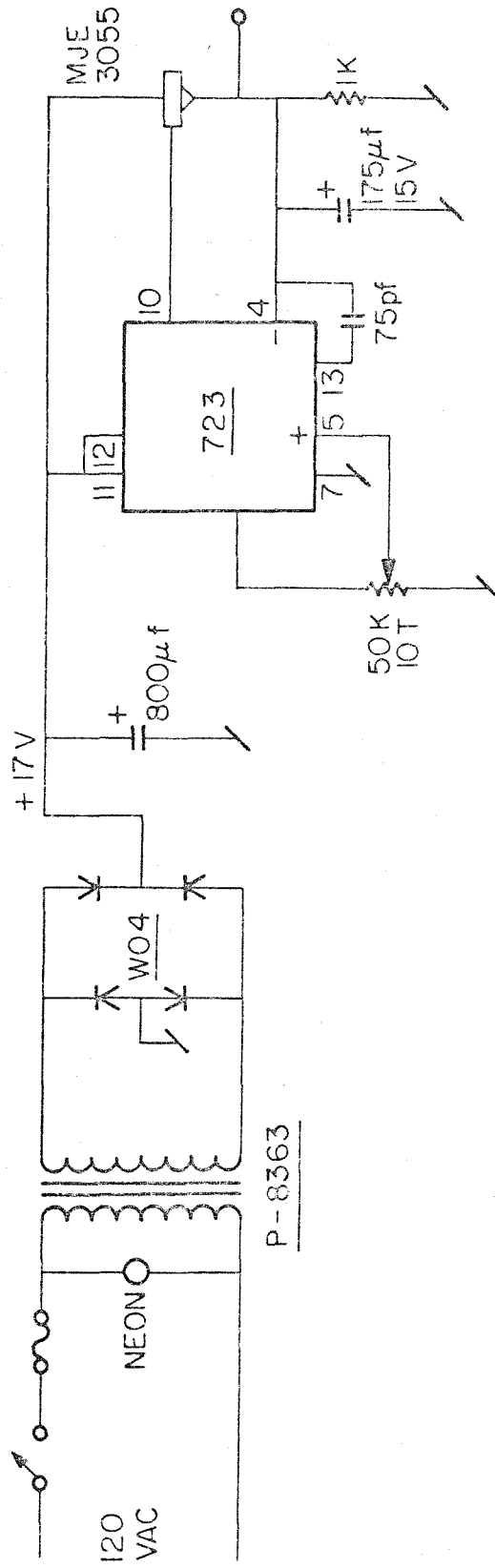
FIGURE 3.25 - CENTRIFUGE POWER SUPPLY TO DRIVE BRIDGE

place at a rate of from 50 to 80 inches per second of recording paper depending on the particular test.

3.5.2. Accelerometers

At the top and bottom of the centerline of the face of each retaining wall is mounted an Entran Devices Inc. Model EGA-125F-500D miniature accelerometer. In most tests there is an additional one located in the backfill approximately half way between the wall and the wall of the bucket and is buried near the surface.

The accelerometers employ a fully active Wheatstone Bridge consisting of semiconductor strain gages. The strain gages are bonded to a simple cantilever beam which is end-loaded with a mass (Figure 3.26). Under acceleration, a "g" force, the force on the cantilever is created by the g effect on the mass (F = ma). The accelerated mass creates a force which in turn provides a bending moment to the beam. The moment creates a strain (proportional to the acceleration) which results in a bridge unbalance. With an applied voltage, this unbalance produces a millivolt deviation at the bridge output, which is proportional to the acceleration vector.

A very attractive feature of this type of accelerometer is its very small size. The entire unit (minus the leads) weighs only 0.02 oz. The accelerometer unit is 0.270" long by 0.145" wide by 0.105" (unit weight of 525 lb/ft^3) high and is mounted on a 0.270" X 0.370" X 0.040" flange as shown in Figure 3.27. The bold-faced arrows indicate the sensitive axis. The accelerometers are attached to the model walls with
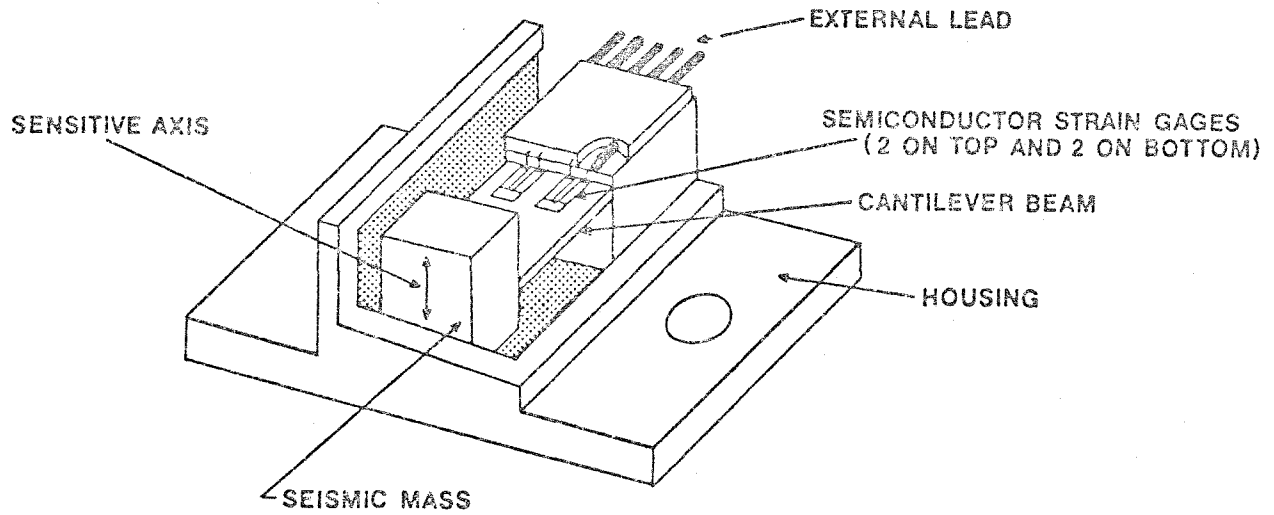
FIGURE 3.26 – ACCELEROMETER CUTAWAY (FROM ENTRAN DEVICES)

FLANGED UNIT
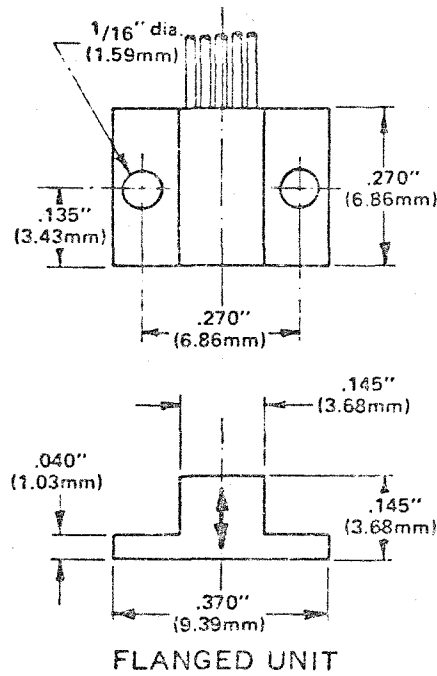
FIGURE 3.27 – ACCELEROMETER DIMENSIONS (FROM ENTRAN DEVICES)

two 0-80 hex screws. The model of accelerometer used has a range of
± 500g with a nominal sensitivity of about 0.5 mV/g (varies slightly
from this with each particular unit), an input impedance of about 1150
Ω, an output impedance of about 550 Ω, and a resonant frequency of 3000
Hz. In addition, the unit is damped to 0.7 of critical using a viscous
fluid medium. This helps to eliminate resonance and allows a useful
frequency range of DC to 1000 Hz. The excitation voltage is 15 V DC.

Similarly, as with the strain gages, the output signals were
suitably amplified and filtered to minimize the high frequency noise
inherent with centrifuge testing. The accelerometer circuit is shown in
Figure 3.28. The gain on the amplifiers was set at 10, and the analog
signals recorded on the Honeywell Visicorder at an amplitude of 200
mV/division. The accelerometer signals were recorded directly alongside
those of the strain gages on the recording paper.

3.5.3. Pressure Transducers

Originally, it was planned to obtain pressure distributions behind
the retaining walls by means of differentiating the moment distributions
twice with respect to the length coordinate x. From elementary rela-
tionships it is well known that the shear Q is:

$$Q = \frac{\partial M}{\partial x}$$

(3.10)

[LF352]   [4558]

(3080)   (4558)
{3080}   {4558}

TRANSDUCER
BRIDGE

TRANSDUCER

SLIPRINGS

HONEYWELL
VISICORDER

[7V – 20V]
+   –
(0V – 7V)
{0V – 7V}
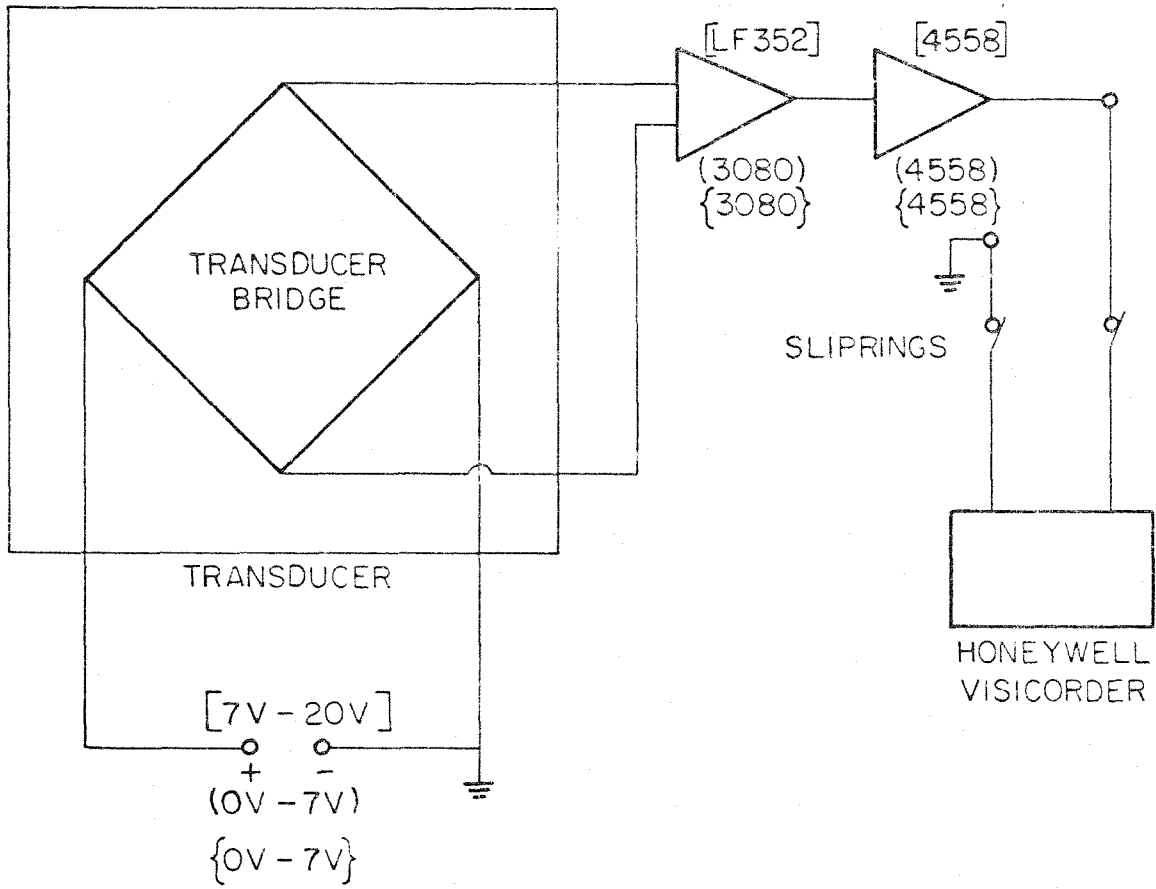
[ACCELEROMETER]

FIGURE 3.28   (PRESSURE TRANSDUCER)   CIRCUIT

{DELTA—BEAM}

where M is the moment distribution. The load (pressure) distribution P is:

$$P = \frac{\partial Q}{\partial x} = \frac{\partial^2 M}{\partial x^2} \tag{3.11}$$

Unfortunately, because of inaccuracies which develop and propagate in numerical differentiation it was found that these simple relations did not give adequate or accurate pressure distributions.

Figure 3.29 (which is fully explained in Section 5.3) shows how inaccurate the use of moment differentiation to arrive at pressure distributions is. It was thus necessary to measure pressure directly by the use of pressure transducers and then integrate the determined pressure distributions (numerical integration is much more stable and accurate than differentiation) to obtain the shear distributions.

Except for test 1CN0001, four miniature, low profile pressure transducers were placed at various locations (depending on the particular test) along the centerline of the back of the walls. In tests 1CN0002, 1CN1003, and 1CN0004, the pressure transducers were located 1.68", 2.78", 3.59", and 4.17" from the top of the wall; in tests 1CN1505, 1CN0006 at 1.79", 2.75", 3.60", 4.16", in tests 1CN0007, 1CN0508, 1CN1009, 1CN1510 at 1.86", 2.77", 3.59", 4.21", and in tests 2CN0011, 2CN0012, 2CN1013, 2CN1514 at 1.83", 2.92", 3.36", 3.91".

The pressure transducers used are Entran Devices Inc. Model EPF-200-50 Flatline Pressure Transducers. The transducer consists of a semiconductor strain gaged circular diaphragm less than 0.2" in diameter constructed of 17-4 PH stainless steel. This is a piezo resistive

FIGURE 3.29 – PRESSURE DISTRIBUTION OBTAINED FROM MOMENT DOUBLE-DIFFERENTIATON
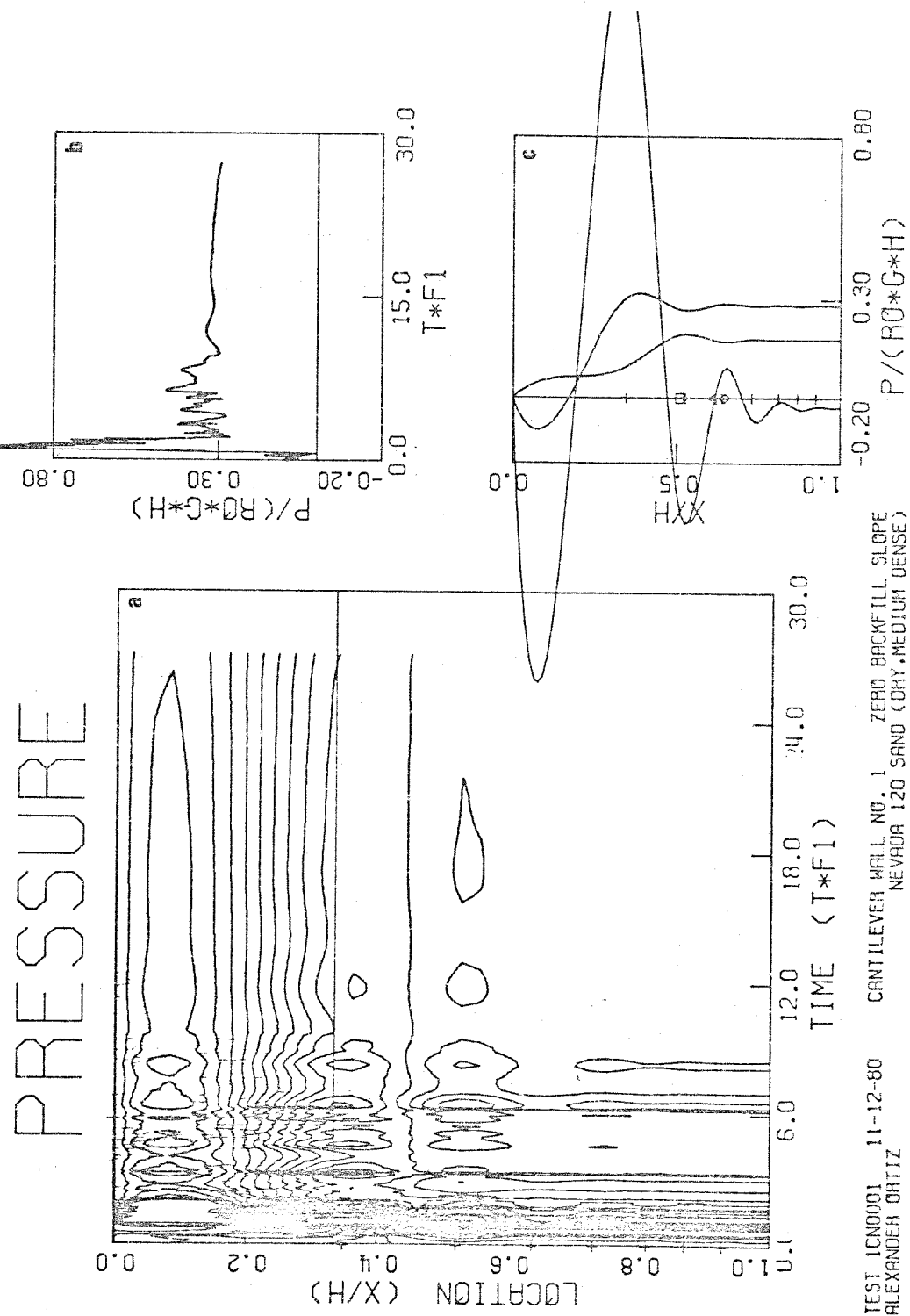
TEST ICN0001   11-12-80   CANTILEVER WALL NO. 1   ZERO BACKFILL SLOPE
ALEXANDER ORTIZ   NEVADA 120 SAND (DRY,MEDIUM DENSE)

pressure transducer with a fully active semiconductor bridge. Similarly, as with the accelerometer, a load on the diaphragm will create a strain (proportional to the pressure) which results in a bridge unbalance. With an applied voltage, this unbalance produces a millivolt deviation at the bridge output, which is proportional to the pressure.

The transducer is very small (Figure 3.30) and thin being only 0.040" thick. It has a range of 0 to 50 psis with a nominal sensitivity of about 2.5 mV/psi (varies slightly from this with each particular unit), an input impedance of about 750 Ω, an output impedance of about 250 Ω and a resonant frequency of 50 kHz. The excitation voltage is 6 V DC.

As previously described with the other types of transducers, the output signal is suitably amplified and filtered. The pressure transducer circuit (Figure 3.28) is similar to that of the accelerometers with the exception that the signals are amplified with a CA3080 amplifier (Figure 3.31). The amplifier gain was 25, and the signals were recorded alongside those of the other transducers on the Honeywell Visicorder at an amplitude of 200 mV/div.

3.5.4. Displacement Transducers (Δ-beams)

In order to determine the relative displacements of the retaining walls with respect to the centrifuge bucket, the moment distribution
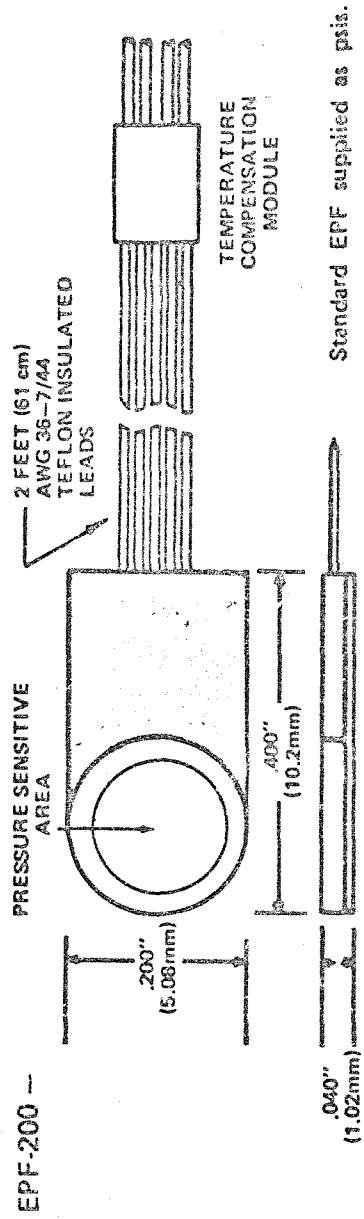
FIGURE 3.30 – PRESSURE TRANSDUCER (FROM ENTRAN DEVICES)
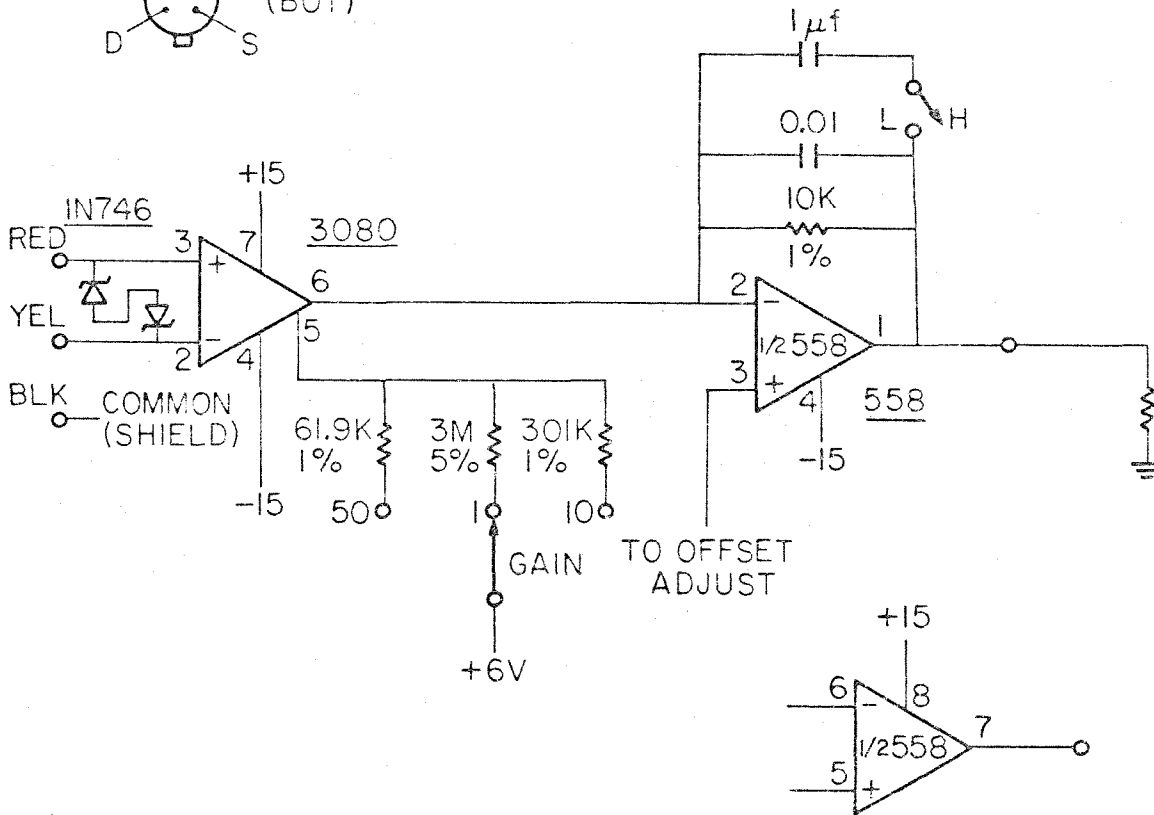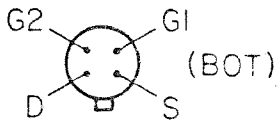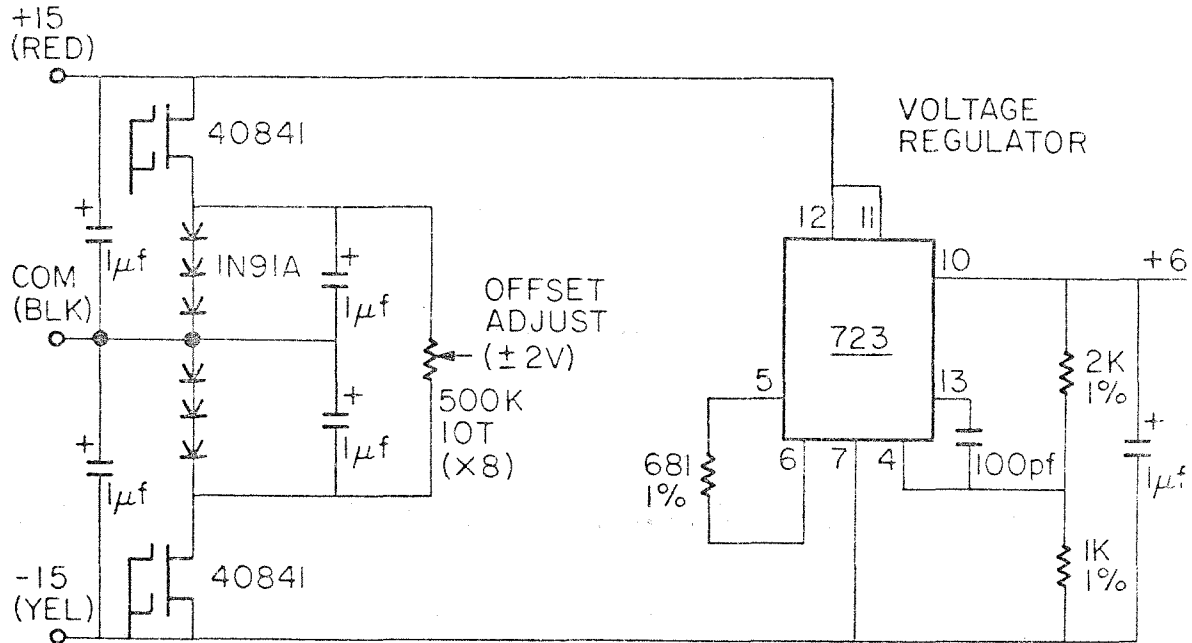
FIGURE 3.31 — AMPLIFIERS FOR PRESSURE TRANSDUCERS AND DELTA—BEAMS

along the wall must be integrated twice with respect to the length

coordinate x. Recalling the equation for a the curvature of the

deflected shape of a simple beam:

$$\frac{\partial^2 y}{\partial x^2} = \frac{-M}{EI}$$

(3.12)

it follows that the deflected shape y is given by:

$$y = \frac{1}{EI} \int_0^H \int_0^H Mdxdx \div Ax + B.$$

(3.13)

where A and B are constants of integration dependent on the boundary

conditions of the wall. A and B can be determined knowing the displace-

ments at the top and the bottom of the wall. The displacements at these

locations can be deduced by integrating the accelerometer records twice

with respect to time. This, however, requires the determination of two

additional constants of integration dependent on time-imposed condi-

tions. At each location if the initial (static), and final (static,

after shaking is over) displacements are known at each of the locations,

the pair of time imposed constants of integration can be determined, and

thus the relative displacements between the walls and bucket can be

determined at the top and bottom of the wall. Knowing this, A, B, and

the full displacement curves can thus be determined.

Initial and final displacements at the top and bottom of the walls

are measured by means of a pair of cantilever beams (called Δ-beams for

simplicity) which are attached to the front of the bucket and connected

by means of a very thin wire to the accelerometer locations on the face

of the wall. These Δ-beams are very thin (0.015" thick) strips 2.25"

long, 1.00" wide of spring steel attached to a rigid base and strain gaged, so that, properly calibrated, they can record displacements over a relatively wide range.

The A-beam circuit is similar to that of the pressure transducers (Figure 3.28). Since the frequency response is very low, the transducer signals are only recorded on the Visicorder during the static portions of the test. The circuit excitation is 5 V, the gain 25, and the Visicorder amplitude is 100 mV/div.

3.6. Calibration of Transducers

All pre-test calibrations were carried out using the entire electronic circuitry, i.e. the calibration signals were routed through those terminals, amplifier channels, filters, sliprings, and Visicorder channels which they would use during the actual testing. The excitations, gains, and recording amplitudes used in calibration were likewise the same as in the tests. The outputs recorded on the Visicorder were converted directly to parameter (moment, displacement, acceleration, etc.) measurements without the use of instrument factors. All transducers are linear and therefore require two calibration factors (slope, intercept) for each. These factors were determined using the linear least-squares function on a Hewlett-Packard 55 pocket calculator.

All calibrations were recorded on the Visicorder and the traces digitized with a Benson-Lehner 099D data reducer unit. The digitizer had a resolution of 790.8 digitizer units (du) per inch of width of recording paper and 792.0 du/inch of length. The calibration slopes

were thus in units of parameter per digitizer unit and the intercepts in units of parameter. Data reduction of the tests will be discussed in Section 4.2.

3.6.1. Strain Gages

The strain gages are calibrated to measure moments directly. To accomplish this, the base of the model retaining walls is rigidly secured to the bottom of the centrifuge magnesium frame which was rotated 90° so that the stem forms as horizontal cantilever beam. Two 1" thick (each) Plexiglas beams were then clamped in sandwich fashion to the free end of the stem and weights hung from the center. The calibration arrangement is shown in Figure 3.32. The Plexiglas beams distribute the load evenly across the width of the wall. This creates in effect a cantilever beam with a concentrated load at the end, moments of which can be readily determined. Weights of 0,1,2,3,4,5,6,and 8 pounds were hung and the output recorded at the Visicorder at the other end of the system.

3.6.2. Accelerometers

In order to calibrate the accelerometers, they were placed with the sensitive axis facing downward on the upper lip of the centrifuge bucket which is at a radius of 30.5 inches from the centrifuge axis. Readings were recorded on the Visicorder with this arrangement, i.e., the accelerometers reading 1g. The centrifuge was then taken up to accelerations of 10, 20, 30, 40, 50, 60, and 70g respectively. It was
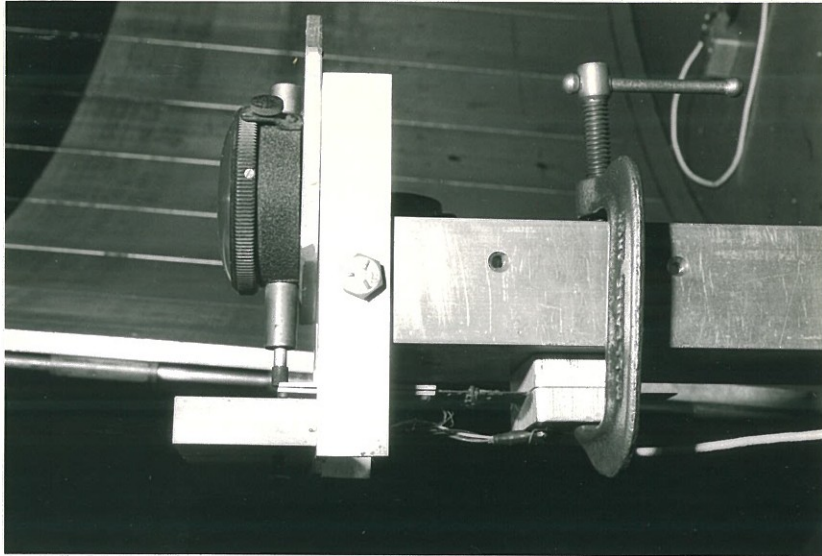
FIGURE 3.33 – DELTA–BEAM CALIBRATION
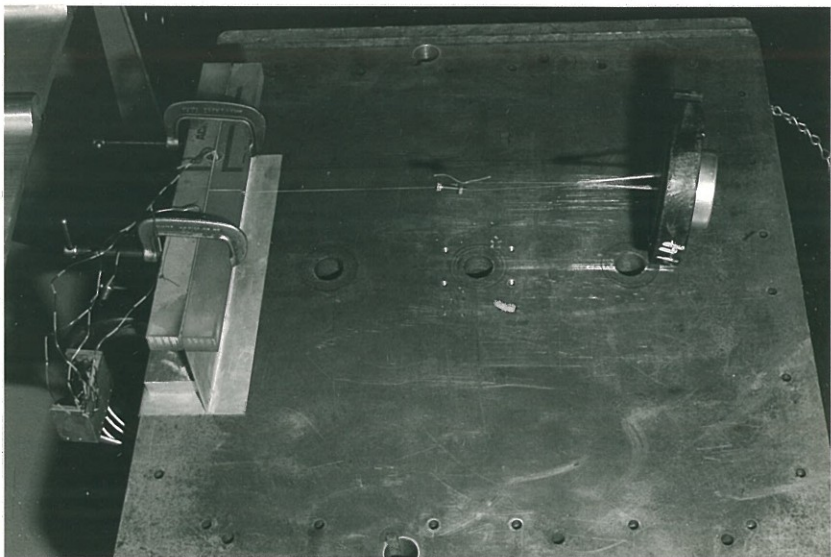
FIGURE 3.32 – STRAIN GAGE CALIBRATION

assumed that an amplitude of 0 du on the Visicorder was 1g. The cali-
brations were then determined in relation to this.

3.6.3. Pressure Transducers

The pressure transducers were calibrated by placing them on the
bottom of the centrifuge bucket at a radius of 40.5 inches from the
centrifuge axis, and placing 4.90" of Nevada 120 sand at a density of
93.3 pcf on top of them. Measurements were then taken with the
centrifuge stationary (at 1g) and spinning at 10,20,30,40, and 50g. The
increase in g-acceleration to N g's causes an increase in the soil unit
weight by N (see Table 2.1) and thus an increase in pressure, the pres-
sure simply being the weight density of the soil (at the particular
acceleration level) times the depth (4.90"). Thus pressures of 38, 381,
762, 1143, 1524, and 1905 psf corresponded to each g level used in the
calibration.

3.6.4. Δ-beams

The Δ-beams were calibrated by fixing them to a vice and measuring
displacements with the aid of a Federal dial gauge accurate to 0.001 in.
Displacements of 0, 0.01, 0.02, 0.03, 0.04, 0.05, and 0.10 inches were
measured (Figure 3.33).

CHAPTER IV

4.1. The Experiment

In every test performed, the following sequence of experimental procedures was carried out.

To begin with, sand was placed on the centrifuge bucket to a depth of about 4 inches (Figure 4.1). If looser conditions were desired, it was just dumped in; if denser, it was tamped and/or vibrated after being placed in one to two inch lifts. Following this, one of the walls, along with all its instrumentation, was placed approximately 6 inches from the front of the bucket (leaving about 8-1/2 inches for backfill) and carefully seated on the sand layer already placed (Figure 4.2). Special care was taken to assure the wall was vertical by following guide lines drawn on the inside of the bucket. Sand was then placed on both sides of the wall following the procedure for looser or denser conditions described above (Figure 4.3). The total depth of sand (for a flat backfill) was 8 inches. For a sloping backfill, it was placed to the desired slope above the 8 inch mark on both sides. The weight of the sand placed was then totalled and, since the bucket dimensions were well known, the unit weight determined.

By placing sand on both sides of the wall and taking the container up to 50g's the transducers were thus zeroed. In this manner, the walls were subjected to no moment, lateral acceleration, or displacement and an accurate zero was recorded on the Visicorder at the test centrifuge
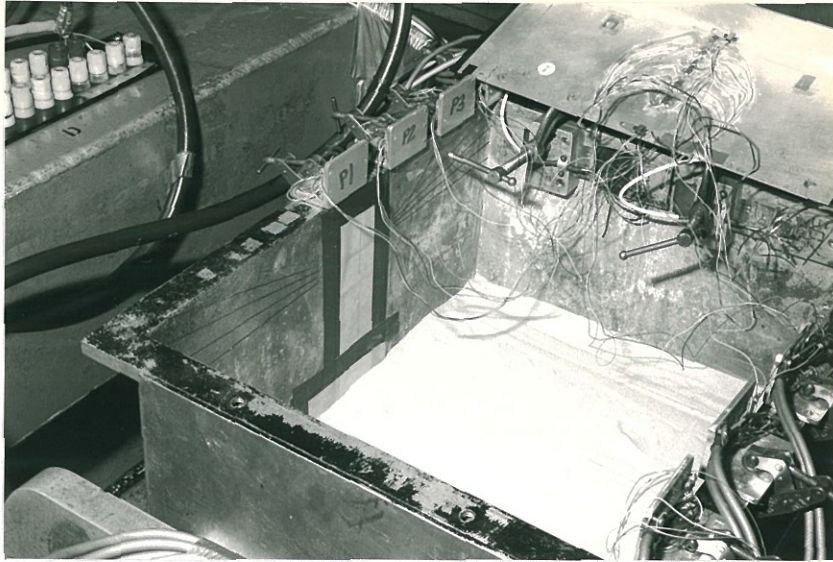
FIGURE 4.1
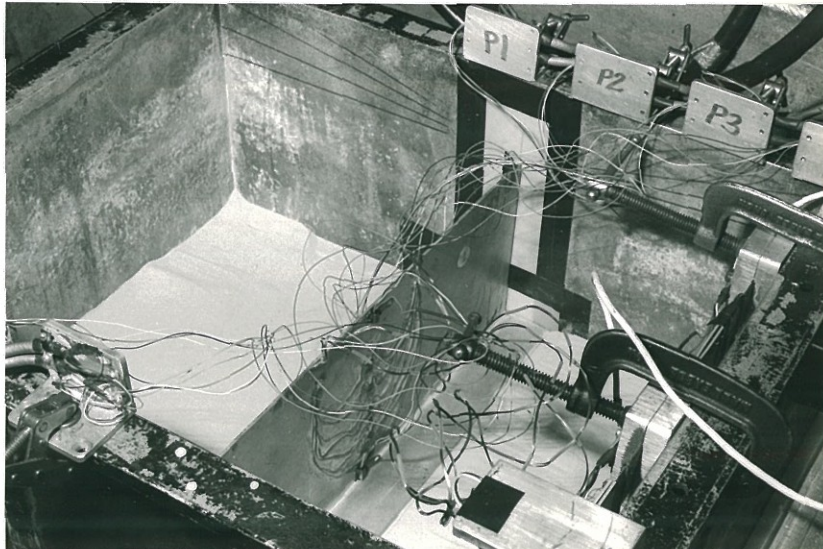
FIGURE 4.2
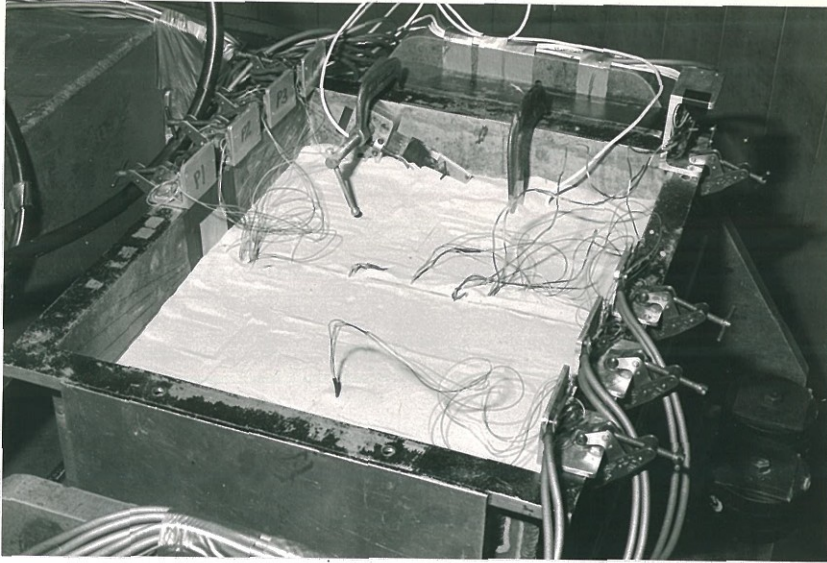
FIGURE 4.3
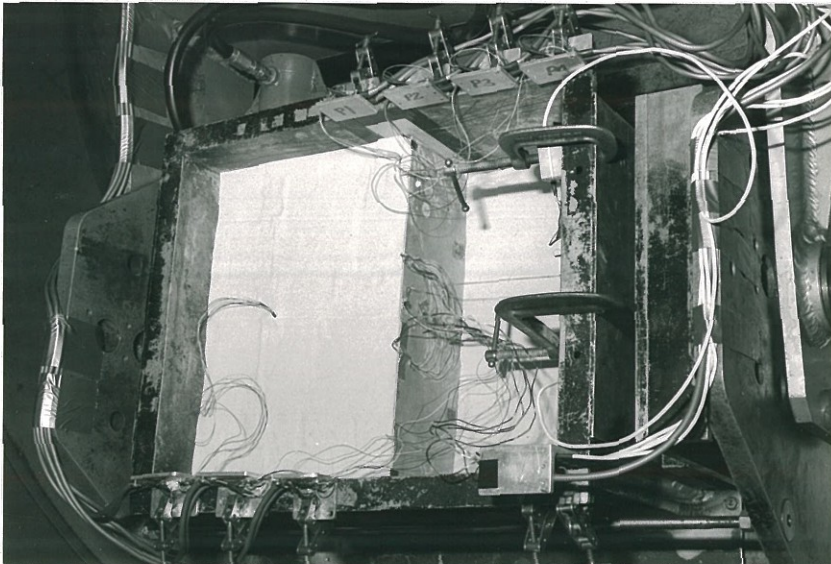
FIGURE 4.4

acceleration. The experiment was then returned to one g where the sand on the front of the walls was removed to the design height (Figure 4.4).

Table 4.1 Soil Densities

Test	Density @ 1g (pcf)	Density @ 50g (pcf)	Test	Density @ 1g (pcf)	Density @ 50g (pcf)
1CN0001	92.6	4630	1CN0508	95.9	4797
1CN0002	91.2	4561	1CN1009	97.0	4849
1CN1003	92.0	4597	1CN1510	95.3	4764
1CN0004	93.9	4695	2CN0011	98.8	4941
1CN1505	92.4	4621	2CN0012	95.8	4790
1CN0006	94.5	4726	2CN1013	97.3	4865
1CN0007	98.1	4906	2CN1514	97.7	4886

The system was next taken back up to 50g's where all the static outputs were recorded on the Visicorder. The channels which carried the signals of the Δ-beams were then turned off since, due to the poor frequency response of the Δ-beams, they were inadequate for dynamic measurements. After this, the container was subjected to the "earthquake" shaking described in Sections 3.2 and 5.2. The output signals were recorded on the Visicorder at a recording paper rate of 50 to 80 inches per second depending on the particular test. Usually there were 4 strain gage, 3 accelerometer and 4 pressure transducer outputs (11 traces total) being recorded on paper only 8 inches wide. Needless to say, there was some overlapping of traces, and a high density of analog data, but the recordings were usually clear and easy to follow when digitizing subsequently.

Figure 4.5 is an example of the traces recorded on the Visicorder during part of the dynamic portion of a typical test (2CN0012 in this case).

Following the shaking, the two A-beam channels were turned back on, and their outputs taken along with those from the other transducers now static once more. The system was then brought back to rest which concluded the actual experiment itself. Data reduction of the Visicorder output followed.

4.2. Data Reduction

The digitizing was performed on a Benson-Lehner 099D data reducer unit and the following procedure used. The cross hairs are manually set to successive x-y coordinates on each record trace. The coordinates are converted to digital position figures by means of a magnetic readout head, and are stored in a 6-digit accumulator system from which they are automatically read out to an IBM 29 card punch. The resolution of the system is 792.0 du/inch in the x and 790.8 du/inch in the y directions. The Visicorder paper is placed on the 24" X 16" digitizing table with the horizontal axis lined up by eye to an estimated zero axis. The lining up of the paper need not be too accurate since it will be corrected with respect to a baseline recorded on the paper. All traces are digitized without moving the record on the table.

First of all, a baseline, which will be used to make corrections for deviation from the horizontal, is digitized. Each trace on the Visicorder paper is then digitized individually as follows. The zero
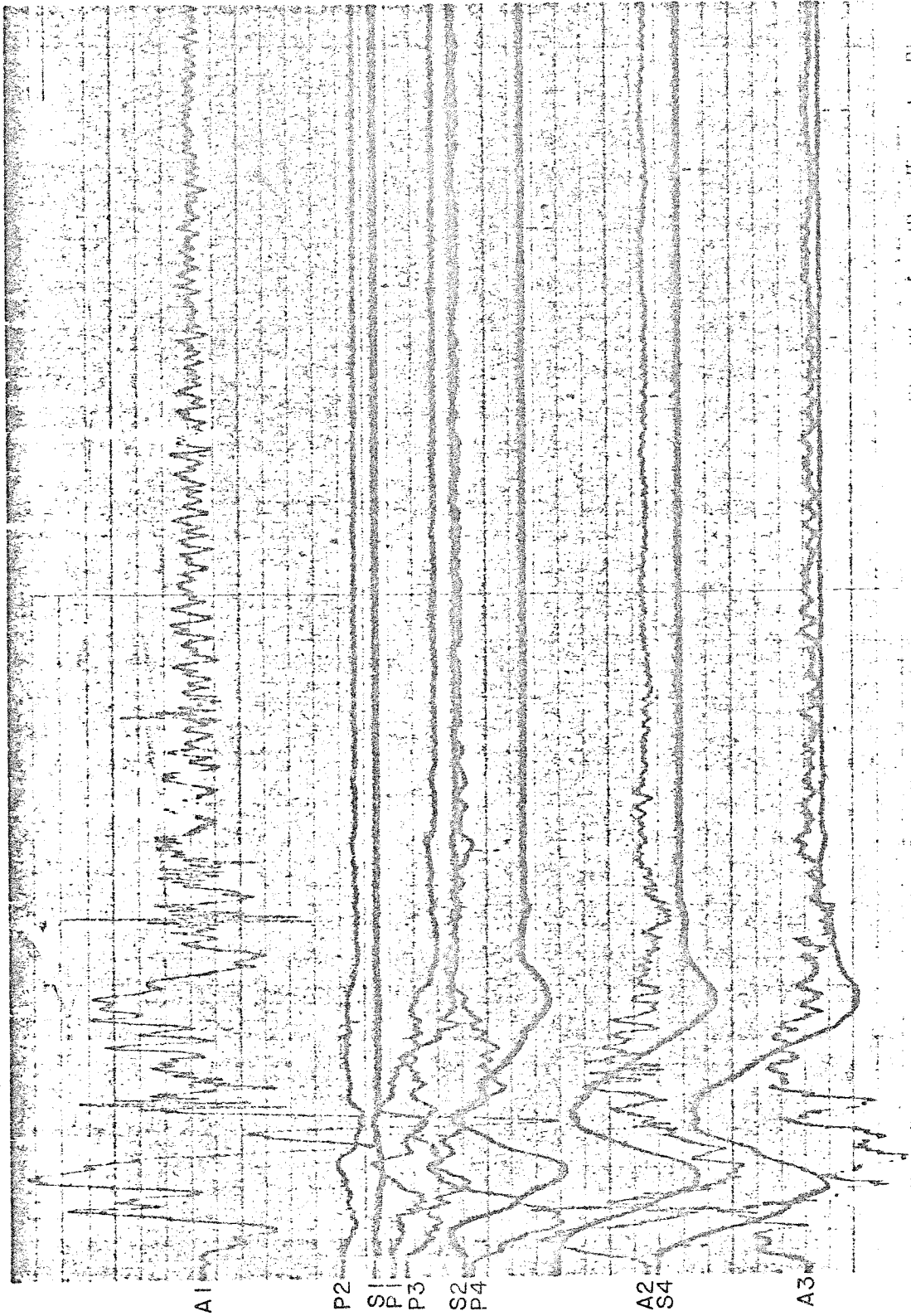
FIGURE 4.5 — TYPICAL VISICORDER RECORD (2CN0012) REDUCED TO 77% OF ORIGINAL
A = ACCELEROMETER   P = PRESSURE GAGE   S = STRAIN GAGE

point of the trace is first digitized. This is the point at 50g where
sand is on both sides of the wall. For the pressure transducers and the
A-beams the zero point is the reading when the centrifuge is at rest.
Next the static point at 50g (normal experiment, backfill sand only) is
digitized followed by the digitization of the dynamic part of the test.
The records are digitized on an unequal time basis since this leads to
the best definition of the trace for a given number of data points. All
significant peaks, points of inflection, etc., are picked, along with as
many intermediate points as are needed for an accurate definition of
shape.

The digitized data are directly punched on cards which are then
read into magnetic disks on a VAX 11 Wordprocessing system. Program
P1CHECK (Trifunac, Lee [63]) reads the data and checks whether the time
coordinates monotonically increase. It also searches for possible
disproportionate jumps of the amplitude data. If any error is found,
the program prints out the message. Small errors are corrected
immediately. The data are then plotted to the same scale as the
digitized record, and the two versions are compared to check the
accuracy of digitization. Any portion that is digitized improperly has
to be redigitized and replotted until the final plot agrees well with
the digitized record.

The corrected digitized data is now fed into the data processing
program WALL which will be described below and which is listed in
Appendix B. WALL prints out static, maximum dynamic, and final static
moment, pressure, shear, and displacement distributions along the wall

to discrete locations; moment, pressure, shear, displacement vs. time
distributions at the location of each maximum response at equal time
steps; accelerometer, velocity and displacement vs. time records for
each of the three accelerometer locations, as well as other data per-
taining to the test, namely, centrifuge operation data, material
properties, and calibration factors. In addition plots are made of the
above-mentioned distributions. Contour plots of moment, pressure,
shear, and displacement distributions with respect to location and time
are also made. This provides a very descriptive and compact representa-
tion of the entire test.

It was sometimes desired to obtain characteristics of the motion
recorded by the accelerometers in order to have a comparison with actual
accelerogram characteristics of real earthquakes. For this purpose,
some of the accelerometer records were given the routine computer
processing of strong-motion accelerograms developed at Caltech by
Trifunac and Lee [63]. Programs P1CHECK, P2SCALE, and P3TAPE form
Volume I of data in which the raw data is converted into uncorrected,
scaled, accelerogram data. Program IIMAIN creates Volume II which con-
tains corrected accelerogram, velocity, and displacement data. Volume
III, which gives the response spectra of the record, is created using
program IIIMAIN. Program IVMAIN creates Volume IV containing the
Fourier Spectra. From this volume, the fundamental frequency of the
system is determined (see Section 3.3.3). As will be seen in the
results, it is the only frequency which contributes significantly to the

response. The standard accelerogram processing is outlined in Figure 4.6.

The results from the tests are obtained by processing the digitized data with the FORTRAN program WALL. The program is run on an IBM 370/3032 Computer System at the Booth Computing Center at Caltech.

After the raw digitized data is checked by program P1CHECK, the corrected data from the transducers is fed into WALL, along with other experimental data, namely centrifuge speed, distance from centrifuge axis to top of wall, wall/soil properties, order of polynomial desired for least-squares fit (see below), type, number, and location of transducers used, and calibration factors.

All the traces are then corrected with respect to the input baseline to avoid errors due to the slight slope which all the records inherently have because of positioning on the digitizer table. This is particularly important in the accelerometer records since double integrations can introduce errors proportional to the square of the running time with just a small initial slope present.

Following this, the data is scaled to model dimensions using the calibration factors.

Since all the separate traces are digitized individually, it is necessary to correlate them to specific, discrete time steps. This is done by smoothing the individual trace data point by point with a cubic spline and then picking off the values from the spline at particular time intervals. For convenience (see Section 5.1), it was decided to use a dimensionless time group tf_1 to express time. t is the real

STANDARD ACCELEROGRAM PROCESSING

RAW DATA

VOL. I PROCESSING:

1. SCALED DATA
2. VOL. I TAPE

VOL. I REPORT

CONTAINING:

1) PLOTS OF SCALED DATA
2) PRINTOUT OF SCALED DATA

VOL. II PROCESSING:

1. CORRECTED DATA
2. VOL. II TAPE

VOL. II REPORT

CONTAINING:

1) PLOTS OF ACCELERATION, VELOCITY, AND DISPLACE-MENT
2) PRINTOUT OF ACCELERATION

VOL. III PROCESSING:

1. RESPONSE SPECTRA
2. VOL. III TAPE
3. VOL. V TAPE

VOL. IV PROCESSING:

1. FOURIER SPECTRA
2. VOL. IV TAPE

VOL. III REPORT

CONTAINING:

1) LOG-LOG PLOT OF PSEUDO-VELOCITY RESPONSE SPECTRA
2) LINEAR PLOT OF TRUE-VELOCITY RESPONSE AND FOURIER SPECTRA
3) PRINTOUT OF ACCEL-ERATION, VELOCITY, DISPLACEMENT, AND PSEUDO-VELOCITY RESPONSE VALUES

VOL. IV REPORT

CONTAINING:

1) LINEAR PLOT OF FOURIER SPECTRA
2) LOG-LOG PLOT OF FOURIER SPECTRA

FIGURE 4.6 - FROM (63)

prototype (or model) time and f_1 is the real prototype (or model) fundamental frequency of the system. tf_1 is the same for both model and prototype. The discrete time steps are chosen at 150 per tf_1 for the first six tf_1 and 75 per tf_1 thereafter. Because of the nature of the experimental shaking, most of the critical (maximum and high frequency) response occurs when $0 \leq tf_1 \leq 6.0$.

The moments are determined from the scaled strain gage data. It is intended to use a quintic (fifth order) spline fit to the data points at each time step. The spline fitting, however, requires six boundary conditions, the moment and the first and second derivatives of the moment, at the top and base of the wall. At the top of the wall, these are known. The moment and shear (first derivative) are zero since this is the free end of a cantilever beam. The pressure (second derivative) is also zero (no load). Since the bottom-most strain gage is located at some distance from the base of the wall (Section 3.5.1), the boundary conditions at this location are thus not known. In order to estimate these a polynomial least-square fit is made of the data points at each time step. A third or fourth order fit is done and the base boundary conditions are determined from this. Once this is done, the quintic spline is fitted to the data points and the moment distribution determined from this fit at each time step.

If no pressure transducers are used, the moment distributions are numerically differentiated with a fourth order finite difference scheme, once to obtain the shears and once more to obtain pressures. (This is why a quintic-spline was used, since a cubic spline would give straight

line segments in the second derivative.) However, due to the instabilities of numerical differentiation, it was determined that first derivatives were marginally satisfactory and second derivatives very inaccurate (recall Figure 3.29). This spawned the use of pressure transducers in tests.

When pressure transducers were used (all the tests except the first one) at each time step, the pressure transducer data points were polynomial fitted and a cubic spline fitted in a manner similar to the moments. An advantage of the cubic spline is that it requires no boundary conditions to be specified. The pressure distribution at each time step is thus read directly from the spline. The location of the resultants is then determined by finding the centroids of the pressure distributions. The shear distributions are obtained by direct trapezoidal rule integration of the pressure distributions. Numerical integration, as opposed to differentiation, is stable and accurate.

The following step is to determine the displacements at the top and bottom of the wall for every time step. The accelerograms are integrated twice and the Δ-beam readings are used to tie in the initial and final conditions. (In the case of the free-field accelerometer, the initial and final displacements are assumed to be zero). The displacement distributions along the wall are then determined by integrating the moments twice and using the end displacements to find the two constants of integration required (see Section 3.5.4). The velocities at the accelerometer locations are also calculated in this process.

After each parameter distribution was determined, the corresponding printing and plotting described in the previous section was done.

The data processing procedure is outlined in the flow chart of program WALL in Figure 4.7.

FLOWCHART FOR PROGRAM "WALL"
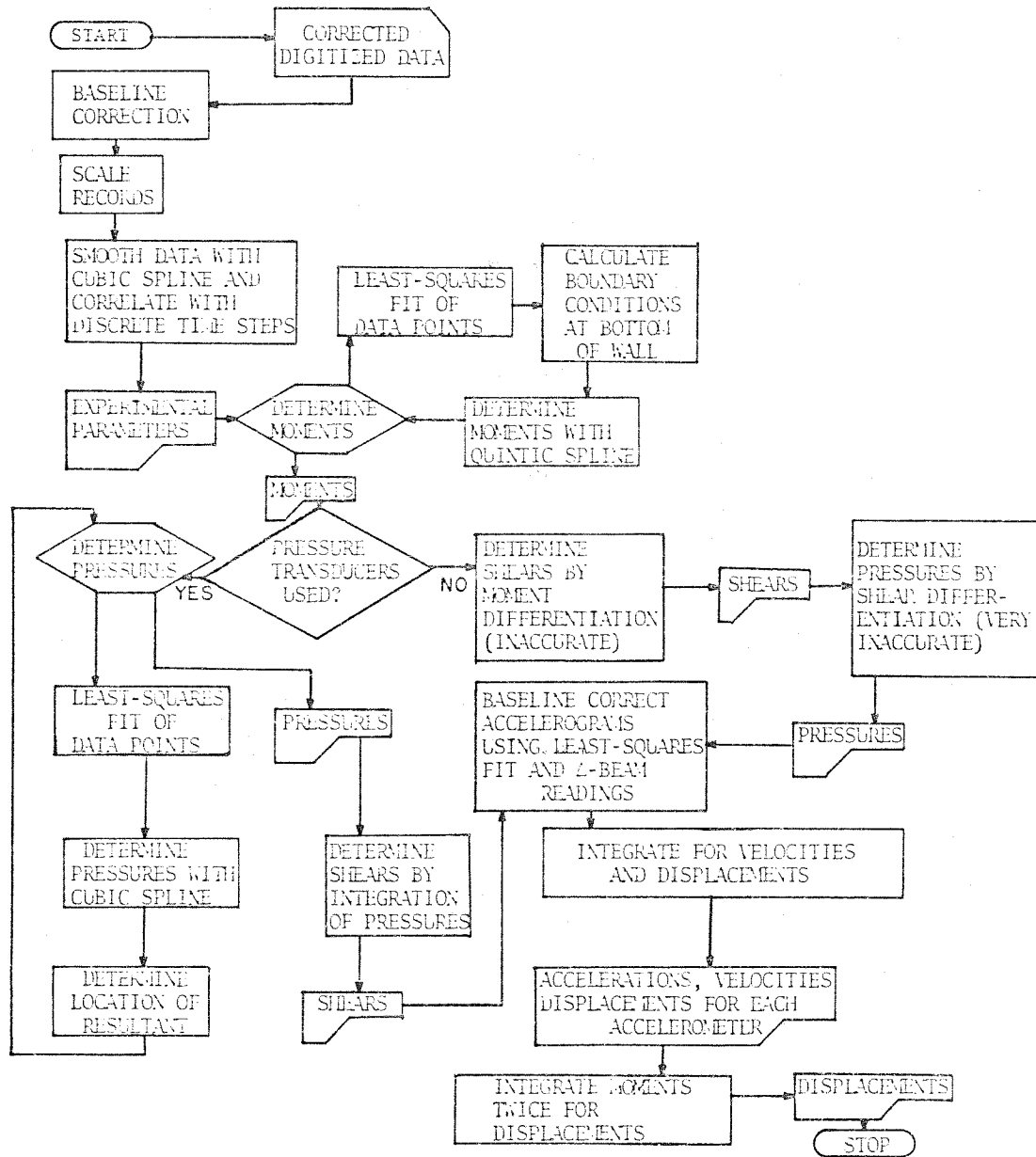
FIGURE 4.7

CHAPTER V

RESULTS

5.1. Dimensionless Groups

Henceforth, for convenience, all parameters will be discussed as dimensionless groups. This will make the discussion indifferent as to model or prototype.

The principles of dimensional analysis (reference [3] and Appendix A) are used to determine the dimensionless groups. From the tests, the following parameters are involved in influencing the results:

TABLE 5.1

Parameters Involved in Tests

x — vertical location
H — height of wall
EI — stiffness of wall*
M — wall moment*
Q — wall shear force*
y — lateral displacement of wall
P — lateral earth pressure
γ — density of soil
ϕ — angle of internal friction of soil
e — soil void ratio
g — gravitational acceleration
a — lateral acceleration
v — lateral velocity
t — time
f_1 — fundamental frequency of system

*per unit width

Parameters like Young's Modulus, Poissons's ratio and wave
velocities for the soil were not used since these imply the soil is
elastic, and are items that can only be assumed, not measured.

Table 5.1 gives a total number of parameters n of 14. From the
Buckingham Π theorem, the total number of independent dimensionless
groups k that can be derived is n minus the rank r of the dimensional
matrix:

$$k = n - r \qquad\qquad (5.1)$$

For the parameters listed the dimensional matrix is shown as Table
5.2.

TABLE 5.2

Dimensional Matrix of Test Parameters

Parameter	Force (F)	Length (L)	Time (T)
x	0	1	0
H	0	1	0
EI	1	1	0
M	1	0	0
Q	1	-1	0
y	0	1	0
P	1	-2	0
γ	1	-3	0
ϕ	0	0	0
e	0	0	0
g	0	1	-2
a	0	1	-2
t	0	0	1
f_1	0	0	1
v	0	1	-1

The rank of the above matrix is 3. From equation (5.1), therefore, 12 independent dimensionless groups can be determined. They were chosen as follows:

TABLE 5.3

Dimensionless Parameters

Parameter	Symbol	Dimensionless Group
Location	x	x/H
Time	t	tf_1
Moment (bending)	M	MH/EI
Moment (overturning)	M	$6M/\gamma H^3$
Shear force	Q	$Q/(1/2\gamma H^2)$
Pressure	P	$P/\gamma H$
Displacement	y	y/H
Velocity	v	$v/f_1 H$
Acceleration	a	a/g
Friction angle	ϕ	ϕ
Void ratio	e	e
–	–	v^2/gH

In addition, the ratio of bending to overturning moment gives the non-independent dimensionless grouping $\gamma H^4/6EI$ which can be used as an indication of the relative stiffness of the wall-soil system.

In the following sections, unless otherwise noted, a reference to Pressure (P) will imply its dimensionless group $(P/\gamma H)$, reference to

time (t) will imply tf_1, and so forth. This will avoid any
model/prototype confusion, and will also simplify the discussion.

5.2. The Experimental "Earthquake"

Although the "earthquake generating" mechanism employed in the
experiment was quite simple, the recorded motions are such that they are
within the realm of strong earthquake ground motions which have been
recorded in reality.

The accelerograms recorded at the top and bottom of the wall, as
well as the free field (i.e., in the backfill some distance behind the
wall) during various experiments, are displayed in Figures 5.1a through
5.40a. Their corresponding velocities and displacements are shown in
Figures 5.1b through 5.40b and 5.1c through 5.40c respectively.

The displacement curves include both the initial static displace-
ments due to the backfill load (assuming that no backfill implies no
wall deflection) plus those generated by the shaking. The magnitudes of
the displacements prior to the earthquake are greater than 1/2% of the
wall height which indicates a state of plastic equilibrium behind the
wall, and thus the development of full active pressure.

From the accelerograms it can be seen that the general pattern of
shaking is such as one would expect from the motion-generating mechanism
involved, namely that of a decaying sinusoid. However, due to the
inherent complexity of the experimental system, this basic pattern is
enhanced by some extra acceleration noise probably generated from
reverberations, collisions, nonlinearities, etc., of the
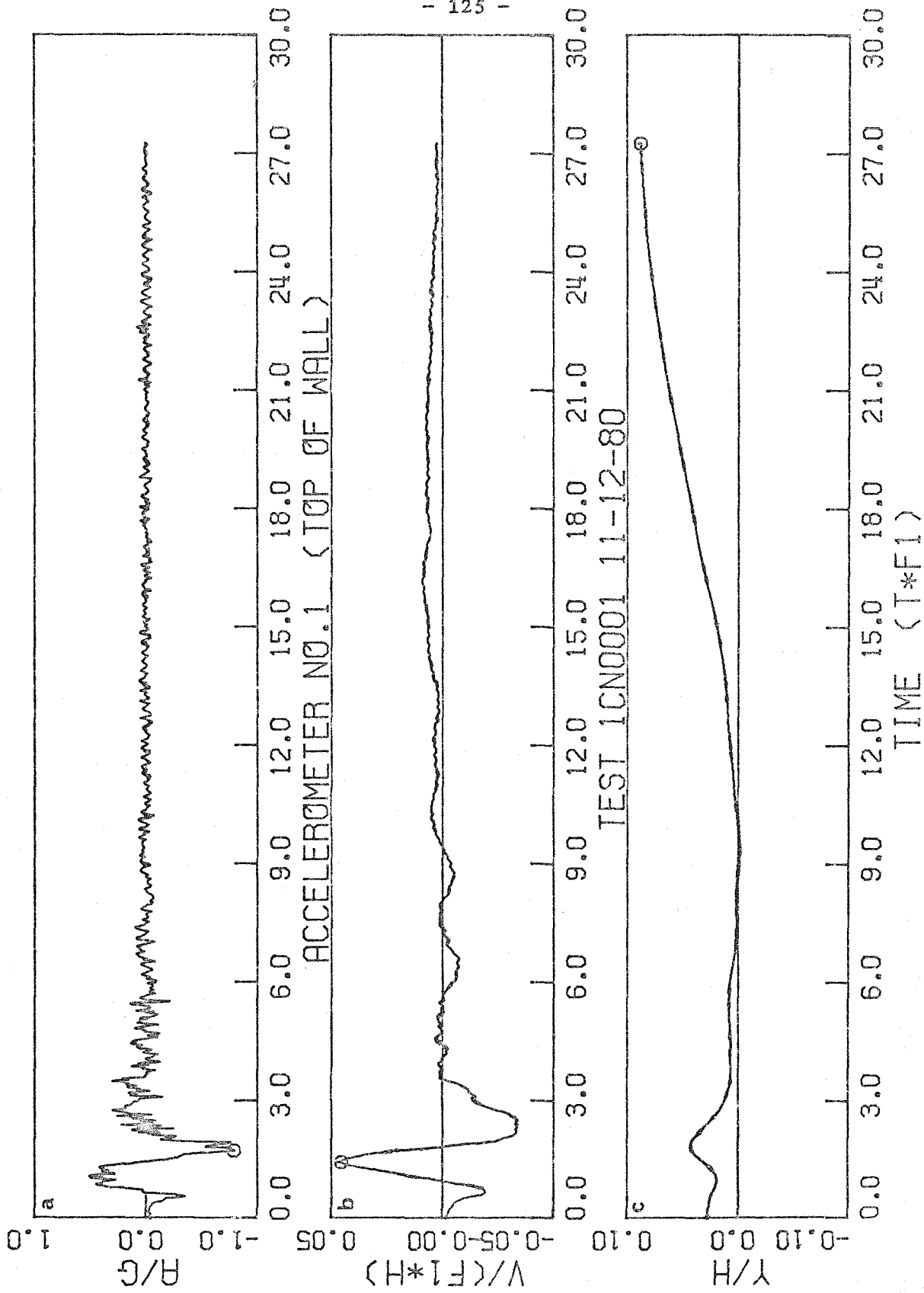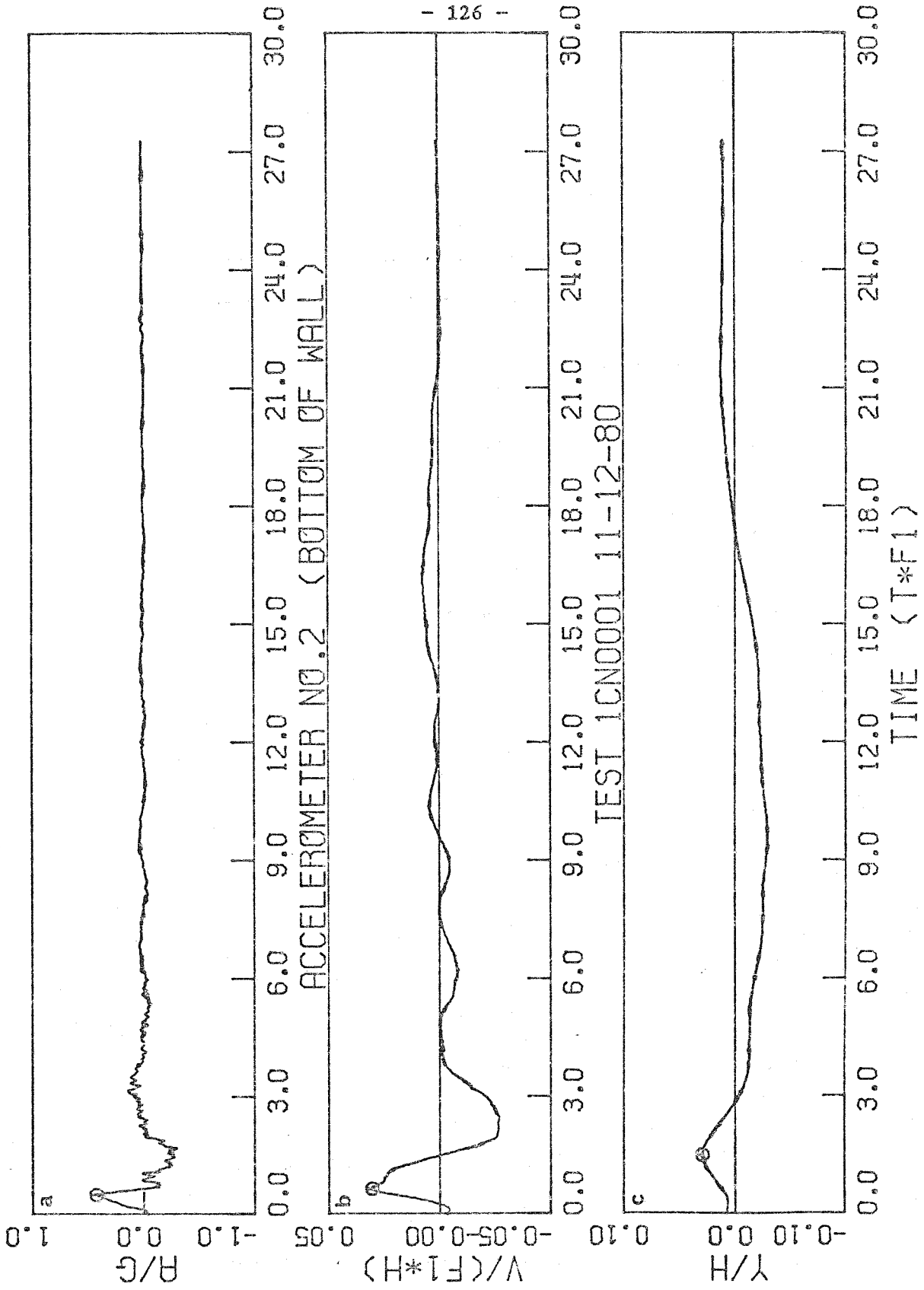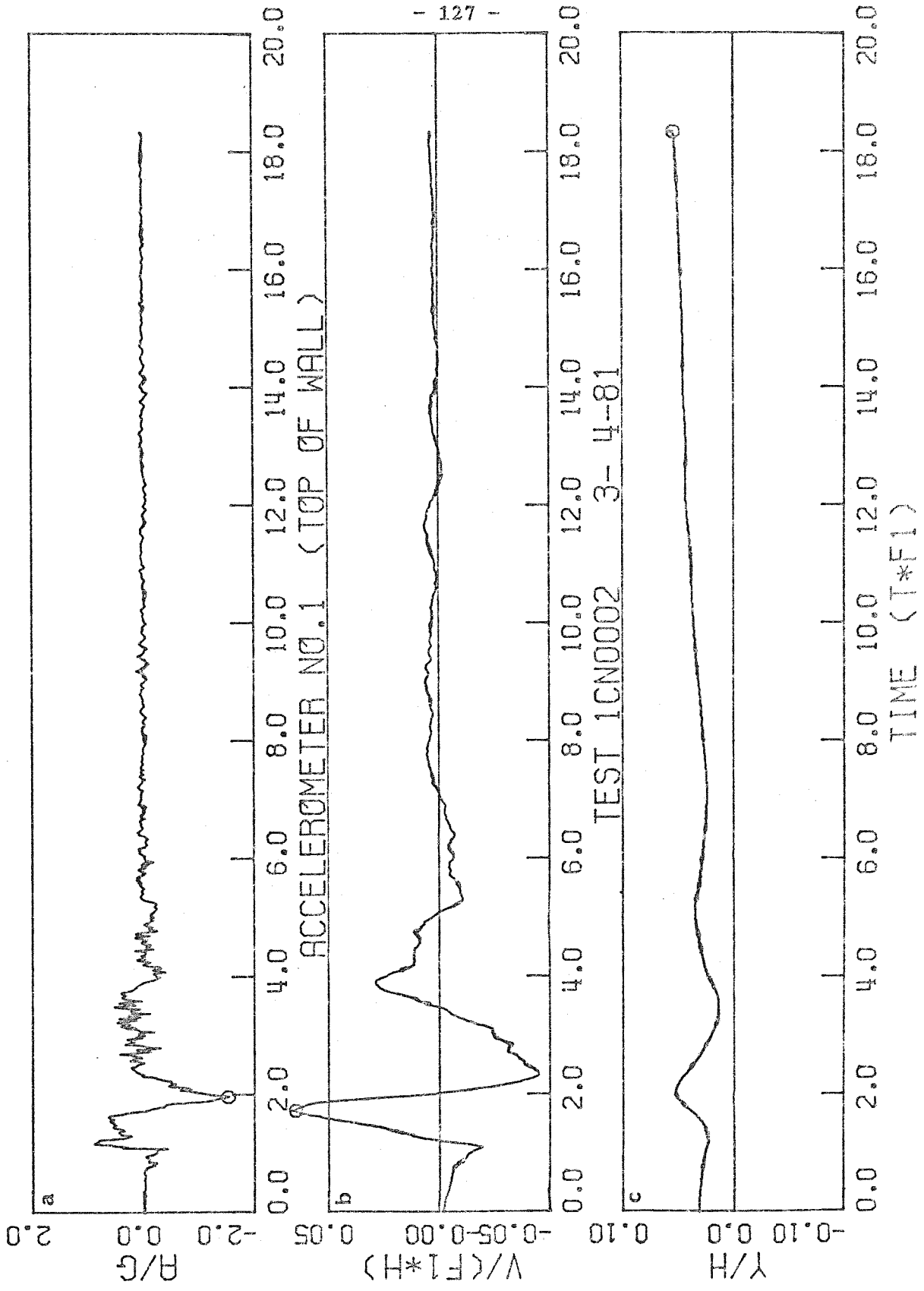
ACCELEROMETER NO. 1 (TOP OF WALL)

TEST 1CN0001 11-12-80

TIME (T*F1)

FIGURE 5.1

ACCELEROMETER NO.2 (BOTTOM OF WALL)

TEST 1CN0001 11-12-80

FIGURE 5.2

FIGURE 5.3

ACCELEROMETER NO.2 (BOTTOM OF WALL)

TEST 1CN0002   3- 4-81

TIME (T*F1)

FIGURE 5.4

FIGURE 5.5

ACCELEROMETER NO.1 (TOP OF WALL)

TEST 1CN1003 3- 9-81

TIME (T*F1)

FIGURE 5.6

FIGURE 5.7

TEST 1CN1003 3- 9-81

ACCELEROMETER NO.2 (BOTTOM OF WALL)

FIGURE 5.8

ACCELEROMETER NO.2 (BOTTOM OF WALL)

TEST 1CN0004 3-16-81

TIME (T*F1)

FIGURE 5.9

FIGURE 5.10

ACCELEROMETER NO.1 (TOP OF WALL)

TEST 1CN1505

TIME (T*F1)
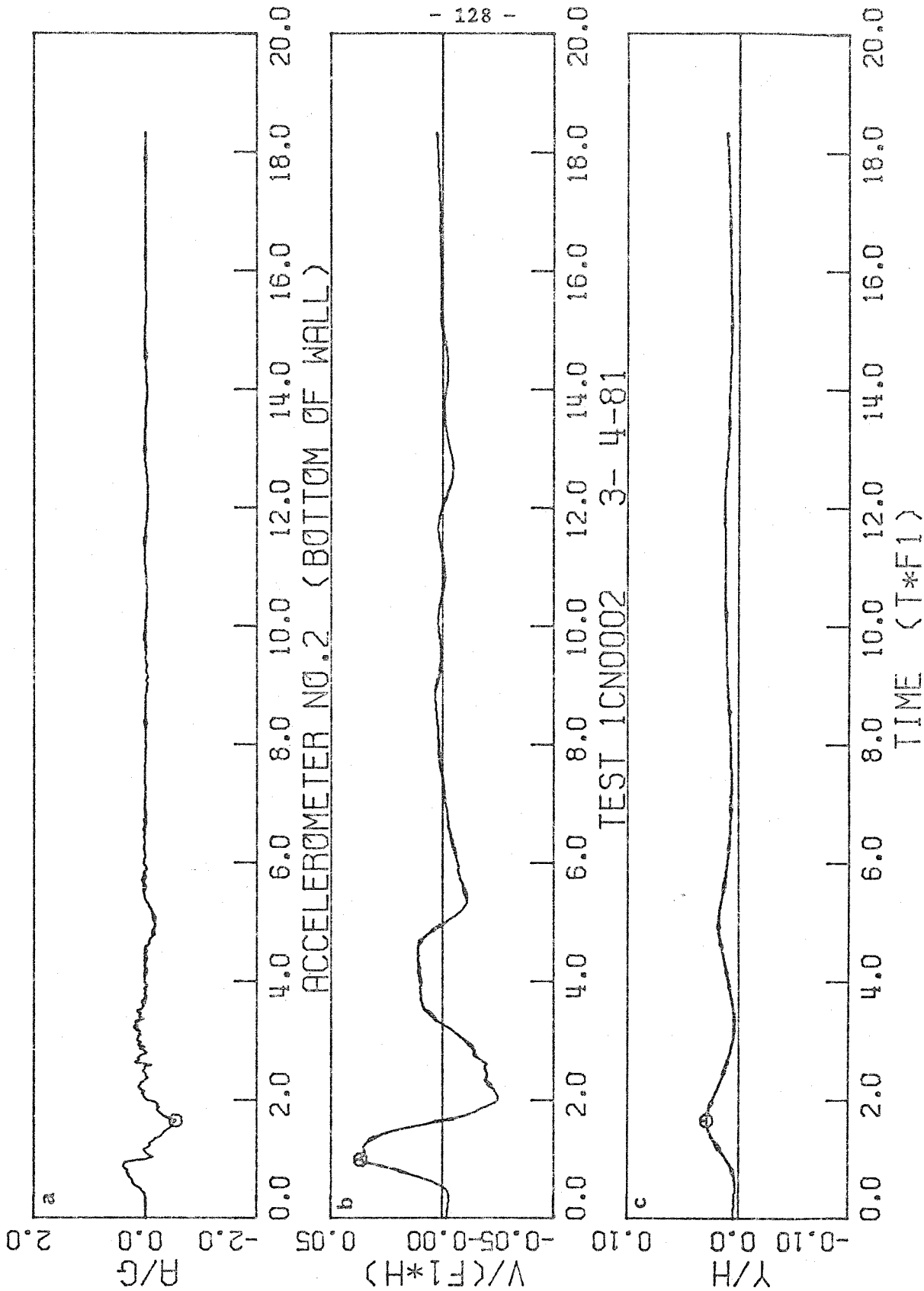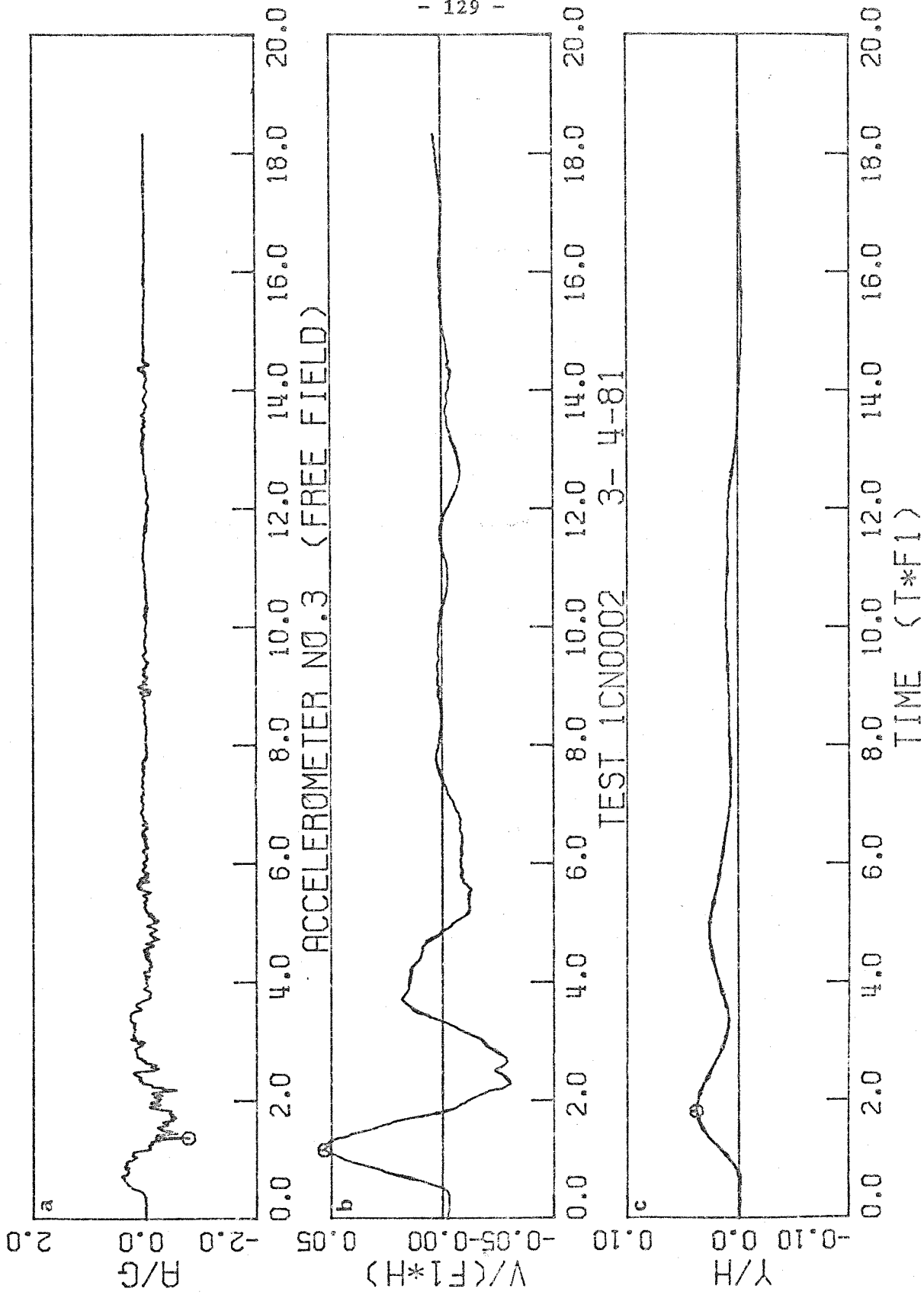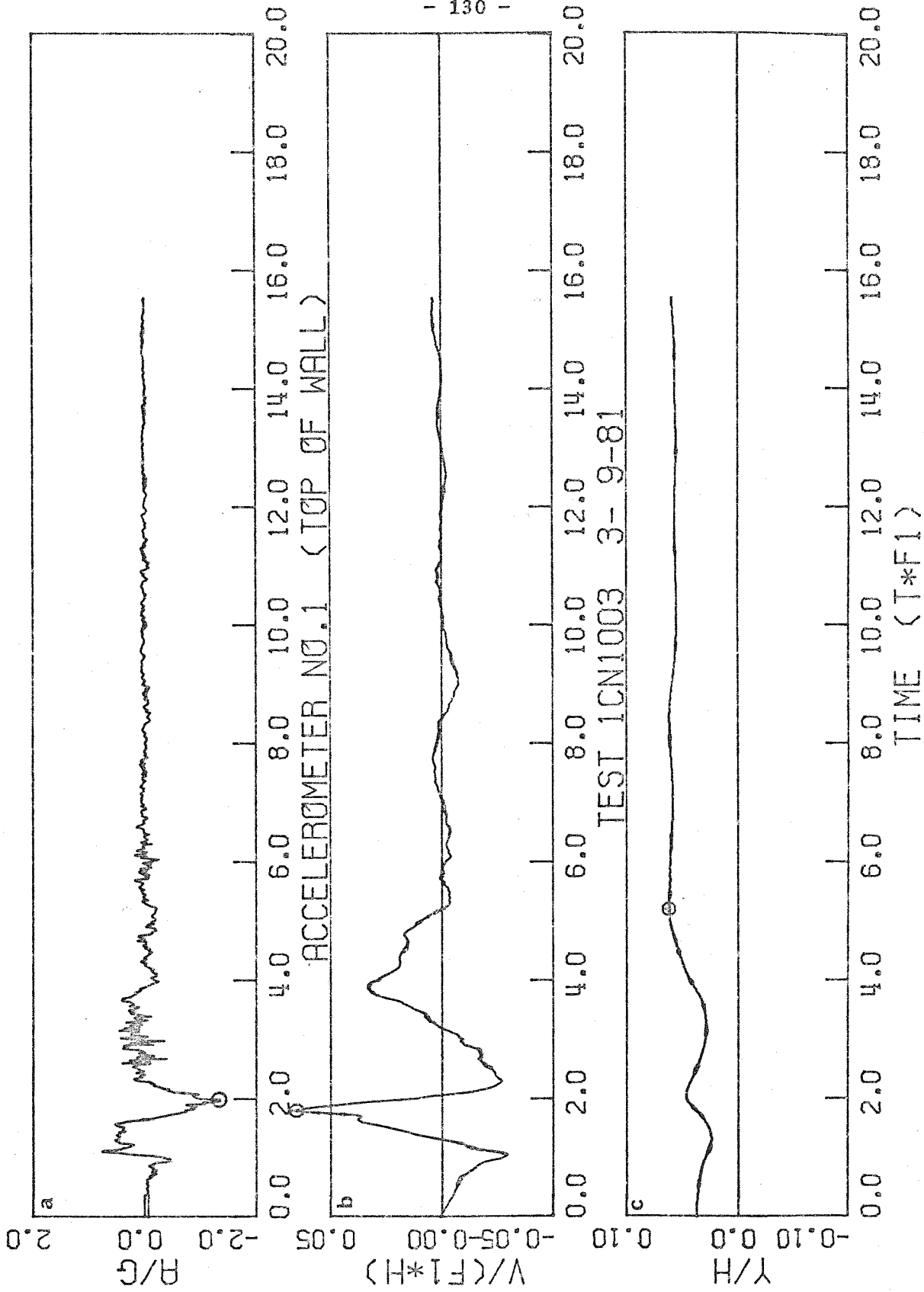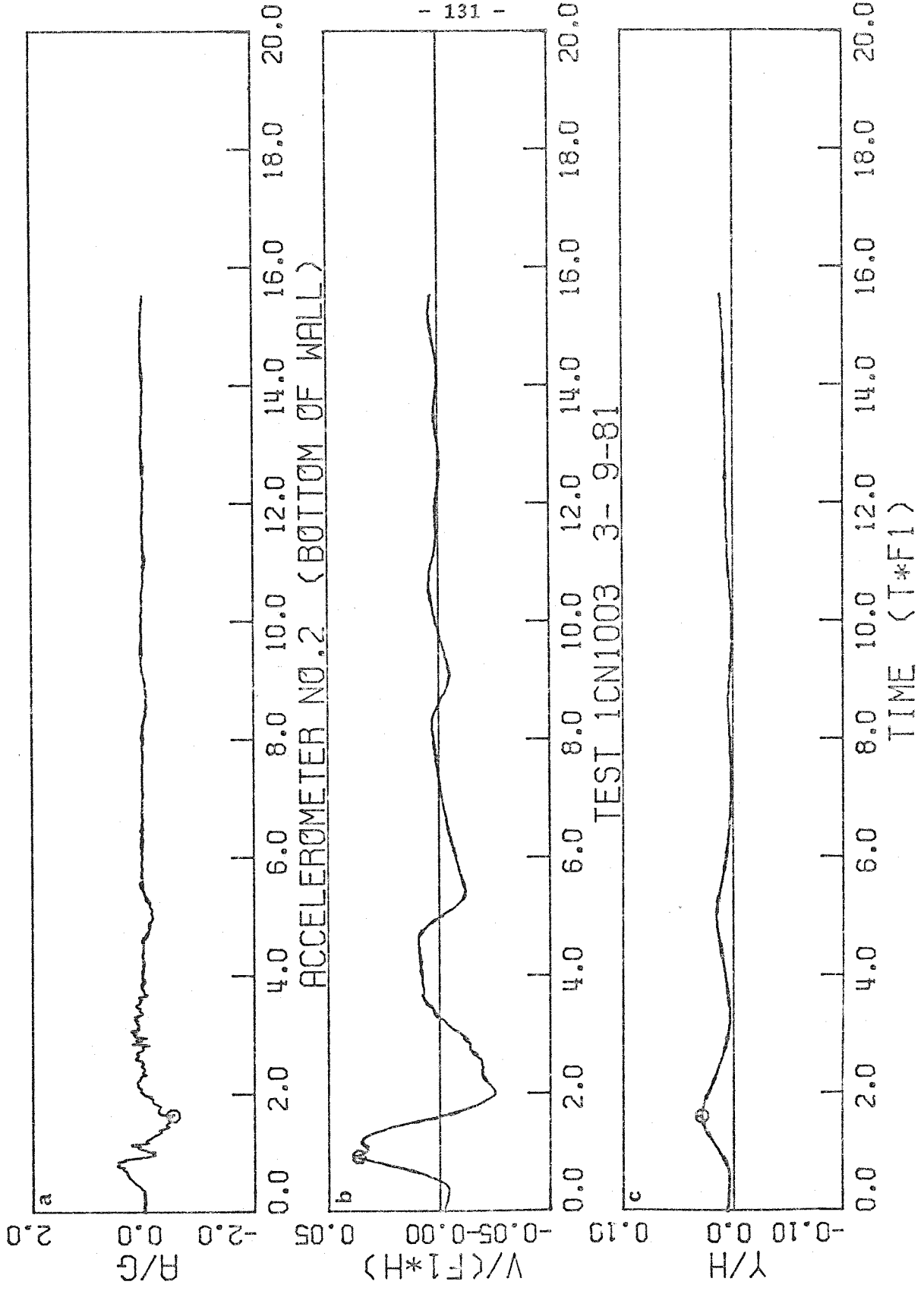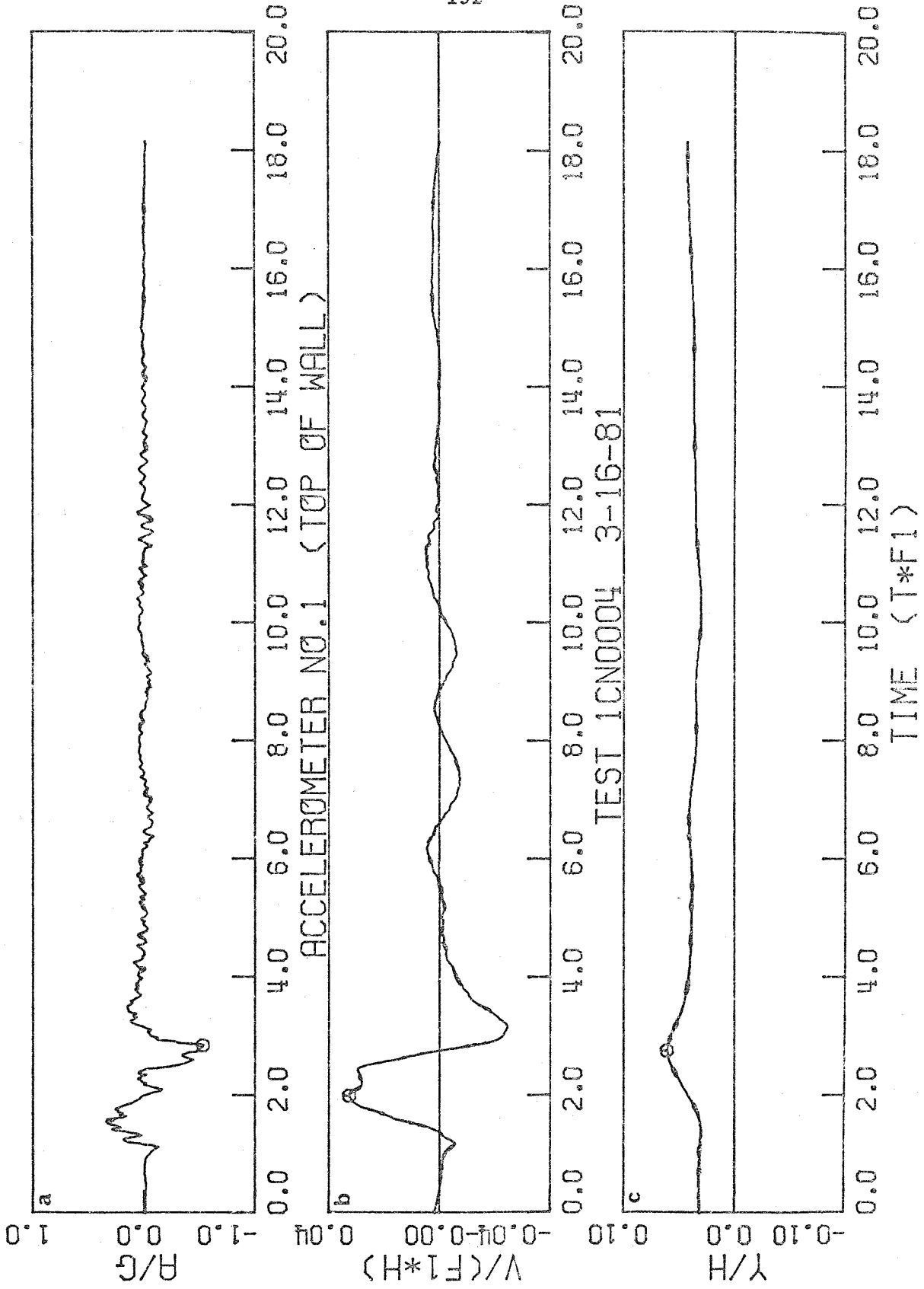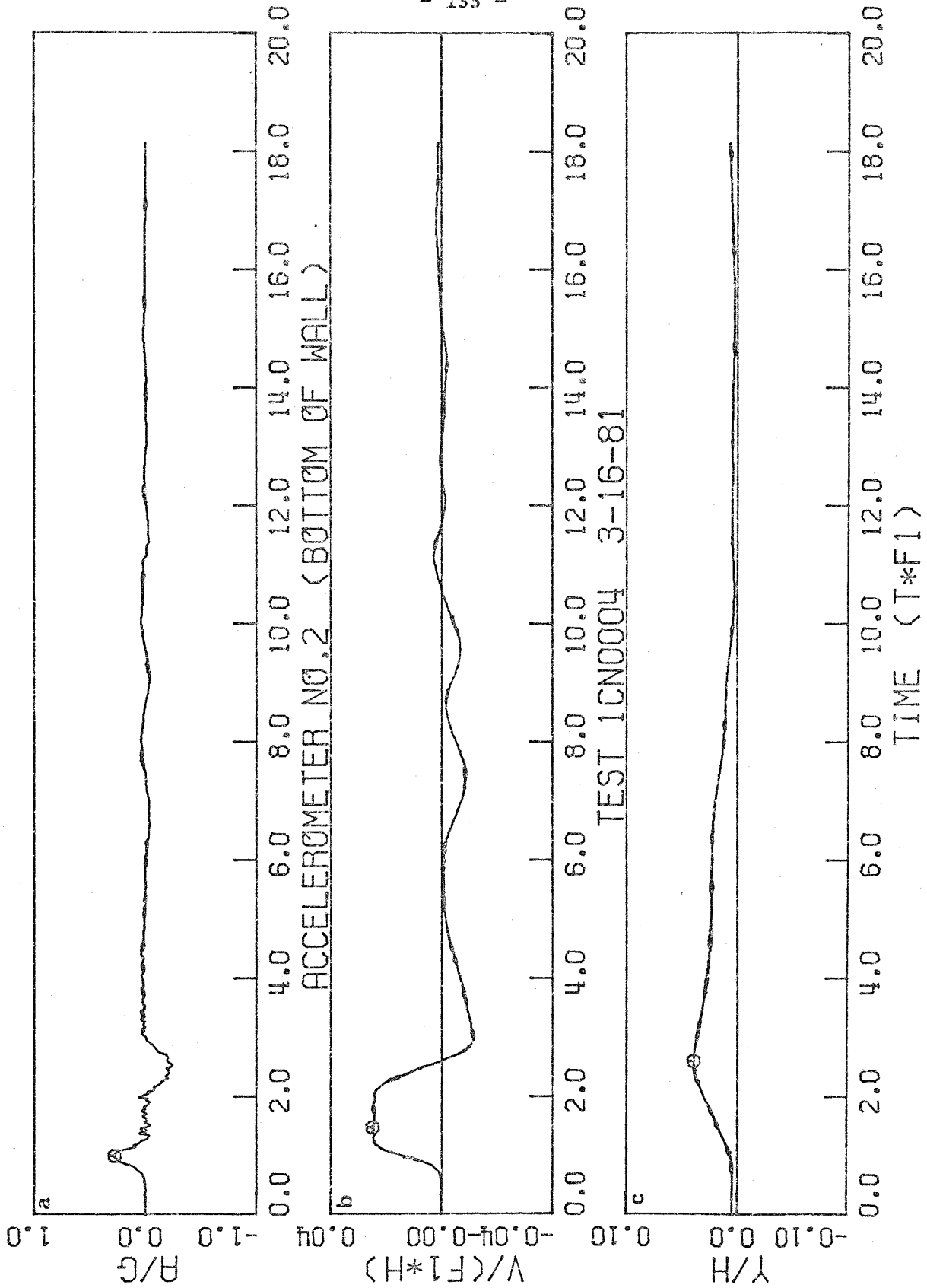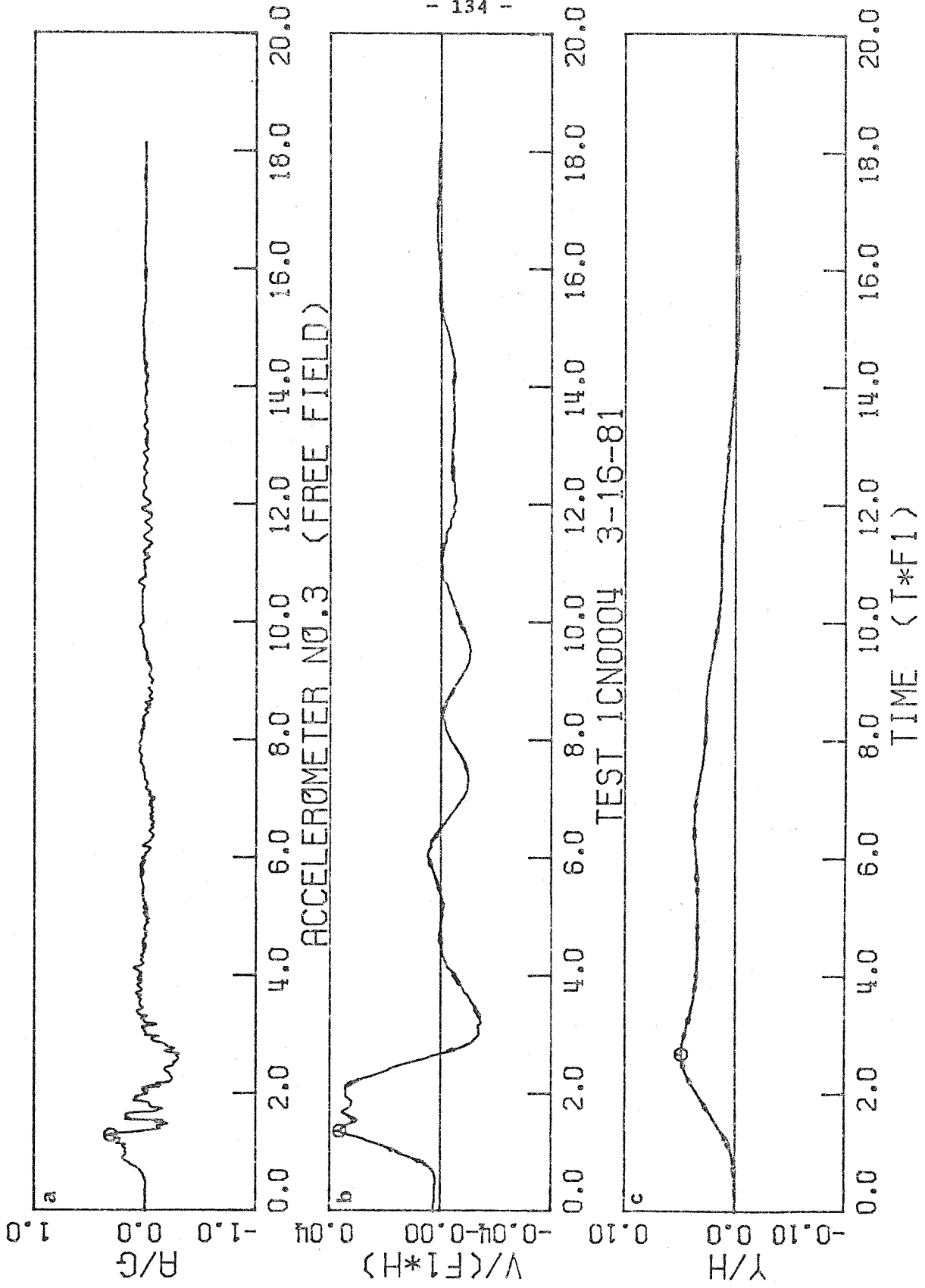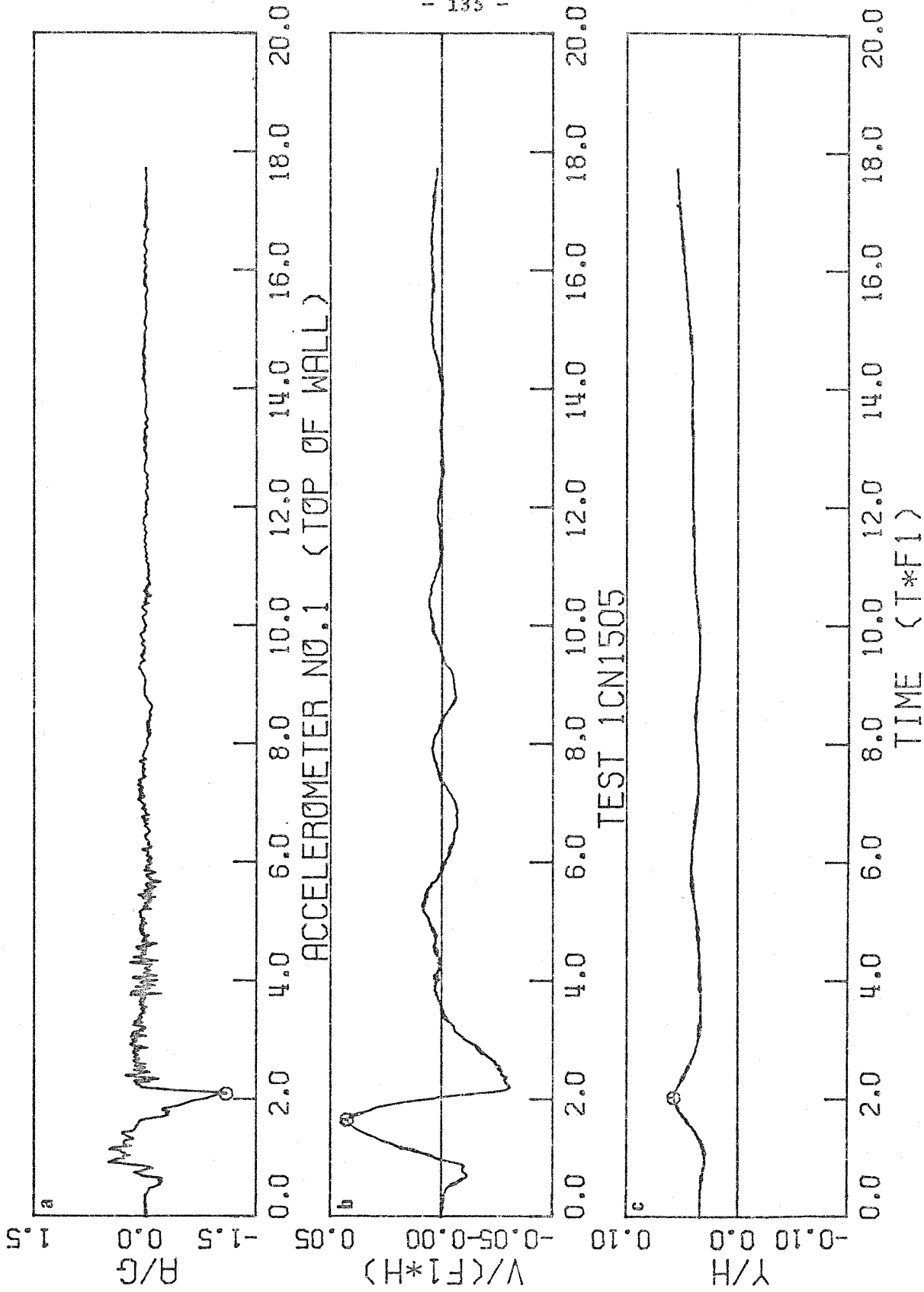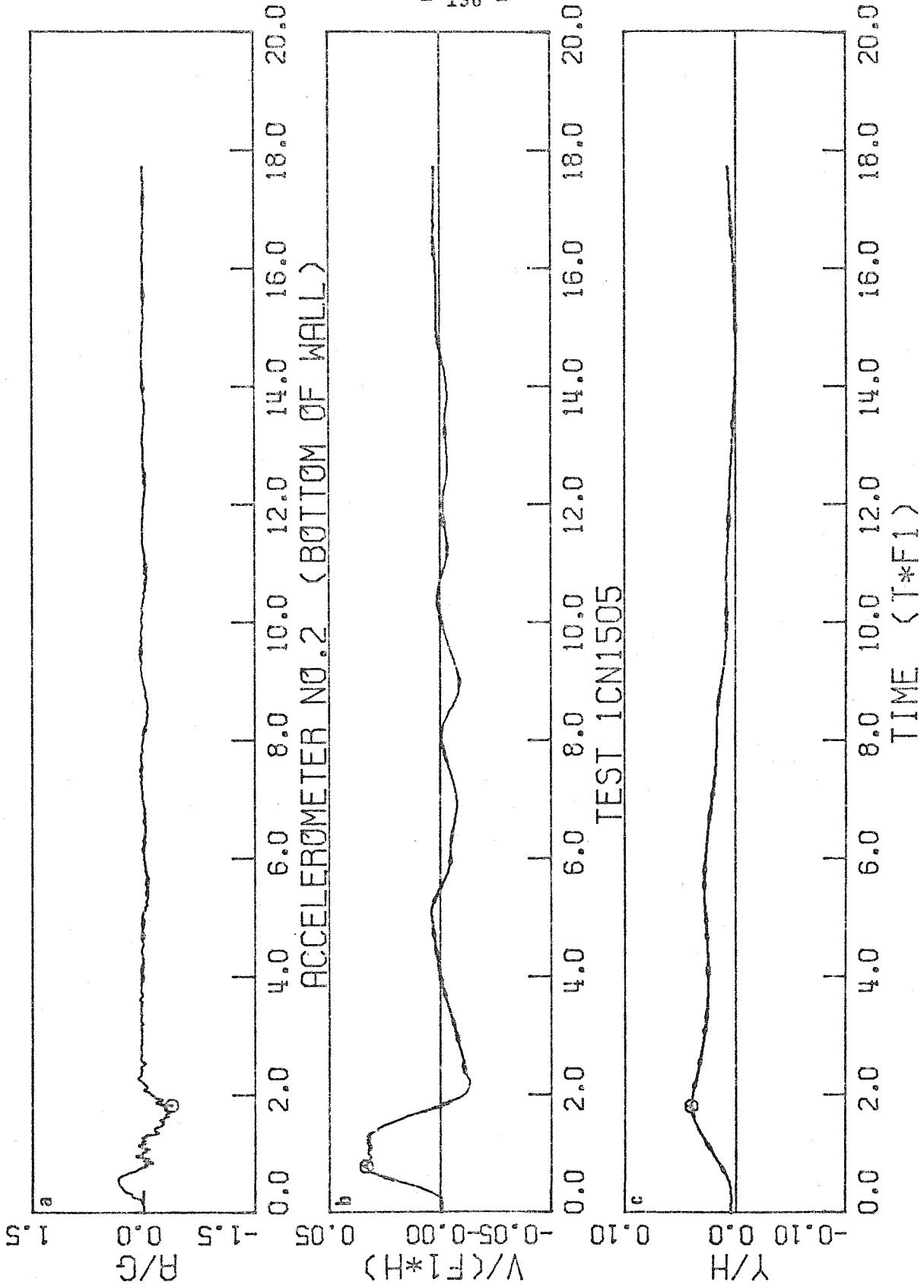
FIGURE 5.11
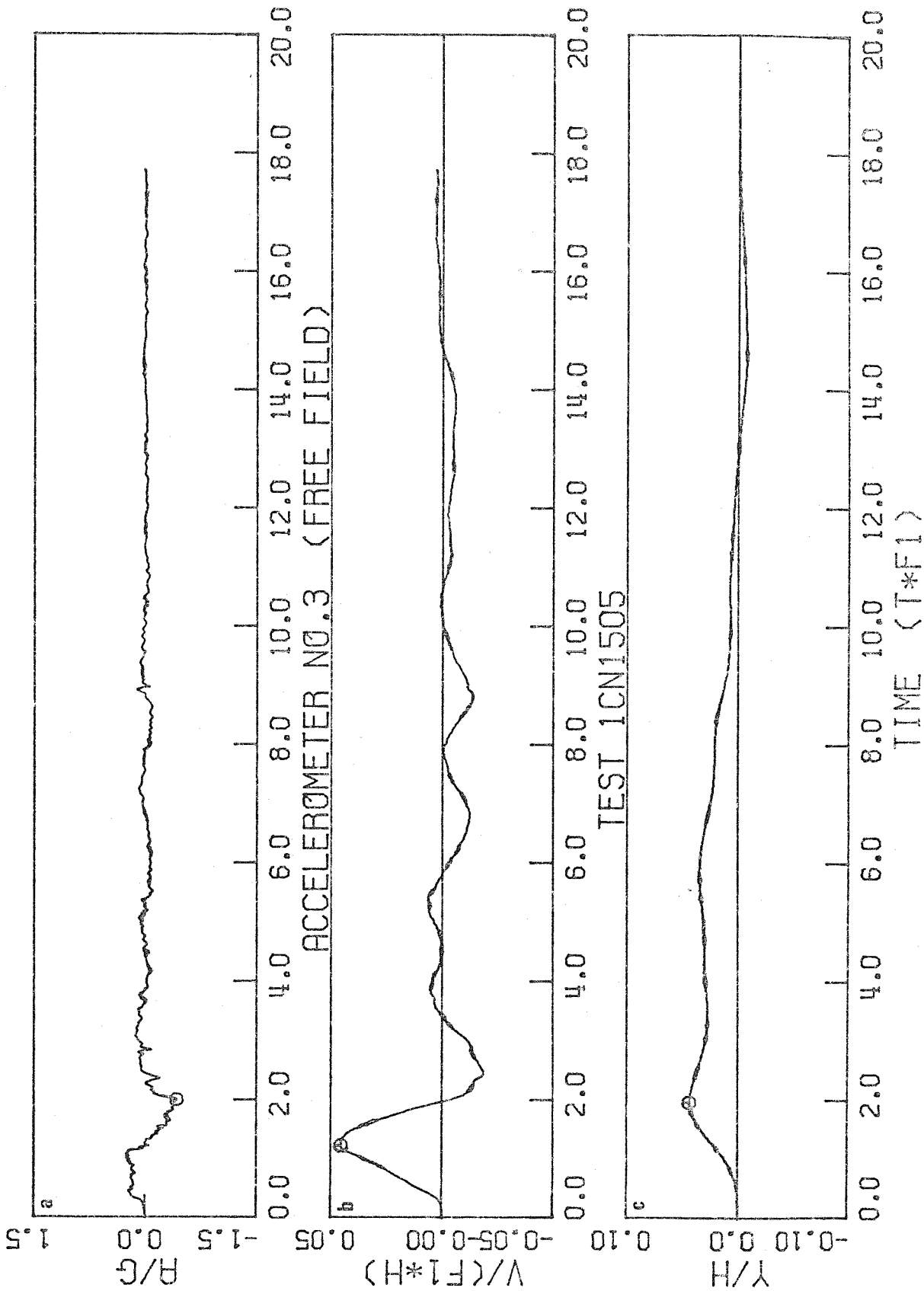
FIGURE 5.12

FIGURE 5.13

FIGURE 5.14

FIGURE 5.15

ACCELEROMETER NO.2 (BOTTOM OF WALL)

TEST 1CN0006 8-6-81

TIME (T*F1)

ACCELEROMETER NO.3 (FREE FIELD)

TEST 1CN0006 8-6-81

TIME (T*F1)

FIGURE 5.16

ACCELEROMETER NO.1 (TOP OF WALL)

TEST 1CN0007 2-15-82

TIME (T*F1)

FIGURE 5.17

FIGURE 5.18

ACCELEROMETER NO.2 (BOTTOM OF WALL)

TEST 1CN0007 2-15-82

ACCELEROMETER NO.3 (FREE FIELD)

TEST 1CN0007 2-15-82

TIME (T*F1)
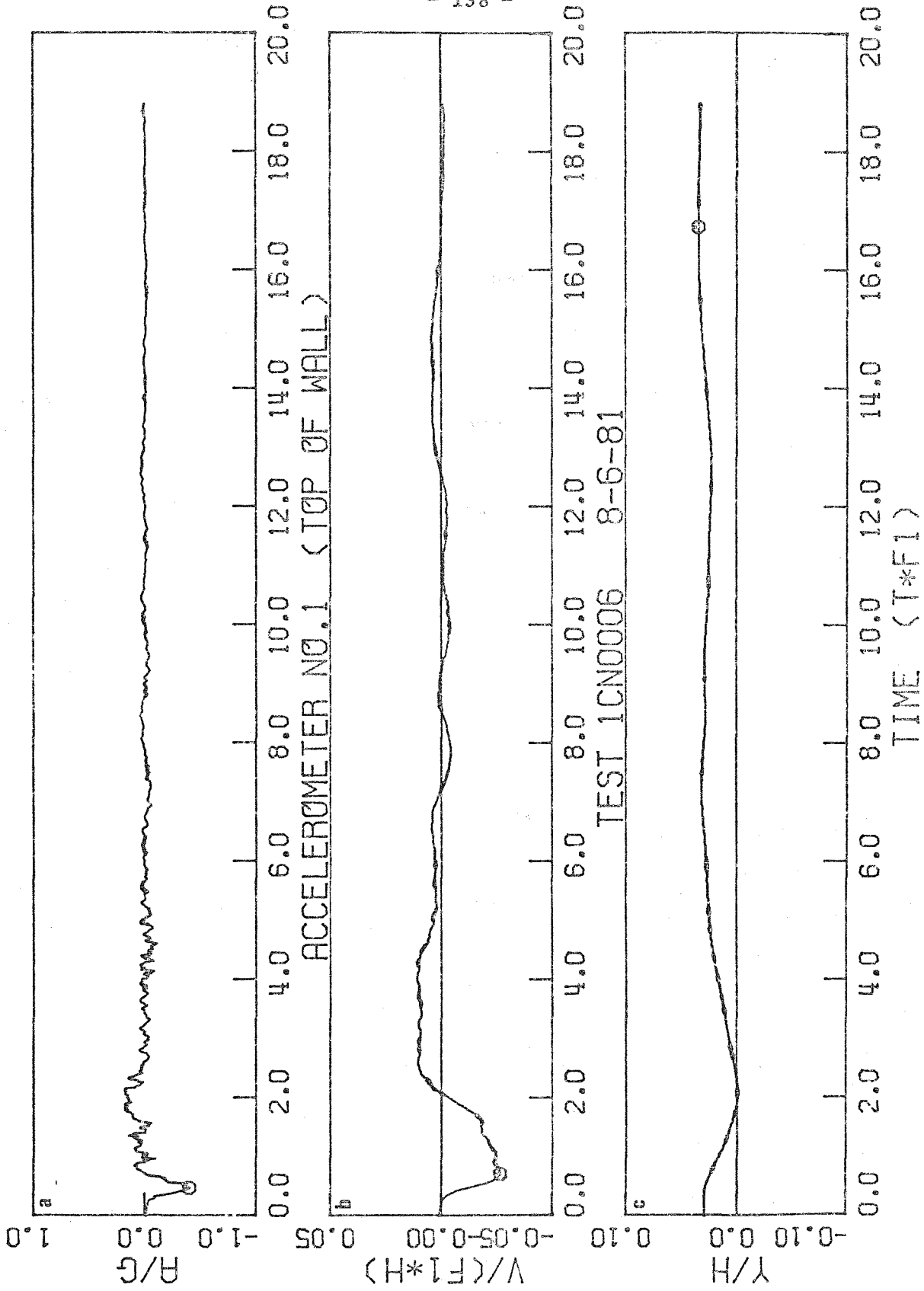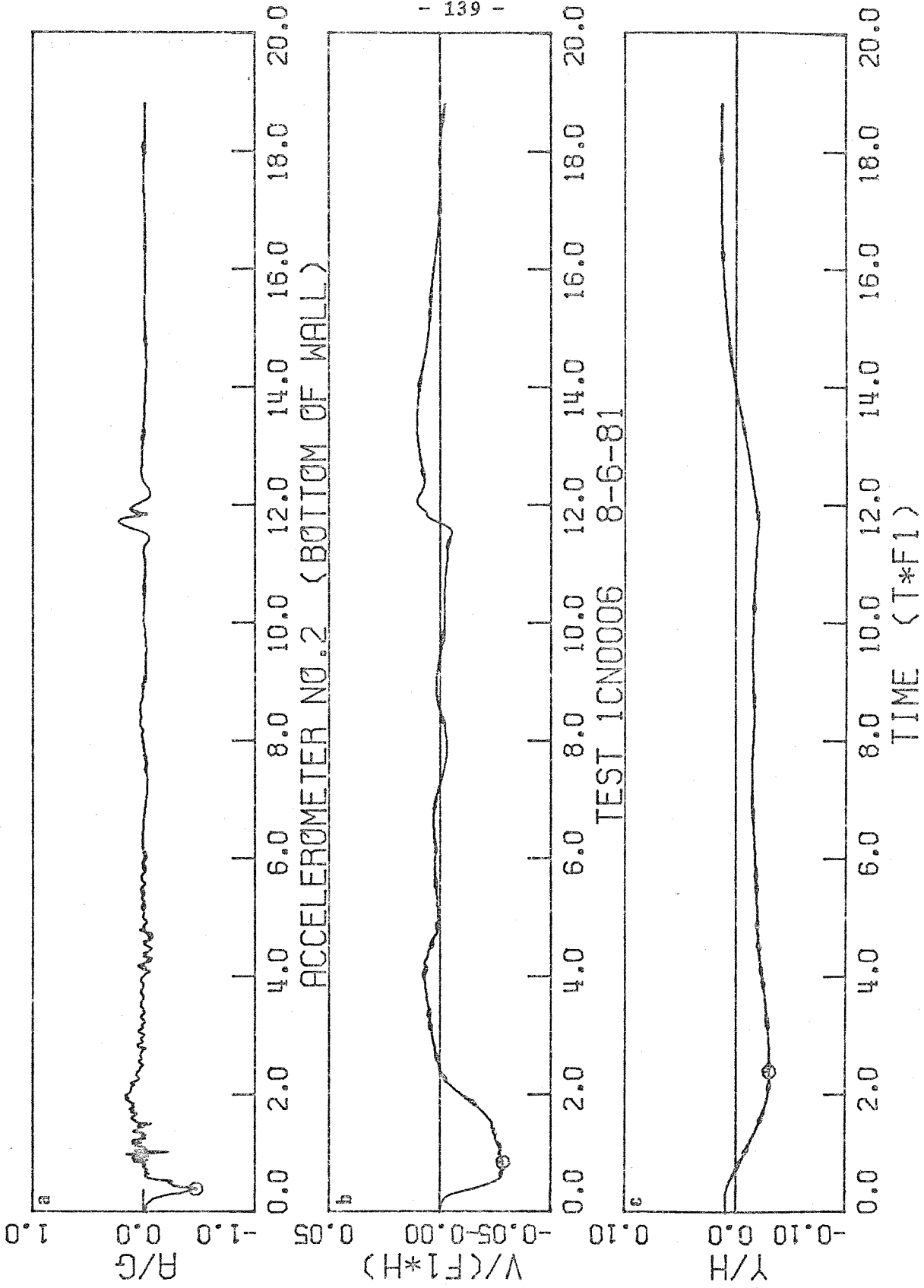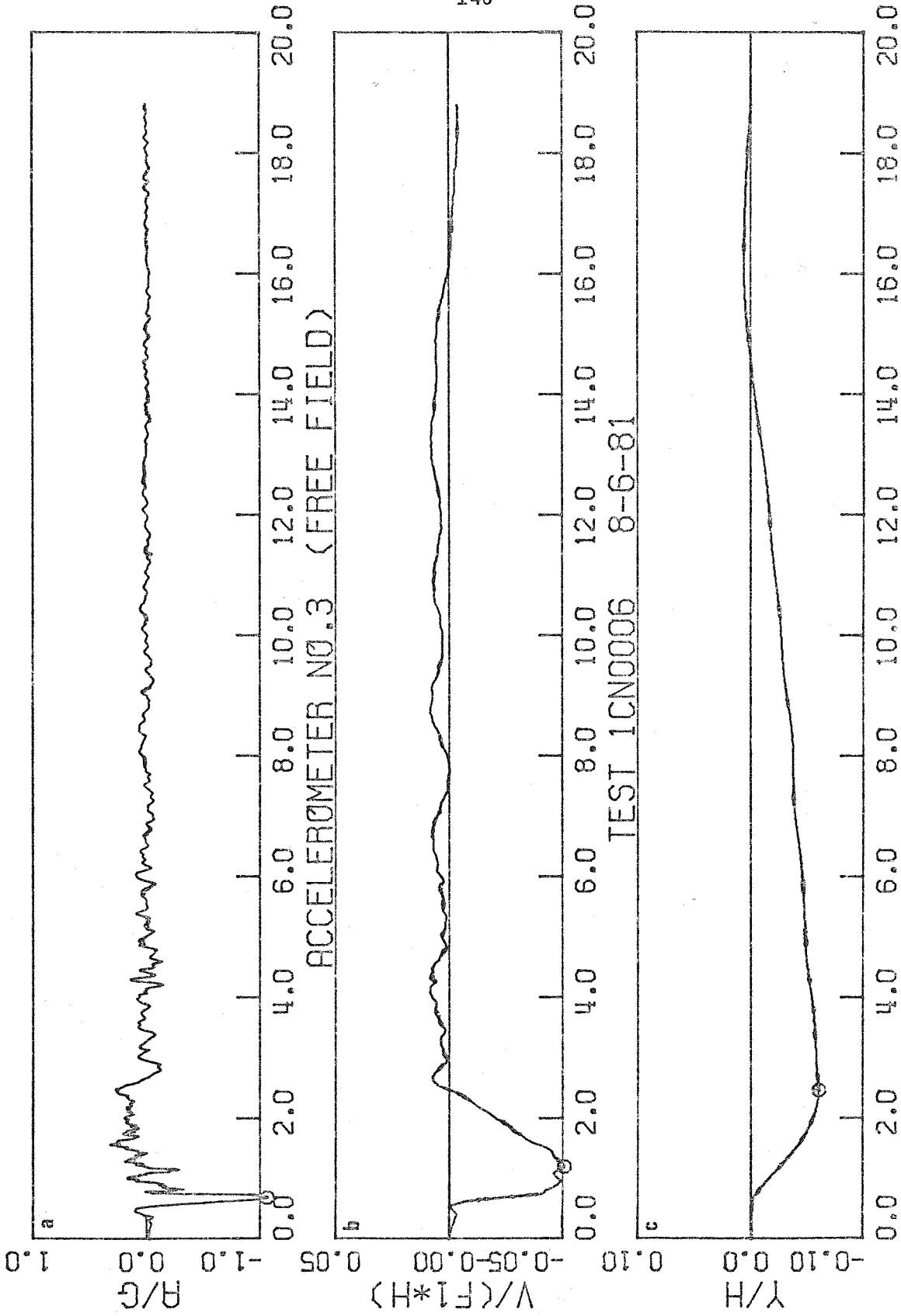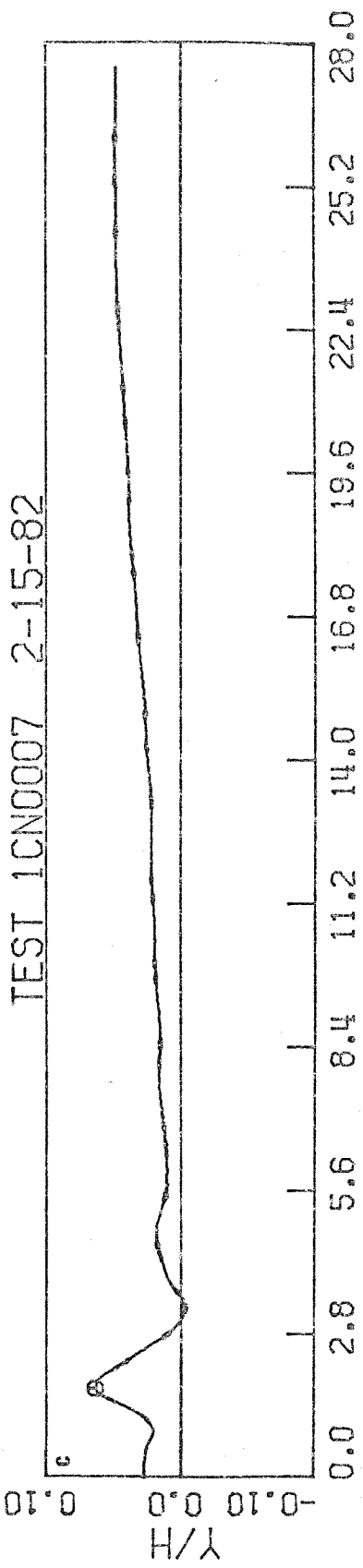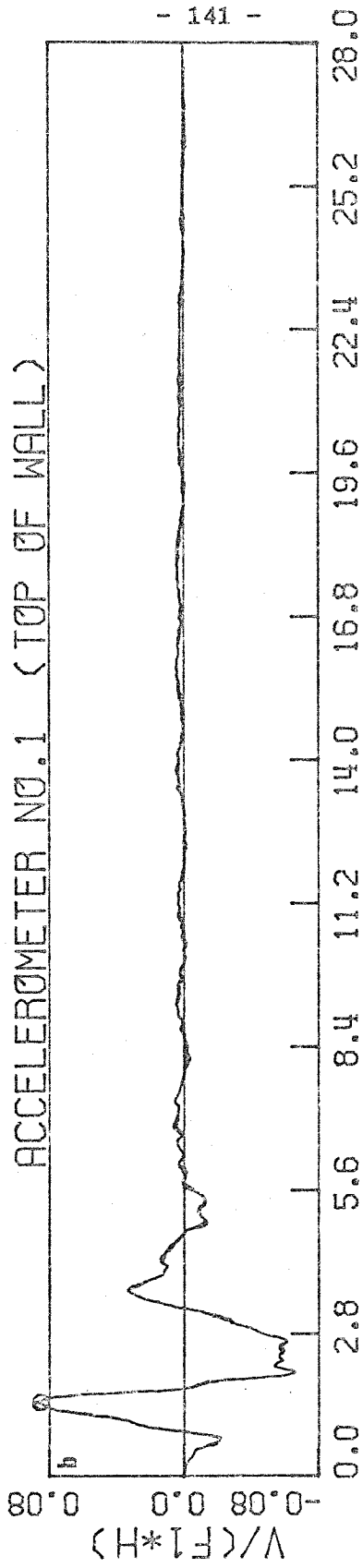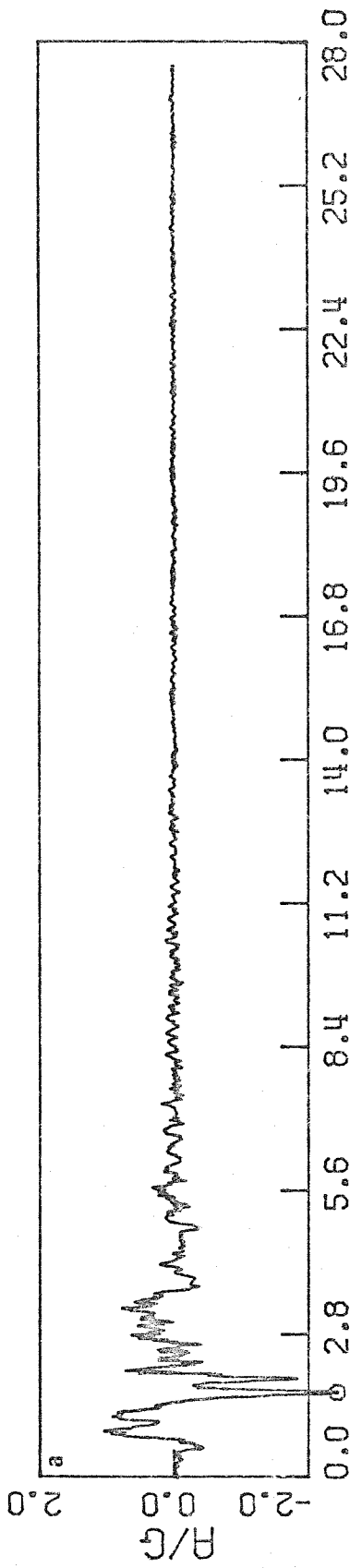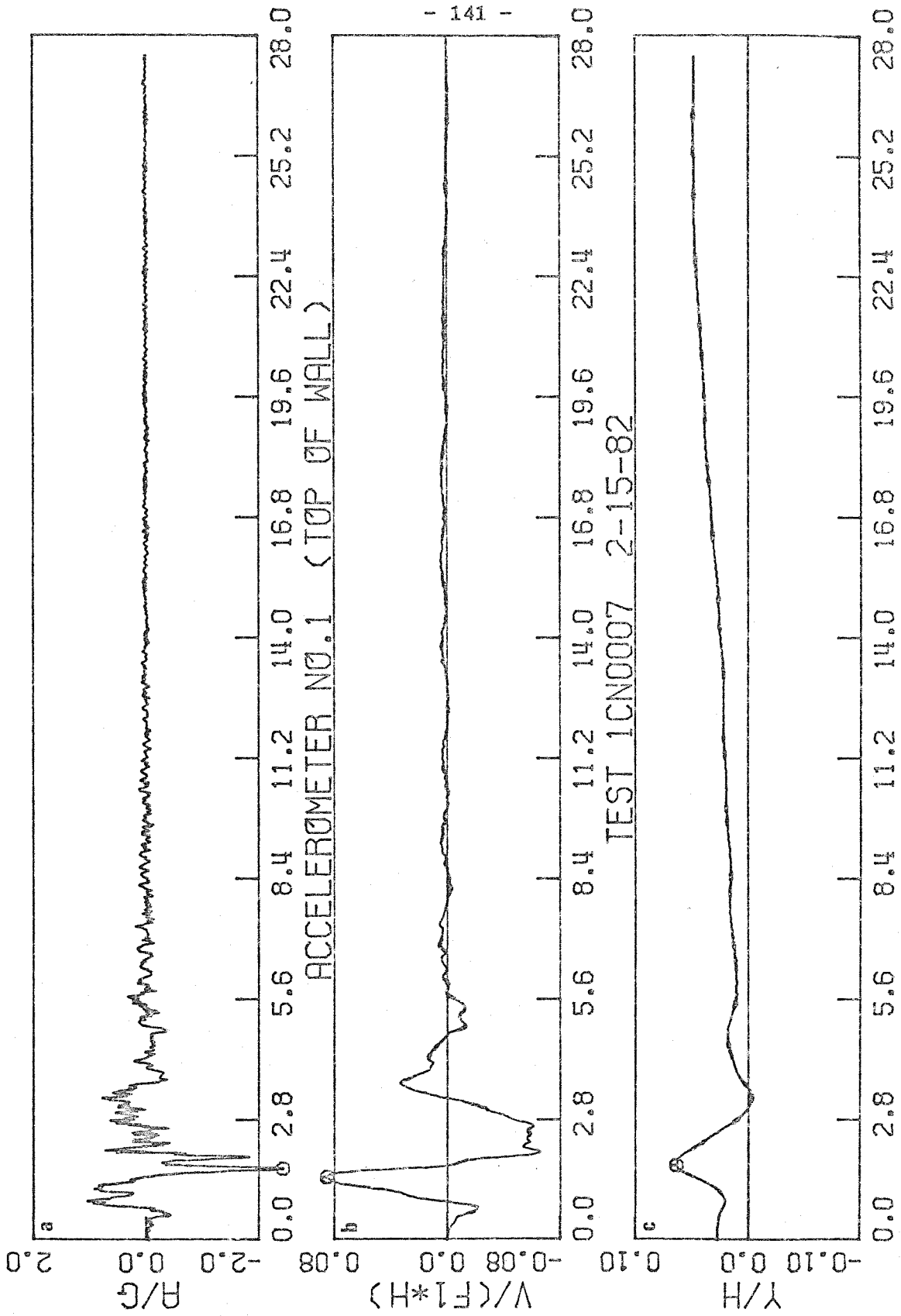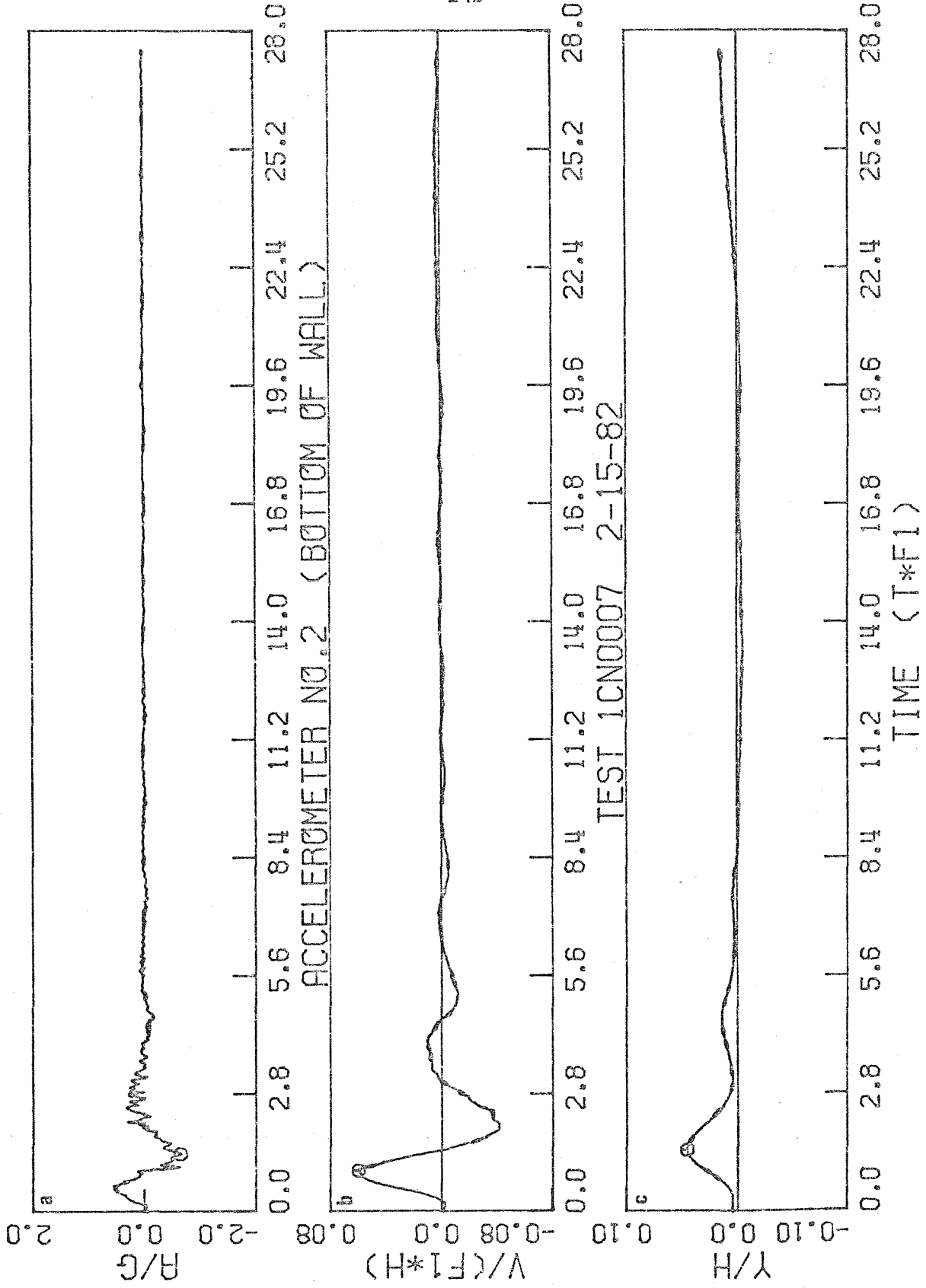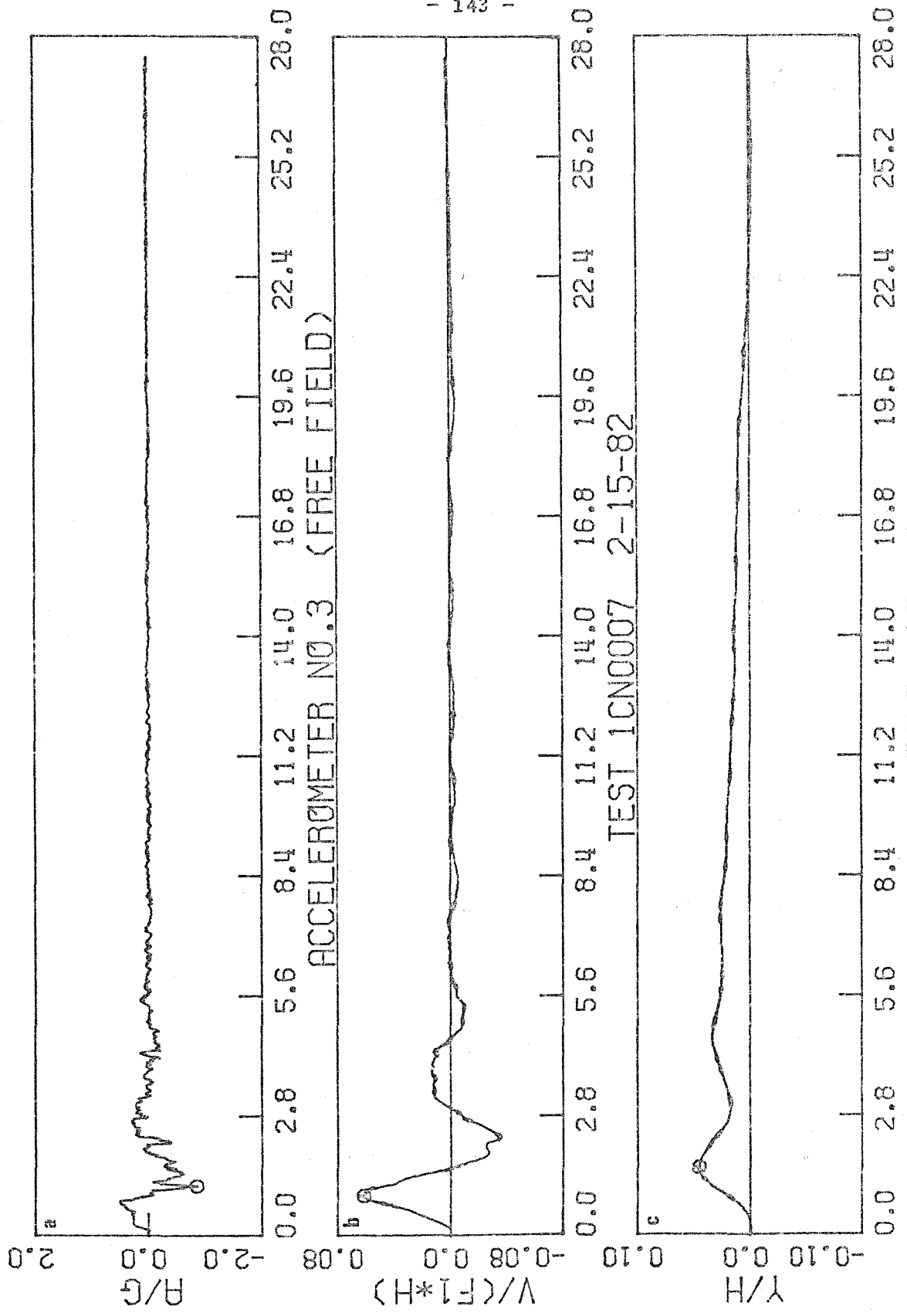
FIGURE 5.19

FIGURE 5.20

FIGURE 5.21

ACCELEROMETER NO.2 (BOTTOM OF WALL)

TEST 1CN0508 2-16-82

TIME (T*F1)

ACCELEROMETER NO.3 (FREE FIELD)

TEST 1CN0508 2-16-82

TIME (T*F1)

FIGURE 5.22

FIGURE 5.23

ACCELEROMETER NO.2 (BOTTOM OF WALL)

TEST 1CN1009 2-17-82

TIME (T*F1)

FIGURE 5.24

ACCELEROMETER NO.3 (FREE FIELD)

TEST 1CN1009 2-17-82

TIME (T*F1)

FIGURE 5.25

ACCELEROMETER NO. 1 (TOP OF WALL)

TEST 1CN1510 2-19-82

TIME (T*F1)

FIGURE 5.26

FIGURE 5.27

ACCELEROMETER NO.3 (FREE FIELD)

TEST 1CN1510 2-19-82

FIGURE 5.28

FIGURE 5.29

ACCELEROMETER NO.1 (TOP OF WALL)

TEST 2CN0011 2-25-82

ACCELEROMETER NO. 2 (BOTTOM OF WALL)

TEST 2CN0011 2-25-82

FIGURE 5.30

ACCELEROMETER NO.3 (FREE FIELD)
TEST 2CN0011 2-25-82

FIGURE 5.31

FIGURE 5.32

FIGURE 5.33

ACCELEROMETER NO. 2 (BOTTOM OF WALL)

TEST 2CN0012 3- 8-82

TIME (T*F1)

FIGURE 5.34

ACCELEROMETER NO. 3 (FREE FIELD)

TEST 2CN0012 3- 8-82

TIME (T*F1)

ACCELEROMETER NO.1 (TOP OF WALL)

TEST 2CN1013 3-8-82

TIME (T*F1)

FIGURE 5.35

ACCELEROMETER NO.2 (BOTTOM OF WALL)

TEST 2CN1013 3- 8-82

FIGURE 5.36

ACCELEROMETER NO.3 (FREE FIELD)

TEST 2CN1013 3- 8-82

TIME (T*F1)
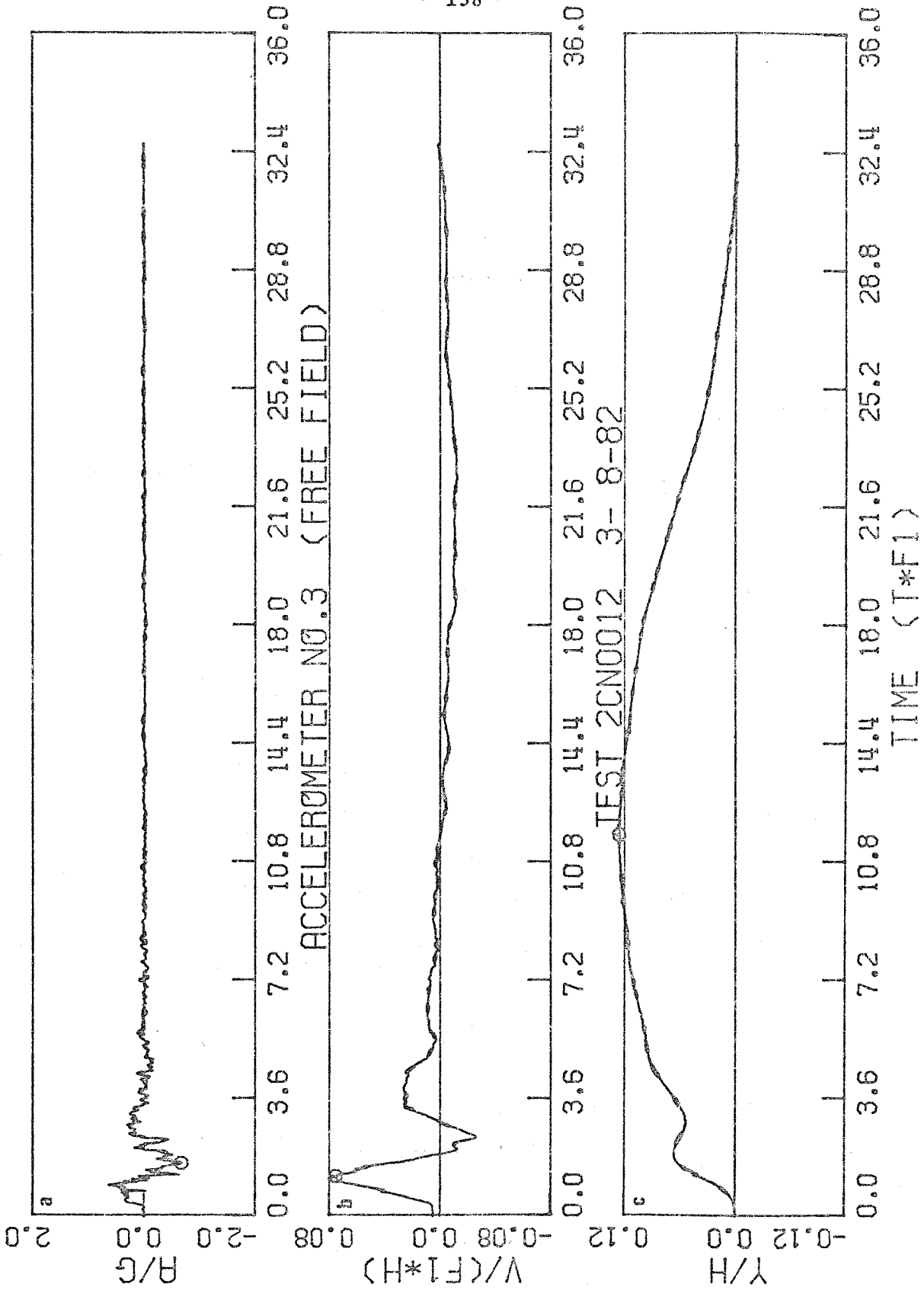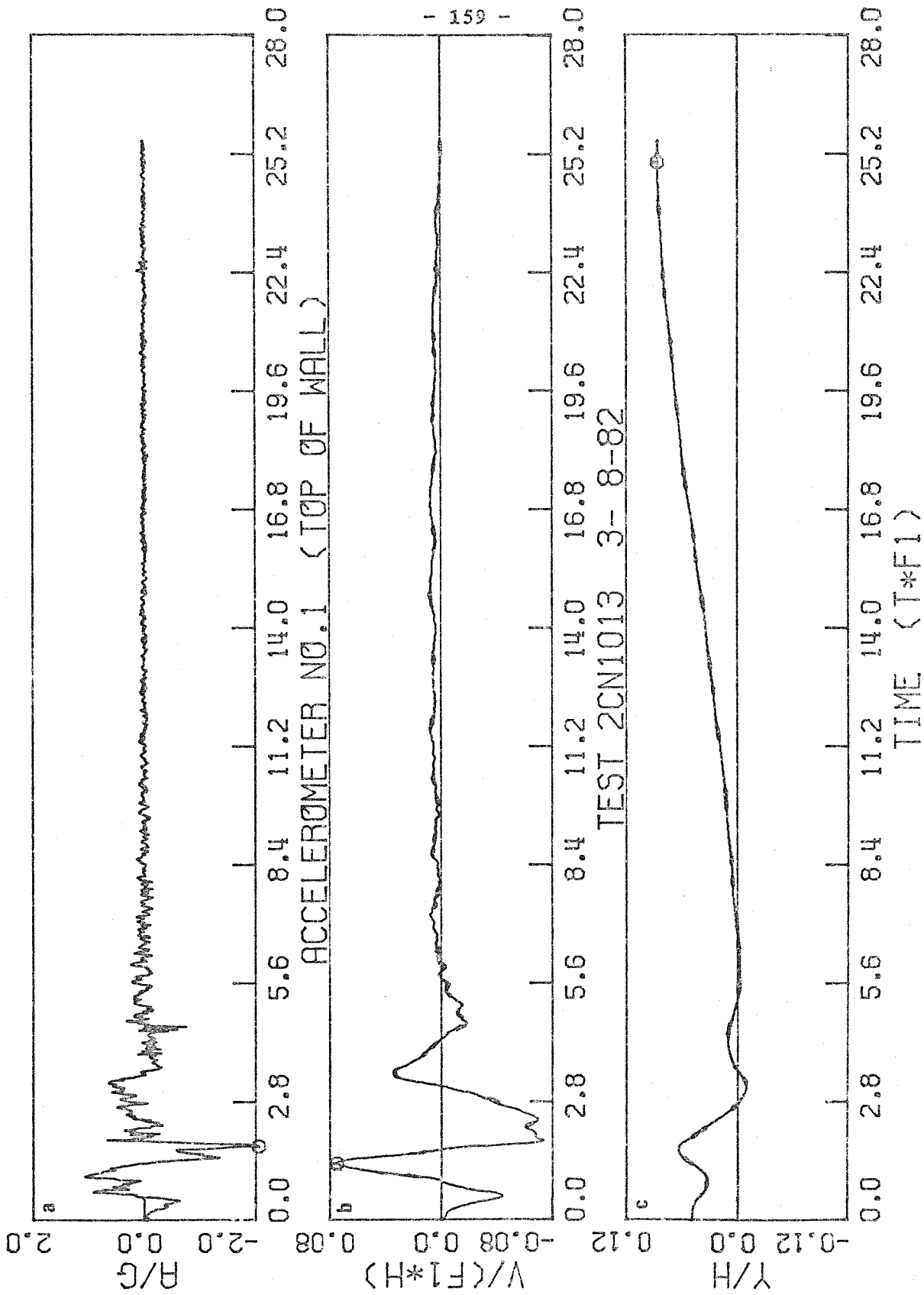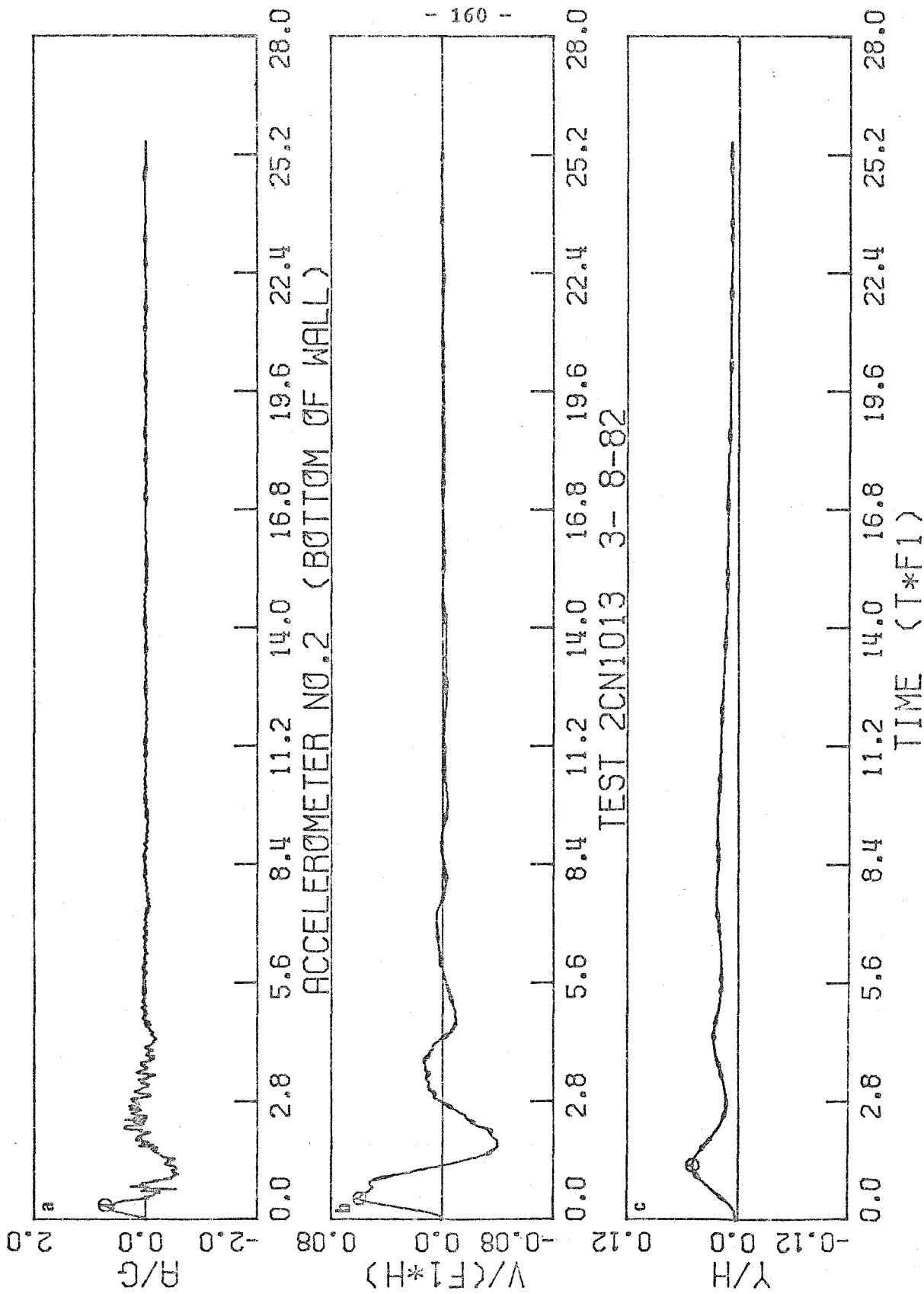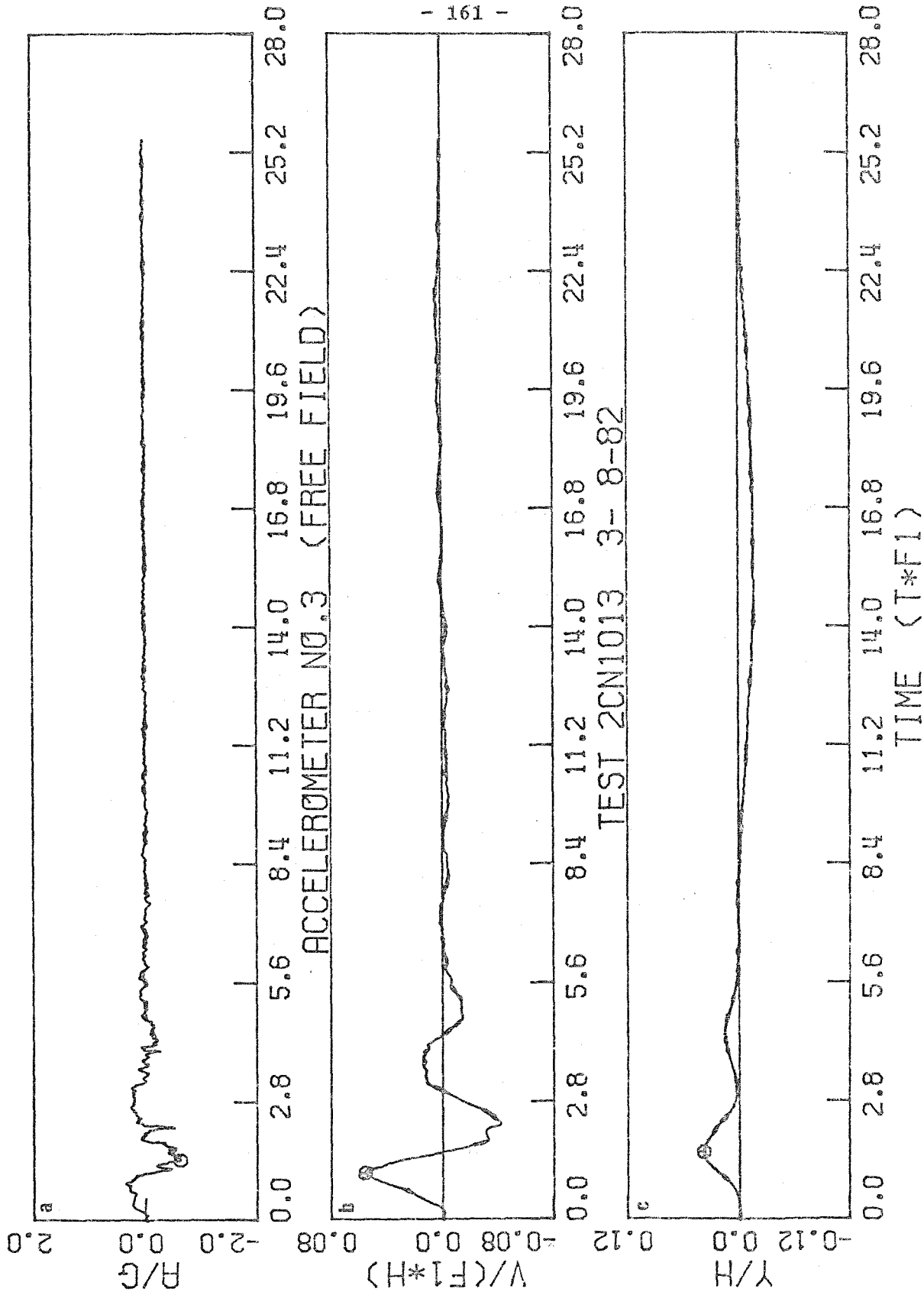
FIGURE 5.37

FIGURE 5.38

FIGURE 5.39

ACCELEROMETER NO.3 (FREE FIELD)

TEST 2CN1514 3-9-82
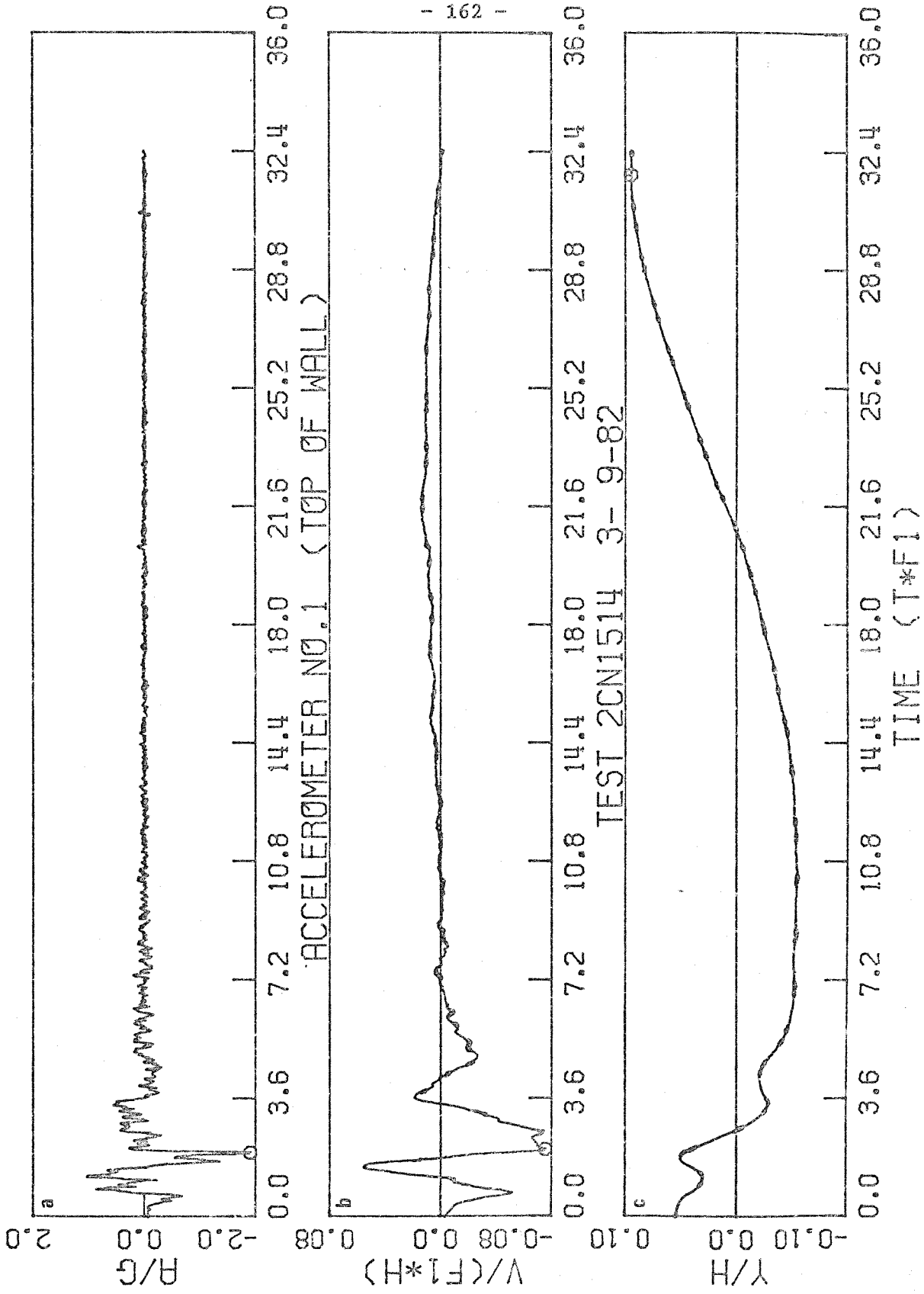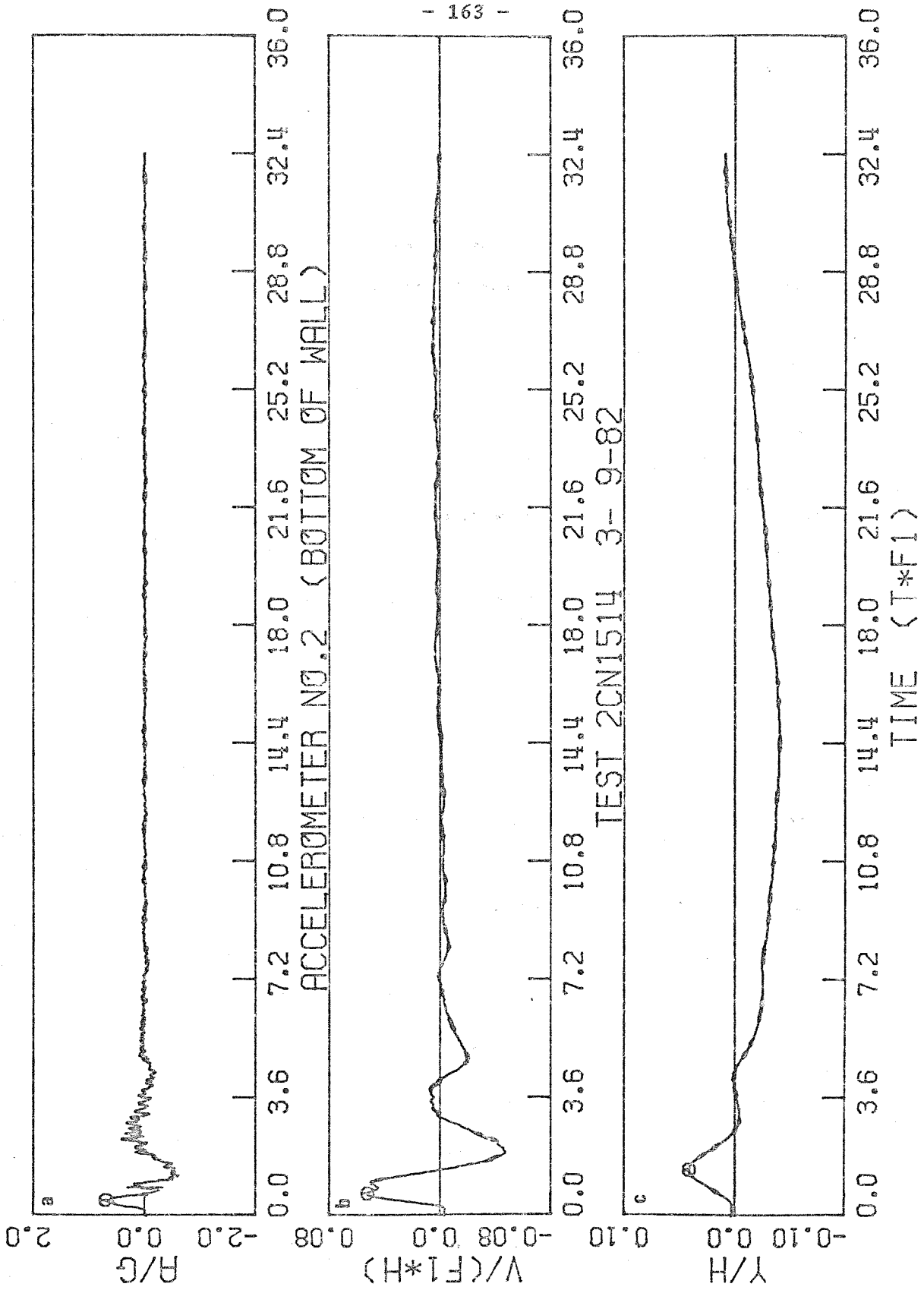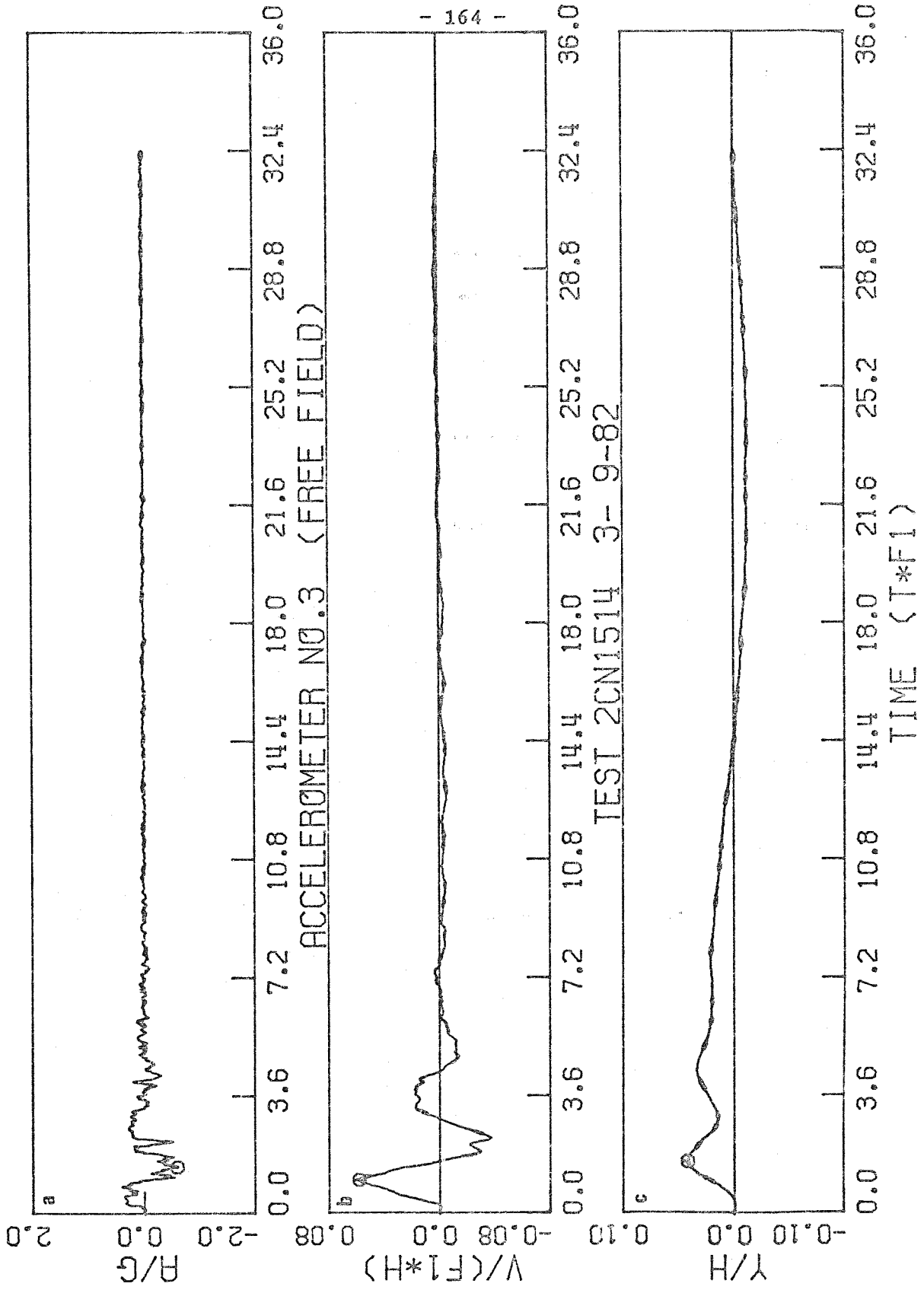
FIGURE 5.40

centrifuge-frame-bucket-toggle-spring-bumper-wall-soil system. The accelerograms recorded in the free-field are very similar to the corresponding ones at the base of the wall (which indicate the input excitation into the wall-soil system), although they are not exactly alike. The peak amplitudes range from about 0.25 to 0.70 depending on the test, and the duration of shaking is from about 18 to about 33 (note the dimensionless variables). The accelerograms recorded at the top of the wall indicate that the motion can be amplified by greater than a factor of 2.0. The "earthquakes" can be generally categorized as short but severe.

The shaking exhibited in the experiments is not unlike that which has been recorded very near a ruptured fault. For example, used for comparison is the accelerogram (Figure 5.41) recorded at Station 2 of the Cholame-Shandon array during the Parkfield, California earthquake of June 27, 1966 (M_L = 5.6). The strong motion accelerograph was located just a few yards from the San Andreas fault trace. This record also exhibits sharp pulse-like accelerations which decay quite quickly. Although the maximum recorded ground acceleration was 50% of gravity, there was little damage to nearby structures presumably because of the narrowness of the acceleration spikes (low energy content) and because of the short duration of the severe shaking [8,16].

From an engineering standpoint, the response spectrum is very important since it gives an indication of how the response of a structure to an earthquake will be. Comparing the response spectra of the centrifuge accelerograms of tests 1CN0001, 1CN0002, 1CN0003, and

PARKFIELD, CALIFORNIA EARTHQUAKE   JUNE 27, 1966 – 2026 PST
IIB033 66.001.0   CHOLAME,SHANDON, CALIFORNIA ARRAY NO. 2   COMP N65E
⊙ PEAK VALUES :   ACCEL = –479.6 CM/SEC/SEC   VELOCITY = –77.9 CM/SEC   DISPL = 26.3 CM
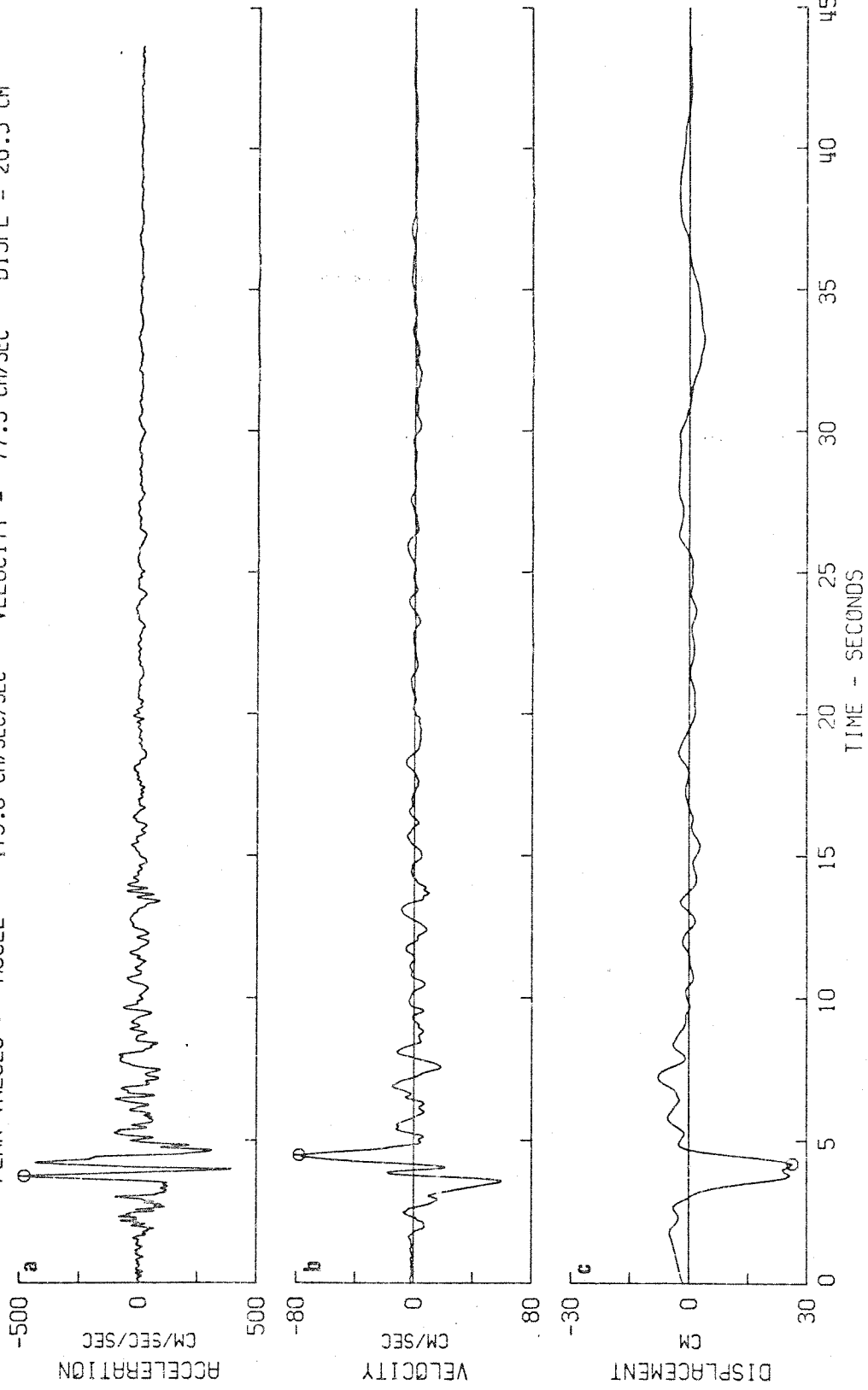
FIGURE 5.41

RESPONSE SPECTRUM

TEST 1CN0001   CENTRIFUGE EARTHQUAKE   11-12-80

IIXX0100 80.001.0 SOIL MECHANICS CENTRIFUGE — TOP OF WALL ACCELEROMETER   COMP HOR

DAMPING VALUES ARE 0, 2, 5, 10 AND 20 PERCENT OF CRITICAL
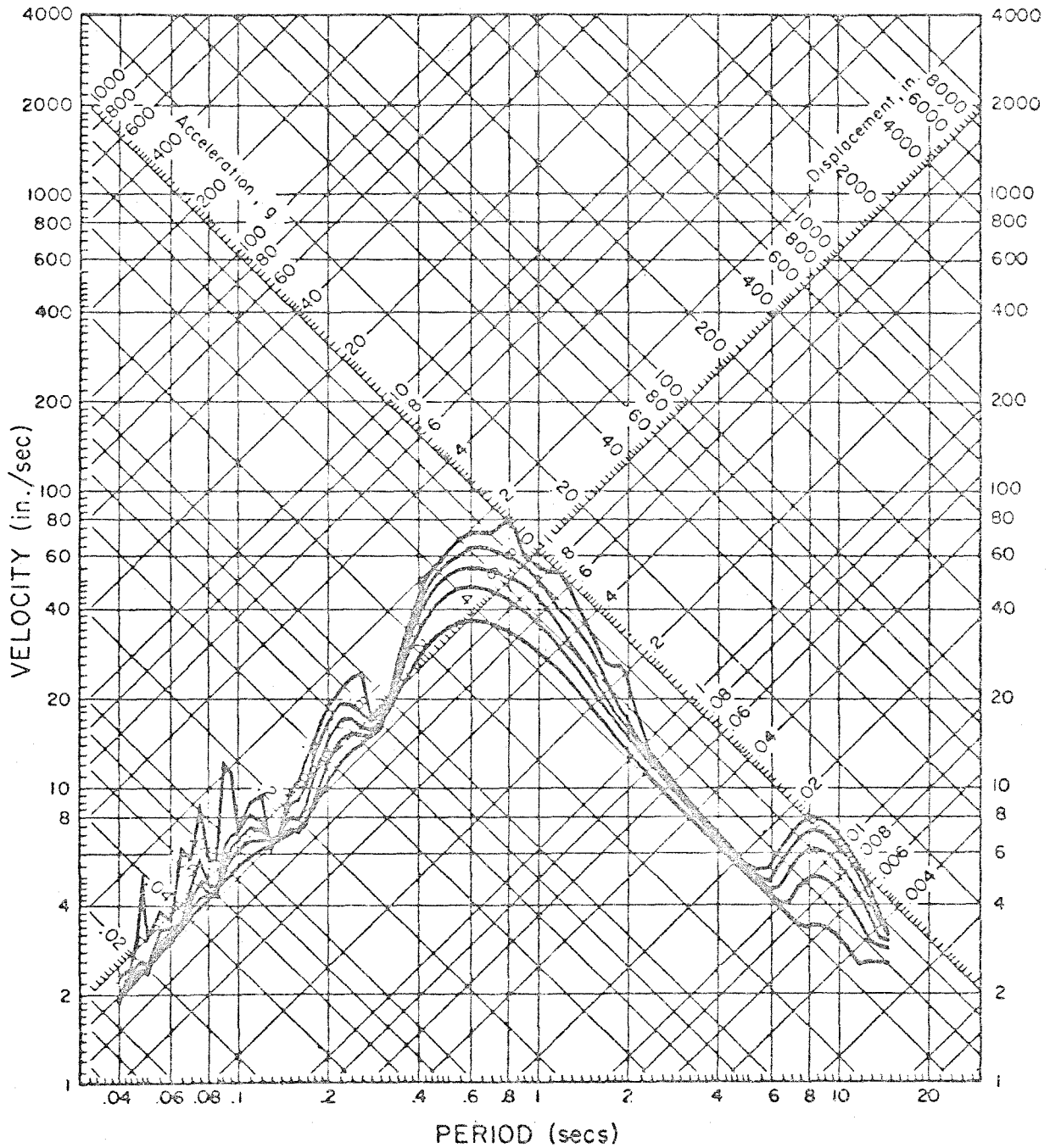
FIGURE 5.42

RESPONSE SPECTRUM

TEST 1CN0001   CENTRIFUGE EARTHQUAKE   11-12-80

IIXX0100 80.001.0   SOIL MECHANICS CENTRIFUGE-BOTTOM OF WALL ACCELEROMETER   COMP HOR

DAMPING VALUES ARE 0, 2, 5, 10 AND 20 PERCENT OF CRITICAL
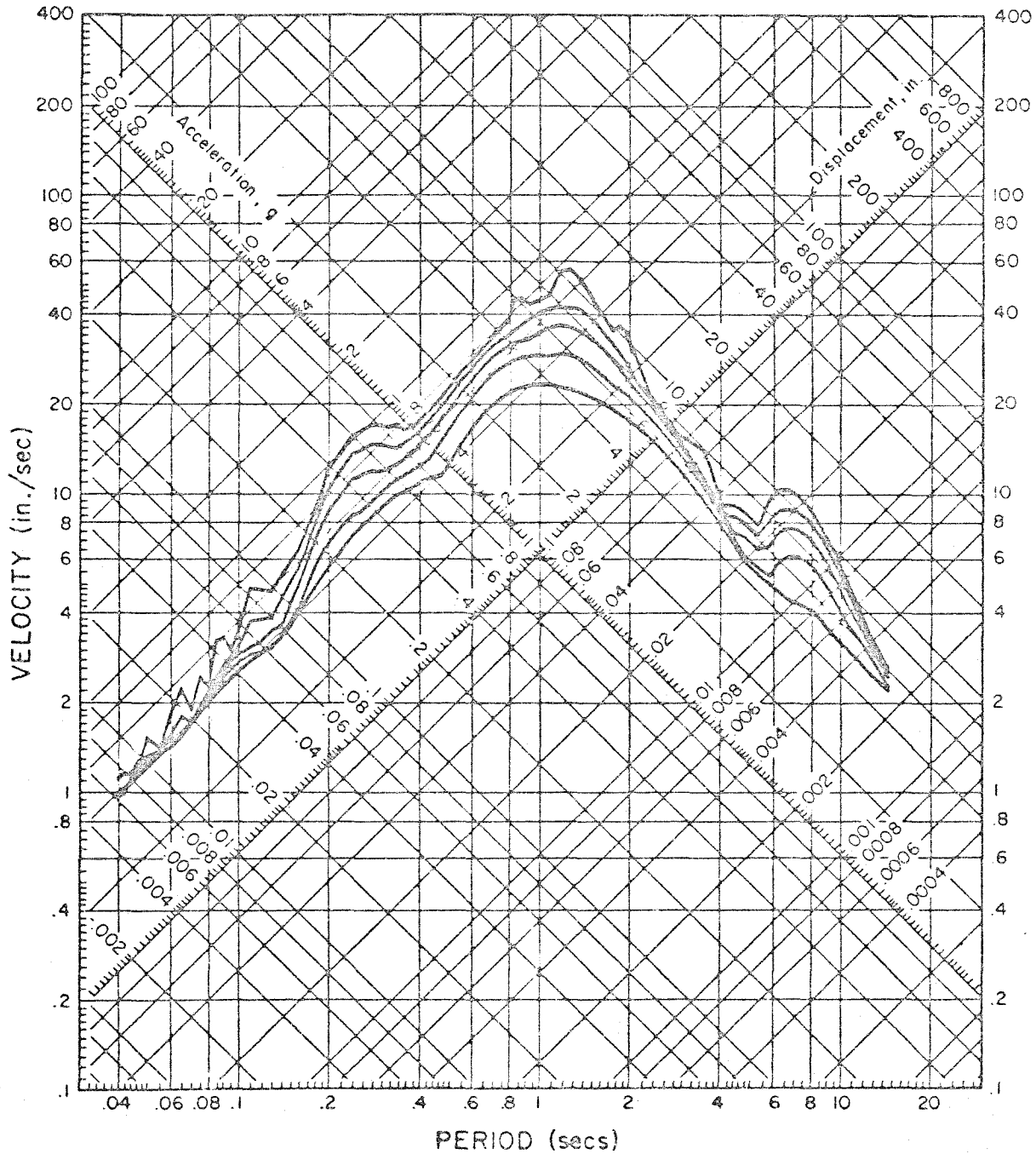
FIGURE 5.43

RESPONSE SPECTRUM

TEST 1CN0002   CENTRIFUGE EARTHQUAKE   3- 4-81

IIXX0200 81.002.0   SOIL MECHANICS CENTRIFUGE -- TOP OF WALL ACCELEROMETER   COMP HOR

DAMPING VALUES ARE 0, 2, 5, 10 AND 20 PERCENT OF CRITICAL

PERIOD (secs)
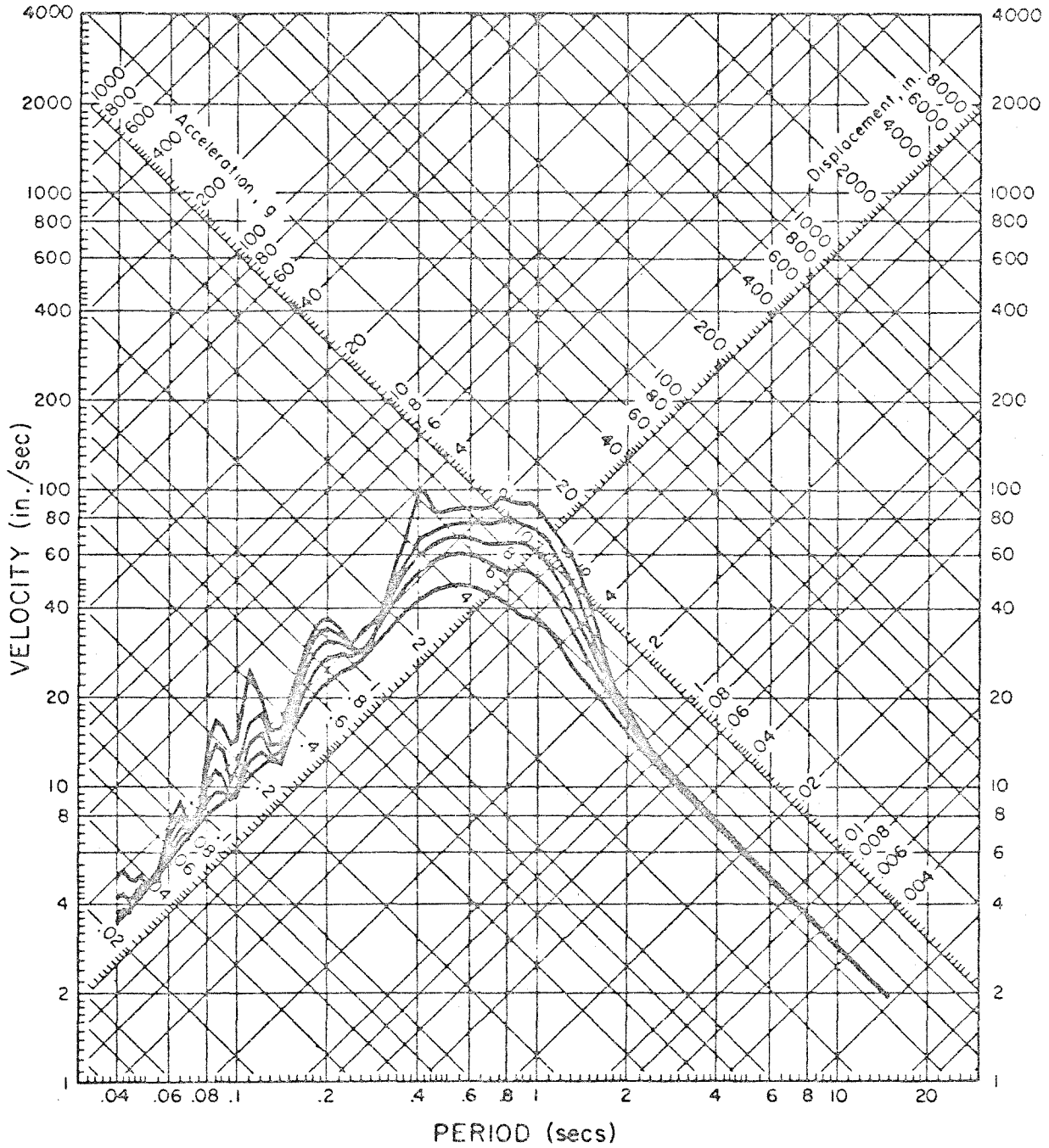
FIGURE 5.44

RESPONSE SPECTRUM

TEST 1CN0002   CENTRIFUGE EARTHQUAKE   3- 4-81

IIXX0200   81.002.0   SOIL MECHANICS CENTRIFUGE-BOTTOM OF WALL ACCELEROMETER   COMP HOR

DAMPING VALUES ARE 0, 2, 5, 10 AND 20 PERCENT OF CRITICAL

PERIOD (secs)

FIGURE 5.45

RESPONSE SPECTRUM

TEST 1CN0002   CENTRIFUGE EARTHQUAKE   3- 4-81

IIXX0200 81.002.0   SOIL MECHANICS CENTRIFUGE – FREE FIELD ACCELEROMETER   COMP HOR

DAMPING VALUES ARE 0, 2, 5, 10 AND 20 PERCENT OF CRITICAL

PERIOD (secs)

FIGURE 5.46

RESPONSE SPECTRUM

TEST 1CN1003   CENTRIFUGE EARTHQUAKE   3- 9-81

IIXX0300 81.003.0   SOIL MECHANICS CENTRIFUGE — TOP OF WALL ACCELEROMETER   COMP HOR

DAMPING VALUES ARE 0, 2, 5, 10 AND 20 PERCENT OF CRITICAL

PERIOD (secs)
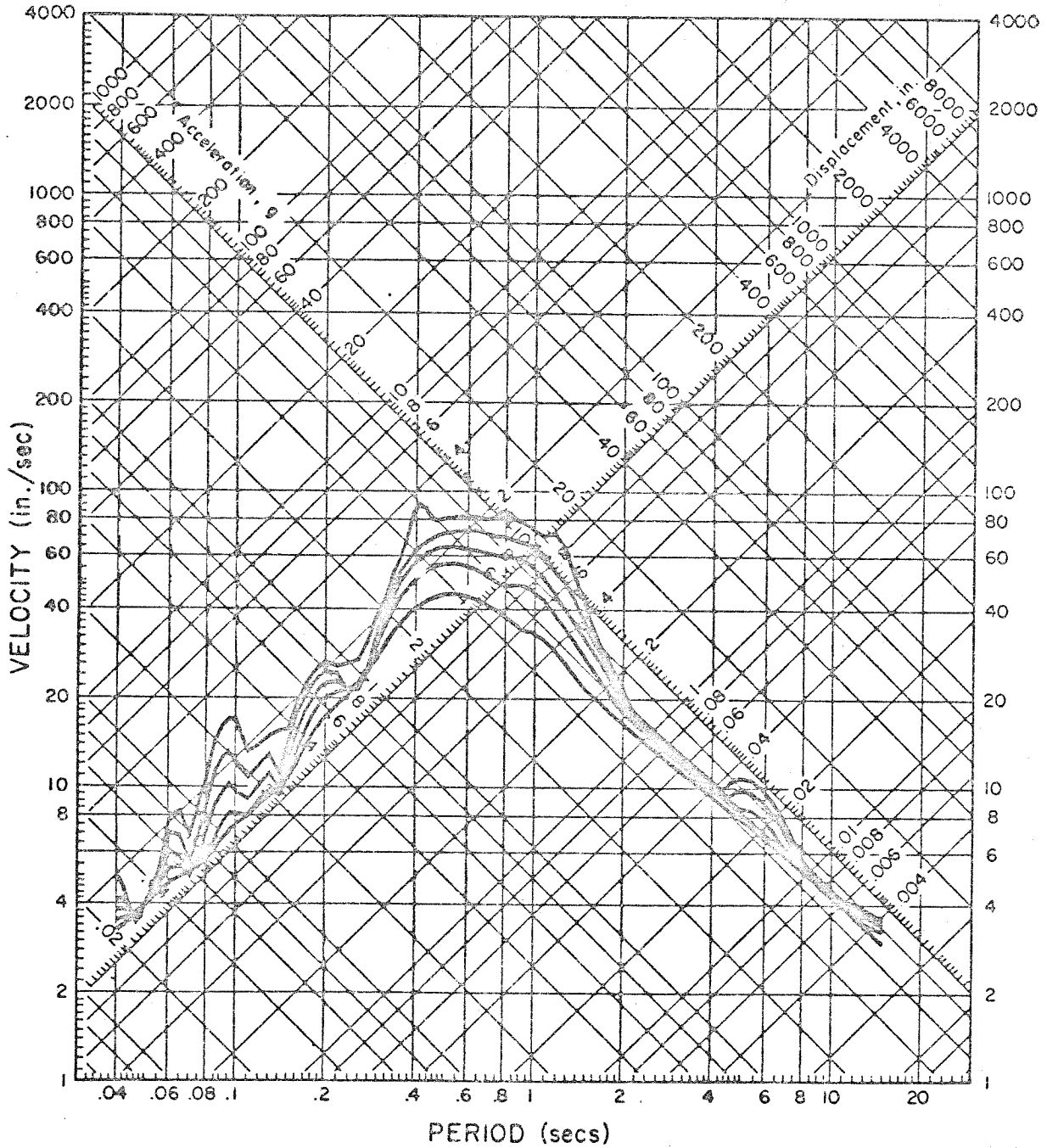
FIGURE 5.47

RESPONSE SPECTRUM

TEST 1CN1003   CENTRIFUGE EARTHQUAKE   3- 9-81

IIXX0300 81.003.0   SOIL MECHANICS CENTRIFUGE-BOTTOM OF WALL ACCELEROMETER   COMP HOR

DAMPING VALUES ARE 0, 2, 5, 10 AND 20 PERCENT OF CRITICAL
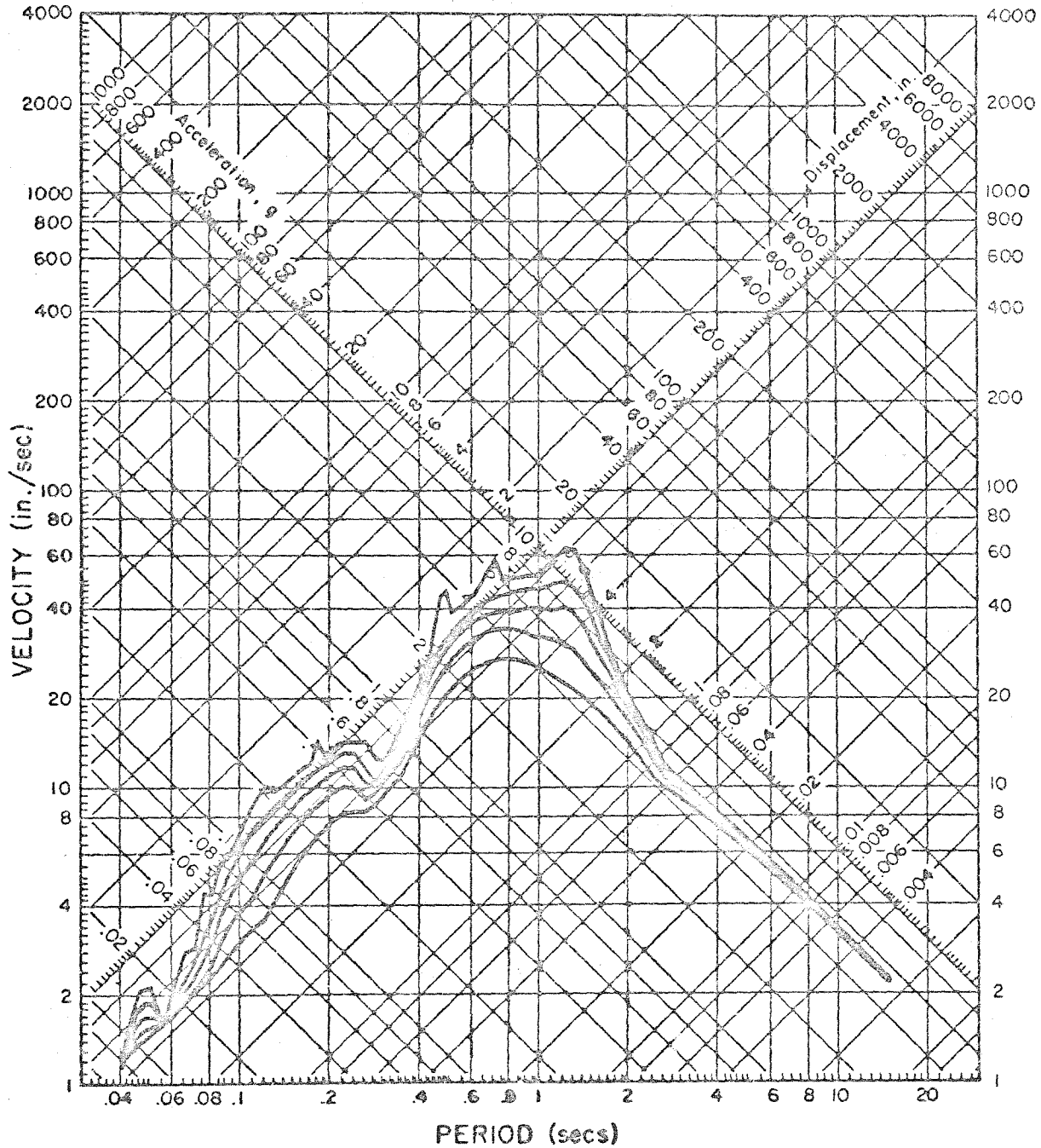
FIGURE 5.48

RESPONSE SPECTRUM

TEST 2CN0011   CENTRIFUGE EARTHQUAKE   2-25-82

IIXX0100 82.011.0 SOIL MECHANICS CENTRIFUGE — TOP OF WALL ACCELEROMETER COMP HOR

DAMPING VALUES ARE 0, 2, 5, 10 AND 20 PERCENT OF CRITICAL

PERIOD (secs)
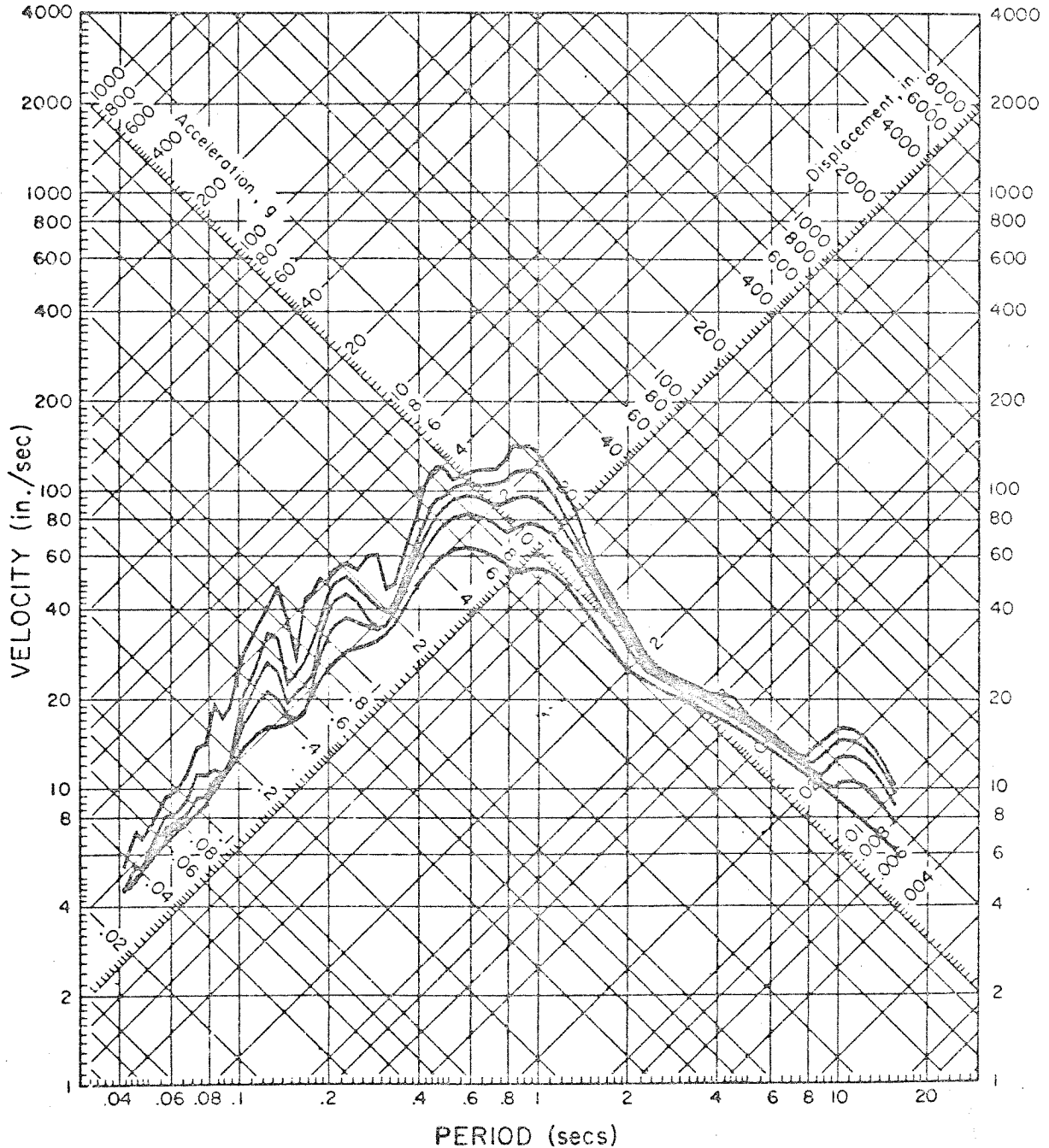
FIGURE 5.49

RESPONSE SPECTRUM

TEST 2CN0011   CENTRIFUGE EARTHQUAKE   2-25-82

IIXX0100 82.011.0   SOIL MECHANICS CENTRIFUGE-BOTTOM OF WALL ACCELEROMETER   COMP HOR

DAMPING VALUES ARE 0, 2, 5, 10 AND 20 PERCENT OF CRITICAL.
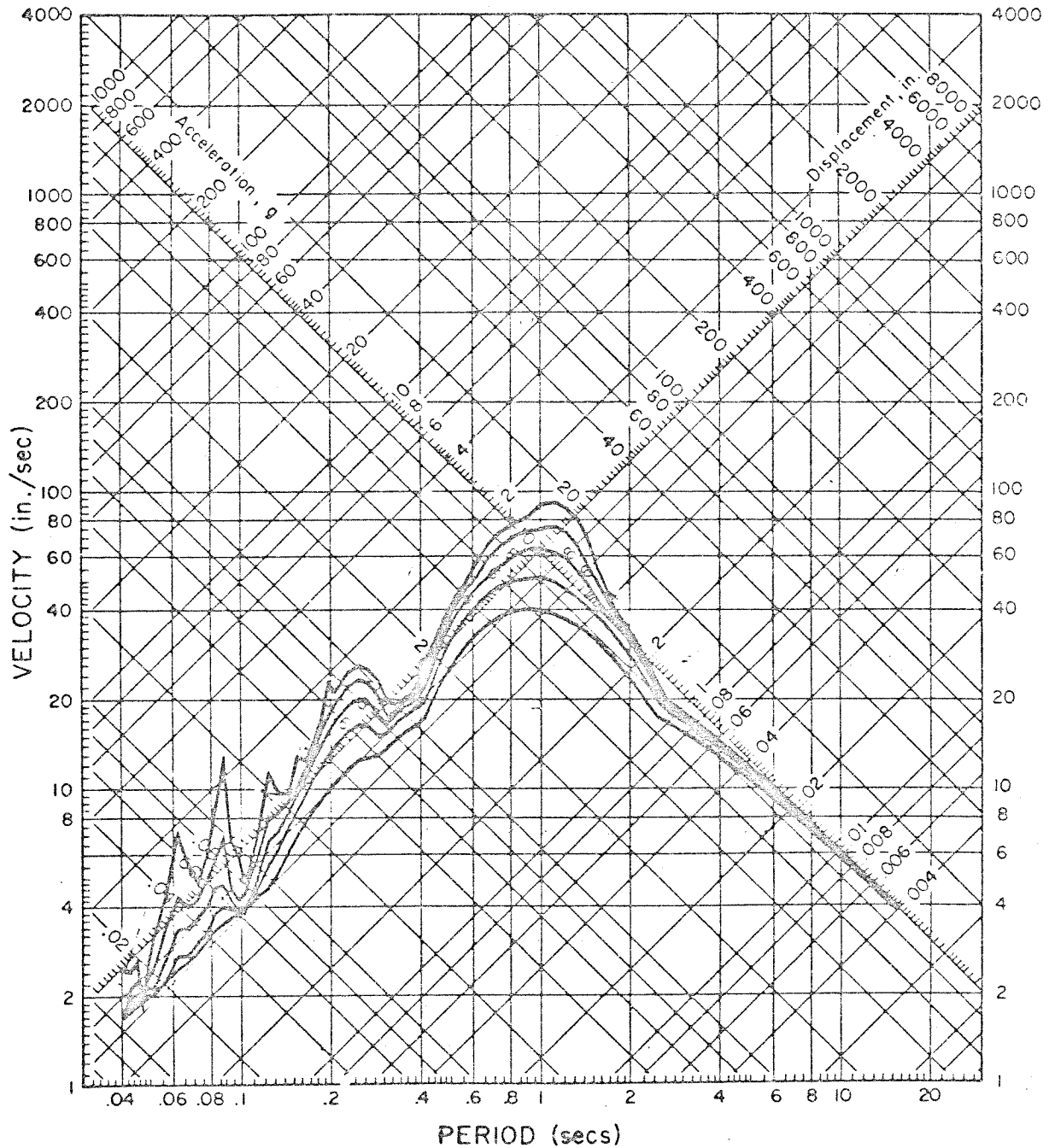
FIGURE 5.50

RESPONSE SPECTRUM

TEST 2CN0011   CENTRIFUGE EARTHQUAKE   2-25-82

IIXX0100 82.011.0   SOIL MECHANICS CENTRIFUGE – FREE FIELD ACCELEROMETER   COMP HOR

DAMPING VALUES ARE 0, 2, 5, 10 AND 20 PERCENT OF CRITICAL
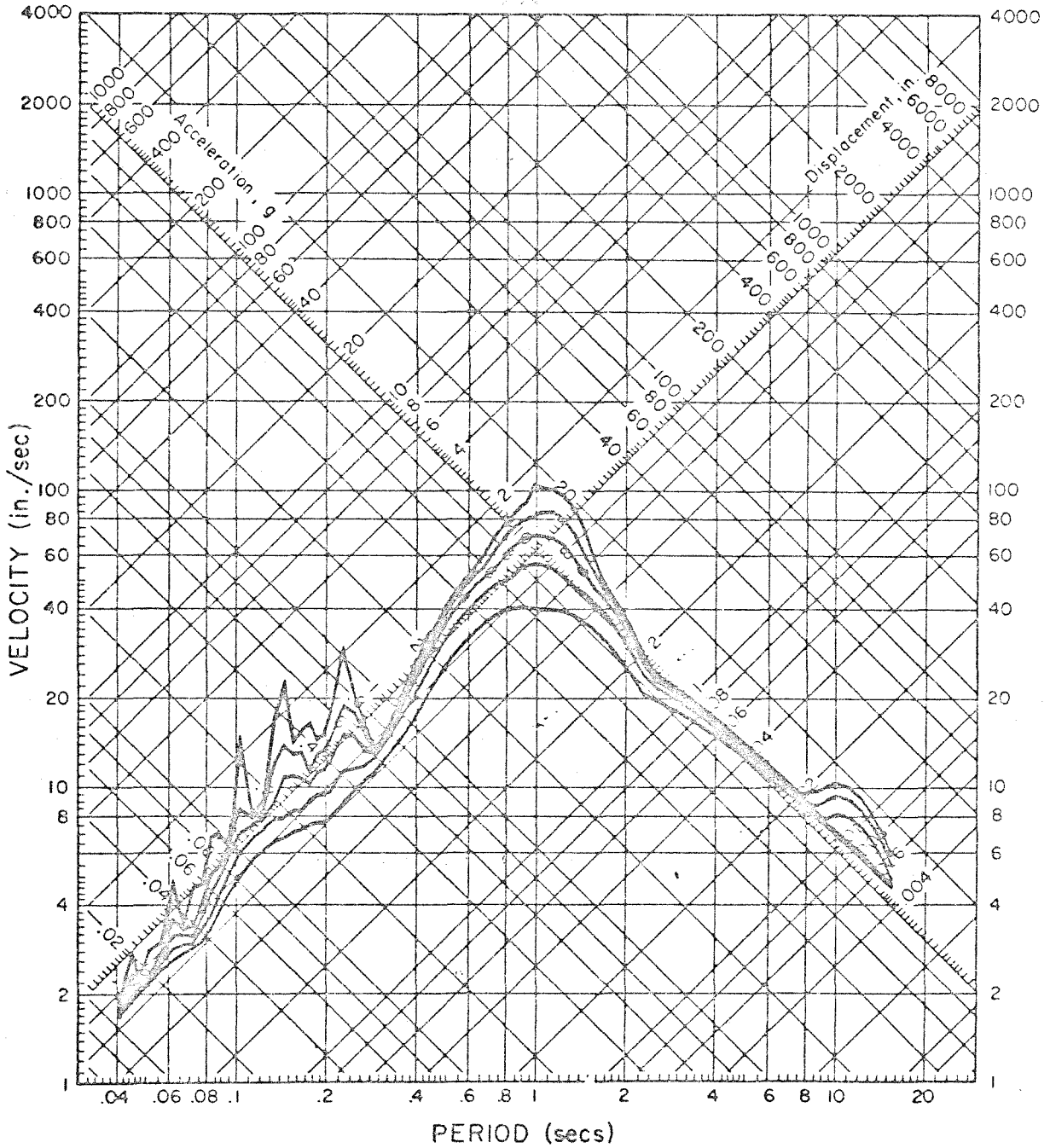
FIGURE 5.51

RESPONSE SPECTRUM

PARKFIELD, CALIFORNIA EARTHQUAKE   JUNE 27, 1966 - 2026 PST

IIIB033 66.001.0   CHOLAME.SHANDON. CALIFORNIA ARRAY NO. 2   COMP N65E

DAMPING VALUES ARE 0, 2, 5, 10 AND 20 PERCENT OF CRITICAL
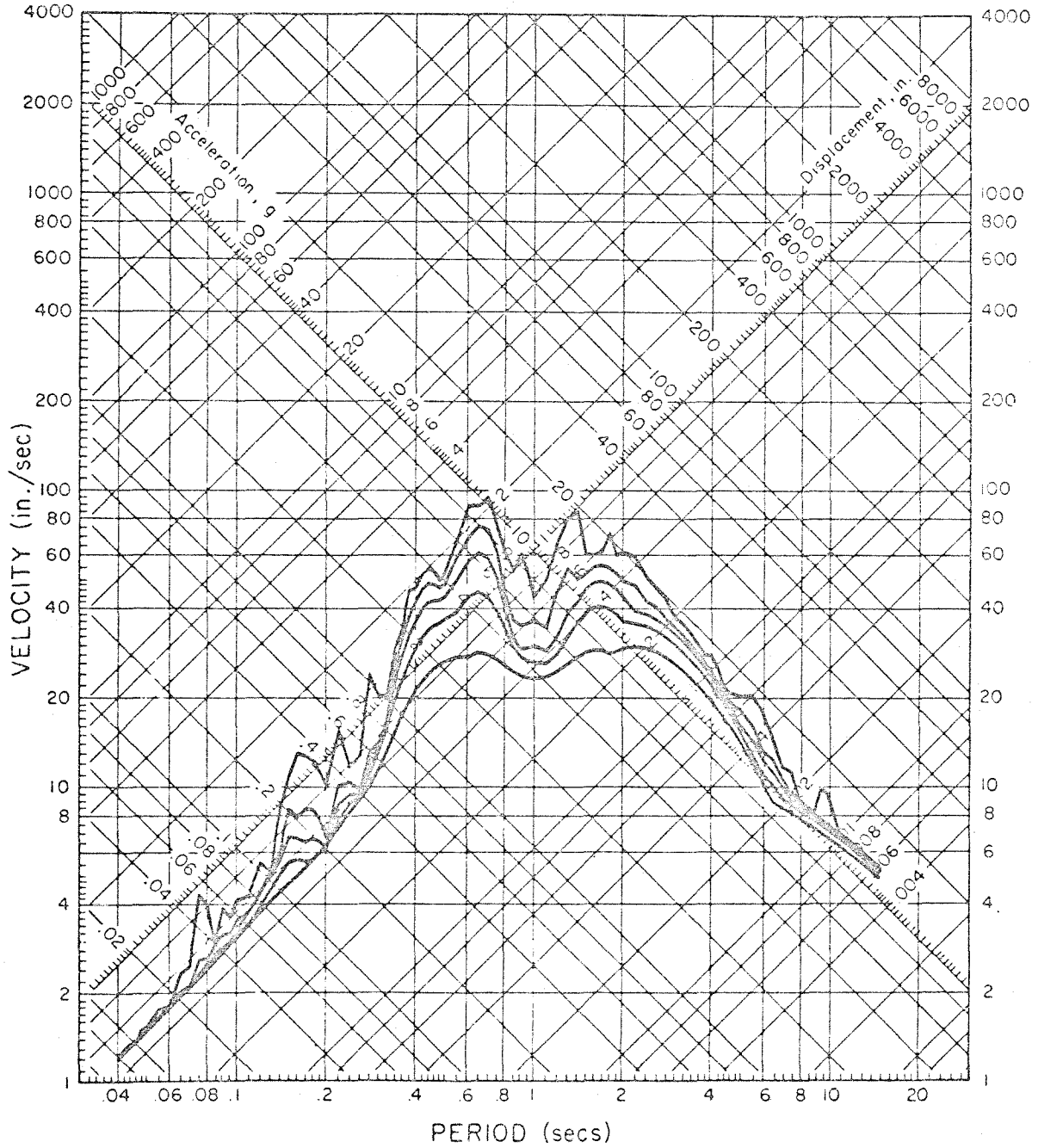
FIGURE 5.52

2CN0011 (Figures 5.42 through 5.51) with that of the stronger horizontal component of Parkfield (Figure 5.52), it can be seen that they are all very similar. They have peaks for periods between 0.4 and 1.5 seconds (prototype) which are at similar levels for similar dampings. The main difference lies in the observation that the centrifuge shaking lacks the longer (> 2.0 sec) period components which the Parkfield motion contains. The above would seem to indicate that the prototype structure of the centrifuge model would have behaved very much like the model during an earthquake similar to Parkfield, had it been close to the rupturing fault.

The comparisons clearly show that, although the shaking mechanism employed in the centrifuge is not sophisticated, it does give motions which have realistic characteristics and thus can be used to provide some real insight into the problem at hand. Longer duration shaking would primarily affect walls retaining saturated backfill in which pore pressure effects might be important.

5.3. Parameter Diagrams

Figures 5.53 through 5.107 show the moment, pressure, shear force, and lateral displacement distributions obtained from the 14 tests performed. As explained in Section 4.2, these figures show the entire response of the system to the particular shaking it was subjected to. Table 5.4 should be used as a key to the interpretation of the figures.

TABLE 5.4
Key To Figures 5.53 Through 5.107

Frame a – Contour map of the parameter distribution with respect to location and time.

Frame b – Parameter distribution with respect to time at location where maximum occurs (Section A-A of contour map).

Frame c – Parameter distribution with respect to location-static, maximum dynamic (section B-B of the contour map), and final static after motion ceases.

+   Location of strain gages

x   Location of pressure transducers

O   Maximum

Δ   Data point

On Frame c of pressure distribution plots, the following symbols appear. [Along $(P/\rho g \, H)$ axis]:

O   Location of static resultant

☐   Location of maximum resultant

◇   Location of final static resultant

Rankine/Coulomb (static) and Mononobe-Okabe (maximum dynamic) pressure distributions are also shown in this frame.

Except for tests 1CN0001, 1CN0002, 1CN1003, 1CN0004, and 1CN1505, the time (tf_1) scales (on Frames a and b) are set up so that the first 20% of the record is displayed over the first 50% of the graph and the final 80% over the other 50%. This was done to enhance the presentation of the more critical part of the tests.

FIGURE 5.53

MOMENT

FIGURE 5.54

TEST 1CN0001 11-12-80   CANTILEVER WALL NO. 1   ZERO BACKFILL SLOPE
ALEXANDER ORTIZ   NEVADA 120 SAND (DRY,MEDIUM DENSE)

FIGURE 5.55

DISPLACEMENT

TEST 1CN0001 11-12-80   CANTILEVER WALL NO. 1   ZERO BACKFILL SLOPE
ALEXANDER ORTIZ   NEVADA 120 SAND (DRY,MEDIUM DENSE)

FIGURE 5.56

MOMENT

TEST 1CN0002   3- 4-81   CANTILEVER WALL NO. 1   ZERO BACKFILL SLOPE
ALEXANDER ORTIZ   NEVADA 120 SAND (DRY,MEDIUM DENSE)

FIGURE 5.57

PRESSURE

TEST 1CN0002   3- 4-81   CANTILEVER WALL NO. 1   ZERO BACKFILL SLOPE
ALEXANDER ORTIZ   NEVADA 120 SAND (DRY,MEDIUM DENSE)

FIGURE 5.58

SHEAR

TEST 1CN0002   3- 4-81   CANTILEVER WALL NO. 1   ZERO BACKFILL SLOPE
ALEXANDER ORTIZ   NEVADA 120 SAND (DRY,MEDIUM DENSE)

FIGURE 5.59

DISPLACEMENT

TEST 1CN0002   3- 4-81   CANTILEVER WALL NO. 1   ZERO BACKFILL SLOPE
ALEXANDER ORTIZ   NEVADA 120 SAND (DRY,MEDIUM DENSE)

FIGURE 5.60

MOMENT

TEST 1CN1003 3- 9-81   CANTILEVER WALL NO. 1   10 DEGREE BACKFILL SLOPE
ALEXANDER ORTIZ   NEVADA 120 SAND (DRY,MEDIUM DENSE)

FIGURE 5.61

TEST 1CN1003 3- 9-81   CANTILEVER WALL NO. 1   10 DEGREE BACKFILL SLOPE
ALEXANDER ORTIZ   NEVADA 120 SAND (DRY,MEDIUM DENSE)

FIGURE 5.62

SHEAR
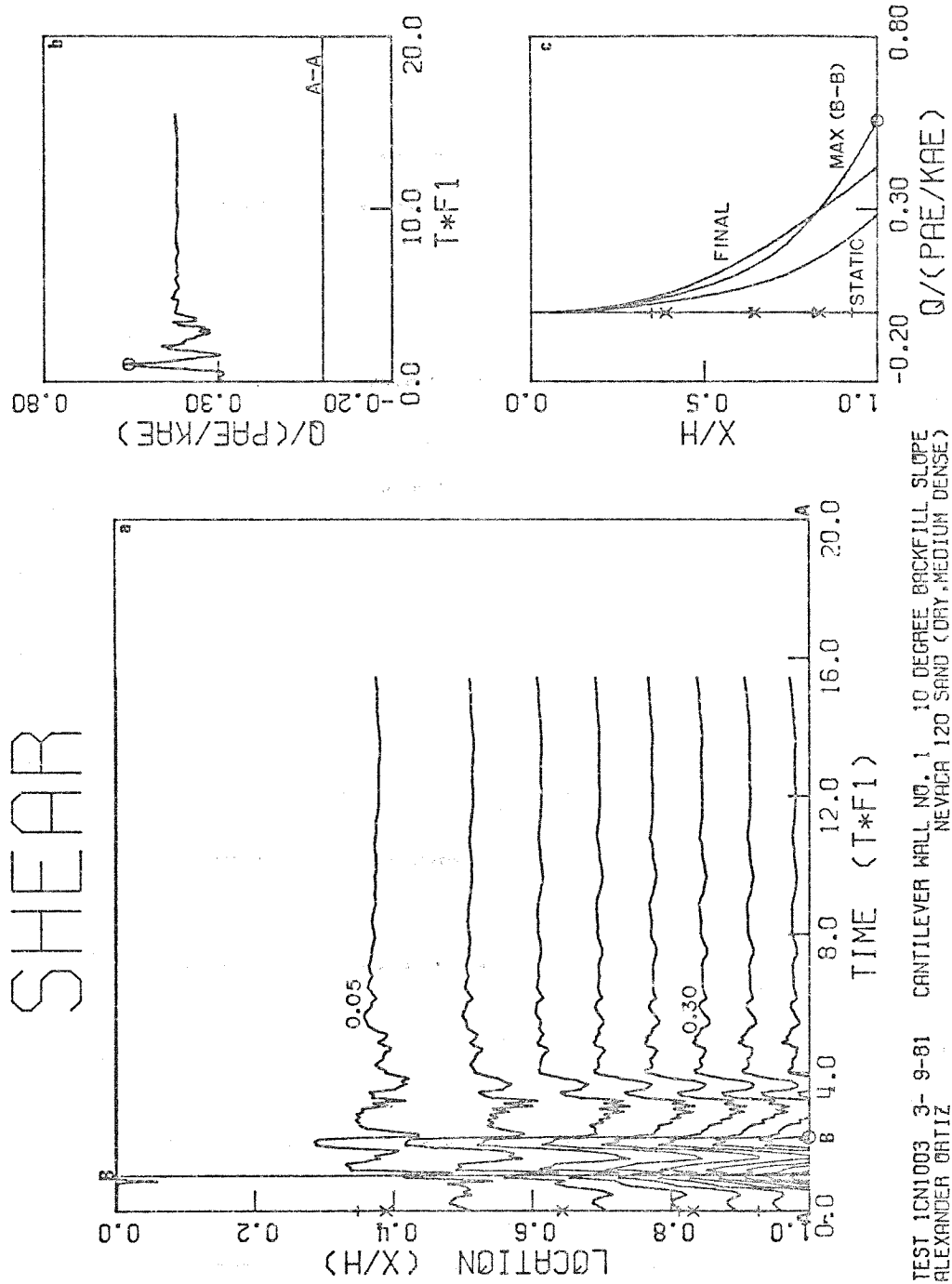
TEST 1CN1003 3- 9-81   CANTILEVER WALL NO. 1   10 DEGREE BACKFILL SLOPE
ALEXANDER ORTIZ   NEVADA 120 SAND (DRY,MEDIUM DENSE)

FIGURE 5.63

DISPLACEMENT
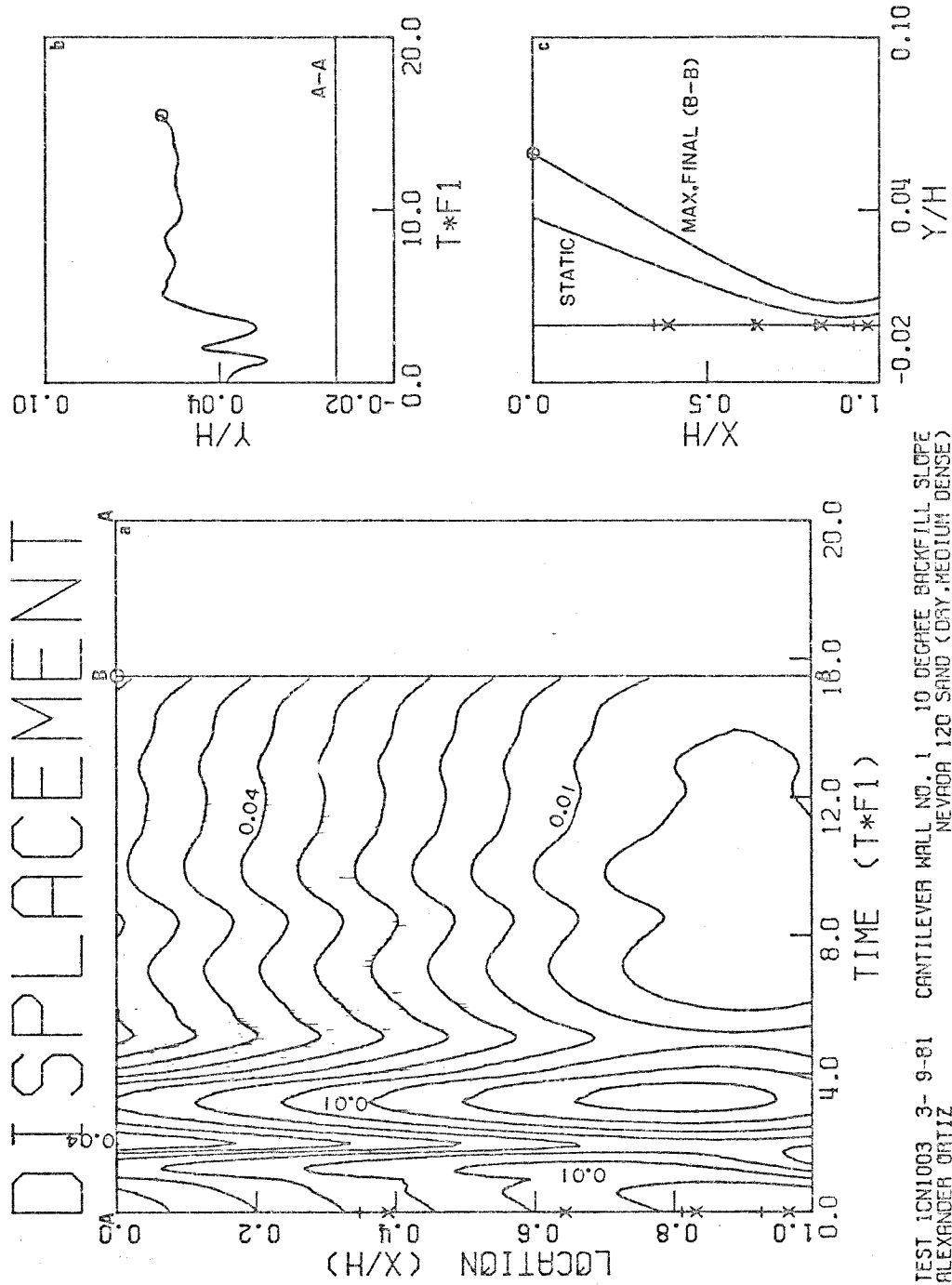
TEST ICN1003 3- 9-81   CANTILEVER WALL NO. 1   10 DEGREE BACKFILL SLOPE
ALEXANDER ORTIZ   NEVADA 120 SAND (DRY,MEDIUM DENSE)

FIGURE 5.64

MOMENT

TEST 1CN0004 3-16-81
ALEXANDER ORTIZ

CANTILEVER WALL NO. 1 ZERO BACKFILL SLOPE
NEVADA 120 SAND (DRY,MEDIUM DENSE)
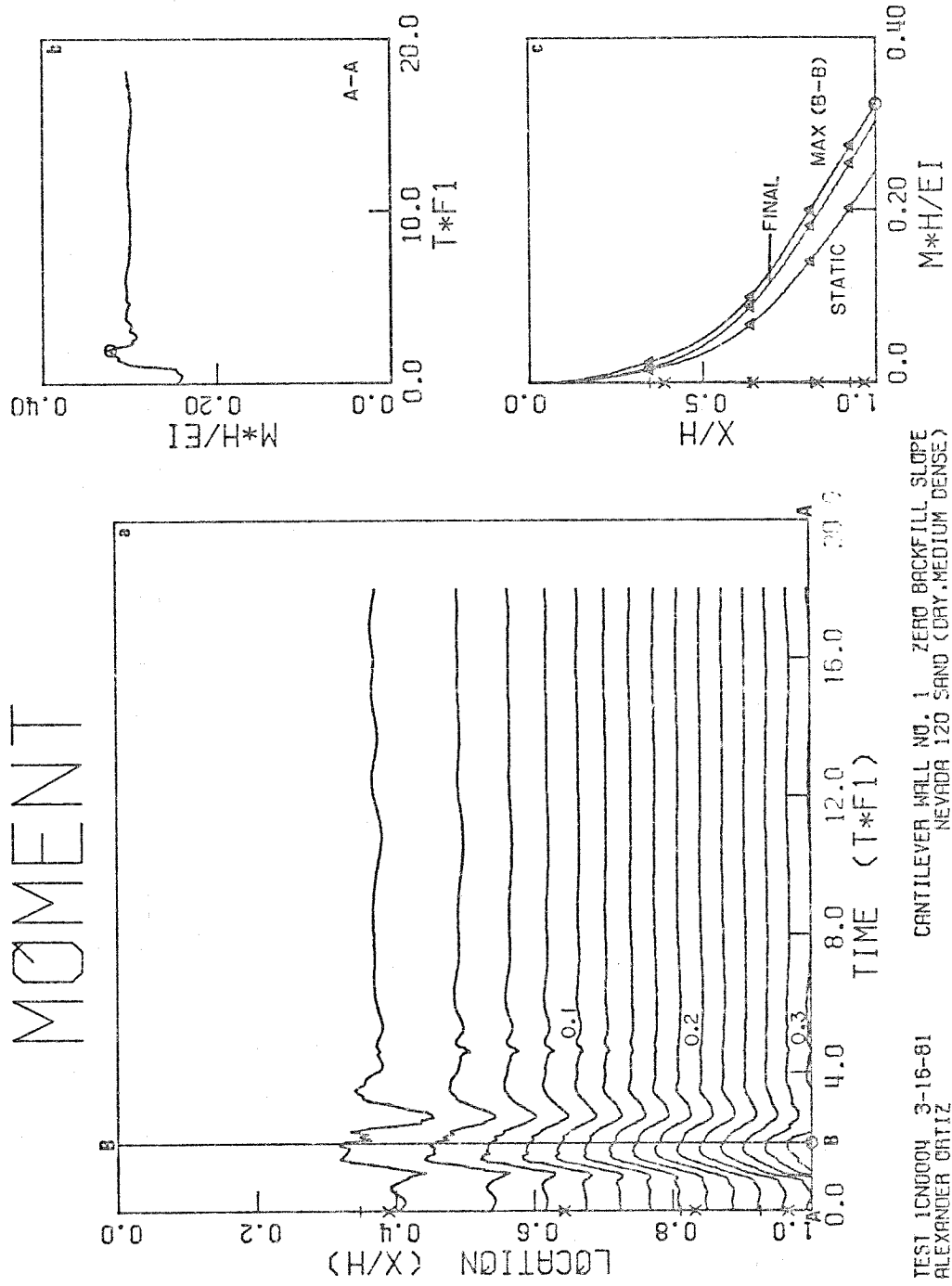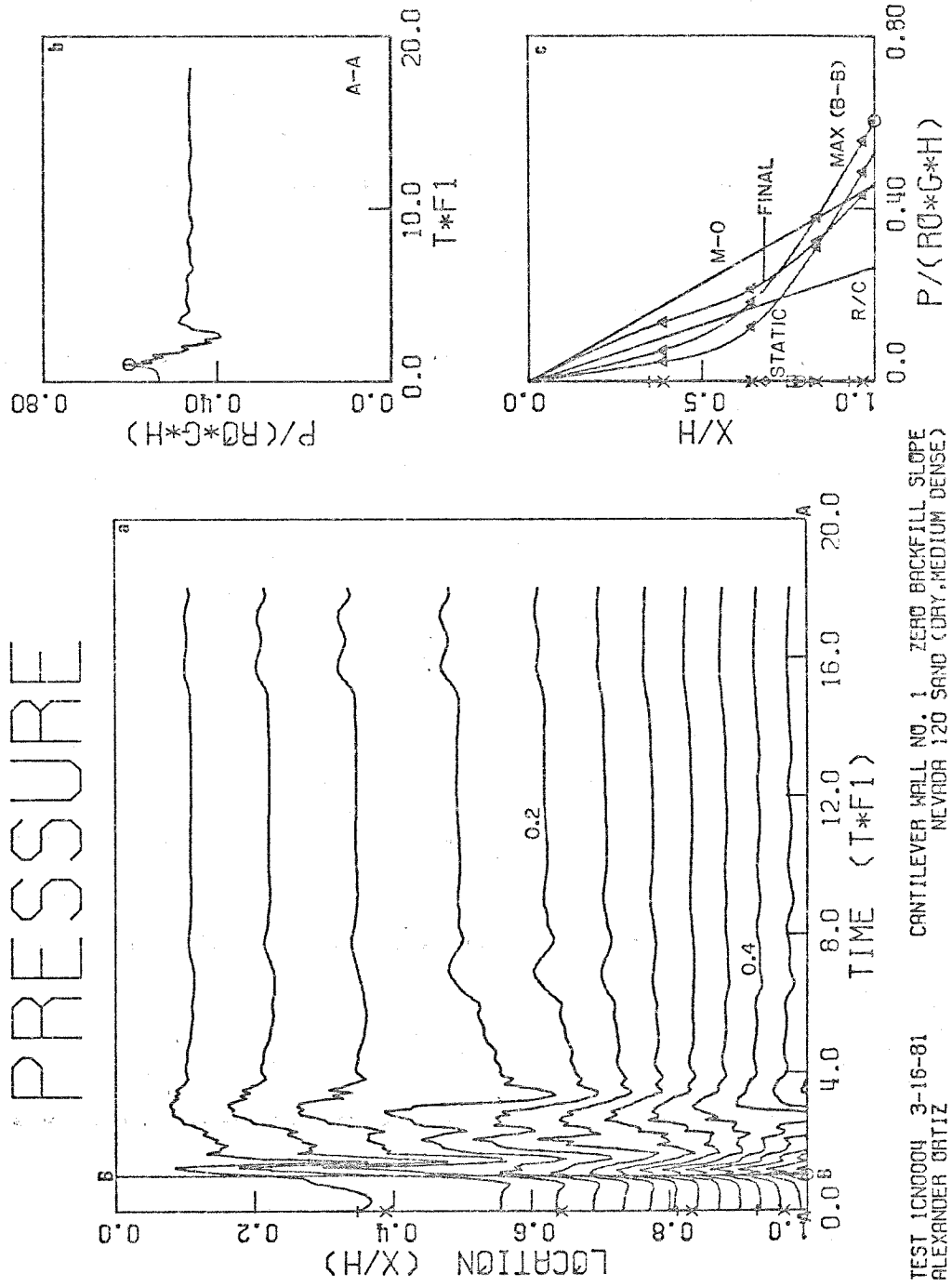
FIGURE 5.65

TEST 1CN0004   3-16-81   CANTILEVER WALL NO. 1   ZERO BACKFILL SLOPE
ALEXANDER ORTIZ   NEVADA 120 SAND (DRY,MEDIUM DENSE)

FIGURE 5.66

FIGURE 5.67

DISPLACEMENT

TEST 1CN0004 3-16-81
ALEXANDER ORTIZ

CANTILEVER WALL NO. 1   ZERO BACKFILL SLOPE
NEVADA 120 SAND (DRY,MEDIUM DENSE)

FIGURE 5.68
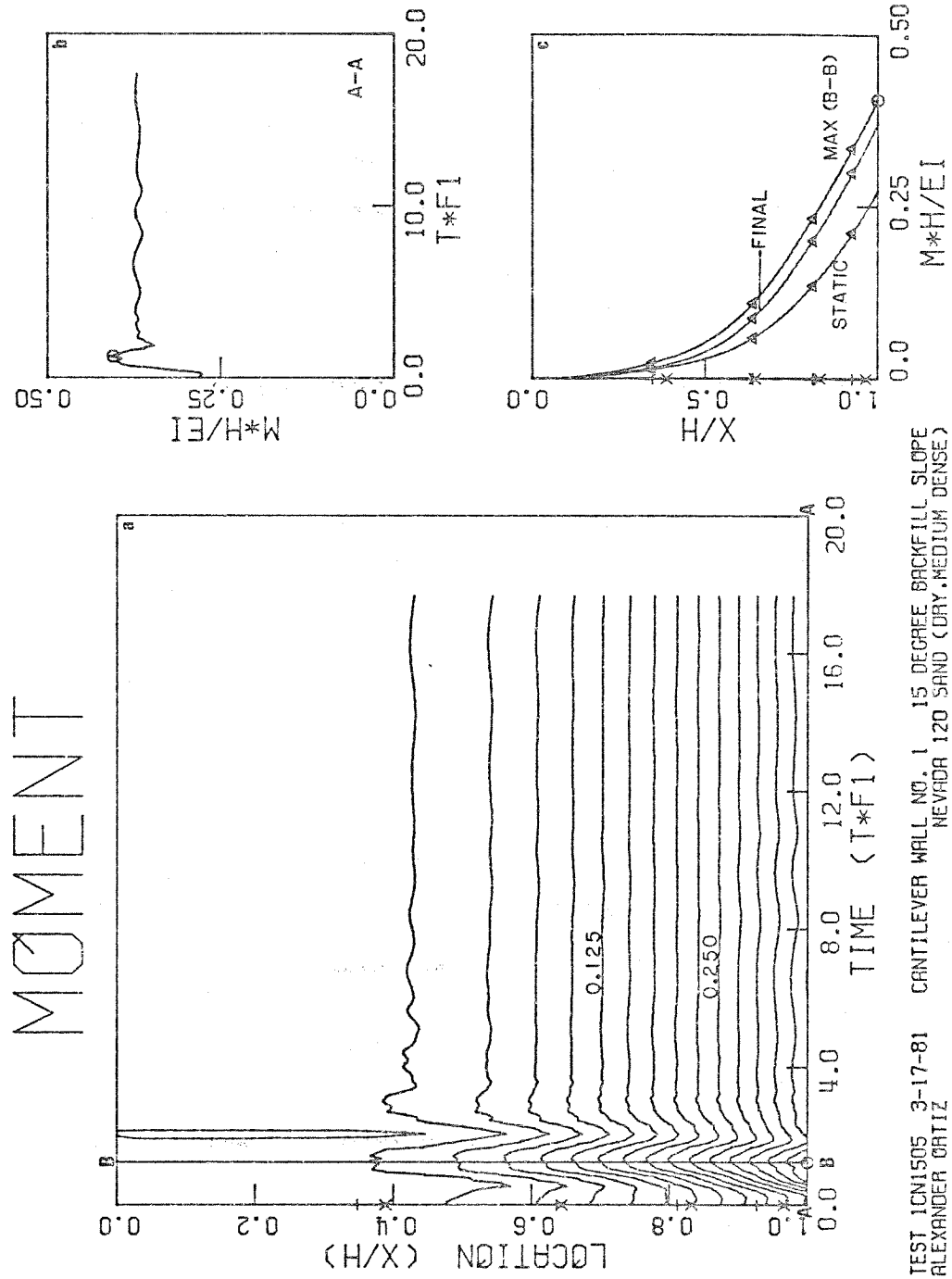
MOMENT

TEST 1CN1505 3-17-81 CANTILEVER WALL NO. 1 15 DEGREE BACKFILL SLOPE
ALEXANDER ORTIZ   NEVADA 120 SAND (DRY,MEDIUM DENSE)

FIGURE 5.69
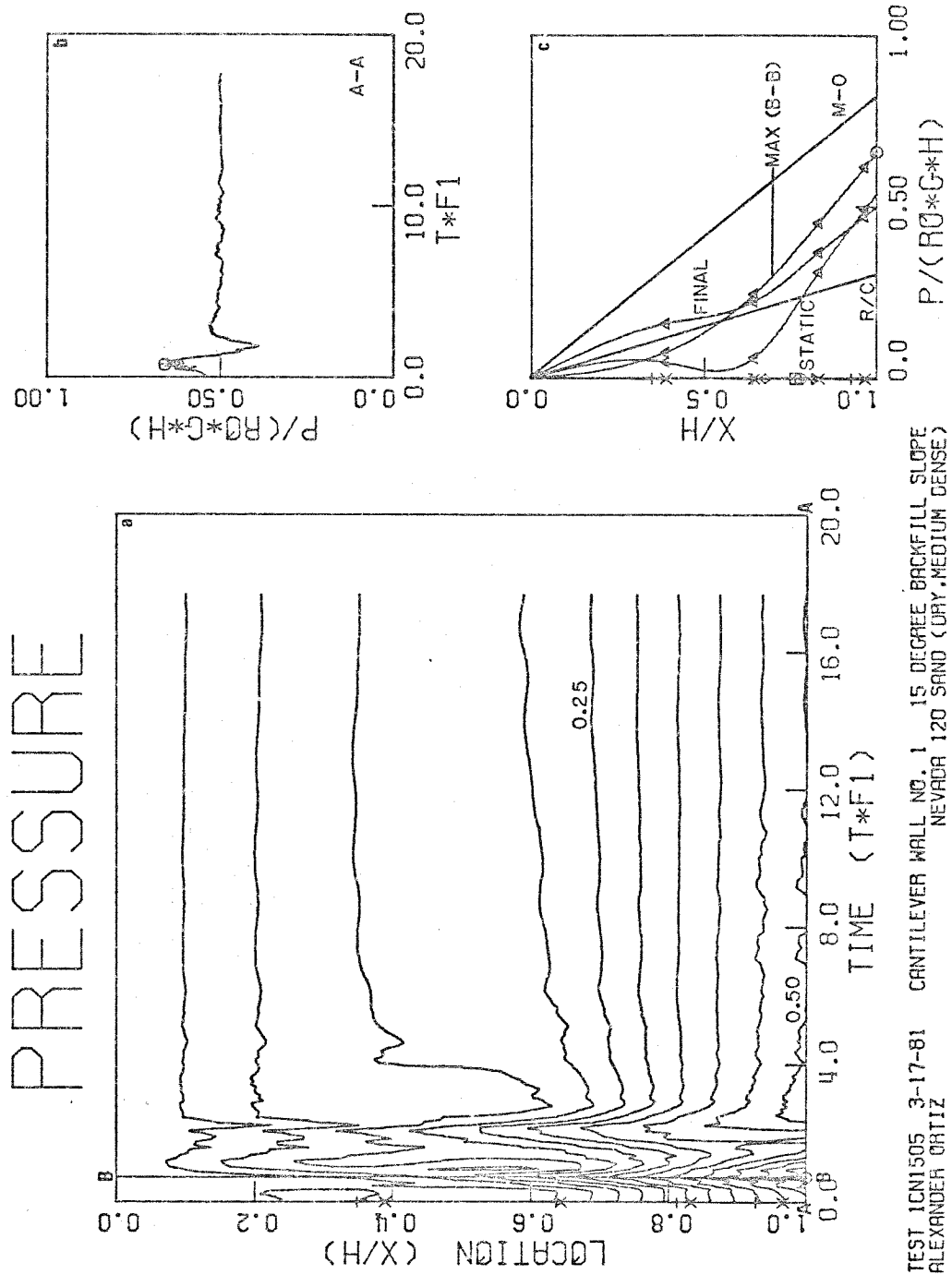
PRESSURE

TEST 1CN1505 3-17-81   CANTILEVER WALL NO. 1   15 DEGREE BACKFILL SLOPE
ALEXANDER ORTIZ   NEVADA 120 SAND (DRY,MEDIUM DENSE)

FIGURE 5.70

SHEAR

TEST 1CN1505 3-17-81   CANTILEVER WALL NO. 1   15 DEGREE BACKFILL SLOPE
ALEXANDER ORTIZ   NEVADA 120 SAND (DRY,MEDIUM DENSE)

FIGURE 5.71

DISPLACEMENT
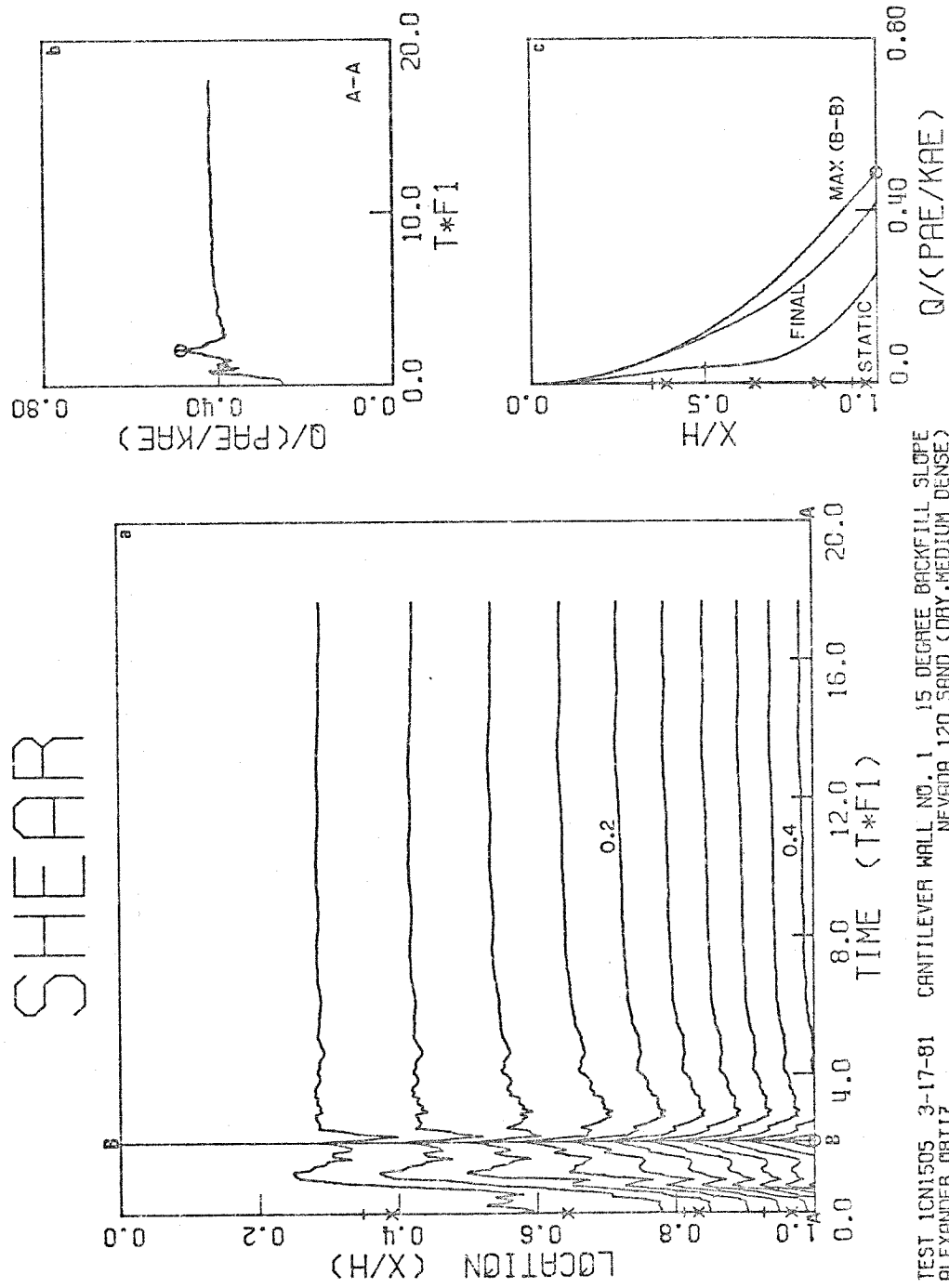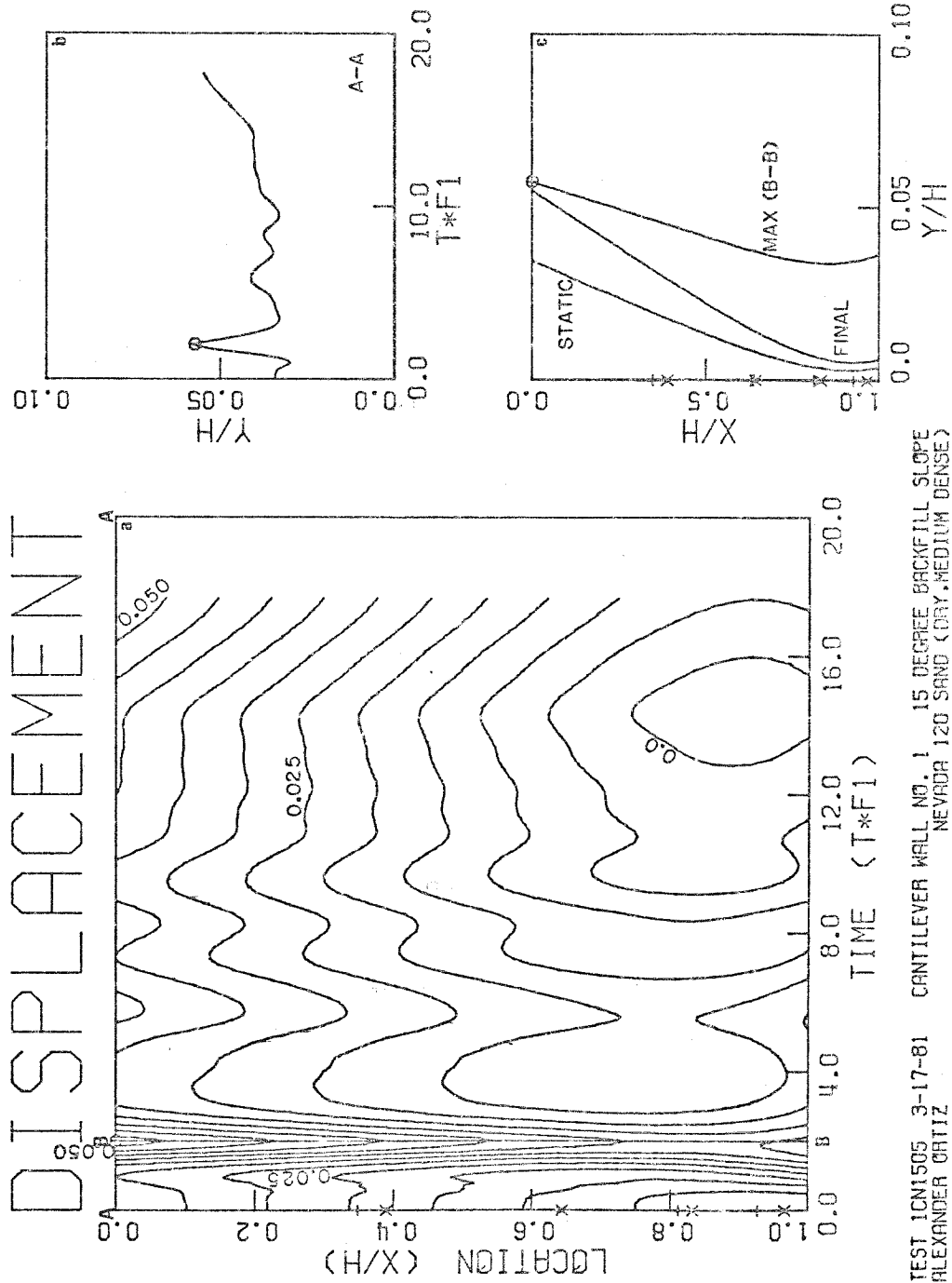
TEST 1CN1505   3-17-81   CANTILEVER WALL NO. 1   15 DEGREE BACKFILL SLOPE
ALEXANDER ORTIZ   NEVADA 120 SAND (DRY,MEDIUM DENSE)

FIGURE 5.72

MOMENT

TEST 1CN0006   8-6-81   CANTILEVER WALL NO. 1 ZERO DEGREE BACKFILL SLOPE
ALEXANDER ORTIZ   NEVADA 120 SAND (DRY,MEDIUM DENSE)

FIGURE 5.73

PRESSURE

TEST 1CND006   8-6-81   CANTILEVER WALL NO. 1 ZERO DEGREE BACKFILL SLOPE
ALEXANDER ORTIZ   NEVADA 120 SAND (DRY,MEDIUM DENSE)

FIGURE 5.74

SHEAR

TEST 1CN0006   8-6-81   CANTILEVER WALL NO. 1   ZERO DEGREE BACKFILL SLOPE
ALEXANDER ORTIZ   NEVADA 120 SAND (DRY,MEDIUM DENSE)

FIGURE 5.75

DISPLACEMENT

FIGURE 5.76

MOMENT

TEST 1CN0007 2-15-82   CANTILEVER WALL NO. 1 ZERO DEGREE BACKFILL SLOPE
ALEXANDER ORTIZ   NEVADA 120 SAND (DRY,DENSE)

FIGURE 5.77

PRESSURE

TEST 1CN0007 2-15-82   CANTILEVER WALL NO. 1 ZERO DEGREE BACKFILL SLOPE
ALEXANDER ORTIZ   NEVADA 120 SAND (DRY, DENSE)

FIGURE 5.78

SHEAR

TEST 1CN0007 2-15-82   CANTILEVER WALL NO. 1 ZERO DEGREE BACKFILL SLOPE
ALEXANDER ORTIZ   NEVADA 120 SAND   (DRY, DENSE)

FIGURE 5.79

DISPLACEMENT
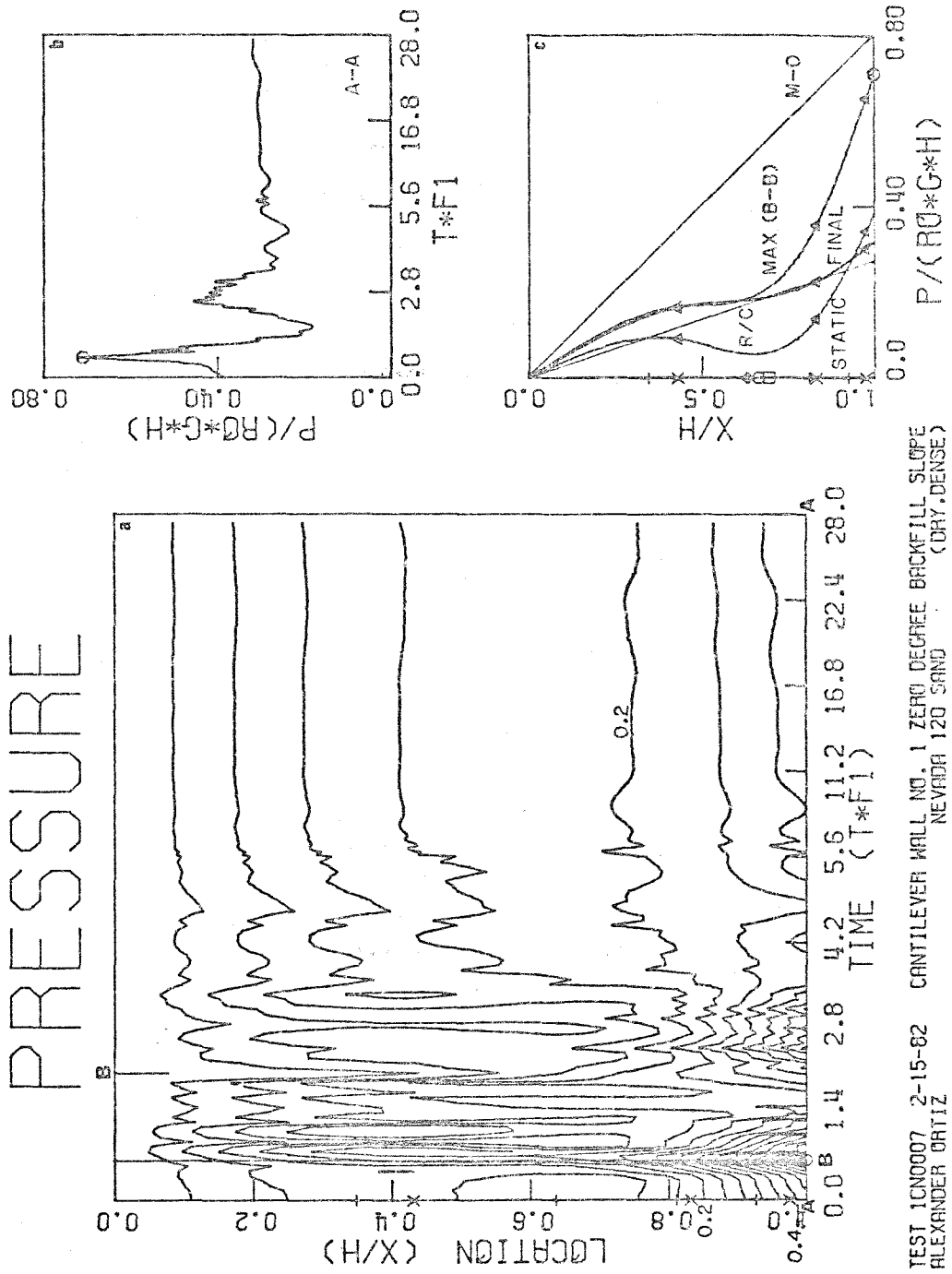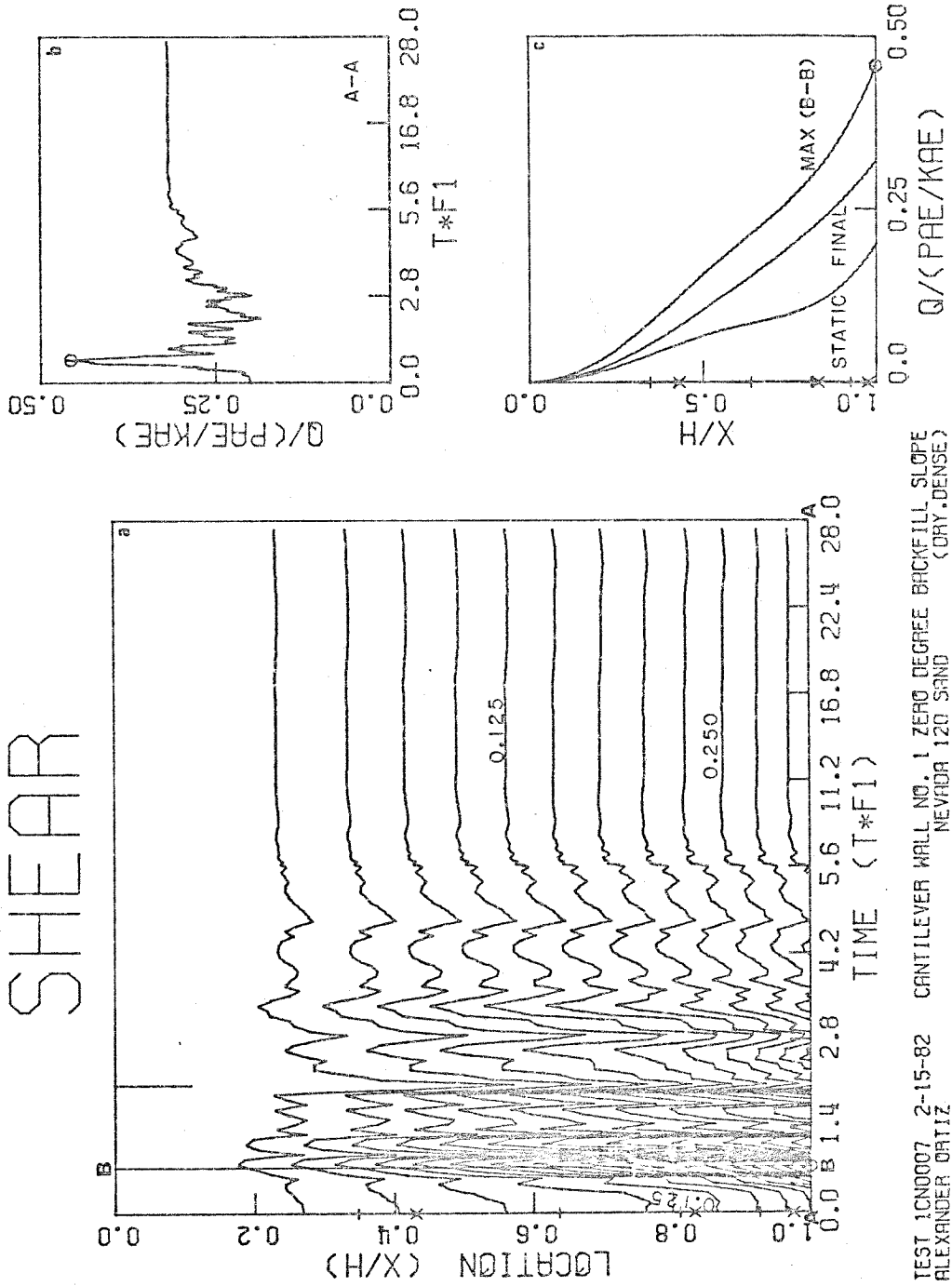
TEST 1CN0007 2-15-82   CANTILEVER WALL NO. 1 ZERO DEGREE BACKFILL SLOPE
ALEXANDER ORTIZ   NEVADA 120 SAND (DRY,DENSE)

FIGURE 5.80

MOMENT

TEST 1CN0508 2-16-82 CANTILEVER WALL NO. 1   5 DEGREE BACKFILL SLOPE
ALEXANDER ORTIZ   NEVADA 120 SAND (DRY,MEDIUM DENSE)

FIGURE 5.81

TEST 1CN0508 2-16-82   CANTILEVER WALL NO. 1   5 DEGREE BACKFILL SLOPE
ALEXANDER ORTIZ   NEVADA 120 SAND (DRY, MEDIUM DENSE)

FIGURE 5.82

SHEAR

TEST 1CN0508 2-16-82   CANTILEVER WALL NO. 1   5 DEGREE BACKFILL SLOPE
ALEXANDER ORTIZ   NEVADA 120 SAND (DRY,MEDIUM DENSE)

Figure 5.55

DISPLACEMENT

TEST 1CN0508 2-16-82   CANTILEVER WALL NO. 1   5 DEGREE BACKFILL SLOPE
ALEXANDER ORTIZ   NEVADA 120 SAND (DRY,MEDIUM DENSE)

FIGURE 5.84

MOMENT

TEST 1CN1009 2-17-82   CANTILEVER WALL NO. 1   10 DEGREE BACKFILL SLOPE
ALEXANDER ORTIZ   NEVADA 120 SAND   (DRY,DENSE)

FIGURE 5.85

PRESSURE

TEST 1CN1009 2-17-82   CANTILEVER WALL NO. 1   10 DEGREE BACKFILL SLOPE
ALEXANDER ORTIZ   NEVADA 120 SAND   (DRY,DENSE)

- 213 -

FIGURE 5.86

SHEAR

TEST 1CN1009 2-17-82   CANTILEVER WALL NO. 1   10 DEGREE BACKFILL SLOPE
ALEXANDER ORTIZ   NEVADA 120 SAND   (DRY.DENSE)

FIGURE 5.87

DISPLACEMENT

TEST 1CN1009 2-17-82   CANTILEVER WALL NO. 1   10 DEGREE BACKFILL SLOPE
ALEXANDER ORTIZ   NEVADA 120 SAND   (DRY.DENSE)

FIGURE 5.88

MOMENT

TEST 1CN1510 2-19-82   CANTILEVER WALL NO. 1   15 DEGREE BACKFILL SLOPE
ALEXANDER ORTIZ   NEVADA 120 SAND (DRY,MEDIUM DENSE)

PRESSURE

FIGURE 5.89

TEST 1CN1510 2-19-82   CANTILEVER WALL NO. 1   15 DEGREE BACKFILL SLOPE
ALEXANDER ORTIZ   NEVADA 120 SAND (DRY,MEDIUM DENSE)

FIGURE 5.90

SHEAR

TEST 1CN1510 2-19-82 CANTILEVER WALL NO. 1 15 DEGREE BACKFILL SLOPE
ALEXANDER ORTIZ   NEVADA 120 SAND (DRY, MEDIUM DENSE)

FIGURE 5.91

DISPLACEMENT

TEST 1CN1510 2-19-82   CANTILEVER WALL NO. 1   15 DEGREE BACKFILL SLOPE
ALEXANDER ORTIZ   NEVADA 120 SAND (DRY,MEDIUM DENSE)

FIGURE 5.92

MOMENT

TEST 2CND011 2-25-82   CANTILEVER WALL NO. 2 ZERO DEGREE BACKFILL SLOPE
ALEXANDER ORTIZ   NEVADA 120 SAND   (DRY,DENSE)

FIGURE 5.93

PRESSURE

TEST 2CND011 2-25-82   CANTILEVER WALL NO. 2 ZERO DEGREE BACKFILL SLOPE
ALEXANDER ORTIZ   NEVADA 120 SAND   (DRY,DENSE)

FIGURE 5.94

SHEAR

TEST 2CN0011 2-25-82   CANTILEVER WALL NO. 2 ZERO DEGREE BACKFILL SLOPE
ALEXANDER ORTIZ   NEVADA 120 SAND   (DRY,DENSE)

FIGURE 5.95

TEST 2CND011 2-25-82   CANTILEVER WALL NO. 2 ZERO DEGREE BACKFILL SLOPE
ALEXANDER OZTIZ   NEVADA 120 SAND   (DRY,DENSE)

FIGURE 5.96
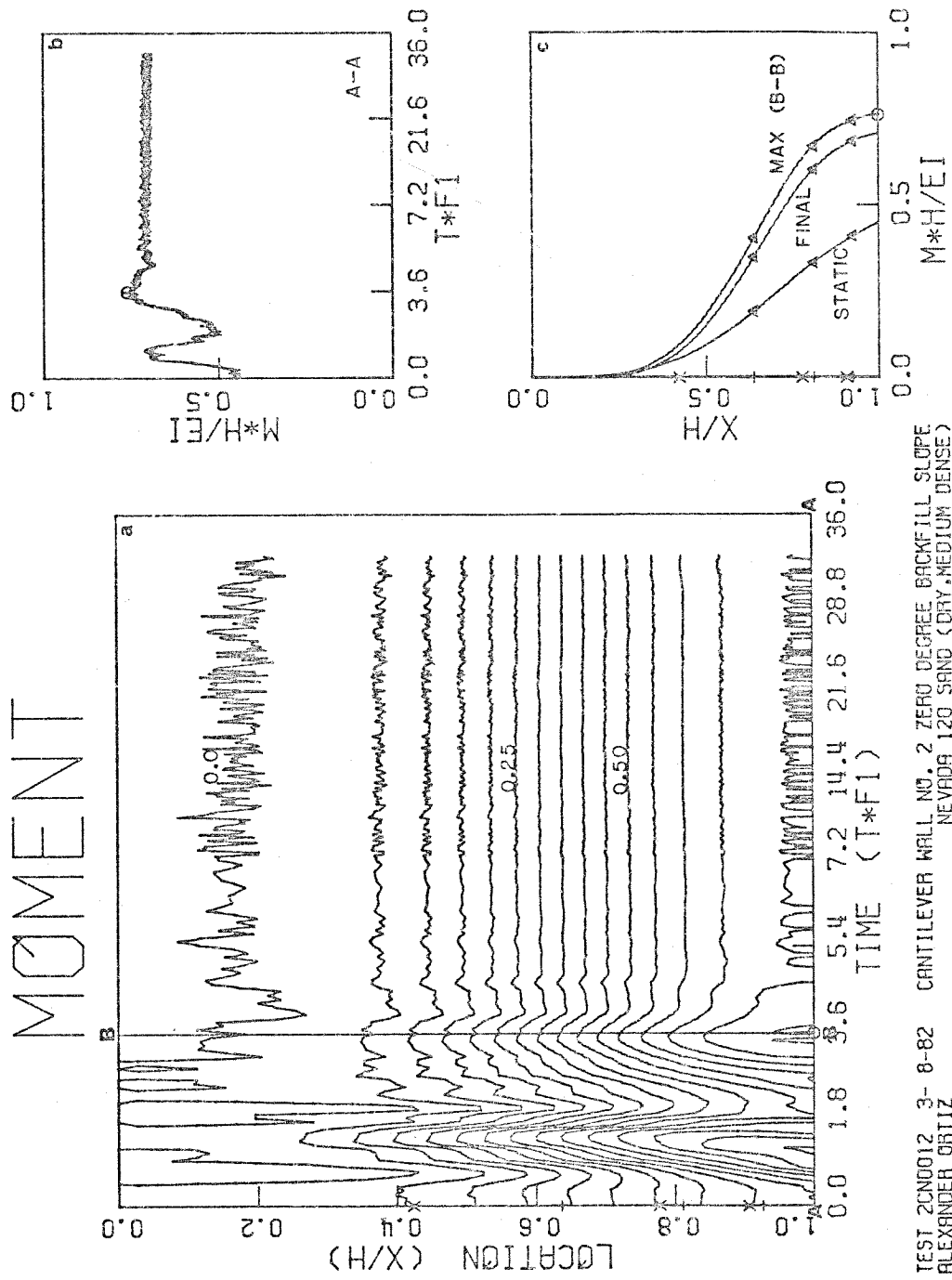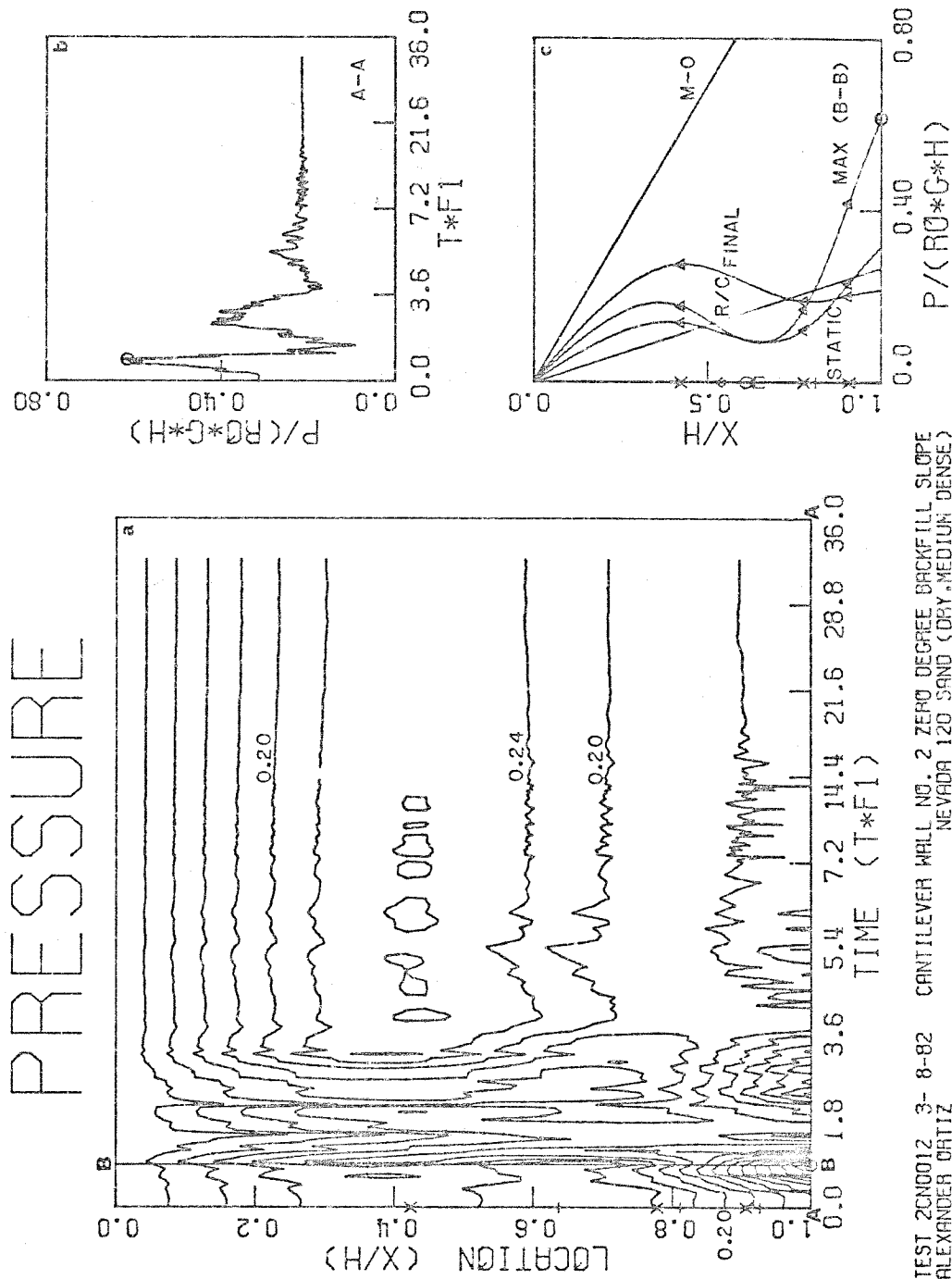
TEST 2CND012 3- 8-82 CANTILEVER WALL NO. 2 ZERO DEGREE BACKFILL SLOPE
ALEXANDER ORTIZ   NEVADA 120 SAND (DRY,MEDIUM DENSE)

FIGURE 5.97

PRESSURE

TEST 2CN0012 3- 8-82   CANTILEVER WALL NO. 2 ZERO DEGREE BACKFILL SLOPE
ALEXANDER ORTIZ   NEVADA 120 SAND (DRY,MEDIUM DENSE)

FIGURE 5.98

SHEAR
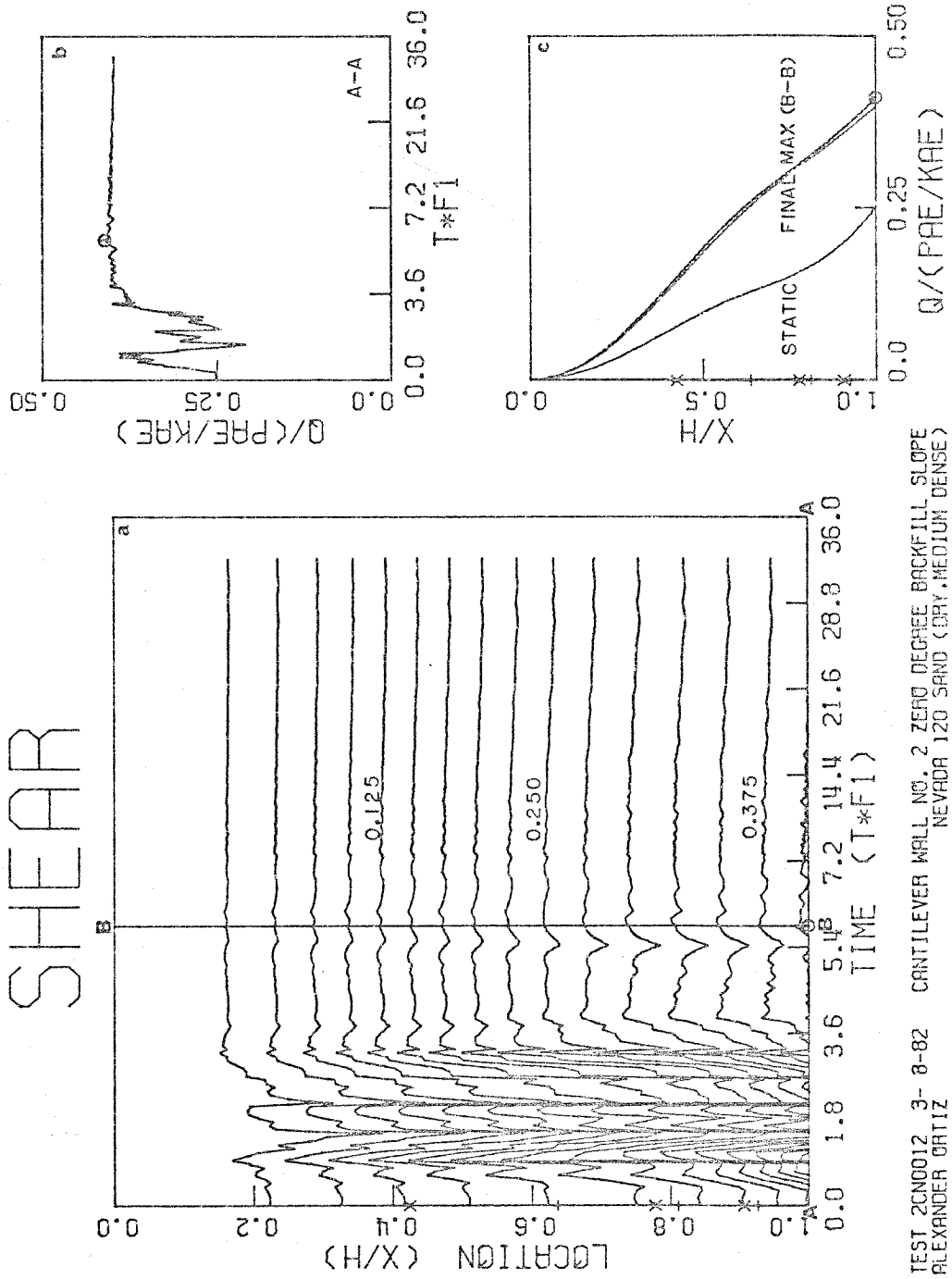
TEST 2CN0012 3- 8-82   CANTILEVER WALL NO. 2 ZERO DEGREE BACKFILL SLOPE
ALEXANDER ORTIZ   NEVADA 120 SAND (DRY,MEDIUM DENSE)

FIGURE 5.99

TEST 2CN0012 3- 8-82 CANTILEVER WALL NO. 2 ZERO DEGREE BACKFILL SLOPE
ALEXANDER ORTIZ   NEVADA 120 SAND (DRY,MEDIUM DENSE)

FIGURE 5.100
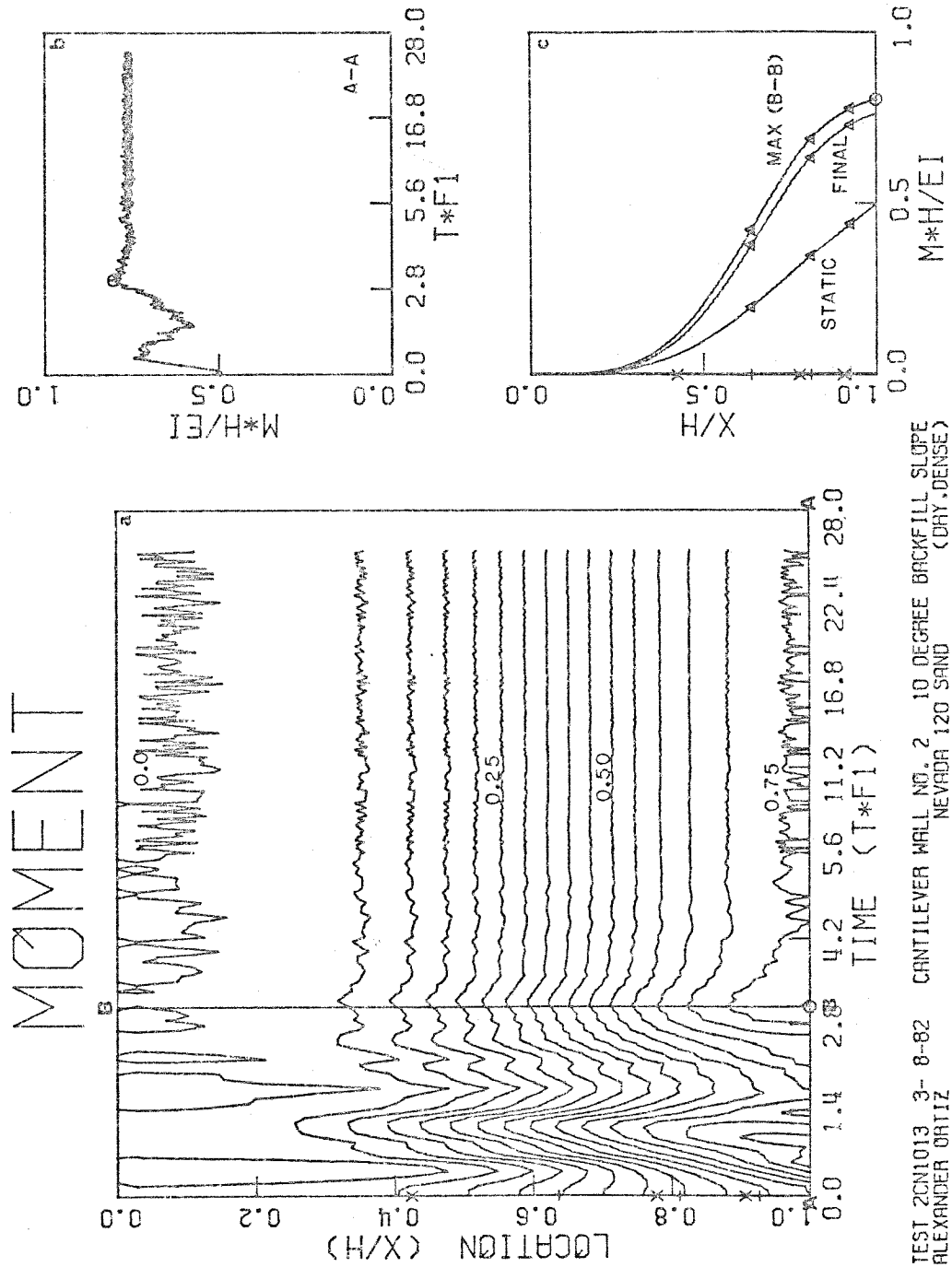
MOMENT

TEST 2CN1013 3- 8-82   CANTILEVER WALL NO. 2   10 DEGREE BACKFILL SLOPE
ALEXANDER ORTIZ   NEVADA 120 SAND   (DRY,DENSE)

FIGURE 5.101
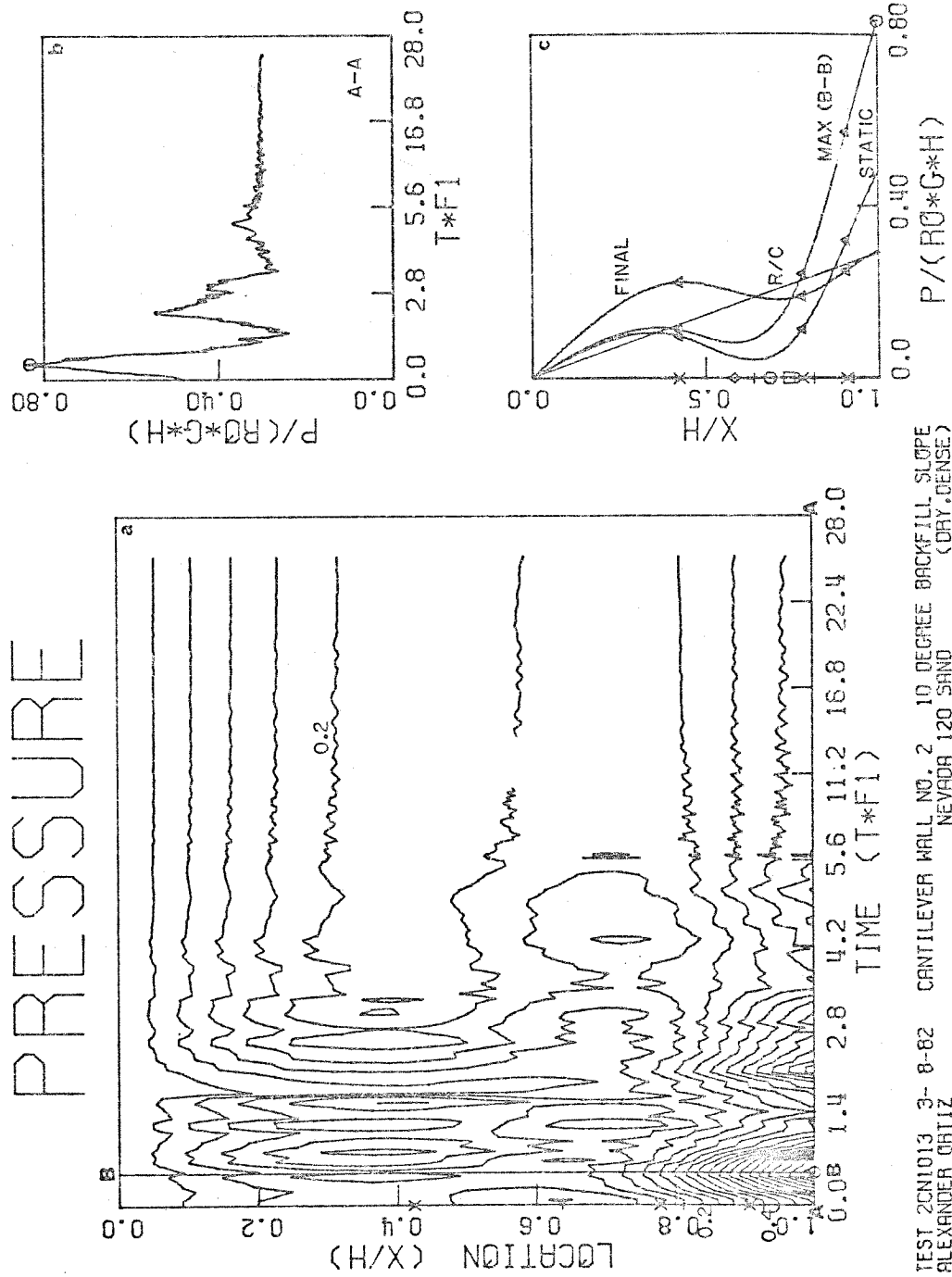
PRESSURE

TEST 2CN1013 3- 8-82   CANTILEVER WALL NO. 2   10 DEGREE BACKFILL SLOPE
ALEXANDER ORTIZ   NEVADA 120 SAND   (DRY,DENSE)

FIGURE 5.102
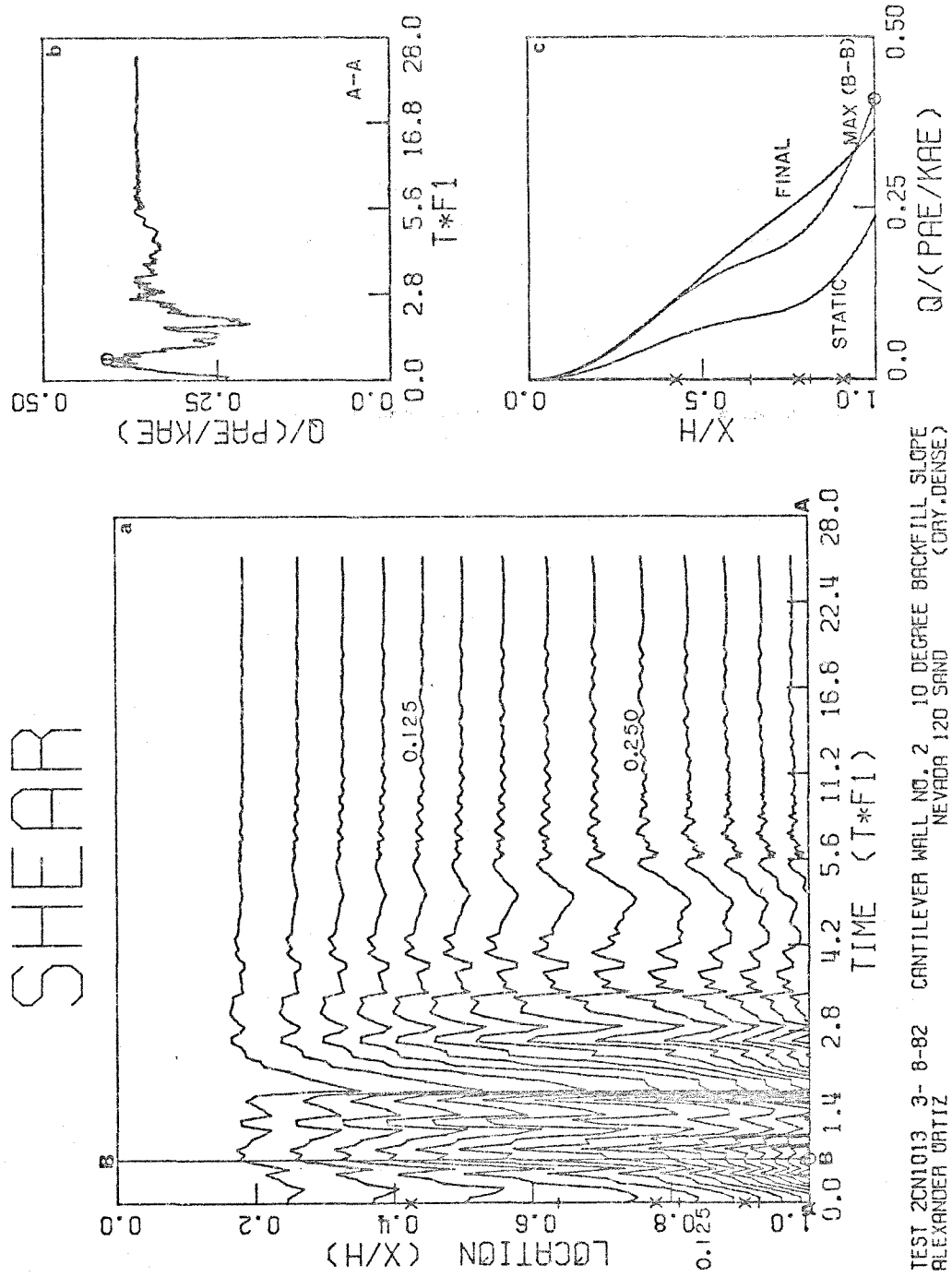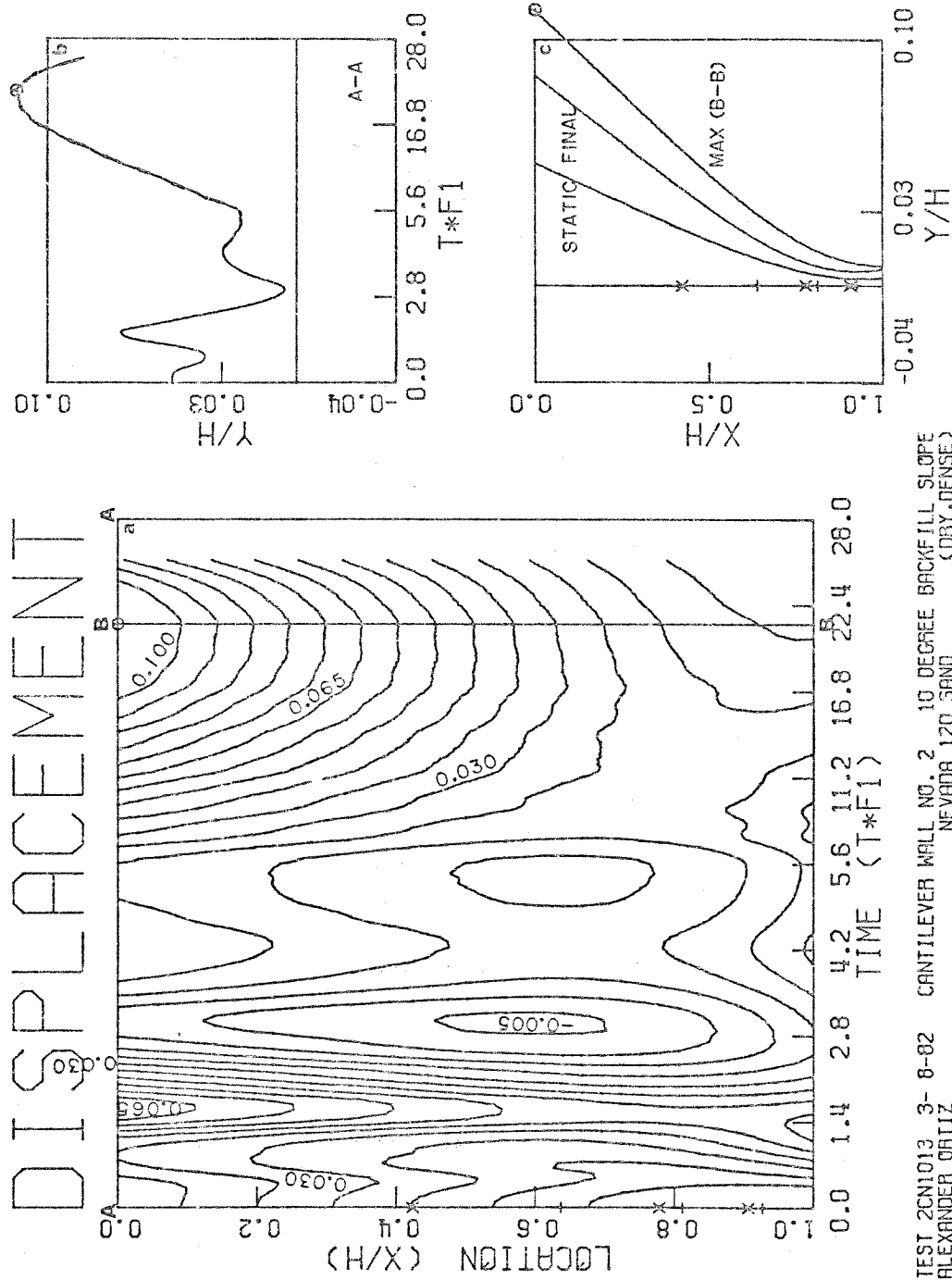
SHEAR

TEST 2CN1013 3- 8-82   CANTILEVER WALL NO. 2   10 DEGREE BACKFILL SLOPE
ALEXANDER ORTIZ   NEVADA 120 SAND   (DRY,DENSE)

FIGURE 5.103

DISPLACEMENT

TEST 2CN1013 3- 8-82   CANTILEVER WALL NO. 2 10 DEGREE BACKFILL SLOPE
ALEXANDER ORTIZ   NEVADA 120 SAND   (DRY,DENSE)

FIGURE 5.104

TEST 2CN1514 3- 9-82   CANTILEVER WALL NO. 2   15 DEGREE BACKFILL SLOPE
ALEXANDER ORTIZ   NEVADA 120 SAND   (DRY,DENSE)

PRESSURE
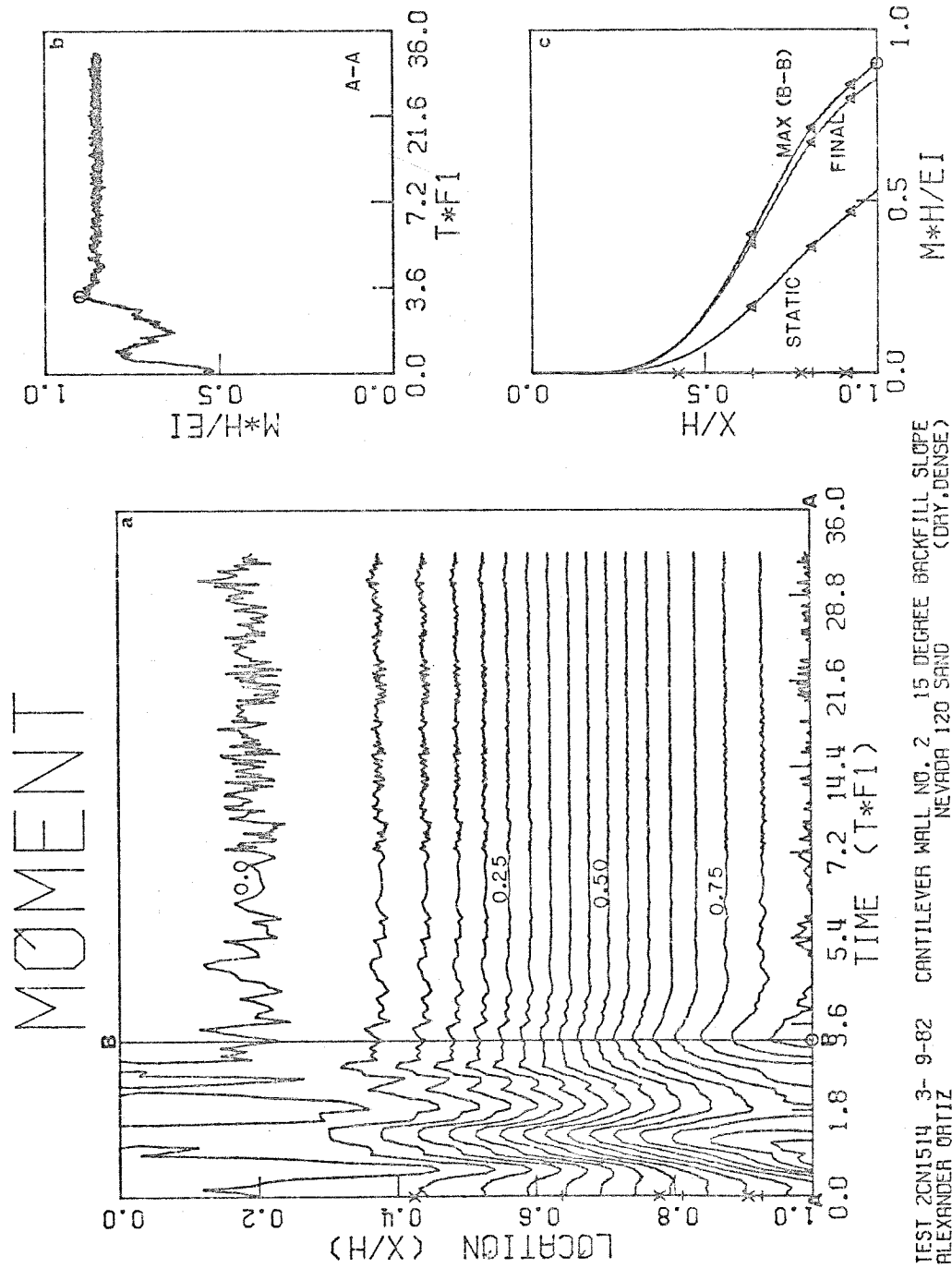
FIGURE 5.105

TEST 2CN1514 3- 9-82   CANTILEVER WALL NO. 2   15 DEGREE BACKFILL SLOPE
ALEXANDER ORTIZ   NEVADA 120 SAND   (DRY,DENSE)
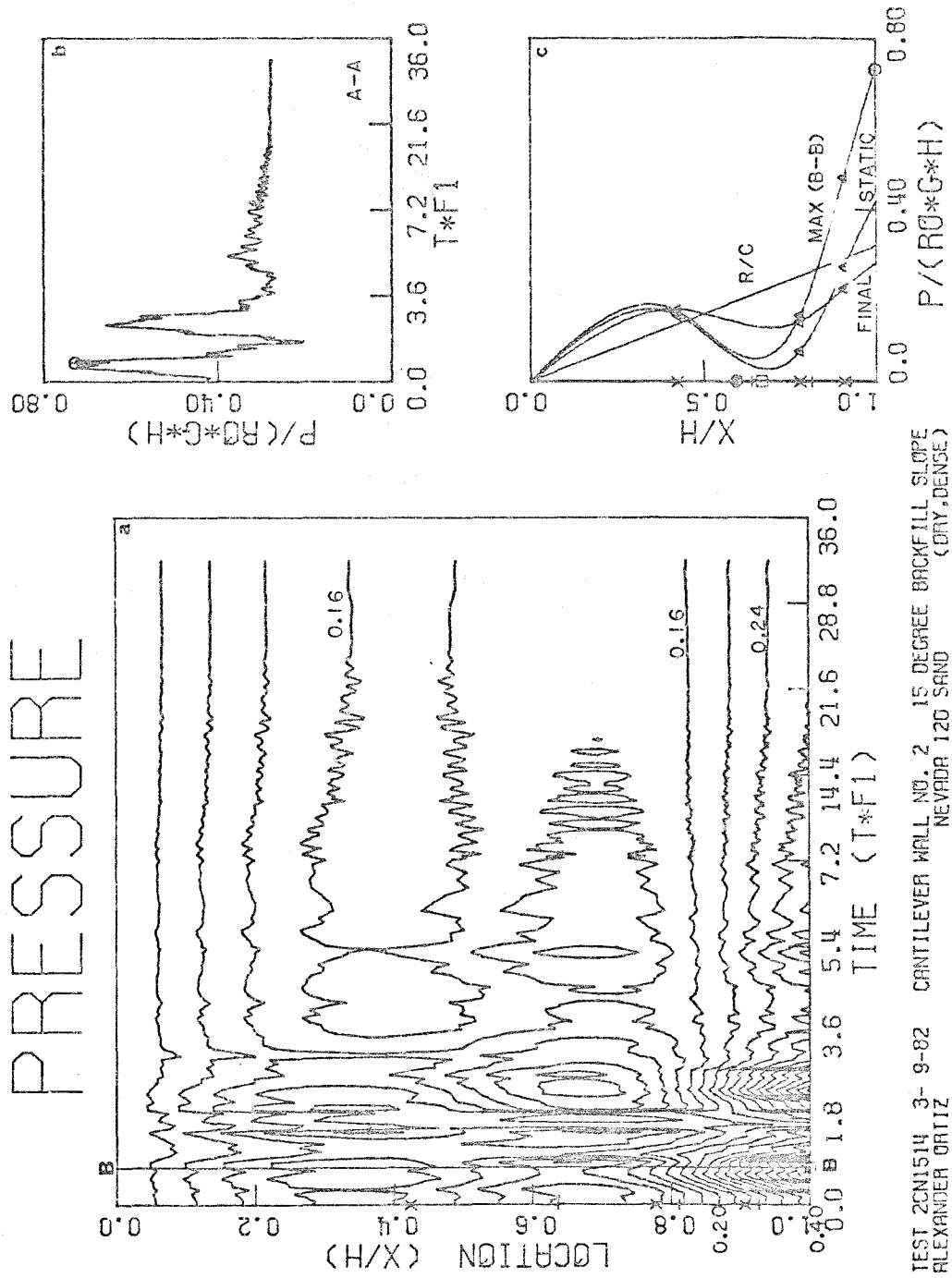
FIGURE 5.106

SHEAR

TEST 2CN1514 3- 9-82   CANTILEVER WALL NO. 2   15 DEGREE BACKFILL SLOPE
ALEXANDER ORTIZ   NEVADA 120 SAND   (DRY.DENSE)

FIGURE 5.107

DISPLACEMENT
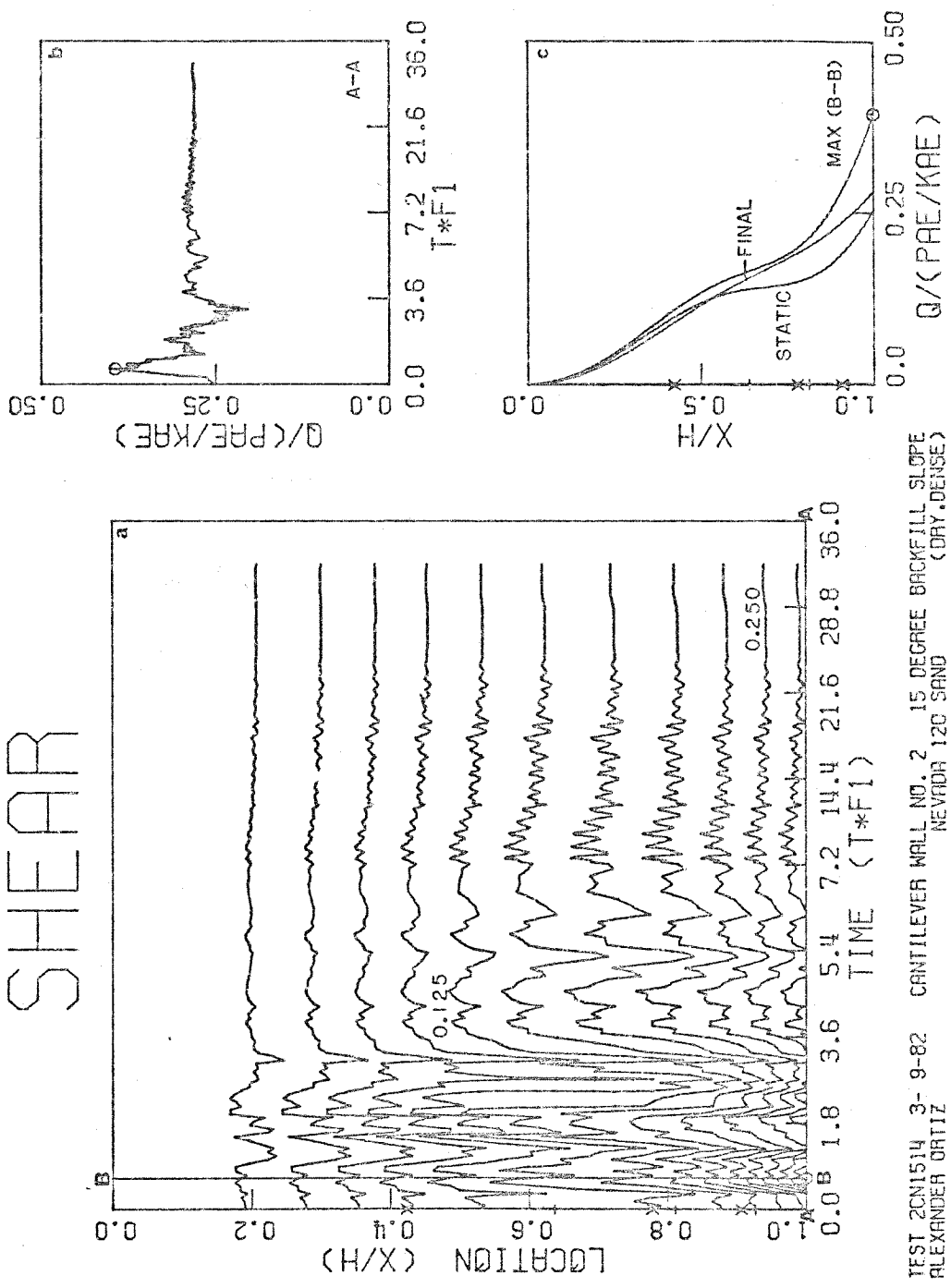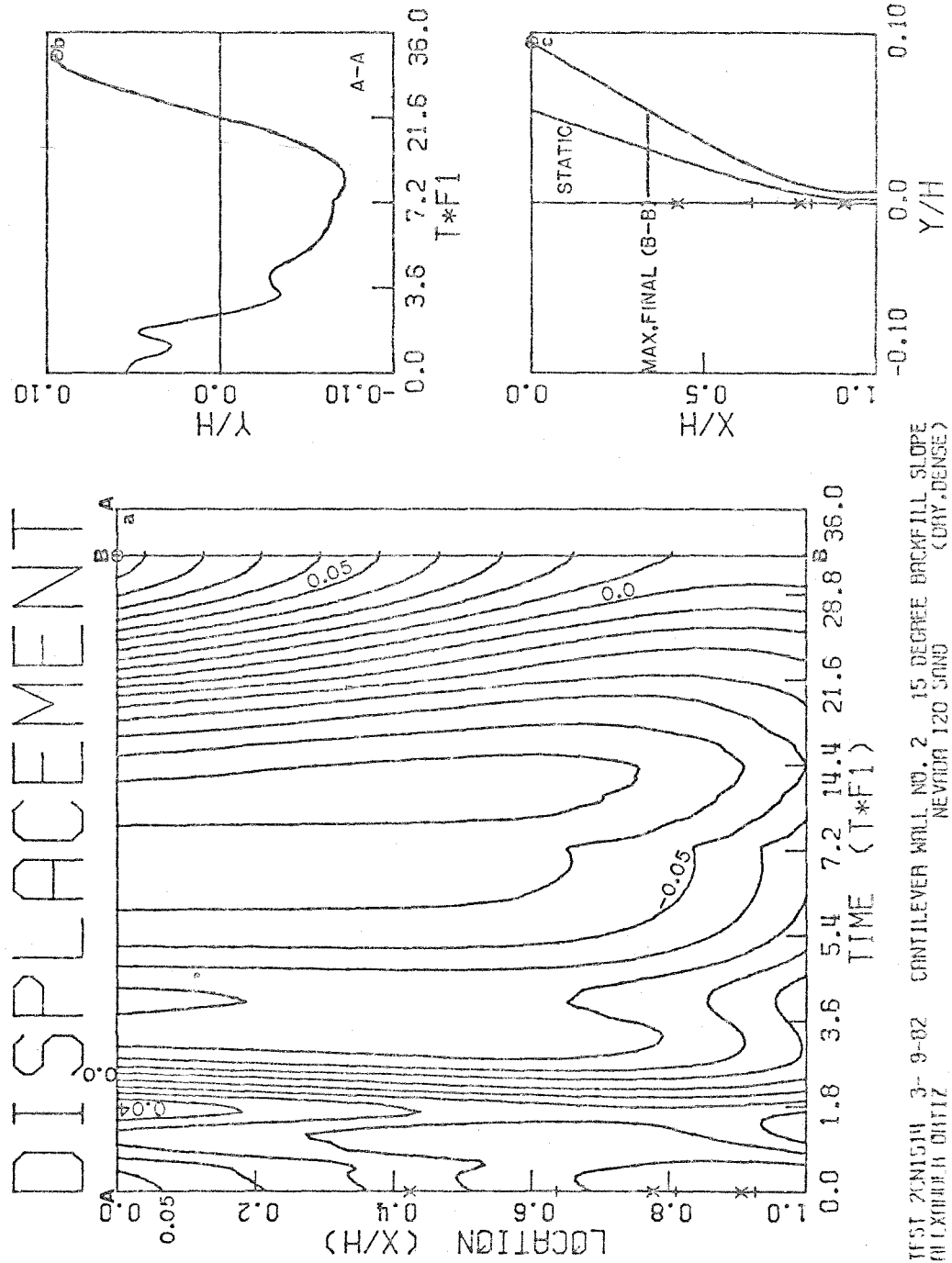
TEST 2GN1514 3- 9-82 CANTILEVER WALL NO. 2 15 DEGREE BACKFILL SLOPE
ALEXANDER ORTIZ NEVADA 120 SAND (DRY,DENSE)

5.4 Static Results

Although the main emphasis of the research project was the study of the dynamic behavior of retaining walls, some interesting results were obtained from a static point of view as well. An important indication that an accurate model has been used is to examine how it behaves statically and compare the results with the accepted Rankine and Coulomb static lateral earth pressure theories.

The Rankine lateral earth pressure theory gives the resultant active force $P_A/(1/2\gamma H^2)$ acting on the retaining wall as:

$$\frac{P_A}{1/2\gamma H^2} = K_A = \frac{(1 - \sin\phi)}{(1 + \sin\phi)} \tag{5.2}$$

The coefficient K_A is referred to as the active earth pressure coefficient. The assumptions under which this theory is formulated are very approximately fulfilled by the model tests which have a horizontal backfill, namely:

- The wall is rigid and vertical.

- The backfill is horizontal.

- There is no friction between soil and wall.

- There is active pressure (wall displaces more than 1/2% of its height).

The Coulomb lateral earth pressure theory (of which the Rankine is only a special case) follows the same assumptions as the Mononobe-Okabe theory (Section 5.5), with the exception that there are no lateral or

vertical acceleration coefficients k_h or k_v (i.e. $\theta = 0^\circ$). The

resultant force acting on the wall is expressed as:

$$\frac{P_A}{1/2\gamma H^2} = K_A = \frac{\cos^2(\phi-\beta)}{\cos^2\beta\,\cos(\delta+\beta)}\left[1+\left(\frac{\sin(\phi+\delta)\,\sin(\phi-i)}{\cos(\delta+\beta)\,\cos(i-\beta)}\right)^{1/2}\right]^{-2} \quad (5.3)$$

For the previously mentioned assumptions, with the exception that

the backfill can be sloping, equation (5.3) can be reduced to:

$$\frac{P_A}{1/2\gamma H^2} = K_A = \cos^2\phi\left[1+\left(\frac{\sin\phi\,\sin(\phi-i)}{\cos i}\right)^{1/2}\right]^{-2} \quad (5.4)$$

This equation will be used as a comparison basis for the tests with

sloping backfills.

In the Rankine and Coulomb theories, under the assumptions listed,

the resultant acts at one third of the height above the wall base since

the pressure distribution is assumed triangular. Therefore, the over-

turning moment $6M/\gamma H^3$ from the Rankine/Coulomb theory is:

$$\frac{6M_A}{\gamma H^3} = K_A \quad (5.5)$$

The maximum bending moment is:

$$\frac{M_A H}{EI} = \frac{\gamma H^4}{6EI}K_A \quad (5.6)$$

Table 5.5 gives a comparison of the maximum measured static parame-

ters from the tests with the Rankine/Coulomb theories, recalling that

the friction angle of the soil used is 35°.

The lateral earth pressure theories (both static and dynamic)

unfortunately only estimate the resultant force and its point of appli-

cation based on the assumption of a triangular pressure distribution.

TABLE 5.5

Maximum Static Values

		Test 1CN0001	Test 1CN0002	Test 1CN1003	Test 1CN0004	Test 1CN1505	Test 1CN0006	Test 1CN0007	Test 1CN0508	Test 1CN1009	Test 1CN1510	Test 2CN0011	Test 2CN0012	Test 2CN1013	Test 2CN1514
$\dfrac{MH}{EI}$	Test	0.241	0.272	0.298	0.246	0.274	0.274	0.168	0.210	0.228	0.291	0.506	0.448	0.498	0.532
	R/C	0.209	0.205	0.229	0.211	0.245	0.213	0.221	0.227	0.242	0.252	0.445	0.432	0.465	0.518
$\dfrac{6M}{\gamma H^3}$	Test	0.313	0.359	0.390	0.315	0.357	0.349	0.206	0.263	0.283	0.367	0.308	0.281	0.508	0.328
	R/C	0.271	0.271	0.300	0.271	0.319	0.271	0.271	0.284	0.300	0.319	0.271	0.271	0.300	0.319
$\dfrac{P}{\gamma H}$	Test	---	0.499	0.442	0.532	0.539	0.419	0.383	0.550	0.430	0.529	0.281	0.315	0.482	0.421
	R/C	0.271	0.271	0.300	0.271	0.319	0.271	0.271	0.284	0.300	0.319	0.271	0.271	0.300	0.319
$\dfrac{Q}{1/2\,\gamma\,H^2}$	Test	0.267	0.297	0.285	0.275	0.255	0.127	0.200	0.304	0.261	0.334	0.215	0.252	0.237	0.255
	R/C	0.271	0.271	0.300	0.271	0.319	0.271	0.271	0.284	0.300	0.319	0.271	0.271	0.300	0.319
y/H	Test	0.0279	0.0319	0.0376	0.0317	0.0344	0.0298	0.0276	0.0294	0.0310	0.0327	0.0439	0.0464	0.0497	0.0047

R/C = Rankine/Coulomb

Maximum $\begin{cases} \text{Moment} \\ \text{Shear-Force} \\ \text{Pressure} \end{cases}$ always at base of wall.

Maximum displacement always at top of wall.

Therefore, the most accurate comparison that can be made is that of the resultant forces.

Comparing the Rankine/Coulomb resultant forces with the maximum shear forces (which are an integration of the pressure distribution behind the wall) it can be concluded that there is reasonable agreement between theory and experiment in this respect, the maximum difference being of the order of 25% between the two. The sole exceptions are tests 1CN1505 and especially 1CN0006 where the pressure distributions show a small magnitude in the upper 60% or so of the height and then increase rapidly below that (Figures 5.69c and 5.73c). This then contains a smaller area under the curve, although the maximum pressures (at the bottom of the wall) are comparable to those of similar tests.

From frames c of the pressure distribution figures, it can be observed that the static pressure distributions are not linear, as the Rankine/Coulomb theories assume, although for the most part, the centroid of the distribution (location of the resultant force) is at around 1/3 of the wall height above the base as a triangular distribution would indicate. It should be noted that, for RW2, the more flexible wall, this centroid does generally creep up to about 40% of the wall height above the base. The maximum pressures (at the bottom of the wall) are much greater in all cases, except 2CN0011 (Figure 5.93c), than those predicted by the Rankine/Coulomb assumption. The maximum static pressures recorded are on an average on the order of 60% higher than those than the Rankine/Coulomb theories would give. From these figures

it can, however, be seen that the traditional theories do seem to predict a correct average pressure distribution.

Since the traditional lateral earth pressure theories are based on the assumption that the wall holding back the soil is rigid, one can only make a qualitative overturning/ bending moment comparison with the test results which are those of two flexible walls. The Rankine/Coulomb overturning moment is assumed to be the resultant force times the moment arm which is 1/3 of the height above the base. The bending (reaction) moments recorded in the tests are generally greater than the overturning (action) moments given by Rankine/Coulomb. The actual test moments generally vary from just a few percent to about 35% greater than those predicted. Since stems of cantilever walls are designed as bending beams, the actual factor of safety could thus actually be much less than the usual 1.7. For a 35% underestimation, the actual safety factor (static) would then only be 1.25.

Looking at the parameters that do not involve the wall stiffness EI, namely, $6M/\gamma H^3$, $P/\gamma H$, and $Q/(1/2\gamma H^2)$, it can be seen that there is correspondingly virtually no difference in the values for the two walls. This indicates that, for the range of wall stiffnesses tested, the system stiffness has little or no effect on the static response. The stiffness of RW1 is about twice that of RW2, but its moments MH/EI are about half. Thus the dimensional moments would be correspondingly similar also demonstrating the independence of wall flexibility on the response.

As far as is known, nobody has ever measured actual moments, static or otherwise, in a cantilever retaining wall, or has ever considered it to be a flexible bending beam, which it obviously is. Thus the moments shown in frames c of the moment distribution figures provide a first insight into actual moments in cantilever walls due to lateral earth pressures.

The measurement of lateral displacements seems also to be unprecedented. The static displacements for all the tests indicate that the wall has initially displaced laterally at least 1/2% of its height and thus a state of plastic equilibrium in the traditional sense can be assumed to exist behind the wall, and thus comparisons with the traditional theories (which use this assumption) can be considered valid. The maximum static displacements are of the order of 3% to 4% in RW1 and 4% to 6% in the less stiff RW2, and, as expected, always occur at the top of the wall. On some of the displacement curves (frames c), one may note a small outward "curl" near the bottom of the wall. This is probably due to slight faults in the measurements of the boundary conditions and should be considered numerical and not physical. This also applies to the maximum dynamic and final static curves.

5.5. Dynamic Results

One can compare the maximum dynamic parameters obtained from the tests with those which would be estimated from the Mononobe-Okabe Theory (discussed in detail in Section 1.1) for similar circumstances. The envelopes (upper bounds) of the various parameters with respect to the

MAXIMUM LATERAL ACCELERATION (A/G)
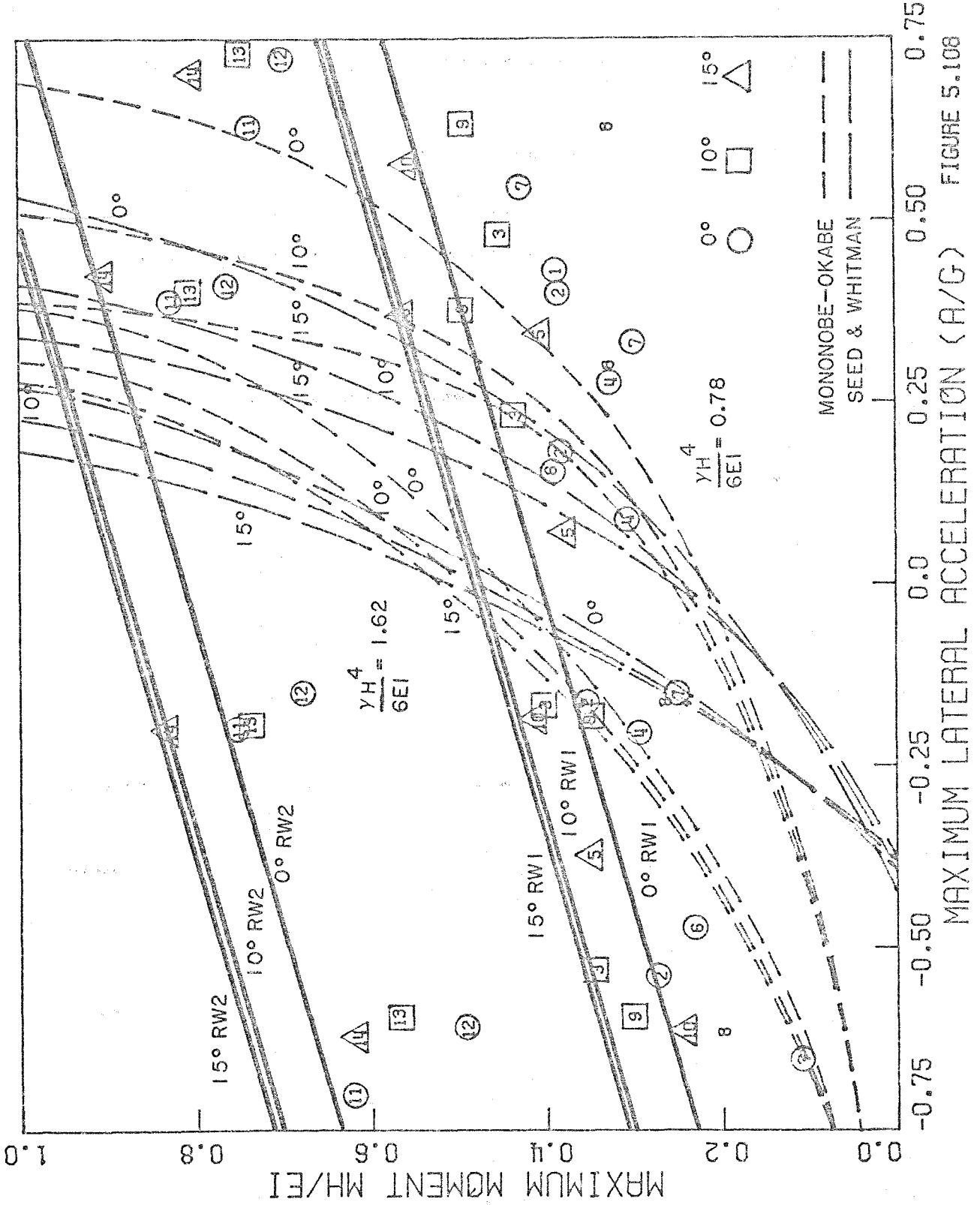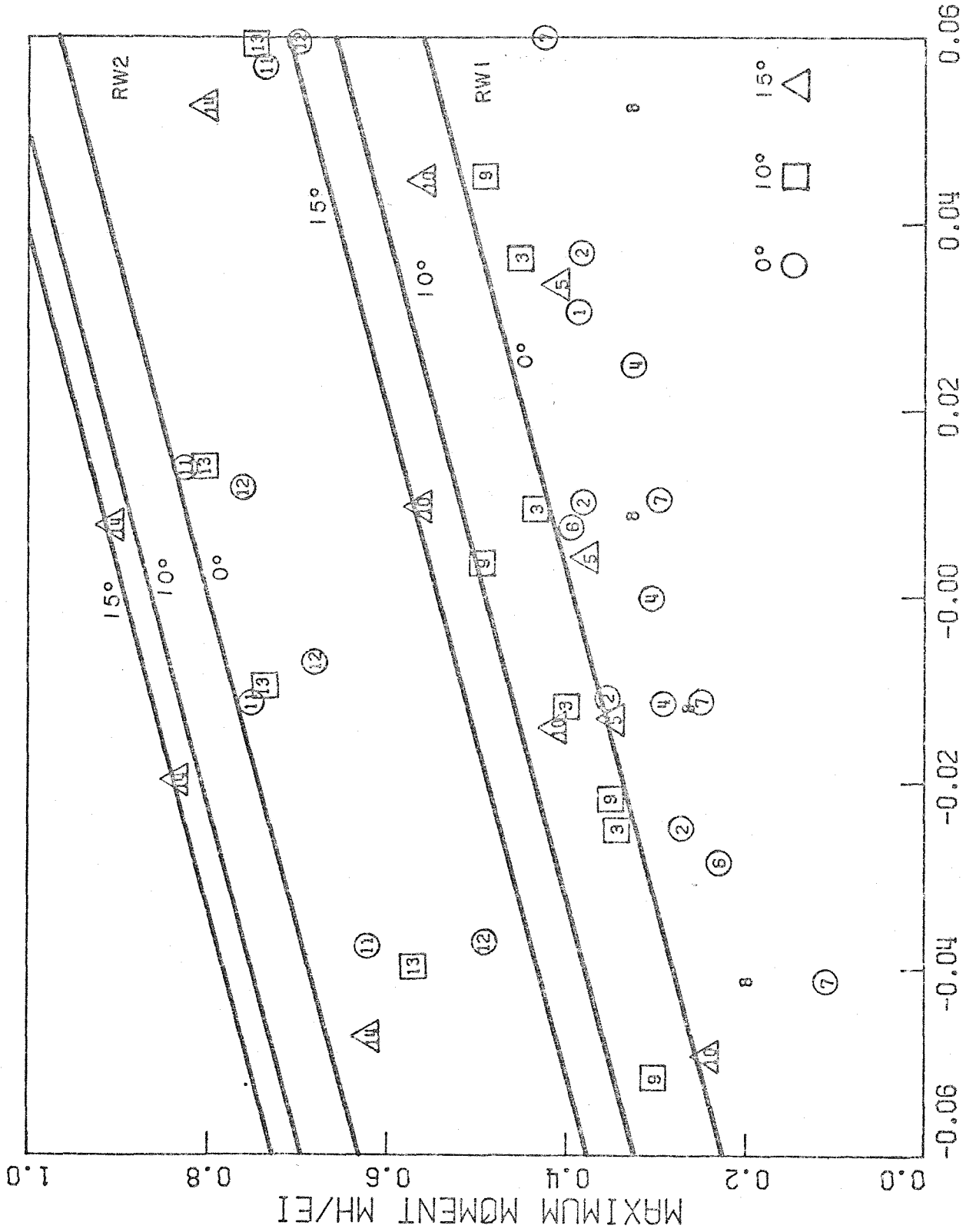
FIGURE 5.108
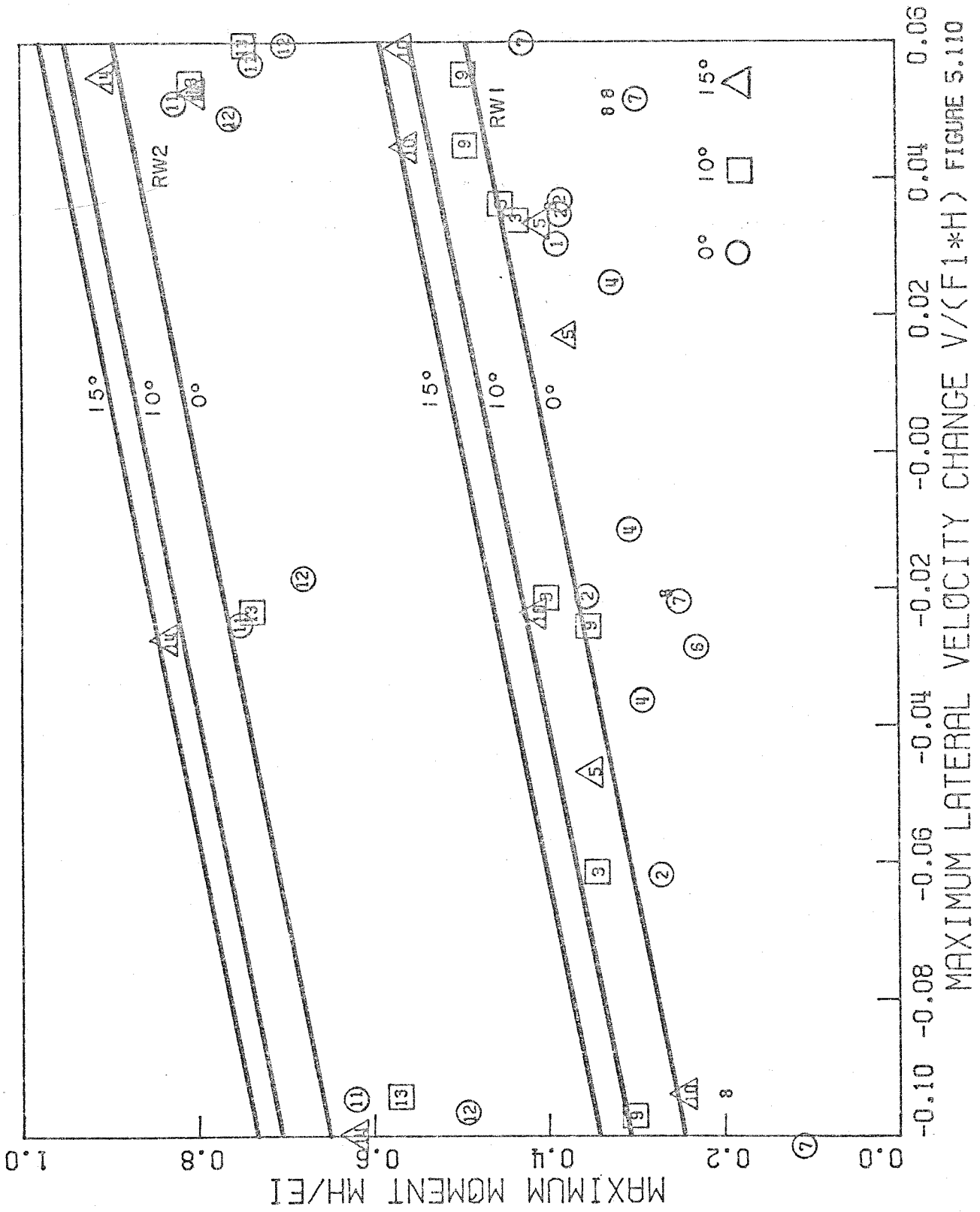
FIGURE 5.109

MAXIMUM LATERAL VELOCITY CHANGE V/(F1*H)   FIGURE 5.110

MAXIMUM LATERAL ACCELERATION (A/G)

MAXIMUM MOMENT 6M/(RØ*G*(H**3))

FIGURE 5.11

FIGURE 5.112

MAXIMUM LATERAL VELOCITY V/(F1*H)

MAXIMUM MOMENT 6M/(R0*G*(H**3))

MAXIMUM LATERAL VELOCITY CHANGE V/(F1*H) FIGURE 5.113

FIGURE 5.114

FIGURE 5.115

FIGURE 5.1.15
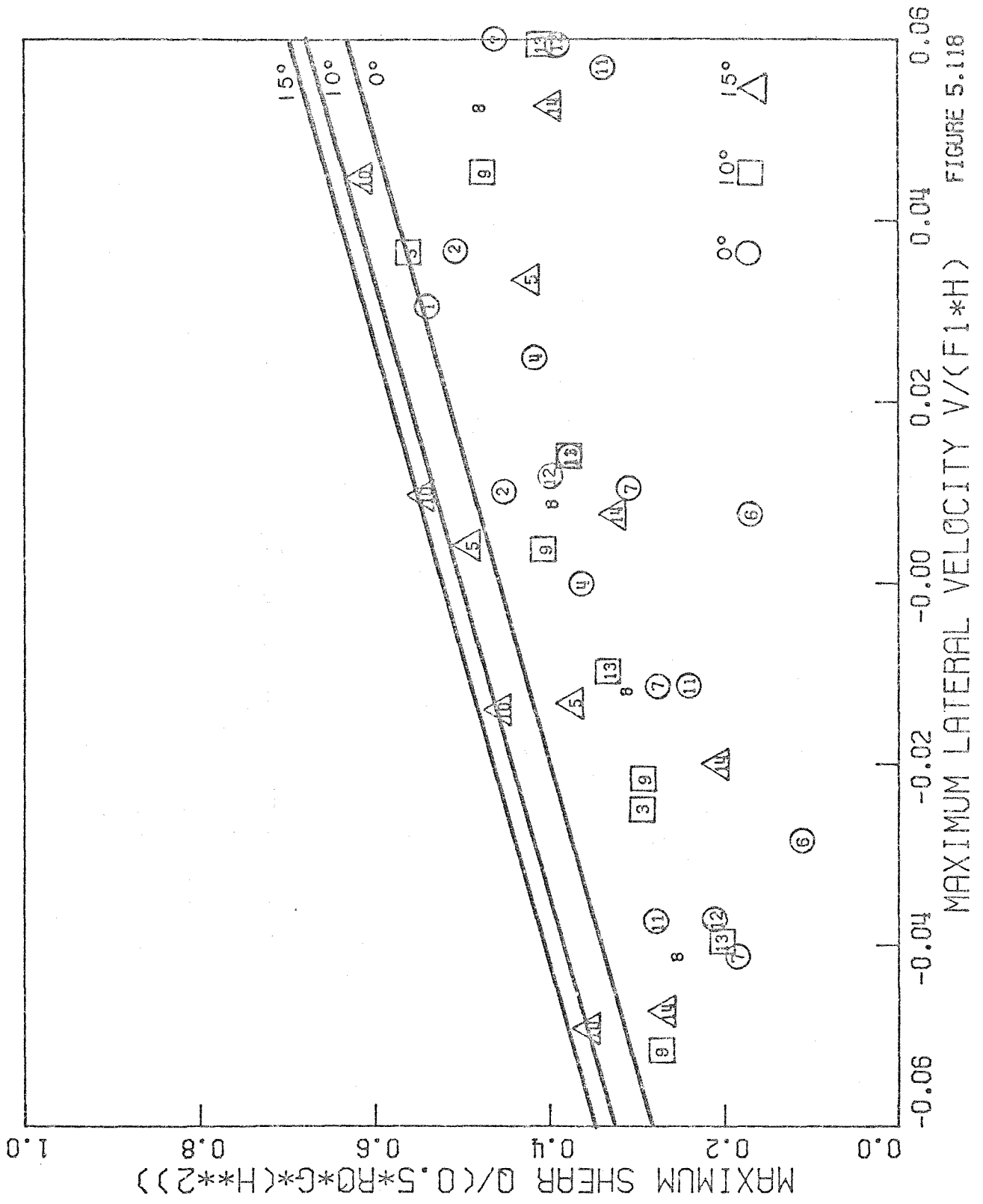
FIGURE 5.117

FIGURE 5.118
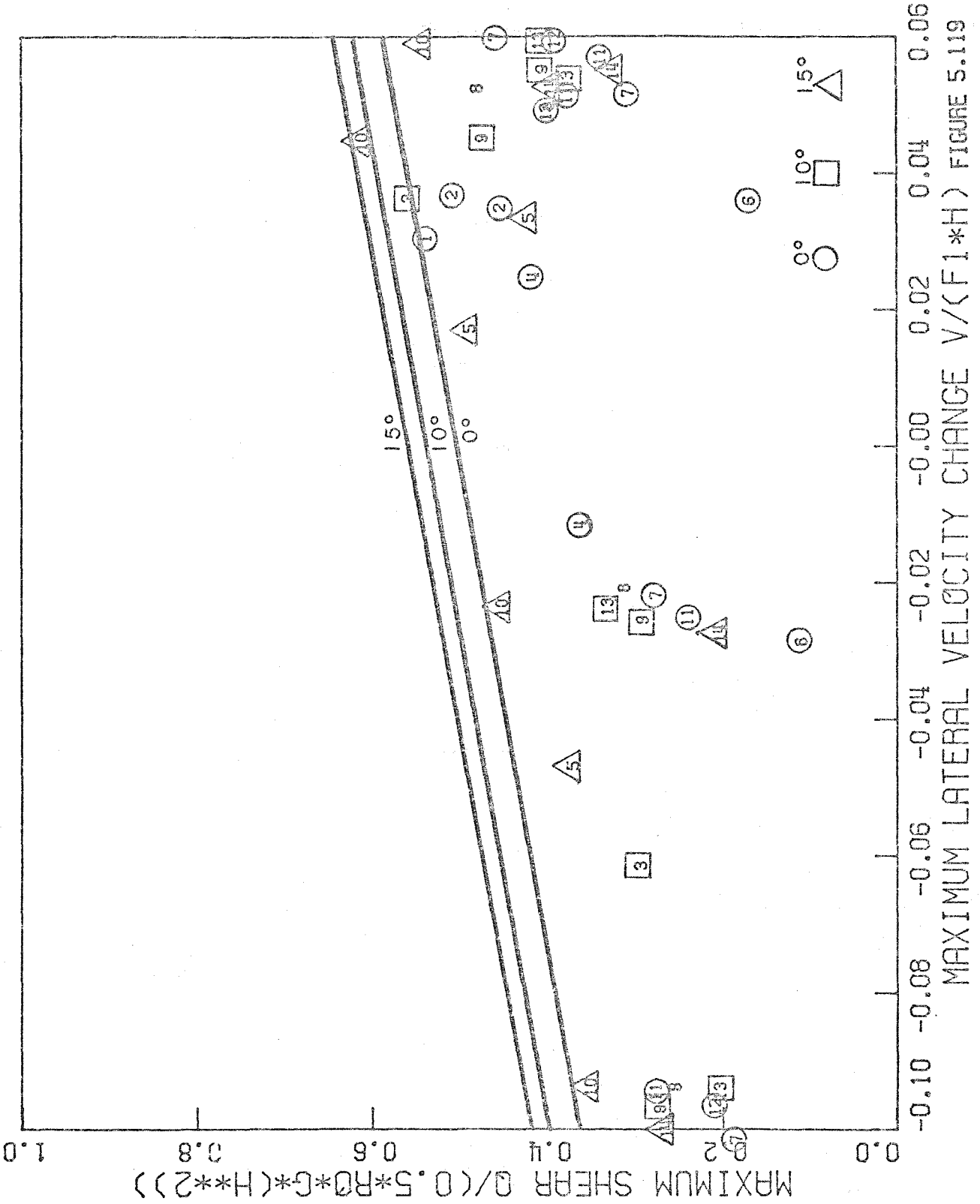
MAXIMUM LATERAL VELOCITY CHANGE V/(F1*H) FIGURE 5.119
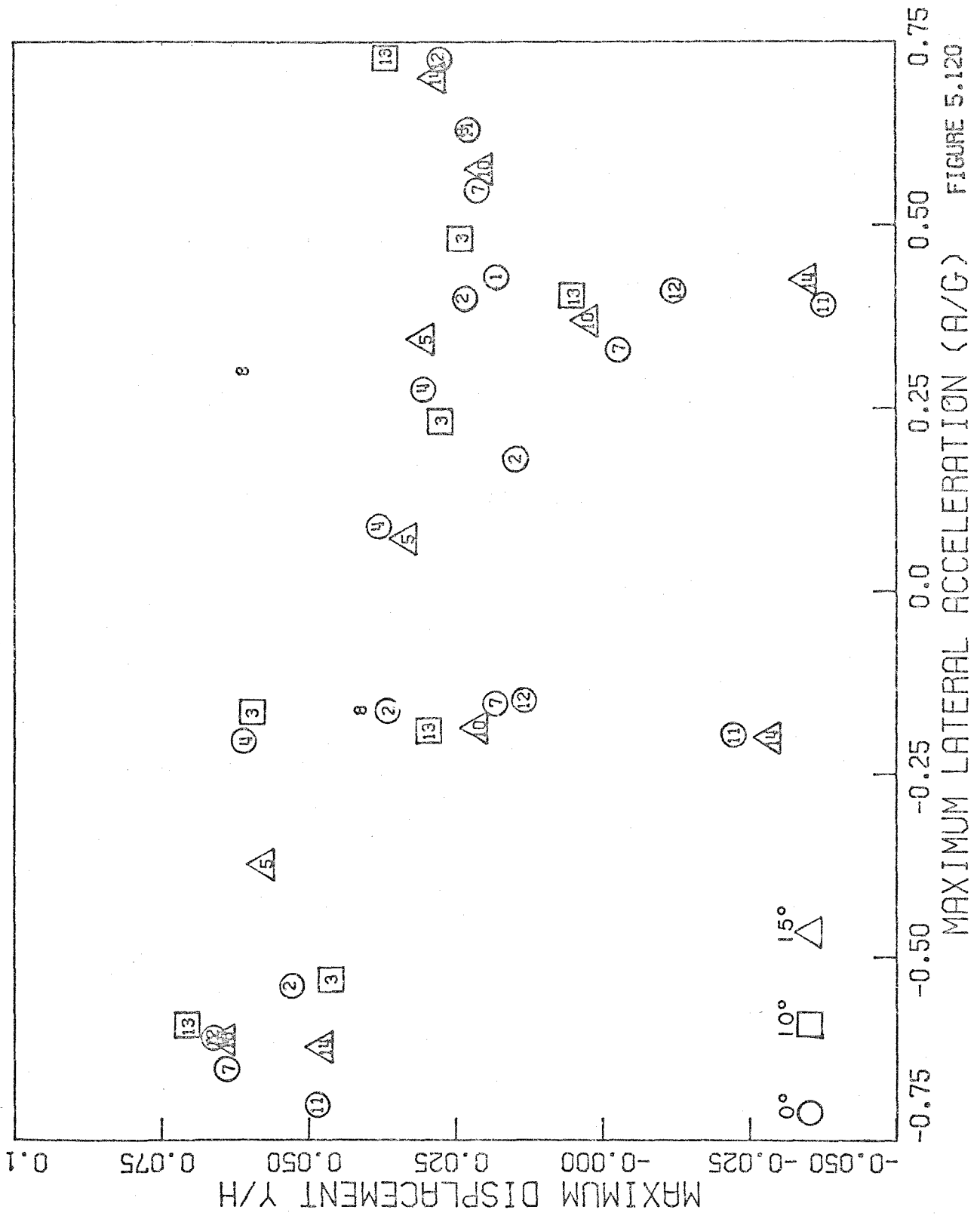
FIGURE 5.120
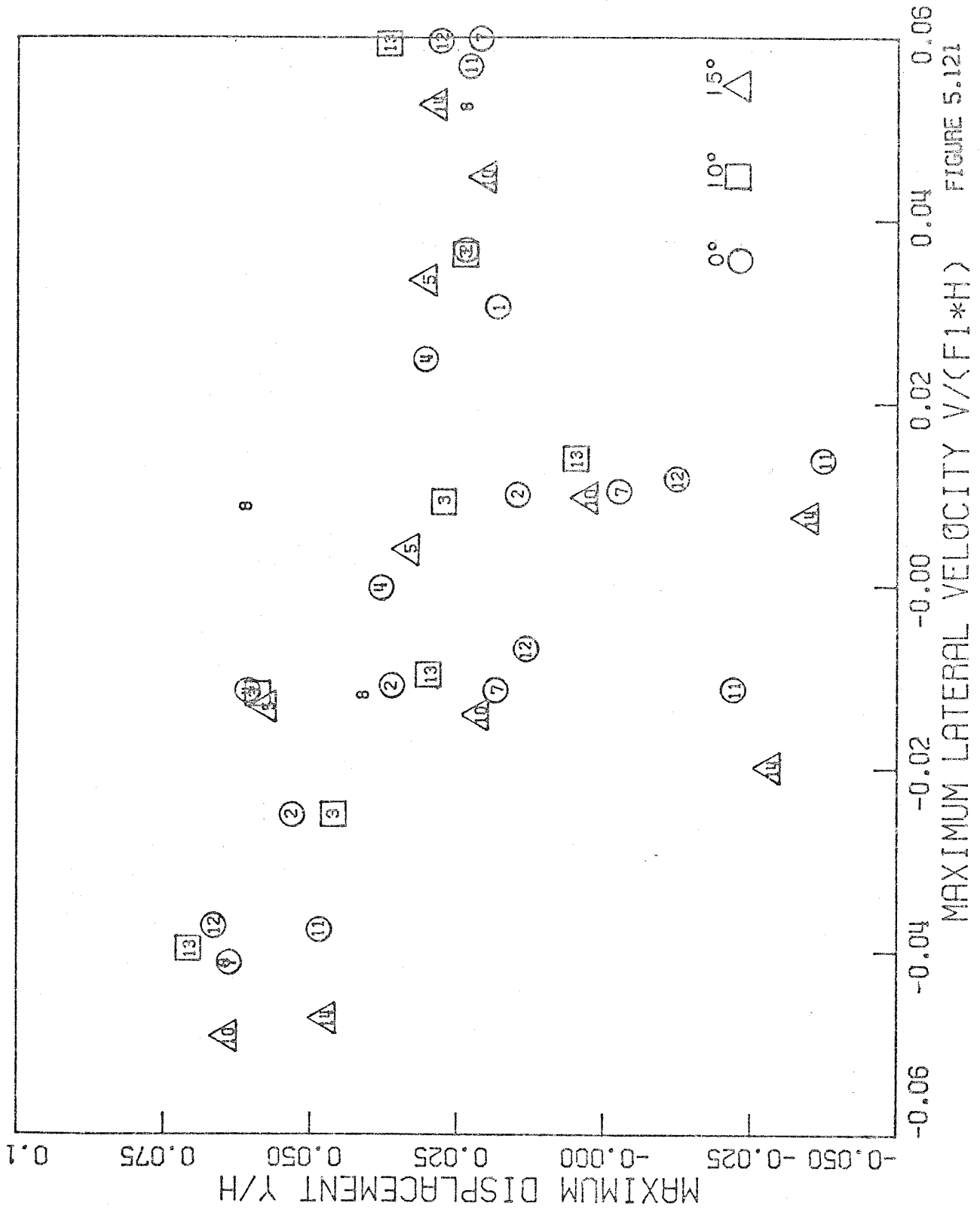
FIGURE 5.121
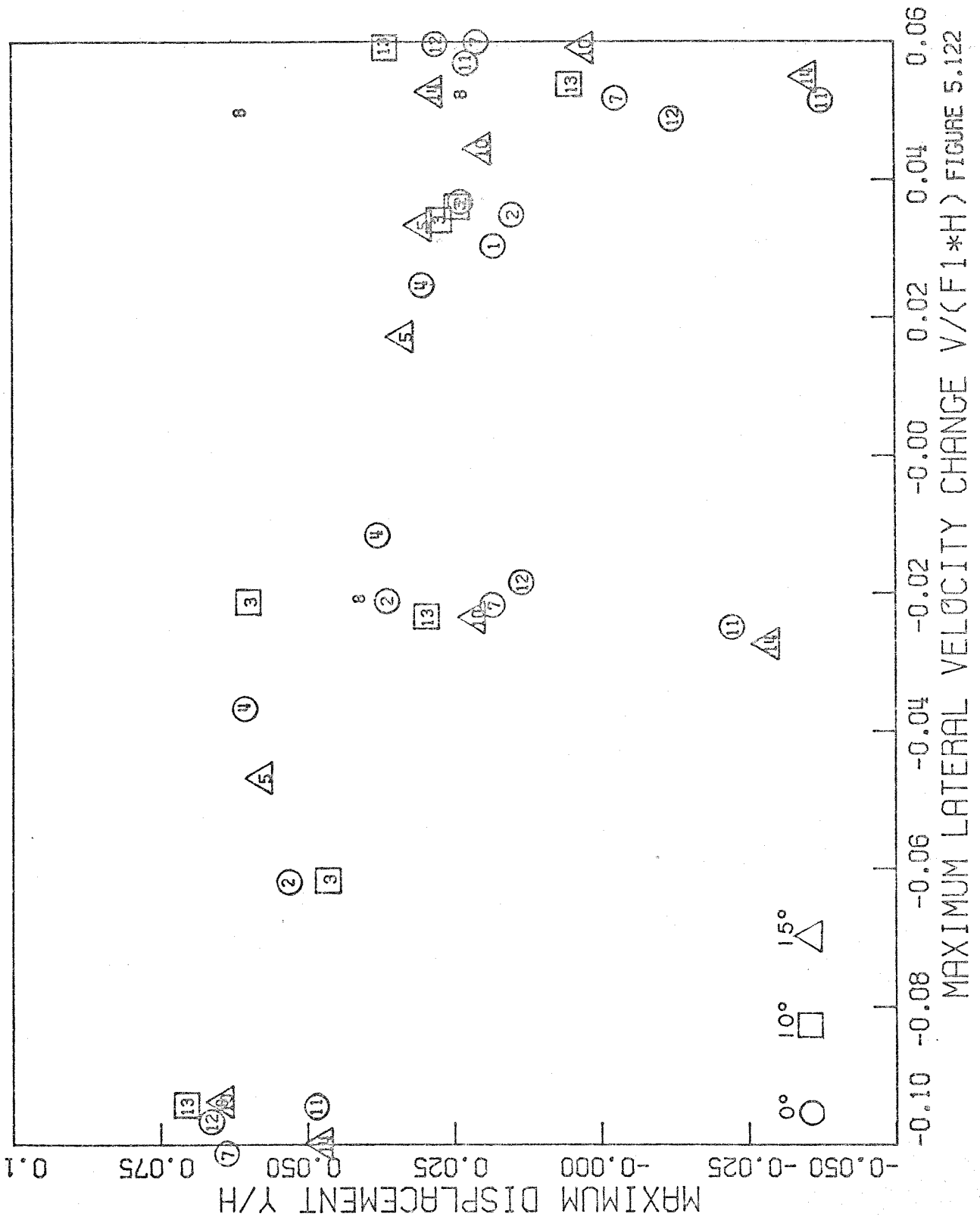
MAXIMUM LATERAL VELOCITY V/(F1*H)

MAXIMUM DISPLACEMENT Y/H

FIGURE 5.122

strong-motion characteristics are illustrated in Figures 5.108 through 5.122. How these envelopes were determined will be explained below. In addition, Mononobe-Okabe distributions with respect to the lateral acceleration coefficients k_h for an average test soil density are shown in Figures 5.108, 5.111, 5.114 and 5.117.

For a flat backfill under the test assumptions (see Section 5.4), the total resultant active force $P_{AE}/(1/2\gamma H^2)$, given by Mononobe-Okabe, reduces from equations (1.1) and (1.2) to:

$$\frac{P_{AE}}{1/2\gamma H^2} = \cos^2 \frac{(\phi-\theta)}{\cos^2 \theta} \left[1 + \left(\frac{\sin \phi \sin (\phi-\theta)}{\cos \theta} \right)^{1/2} \right]^{-2} \tag{5.8}$$

For a sloping backfill of angle i, the resultant force is expressed as:

$$\frac{P_{AE}}{1/2\gamma H^2} = K_{AE} = \frac{\cos^2 (\phi-\theta)}{\cos^2 \theta} \left[1 + \left(\frac{\sin \phi \sin (\phi-\theta-i)}{\cos \theta \cos i} \right)^{1/2} \right]^{-2} \tag{5.9}$$

These equations form the basis for comparison with the maximum dynamic results obtained from the tests.

In the Mononobe-Okabe theory, the resultant force is assumed to act at one third of the height above the base of the wall. Therefore, the overturning moment $6M_{AE}/\gamma H^3$ from the Mononobe-Okabe theory is:

$$\frac{6M_{AE}}{\gamma H^3} = K_{AE} \tag{5.10}$$

The maximum bending moment is:

$$\frac{M_{AE}H}{EI} = \frac{\gamma H^4}{6EI} K_{AE} \tag{5.11}$$

On the basis of previous studies (up to 1970), Seed and Whitman [55] suggest that the dynamic portion of the moment acts at 0.6 of the height above the base of the wall. Therefore the overturning moment is:

$$\frac{6M_{AE}}{\gamma H^3} = K_A + 1.8\Delta K_{AE} = 1.8K_{AE} - 0.8K_A \qquad (5.12)$$

where:

$$\Delta K_{AE} = K_{AE} - K_A \qquad (5.13)$$

Likewise, the bending moment is:

$$\frac{M_{AE}H}{EI} = \frac{\gamma H^4}{6EI}\left(K_A + 1.8\Delta K_{AE}\right) = \frac{\gamma H^4}{6EI}\left(1.8K_{AE} - 0.8K_A\right) \qquad (5.14)$$

This suggestion is also used in the moment comparisons with the experiments, and is shown (for an average test soil density) in Figures 5.108 and 5.111.

The maximum pressure $R_{AE}/\gamma H$ at the base of the wall is:

$$\frac{R_{AE}}{\gamma H} = K_{AE} \qquad (5.15)$$

One should keep in mind that the Mononobe-Okabe Theory is based on the assumption that the coefficient of lateral earth pressure k_h is representative of a constant lateral acceleration which provides a constant lateral body-type force to the system. There are no inertia effects. The wall is also assumed to be rigid. In the experiment however, the lateral acceleration was rapidly varying in time, providing for inertia effects, and the retaining walls were flexible.

From equation (5.9) it can be seen that the Mononobe-Okabe equation goes singular when $(\delta - \theta - i)$ is less than zero since the term under the radical goes negative. For $\delta = 35^\circ$ and a flat backfill ($i = 0^\circ$) this means that θ has to be less than or equal to 35° or $k_h \leq 0.70$. Likewise, for a 5° backfill slope $\theta \leq 30^\circ$ or $k_h \leq 0.58$, for a 10° backfill slope $\theta \leq 25^\circ$ or $k_h \leq 0.47$ and for a 15° backfill slope, $\theta \leq 20^\circ$ or $k_h \leq 0.36$. From the lateral acceleration values (comparable to k_h) listed in Table 5.6, it can be seen that the upper limits just mentioned are exceeded, or very nearly exceeded, in some of the tests, especially in those where sloping backfills were used. From a Mononobe-Okabe analysis one would then have expected a complete collapse of the walls. In fact, there was never a complete collapse in any of the tests although lateral displacements were in some cases quite high (about 10% of the wall height in tests 1CN0508, 2CN1013, and 2CN1514). Complete collapse would probably have occurred if the lateral acceleration was constant and inertialess as assumed by Mononobe-Okabe. The level of maximum acceleration was only achieved momentarily, however, being followed by changes in acceleration which in time would lead to a restoring force holding the wall back. There might have been a momentary collapse of the system in some cases, which was quickly arrested. It should be noted that in most tests the maximum accelerations recorded (especially at the top of the wall) occur while the wall is being

"pushed" back into the backfill (i.e., while the system is being restrained from collapse).

The envelopes of the various parameters with respect to the strong motion characteristics were arrived at in the following manner:

As mentioned in Section 5.2, the ground motion of the centrifuge earthquakes has the shape mainly of a decaying sinusoid with some additional noise added (see the bottom-of-wall accelerograms). In most of the tests there is an initial acceleration spike (positive acceleration) followed by a trough (negative acceleration), then a smaller spike, then a smaller trough, and thereafter low amplitude accelerations. The corresponding velocity diagrams, which, as one would expect, have their extreme values when the acceleration curves cross the zero axis, give the total area under the acceleration curves. The velocity changes from one extreme velocity to the other thus give the area under their respective acceleration spikes. The velocity and velocity changes are important in that they can be used as an indication of the energy content of the acceleration spikes, which is thus an indication of the energy put into the system by the earthquake. Recall that there was little damage from the Parkfield earthquake (Section 5.2), although there were high accelerations, because of the low energy content of the acceleration spikes.

It was observed, from the frames b of the parameter diagrams (Figures 5.53b through 5.107b) that, in almost every experiment, peaks in the maximum moment, pressure and shear distributions at the base of the walls with respect to time were obtained in between the time when

the acceleration spikes reached their peaks and the time when they crossed the zero axis (where the corresponding velocities reached their peaks). It was likewise observed that troughs in the maximum moment, pressure and shear distributions were obtained in between the times when accelerations reached troughs (negative maxima) and the times when they recrossed the zero axis (where the corresponding velocities reached their negative maxima). The opposite correlation between acceleration/velocity extremes and the maximum displacements at the top of the walls was also observed.

The peaks and troughs of the parameter distributions were then plotted with respect to their corresponding accelerations, velocities, and velocity changes (which are the areas under individual acceleration spikes) in Figures 5.108 through 5.122. These values are also tabulated in Table 5.6. It should be noted that static values were not included as peaks or troughs in the analysis, as they are probably neither. These values would have been plotted along the axis where acceleration and velocity are zero. However, in dynamic motion, when the acceleration is zero, the velocity might not be, and vice-versa, so the inclusion of static values in the envelope analysis would not have been appropriate to the other dynamic points. Only dynamic values were included.

It should also be noted that the Mononobe-Okabe analysis reduces to the static Rankine/Coulomb analysis for no lateral acceleration which does not seem accurate from a dynamic motion point of view.

TABLE 5.6

Maximum Extreme Dynamic Values (Peaks and Troughs)

	1CN0001			1CN0002			1CN1003			1CN0004			1CN1505		
M/EI	0.387	0.383	0.271[T]	0.382	0.354[T]	0.450	0.343[T]	0.433	0.401[T]	0.323	0.292	0.305[T]	0.406	0.346[T]	0.314
$\delta M/\gamma H^3$	0.503	0.505	0.358[T]	0.504	0.467[T]	0.589	0.489[T]	0.566	0.525[T]	0.414	0.374[T]	0.391	0.529	0.451[T]	0.437
$P/\gamma H$	–	0.813	0.318[T]	0.622	0.430[T]	0.929	0.324[T]	0.560	0.378[T]	0.605	0.391[T]	0.489	0.661	0.389[T]	0.532
$Q/(\tfrac{1}{2}\gamma H^2)$	0.538	0.518	–	0.452	–	0.558	0.293[T]	–	–	0.415	–	0.362	0.420	0.370[T]	0.488
y/H	0.0181[T]	0.0238[T]	0.0149[T]	0.0365	0.0238	0.0462	0.0274	0.0596	0.0305[T]	0.0607	0.0383[T]	0.0300[T]	0.0572	0.0331[T]	–
a/g	0.430	0.401	-0.538	0.181	-0.162	0.483	-0.529	0.234	-0.165	0.279	-0.203	0.090	0.344	-0.371	0.072
$v/f_1 H$	0.0305	0.0369	-0.0249	0.0101	-0.0109	0.0364	-0.0249	0.0094	-0.0117	0.0249	-0.0114	-0.0001	0.0335	-0.0132	0.0041
$\Delta v/f_1 H$	0.0305	0.0369	-0.0618	0.0350	-0.0210	0.0364	-0.0613	0.0343	-0.0211	0.0249	-0.0363	0.0113	0.0335	-0.0467	0.0173

	1CN0006			1CN0007			1CN0508			1CN1069			1CN1510		
M/EI	0.229[T]	0.393	–	0.423	0.108[T]	0.296	0.327	0.199[T]	0.327	0.264[T]	0.491	0.301[T]	0.493	0.351[T]	0.554
$\delta M/\gamma H^3$	0.292[T]	0.500	–	0.519	0.133[T]	0.363	0.410	0.250[T]	0.410	0.331[T]	0.609	0.373[T]	0.611	0.436[T]	0.700
$P/\gamma H$	0.250[T]	0.366	–	0.712	0.179[T]	0.455	0.723	0.300[T]	0.549	0.306[T]	0.557	0.233[T]	0.506	0.322[T]	0.673
$Q/(\tfrac{1}{2}\gamma H^2)$	0.110[T]	0.169	–	0.458	0.185[T]	0.307	0.479	0.254[T]	0.397	0.312[T]	0.473	0.272[T]	0.404	0.291[T]	0.511
y/H	–	–	–	0.0210[T]	0.0638	-0.0029[T]	0.0236[T]	0.0647	0.0612[T]	0.0412[T]	–	–	–	–	0.0200[T]
a/g	-0.472	0.157	–	0.549	-0.652	0.332	0.629	-0.614	0.302	-0.161	0.634	-0.593	0.379	-0.185	0.575
$v/f_1 H$	-0.0285	0.0075	–	0.0601	-0.0413	0.0104	0.0525	-0.0412	0.0087	-0.0119	0.0452	-0.0517	0.0036	-0.0217	0.0445
$\Delta v/f_1 H$	-0.0285	0.0360	–	0.0601	-0.1014	0.0517	0.0525	-0.0937	0.0499	-0.0206	0.0452	-0.0969	0.0553	-0.0253	0.0445

	Test 1CN1510(Cont.)			Test 2CN0011				Test 2CN0012				Test 2CN1013			
MH/EI	0.239^T	0.560	0.409^T	0.736	0.622^T	0.826	0.752^T	0.698	0.492^T	0.762	0.680^T	0.746	0.570^T	0.804	0.738^T
$6M/\gamma H^3$	0.302^T	0.707	0.517^T	0.448	0.379^T	0.503	0.453^T	0.438	0.309^T	0.478	0.427^T	0.461	0.352^T	0.497	0.456^T
$P/\gamma H$	0.374^T	0.578	0.426^T	0.703	0.142^T	0.414	–	0.615	0.090^T	0.423	–	0.814	0.239^T	0.456	0.261^T
$Q/(1/2\gamma H^2)$	0.331^T	0.541	0.452^T	0.338	0.277^T	0.377	0.240^T	0.390	0.209^T	0.400	–	0.408	0.203^T	0.375	0.331^T
v/H	0.0640	0.0024^T	0.0210	0.0229^T	0.0488	-0.0376	-0.0222	0.0279^T	0.0666	-0.0124^T	0.0135	0.0368^T	0.0706	0.0048^T	0.0296
a/g	-0.615	0.367	-0.190	0.629	-0.703	0.590	-0.198	0.723	-0.612	0.408	-0.151	0.729	-0.596	0.400	-0.193
v/f_1H	-0.494	0.0095	-0.0142	0.0569	-0.0376	0.0137	-0.0114	0.0595	-0.0373	0.0113	-0.0071	-0.0593	-0.0398	0.0138	-0.0098
$\Delta v/f_1H$	-0.0939	0.0589	-0.0237	0.0569	-0.0945	0.0513	-0.0251	0.0595	-0.0968	0.0488	-0.0186	0.0593	-0.0944	0.0536	-0.0236

	Test 2CN1514			
MH/EI	0.798	0.616^T	0.902	0.830
$6M/\gamma H^3$	0.491	0.379^T	0.555	0.511^T
$P/\gamma H$	0.730	0.202^T	0.659	0.267^T
$Q/(1/2\gamma H^2)$	0.394	0.263^T	0.323	0.203^T
v/H	0.0282^T	0.0472	-0.0331^T	-0.0288
a/g	0.701	-0.624	0.422	-0.202
v/f_1H	0.0526	-0.0474	0.0074	-0.0200
$\Delta v/f_1H$	0.0526	-0.1000	0.0548	-0.0274

T = Trough (local minimum) Peak value otherwise.

Maximum $\left\{\begin{array}{l}\text{Moment} \\ \text{Shear-Force} \\ \text{Pressure}\end{array}\right\}$ always at bottom of wall.

Maximum displacement always at top of wall.

The extreme points seem to follow, with the exception of the displacement, a general trend; that is, the higher the lateral acceleration, velocity or change in velocity, the higher the extreme. It was decided to fit least-squares straight lines through each of the sets of points one for each backfill slope; 0°, 10°, 15°. The maximum slope from each of the three sets of data was taken as the slope for the envelopes. The envelopes were drawn with these slopes as tangents to the individual sets of points. From the linear correlation coefficients of the least-squares fits, it was determined that the best fits were the maximum moment vs. change in velocity (Figures 5.110 and 5.113), the maximum pressure vs. velocity (Figure 5.115) and, the maximum shear vs. acceleration (Figure 5.117). No conclusions could be drawn from the displacement curves (Figures 5.120 through 5.122).

The best fits would indicate that moment and pressure are more momentum- or energy-governed parameters since they are better related to velocity effects. Similarly, the shear force is more a force-governed parameter (which is logical) since it is better related to acceleration.

The envelopes presented thus provide an upper bound for the various parameters with respect to actual dynamic strong motion characteristics for at least a range of system stiffnesses ($\gamma H^4/6EI$) between about 0.75 and 1.75 which the experiments encompassed (for $\phi \approx 35^\circ$).

As in the static case, the various parameters are indicated to be independent of the stiffness of the walls at least for the range of stiffnesses tested. It would be difficult to say if this would hold for

rigid walls, or very flexible walls, since the actual walls tested appeared quite flexible as indicated by the deflection shapes.

The only logical comparisons that can be made are those between the envelopes obtained and the corresponding Mononobe-Okabe predictions (which have been simplified for an average of the soil densities encountered). These can be seen in Figures 5.108 and 5.111 for moments, 5.114 for pressures, and 5.117 for shears. In addition, Figures 5.108 and 5.111 show the values for moments suggested by Seed and Whitman which were previously discussed. No comparisons with previous investigators can be made in terms of the envelopes involving the velocity parameters since this does not seem to have been examined before. Having the envelopes with respect to accelerations, velocity and change in velocity should, however, help in better understanding the problem at hand.

Since the Mononobe-Okabe curves and Seed and Whitman curves (in the moment diagrams) generally intersect at one point and at relatively steep angles to each other, it appears that the traditional methods underestimate the actual values of maximum moments below the point of intersection and overestimate them above. It appears that going even a small distance above or below the intersection points leads to large differences between the actual experimental maximum values and those predicted by the theory. For example, from Figure 5.111, for a flat backfill and a lateral acceleration of 0.25g the Mononobe-Okabe method gives a maximum moment around 60% as large as that determined from the envelope. Seed and Whitman indicate one about 80% as large. For 0.50g,

however, Mononobe-Okabe predicts a maximum moment about as large as the envelope while Seed and Whitman shows one 1.5 times larger. Similar comparisons can readily be made for the other parameters as well by examining the respective diagrams. The designer would observe, therefore, that the envelopes obtained from the experiments generally give what appear to be conservative values for lateral accelerations less than about 0.50g (which is probably the practical extreme for the use of the Mononobe-Okabe theory in any case). It should also be noted that the envelopes do not seem to be as sensitive to backfill slope as the Mononobe-Okabe theory is.

From the parameter diagrams (Figures 5.53 through 5.107) it can be observed that the maximum moments recorded ranged from about 40% to about 100% higher than the maxima recorded statically (with the exception of test 1CN0007 which had a relatively very low static maximum moment). As mentioned previously, this ratio is more dependent on the energy input into the system (represented by the velocity) than on the peak accelerations. The moment distributions with respect to the location (frames c and vertical cuts of frames a) seem to be smooth curves which could possibly be approximated using low order polynomials, for example, quadratic functions.

The maximum dynamic pressures ranged anywhere from 1 to 2-1/2 times the maximum static ones and like the moments this ratio was more dependent on the velocities recorded. Although the pressure distributions are by no means linear (as assumed by the Mononobe-Okabe theory), their centroids (locations of resultants) generally appear to be at or

very near the location of the static centroids, that is, somewhere between 30% to 40% above the wall base. As with the static pressure distributions, this indicates that the distributions are like an "average" of a linear pressure distribution although they are generally difficult to relate to a Mononobe-Okabe distribution. In any case, the dynamic centroid appears to hold steady at around 1/3 the height above the base in contradiction to Seed and Whitman [55] and Prakash and Basavanna [42] (see Section 1.3).

The maximum shear forces recorded in the tests are generally 50% to 100% higher than the maximum recorded statically for the range of maximum test accelerations. It appears that the percentage is more closely associated with the acceleration than the velocity levels. One should keep in mind that shear requirements are usually amply met if a bending design is used unless the beam is short with respect to its thickness (behaving like a shear beam). For reinforced concrete beams, shear is important, however, and some shear reinforcement is usually required by design.

As can be seen from Figures 5.120 through 5.122 no clear trend could be determined between the maximum displacements (at the top of the wall) and the strong motion characteristics.

Richards and Elms [43] performed some tests on a gravity retaining wall on a (1g) shaking table which was subjected to a scaled El Centro, California (1940) earthquake record. They measured the displacements on the wall and noted that the wall always moved outward away from the backfill and continued to move outward until the shaking ceased. By

contrast, barring the author's prejudice toward 1g shaking table tests (Section 1.2), in the cantilever retaining wall tests of this investigation, the walls were observed to displace both outwardly and inwardly with respect to the backfill. The maximum displacements were observed to be not necessarily the final ones although in some tests they were. This is as it should be. At 1g, the soil grains are under low stresses and are rigid, so the only displacements are due to grain slipping which is all irreversible. In the centrifuge, the soil behavior is properly elastic/plastic so dynamic to and fro movements are observed. In addition to the sliding and rotation of the base, there is also the flexing of the stem (and base) so the elastic wall can rebound somewhat as well. The maximum deflections ranged from 5% to 9% of the wall height for RW1 and from 7% to 11% for the more flexible RW2. These magnitudes of deflections could lead to some severe cracking in reinforced concrete walls although it should be remembered that part of the deflection is due to a rotation of the base.

From the shape of the deflection curves (frames c and vertical sections through frames a of the parameter diagrams) it can be seen that the wall motion is basically in the first mode with apparently little or no contribution from other modes. This is also confirmed by the Fourier Spectra discussed in Section 3.3.3.

5.6. Final Static (Residual) Results

A visual idea of the results of the earthquake on the retaining walls can be observed from Figures 5.123 (Test 1CN0007), 5.124 (Test
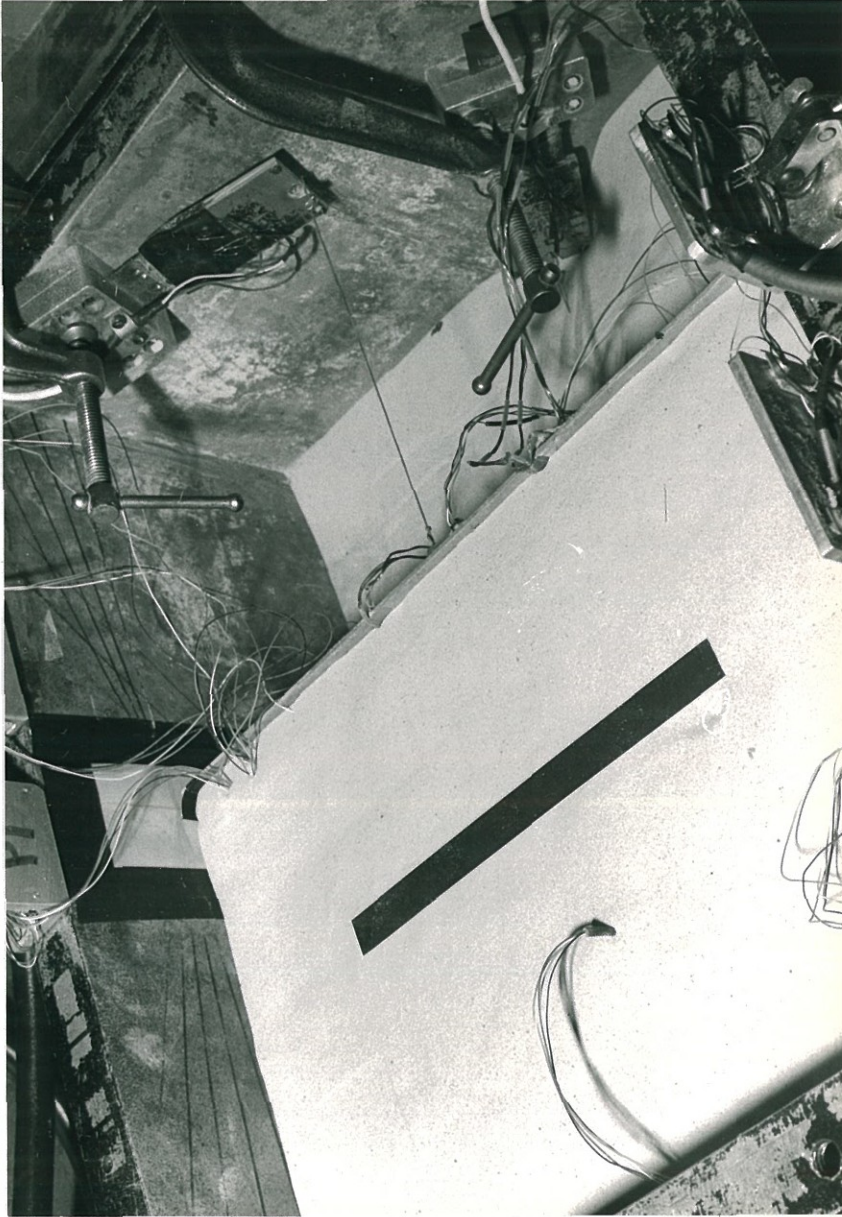
FIGURE 5.123 – TEST 1CN0007, POST TEST VIEW (AT 1 G)
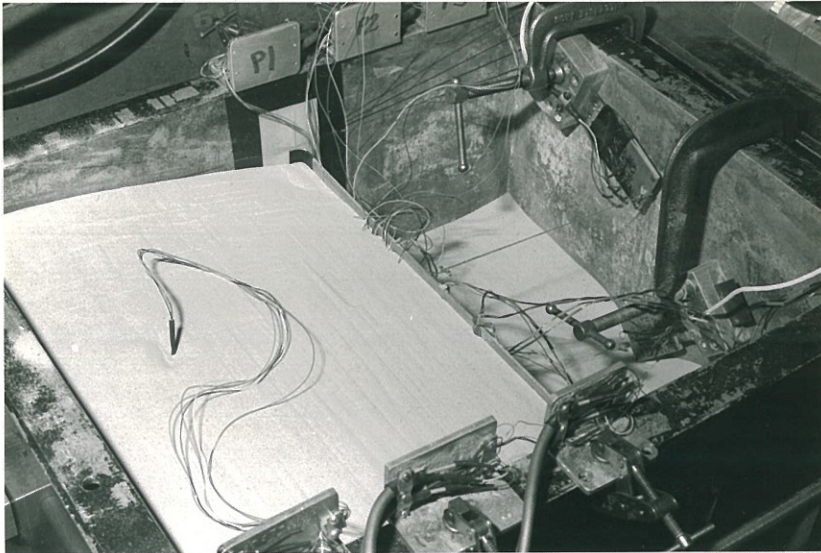
FIGURE 5.124 – TEST 1CN1009, POST TEST VIEW (AT 1 G)
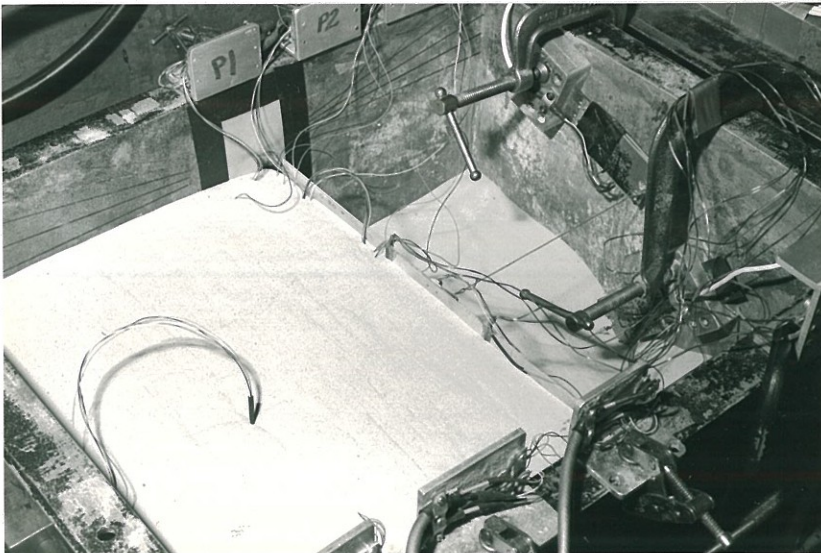
FIGURE 5.125 – TEST 2CN0011, POST TEST VIEW (AT 1 G)

1CN1009), and 5.125 (Test 2CN0011). Although the photographs were taken after the centrifuge was brought back down to rest, one can see that there was a large amount of motion of the backfill and wall. There was, of course, an amount of "rebounding" of the system as the artificial gravitational field decreased. One can observe that the backfill, which was originally flush with the lip of the wall, has displaced downward 1/4 to 1/2 of an inch. These kinds of displacements are quite sizeable and it can be safe to speculate that, if colored sand, or slightly moistened sand (with some apparent cohesion) had been used, some cracks in the backfill would have been observed.

Not apparent from the photographs is a "mounding" of the sand observed at the base of the wall. This was obviously produced by the outward movement of the wall during the tests.

An important observation related to the downward sliding of the backfill and the "mounding" at the base is that these features were uniform across the width of the wall and there was no apparent change near the edges. This can be taken as a good indication that the system behaved in a plane strain fashion (as assumed) and that the edge effects (if any) were minimal.

Seed and Whitman [55] mention the fact that after a retaining structure with granular backfill has been subjected to a base excitation, a residual pressure acts on it which is substantially greater than the initial pressure before base excitation. This pressure is also a

TABLE 5.7

Maximum Final (Residual) Static Values From Tests

	Test 1CN0001	Test 1CN0002	Test 1CN1003	Test 1CN0004	Test 1CN1505	Test 1CN0006	Test 1CN0007	Test 1CN0508	Test 1CN1009	Test 1CN1510	Test 2CN0011	Test 2CN0012	Test 2CN1013	Test 2CN1514
Moment MH/EI	0.338	0.358	0.409	0.303	0.371	0.381	0.302	0.270	0.423	0.456	0.790	0.708	0.760	0.856
Moment $6M/\gamma H^3$	0.439	0.472	0.535	0.388	0.483	0.485	0.370	0.379	0.525	0.576	0.481	0.445	0.470	0.527
Pressure $P/\gamma H$	-	0.478	0.408	0.461	0.501	0.314	0.318	0.308	0.354	0.444	0.268*	0.275**	0.297	0.276
Shear $Q/(1/2 \gamma H^2)$	0.413	0.428	0.423	0.375	0.419	0.177	0.320	0.317	0.381	0.482	0.359	0.398	0.365	0.282
Displacement y/H	0.0474	0.0536	0.0599	0.0433	0.0548	0.0328	0.0481	0.0552	0.0580	0.0561	0.0653	0.0721	0.0856	0.0947

Maximum Moment always at bottom of wall unless otherwise specified.

Maximum Pressure always at bottom of wall unless otherwise specified.

Maximum Shear Force always at bottom of wall unless otherwise specified.

Maximum Displacement always at top of wall.

*. Occurs at $x/H = 0.625$

**. Occurs at $x/H = 0.431$

TABLE 5.8

Ratios of Final Residual to Maximum Static and Maximum Dynamic Values (Test only).

	Test 1CN0001		Test 1CN0002		Test 1CN0003		Test 1CN0004	
	Static	Dynamic	Static	Dynamic	Static	Dynamic	Static	Dynamic
Moment $M_H/El\Delta 6M/\gamma H^3$	1.40	0.87	1.32	0.93	1.37	0.91	1.23	0.94
Pressure $P/\gamma H$	-	-	0.96	0.59	0.92	0.44	0.87	0.76
Shear Force $Q/(1/2\ \gamma\ H^2)$	1.55	0.77	1.44	0.84	1.48	0.76	1.36	0.90
Displacement y/H	1.70	1.00*	1.68	1.00*	1.59	1.00*	1.37	0.71

Test 1CN1505		Test 1CN0006		Test 1CN0007		Test 2CN0012		Test 1CN0508		Test 1CN1009	
Static	Dynamic	Static	Dynamic	Static	Dynamic	Static	Dynamic	Static	Dynamic	Static	Dynamic
1.35	0.91	1.39	0.97	1.80	0.71	1.58	0.93	1.29	0.83	1.86	0.86
0.93	0.76	0.75	0.75	0.83	0.45	0.87	0.45	0.56	0.43	0.82	0.64
1.64	0.86	1.39	1.00	1.60	0.70	1.58	0.97	1.04	0.69	1.46	0.81
1.59	0.96	1.10	-0.92	1.61	0.75	1.58	1.00*	1.88	0.59	1.87	-0.83

Test 1CN1510		Test 2CN0011		Test 2CN1013		Test 2CN1514	
Static	Dynamic	Static	Dynamic	Static	Dynamic	Static	Dynamic
1.57	0.81	1.56	0.97	1.53	0.95	1.61	0.95
0.84	0.66	0.95	0.38	0.62	0.36	0.66	0.38
1.44	0.79	1.07	0.95	1.54	0.89	1.11	0.72
1.72	0.88	1.49	1.00	1.72	0.76	1.73	1.00

* Final = Maximum

substantial portion of the maximum pressure developed during the excitation. This statement is quantitatively demonstrated by the experiments.

The maximum residual parameters are listed in Table 5.7 and their ratios to maximum static and maximum dynamic values in Table 5.8.

One can observe that, although the maximum residual pressure is always somewhat lower than the maximum static pressure (5% to 25%), and considerably lower than the maximum dynamic (25% to 60% lower), the resultant (shear) forces (i.e., the areas under the pressure distributions) are in accordance with the Seed and Whitman observation. The residual resultants can be up to 60% higher than the static! This appears to be random with respect to the slope. From frames c of the pressure distribution diagrams, it can also be observed that the final residual resultant is usually located some 20% to 40% above the static and dynamic resultants indicating that a triangular (or "average triangular") pressure distribution no longer exists.

The residual moments are also substantially higher than the static and are only a few percent lower than the maximum. This, again, develops regardless of the magnitude of the shaking the wall was subjected to. This could indicate that a retaining wall which has survived an earthquake intact could be pre-stressed for the following earthquake or aftershock to the point where there is virtually no safety factor and thus fail under an even mild event. It should be noted that in Test 1CN1505 the centrifuge was left running for 3 hours after the shaking occurred. This is the equivalent of 150 hours (over 6 days) in prototype time, and in this period, no rebounding or relaxation was

observed in either the strain gage (moment) or pressure transducer readings.

As mentioned in Section 5.5 the walls displaced out and in with respect to the backfill and then generally crept out toward some final displacement which in some tests was the maximum observed. The final displacements were found to be much greater than the static ones in any case. This then gives rise to the question of whether or not such large displacements can be tolerated from a safety or aesthetic point of view although the retaining wall survived the earthquake.

CHAPTER VI

CONCLUSIONS AND RECOMMENDATIONS

The purpose of this investigation was to observe the natural behavior of an 18 ft high cantilever retaining wall when subjected to only a gravity body force with a dynamic lateral earthquake excitation. The retaining walls were properly modelled and were subjected to some earthquake-like motions which were considered to be in a realistic range. Moment, pressure, shear, and displacement distributions (static, dynamic, and residual) were obtained. It was also novel that the retaining walls were considered flexible (as they are in real life) as opposed to rigid, which seems to be the norm in 1g model retaining wall studies and in theoretical analyses. A large amount of data was obtained directly from transducers and indirectly from simple mathematical manipulations of transducer data and was presented in as concise a manner as possible. Some empirical curves for relating the upper bound responses of the retaining walls to strong motion characteristics were also obtained.

From the information acquired from the tests, the following conclusions and recommendations can be made.

6.1. Conclusions

1. The simple "earthquake generating" mechanism employed was found to give realistic characteristics and could thus be employed in the

studies of other earthquake-related problems in geotechnics in the centrifuge.

2. The static earth pressure distributions obtained were not triangular as the Rankine/Coulomb lateral earth pressures assume. The experimental centroids were generally located at about 1/3 the height above the base of the wall. The resultant forces (areas under the pressure curves) were in reasonable agreement with the Rankine/Coulomb theory. This indicates that the Rankine/Coulomb theory estimates an "average" pressure distribution which is taken as triangular.

3. The static moments measured were generally higher than those which would be obtained using a Rankine/Coulomb resultant force with a 1/3 of the height moment arm (by as much as 35%), indicating that the properly designed wall might have a safety factor lower than estimated.

4. Static displacements were sufficiently large to create a state of full active pressure behind the wall.

5. Static and dynamic reaction parameters (moments, pressures, etc.) appear to be independent of wall stiffness, at least for the range of experimental system stiffnesses ($0.75 \leq \gamma H^4/6EI \leq 1.75$, $\phi \approx 35^{\circ}$)

6a. The only significant dynamic response of the system is in the fundamental mode.

6b. The two walls had fundamental frequencies of 2.6 Hz and 2.5 Hz with the soils employed.

7. The dynamic response of the system is not only dependent on lateral accelerations, as the Mononobe-Okabe theory assumes, but also on the energy content of the earthquake indicated by the velocities. Maximum moments were found to be more closely associated with the areas under the individual acceleration spikes (changes in velocity), maximum pressures with the velocities, and maximum shear (resultant) forces with the accelerations, although there is a general dependence on all the strong motion characteristics. There is a strong correlation between maximum and minimum (maximum negative) accelerations, velocities, and changes in velocities; and peaks and troughs in the maximum response curves.

8. The experimental envelopes presented in Chapter V provide an upper bound for the various parameters with respect to actual dynamic strong motion characteristics for at least the system stiffness range $(0.75 \leq \gamma H^4/6EI \leq 1.75, \phi \approx 35^\circ)$ which was studied. These envelopes can be used as a design aid (Section 6.2).

9. The Mononobe-Okabe theory underestimates responses (in some cases severely) below certain lateral acceleration levels for each individual case (Figures 5.108, 5.111, 5.114, and 5.117) and overestimates them above that acceleration when compared to the experimental envelopes. This is due to the steep slope of intersection (at only one point) between the recorded parameter envelopes and the Mononobe-Okabe curves. This makes the envelopes appear conservative for k_h values less than 0.5g, but they are not, because they came from tests.

10. The experimental envelopes are not as sensitive to backfill slope as the Mononobe-Okabe theory is.

11. Dynamic moment distributions with respect to wall location are generally smooth, monotonic curves which resemble some low order polynomial, possibly quadratic.

12. As in the static cases, the dynamic pressures were not triangular as the Mononobe-Okabe theory assumes, although the centroids did remain at about 1/3 the height above the base, contradicting other investigators which state that it rises to between 1/2 and 2/3 of the height. The dynamic pressure distributions could thus be considered an "average" of a linear distribution, although they could not generally be related to Mononobe-Okabe.

13. The walls displaced both outwardly and inwardly with respect to the backfills during the severe parts of the shaking and crept outwardly during the milder shaking towards the end. Maximum deflections could be considered excessive in some cases even though the structure survived the event intact. Deflected shapes gave an indication of first mode (only) flexible bending beam behavior.

14. The fact was confirmed that, after a retaining structure with a granular backfill undergoes severe dynamic excitation, a residual pressure acts on it which is substantially greater than the initial pressure before excitation, and is a substantial portion of the maximum pressure developed during the excitation. This also applies to moments, shears, and displacements.

15. No noticeable experimental "edge effects" were observed, and a
    plane strain condition for the tests could be assumed to hold.

16. Elastic solutions for retaining wall problems should be avoided.
    This includes the use of elastic finite elements (Appendix D).

6.2. Recommendations

Based on the concluded investigation, it is highly recommended
that some type of dynamic analysis in the design of large retaining
structures be employed, as the dynamic responses generated can be
considerably greater than the static ones. There should be extreme cau-
tion in accepting the following quote from Seed and Whitman [55]:

"Thus many walls adequately designed for static earth pressures
will automatically have the capacity to withstand earthquake ground
motions of substantial magnitudes and in many cases, special seismic
earth pressure provisions need not be required".

As an example of how the experimental data from this investigation
might be used as a design aid consider the following practical problem:

It is required to design a 20 ft high cantilever retaining wall
with a flat, granular backfill with $\phi = 35^{\circ}$. The wall is to be
subjected to a scaled down Parkfield Earthquake (Figure 5.41a) to one
half the magnitude shown.

Since the wall/soil description is similar to that of the experi-
ments, the fundamental frequency can be assumed to be about 2.5 Hz.
From Figure 5.41, based on test experience, the second acceleration
spike (that whose peak is at about 4.1 seconds) should probably generate

the critical response. The peak design acceleration is then 215 cm/sec^2, the corresponding velocity 39 cm/sec (which occurs at about 4.6 sec) and the area under the acceleration spike is 49 cm/sec (which is the peak-trough difference on the velocity curve). Based on test experience, the peak response of the wall should then occur sometime between the 4 and 5 second mark.

For a = 215 cm/sec^2, a/g = 0.22. Therefore, from Figure 5.111

$$\frac{6M}{\gamma H^3} = 0.58.$$

For v = 39 cm/sec, (f_1 = 2.5 Hz).

$$\frac{v}{f_1 H} = \frac{39}{(2.5)(20)(30.48)} = 0.026.$$

Therefore, from Figure 5.112,

$$\frac{6M}{\gamma H^3} = 0.55$$

For Δv = 49 cm/sec, (f_1 = 2.5 Hz).

$$\frac{\Delta v}{f_1 H} = 0.032.$$

Therefore, from Figure 5.113,

$$\frac{6M}{\gamma H^3} = 0.57$$

The maximum moment could then be taken as the average of the three values obtained from the envelopes, therefore

$$\left(\frac{6M}{\gamma H^3}\right)_{MAX} = 0.57.$$

Having this value, the stem could then be designed as a regular bending beam using, for example, a quadratic moment distribution for simplicity and having all the design requirements (as was done in Section 3.3.1).

It should be noted that had a Mononobe-Okabe analysis been performed, using the maximum scaled Parkfield acceleration of 240 cm/sec^2 and equation (5.10), the maximum moment would have been:

$$\left(\frac{6M}{\gamma H^3}\right)_{MAX} = 0.42$$

which is 35% below the one obtained from the other analysis. It was based on one dynamic parameter (the peak acceleration) whereas, the other was based on three. If a standard factor of safety of 1.7 is used, it would in actuality only be 1.25 when compared to the previous analysis.

One could also use a similar analysis to investigate the pressures and shears and perhaps refine the design.

Future research could be done using identical types of tests with different wall heights, stiffnesses, different soils and longer earthquake durations.

The data analysis should concentrate more on the highlights (peaks, troughs, etc.) of the dynamic characteristics related to the system responses instead of the detailed, time-consuming, expensive, and tedious data analysis which was performed in this investigation.

Sheetpile walls, channel sections, and other types of bending beam retaining walls should also be studied.

Retaining wall problems with wet or saturated soils should also be examined with the centrifuge, although there could be some problems with retaining the water in the backfill as well as having two time scales (dynamic and consolidation -- see Appendix A).

The centrifuge would also be an ideal tool for studying static and dynamic retaining wall behavior with clays.

It would be desirable to develop a better shaker which could be implemented into a centrifuge. There is also a need for some full-scale testing of bending beam retaining structures. Sinusoidal shakers could be used on actual retaining structures to determine some natural frequencies and modes of vibration and perhaps test some to failure.

An actual retaining wall should also be instrumented with two strong motion accelerographs (one at the base and one at the top) and with at least some kind of pressure transducers which could record pressures during an actual earthquake. The recording devices could be triggered by the accelerographs.

BIBLIOGRAPHY

1. K.J. Bathe, E.L. Wilson, F.E. Peterson (1973), "SAPIV - A Structural Analysis Program for Static and Dynamic Response of Linear Systems", Report No. EERC 73-11, College of Engineering, University of California, Berkeley, California, June.

2. Biggs, J.M. (1964), Introduction to Structural Dynamics, McGraw-Hill Book Company, San Francisco.

3. Bridgman, P.W. (1943), Dimensional Analysis, Yale University Press.

4. Bucky, P.B. (1931), "Use of Models for the Study of Mining Problems", American Institute of Mining and Metallurgical Engineers Technical Publication No. 425.

5. Chakrabarti, S., Husak, A.D., Christiano, P.P., Troxell, D.E. (1978), "Seismic Design of Retaining Walls and Cellular Cofferdams", Proceedings of the ASCE Geotechnical Conference, Earthquake Engineering and Soil Dynamics, Pasadena, California.

6. Chang, M.F., Chen, W.F. (1981), "Limit Analysis of Lateral Earth Pressures on Rigid Walls Retaining Cohesionless Soils", Report CE-STR-81-2, School of Civil Engineering, Purdue University, January.

7. Chang, M.F., Chen, W.F. (1981), "Lateral Earth Pressures on Rigid Retaining Walls Subjected to Earthquake Forces", Report CE-STR-81-20, School of Civil Engineering, Purdue University, June.

8. Cloud, W.K. (1967), "Intensity Map and Structural Damage, Parkfield, California Earthquake of June 27, 1966", Bulletin of the Seismological Society of America, Vol. 57, No. 6, December.

9. Cloud, W.K., Perez, V. (1967), "Accelerograms - Parkfield Earthquake", Bulletin of the Seismological Society of America, Vol. 57, No. 6, December.

10. CNEN-ENEL Commission on Seismic Problems Associated with the Installation of Nuclear Power Plants (1976), Contribution to the Study of the Friuli Earthquake of May, 1976.

11. Duke, C.M., Leeds, D.J. (1963), "Response of Soils, Foundations, and Earth Structures to the Chilean Earthquakes of 1960", Bulletin of the Seismological Society of America, Vol. 53, No. 2, February.

12. Ellingwood, B.R., Editor (1980), "An Investigation of the Miyagi-Ken-Oki, Japan Earthquake of June 12, 1978", U.S. Department of Commerce, Bureau of Standards Special Publication 592, October.

13. Greville, T.N.E. (1970), Spline Functions and Applications, National Technical Information Service, Springfield, Virginia.

14. Hayoshi, S., Kubo, K., Nakase, A. (1966), "Damage to Harbor Structures in the Niigata Earthquake", Soils and Foundations, Tokyo.

15. Hoek, E. (1965), "The Design of a Centrifuge for Simulation of Gravitational Force Fields in Mine Models", Journal of the South African Institute of Mining and Metallurgy, Vol. 65, No. 9.

16. Housner, G.W., Trifunac, M.D. (1967), "Analysis of Accelerograms - Parkfield Earthquake", Bulletin of the Seismological Society of America, Vol 57, No. 6, December.

17. International Association for Earthquake Engineering (1970), "Earthquake Engineering Regulations: A World List", November.

18. Ishii, T., Arai, M., Tsuchida, H. (1960), "Lateral Earth Pressures in an Earthquake", Proceedings, Second World Conference on Earthquake Engineering, Tokyo, Japan.

19. Jacobsen, L.S. (1939), Appendix D of "The Kentucky Project", Technical Report No. 13, Tennessee Valley Authority, 1951.

20. Japan Society of Civil Engineers (1980), Earthquake Resistant Design of Civil Engineering Structures and Foundations in Japan.

21. Jennings, P.C., Editor (1971), Engineering Features of the San Fernando Earthquake, Report No. EERL 71-02, Earthquake Engineering Research Laboratory, California Institute of Technology, Pasadena, California.

22. Kawasumi, H. (1968), General Report on the Niigata Earthquake of 1964, Tokyo Electrical Engineering College Press, Tokyo, Japan.

23. Ketter, R.L., Prawel, S.P., Jr. (1969), Modern Methods in Engineering Computation, McGraw-Hill Book Company, New York.

24. Lew, H.S., Leyendecker, E.V., Dikkers, R.D. (1971), "Engineering Aspects of the 1971 San Fernando Earthquake", Building Research Division, Institute for Applied Technology, National Bureau of Standards, Washington, D.C., Building Science Series 40, December.

25. Liu, H-P., Hagman, R.L., Scott, R.F. (1978), "Centrifuge Modeling of Earthquakes", Geophysical Research Letters, Vol. 5, No. 5, May.

26. Matsuo, H. (1941), "Experimental Study on the Distribution of Earth Pressures Acting on a Vertical Wall During Earthquakes", Journal of the Japanese Society of Civil Engineers, Vol. 27, No. 2.

27. Matsuo, M., Ohara, S. (1955), "Seismic Earth Pressure Due to Saturated Soils", Journal of the Japanese Society of Civil Engineers, Vol. 40, No. 6.

28. Matsuo, M., Ohara, S. (1960), "Lateral Earth Pressures and Stability of Quay Walls During Earthquakes", Proceedings, Second World Conference of Earthquake Engineering, Tokyo, Japan.

29. Matsuo, M., Ohara, S. (1965), "Dynamic Pore Water Pressure Acting on Quay Walls During Earthquakes", Proceedings, Third World Conference on Earthquake Engineering, New Zealand.

30. Mononobe, N. (1929), "Earthquake Proof Construction of Masonry Dams", Proceedings, World Engineering Conference, Japan, Vol. 9.

31. Mononobe, N., Matsuo, M. (1929), "On the Determination of Earth Pressures During Earthquakes", Proceedings, World Engineering Conference, Japan, Vol. 9.

32. Murphy, L.M., Scientific coordinator (1973), "Earthquake Damage to Water and Sewerage Facilities: Subcommittee on Water and Sewerage Systems", San Fernando, California, Earthquake of February 9, 1971, U.S. Department of Commerce, National Oceanic and Atmospheric Administration, Environmental Research Laboratories, Washington, D.C.

33. Murphy, V.A. (1960), "The Effect of Ground Characteristics on the Aseismic Design of Structures", Proceedings, Second World Conference on Earthquake Engineering, Tokyo, Japan.

34. Murray, W.M., Stein, P.K. (1958), Strain Gage Techniques, M.I.T. Press.

35. Newmark, N.M. (1965), "Effects of Earthquakes on Dams and Embankments", Geotechnique, Vol. XV, No. 2, June.

36. Niwa, S. (1960), "An Experimental Study of Oscillating Earth Pressures Acting on a Quay Wall", Proceedings, Second World Conference on Earthquake Engineering, Tokyo, Japan.

37. Oberg, E., Jones, F.D., Horton, H. L., Schubert, P.B., Garratt, G., Semioli, W.J., Moltrecht, K.H. (1975) Machinery's Handbook, 20th Edition, Industrial Press, Inc., New York.

38. Ohara, S. (1960), "Experimental Studies of Seismic Active and Seismic Passive Earth Pressure", Proceedings, Third Japanese Earthquake Engineering Symposium, Tokyo, November.

39. Okabe, S. (1926), "General Theory of Earth Pressure", Journal of the Japanese Society of Civil Engineers, Vol. 12, No. 1.

40. Pokrovsky, G.I., Fyodorov, I.S. (1975), "Centrifugal Model Testing in the Construction Industry", Draft translation prepared by Building Research Establishment Library Translation Service, Great Britain, Vols. I and II.

41. Polshin, D.E., Rudnitski, N.Y., Chizhikov, P.G., Yakovleva, T.G. (1973), "Centrifugal Model Testing of Foundation Soils of Building Structures", Proceedings, 8th International Conference of Soil Mechanics and Foundation Engineering, Moscow.

42. Prakash, S., Basavanna, B.M. (1969), "Earth Pressure Distribution Behind Retaining Wall During Earthquake", Proceedings, Fourth World conference on Earthquake Engineering, Santiago, Chile.

43. Richards, R., Jr., Elms, D.G. (1977), "Seismic Behavior of Gravity Retaining Walls", Research Report No. 77-10, University of Delaware, Newark, Delaware, University of Canterbury, Christchurch, New Zealand.

44. Richart, F.E., Jr., Hall, J. R., Jr., Woods, R.D. (1970), Vibration of Soils and Foundations, Prentice Hall.

45. Ross, G.A., Seed, H.B., Migliaccio, R. (1969), "Bridge Foundation Behavior in Alaska Earthquake", Journal of the Soil Mechanics and Foundation Division, American Society of Civil Engineers, July.

46. Rowe, P.W. (1975), "Application of Centrifugal Models to Geotechnical Structures", Proceedings, Symposium on Geotechnical Structures, University of New South Wales, Australia, July.

47. Satake, M. (1979), Investigation of Disasters Caused by the 1978 Miyagi-Ken-Oki Earthquake.

48. Scott, R.F. (1963), Principles of Soil Mechanics, Addison-Wesley Publishing Co., Inc., Reading, Massachusetts.

49. Scott, R.F. (1973), "Earthquake-Induced Earth Pressures on Retaining Walls", Proceedings, Fifth World Conference on Earthquake Engineering, Rome, Italy.

50. Scott, R.F. (1975), "The Centrifugal Technique in Geotechnology-Selected Papers", Soil Mechanics Laboratory, California Institute of Technology, Pasadena, California, November.

51. Scott, R.F., Liu, H-P., Ting, J. (1977), "Dynamic Pile Tests by Centrifuge Modeling", Proceedings, Sixth World Conference on Earthquake Engineering, Paper 4-50, New Delhi, January.

52. Scott, R.F. (1977), "Centrifuge Studies of Cyclic Lateral Load-Displacement Behavior of Single Piles", Soil Mechanics Laboratory, Division of Engineering and Applied Science, California Institute of Technology, Pasadena, California.

53. Scott, R.F. (1979), "Cyclic Static Model Pile Tests in a Centrifuge", Offshore Technology Conference, Paper no. 3492.

54. Seed, H.B., Idriss, I.M. (1970), "Soil Moduli and Damping Factors for Dynamic Response Analyses", Report No. EERC, 70-10, Earthquake Engineering Center, University of California, Berkeley, December.

55. Seed, H.B., Whitman, R.V. (1970), "Design of Earth Retaining Structures for Dynamic Loads", ASCE Specialty Conference, Lateral Stresses in the Ground and the Design of Earth Retaining Structures, Cornell University Ithaca, New York.

56. Sim, L.C. (1979), "Behavior of Retaining Walls Under Seismic Loading", Research Report 79/9, Department of Civil Engineering, University of Canterbury, Christchurch, New Zealand, February.

57. Stratta, J.L., Wyllie, L.A., Jr. (1979), "Reconnaissance Report, Friuli, Italy Earthquakes of 1976", Earthquake Engineering Research Institute, August.

58. Tagaya, K., Scott, R.F., Aboshi, H. (1977), "Fundamental Study on Extraction of Buried Anchors", Proceedings, 12th Conference on Soil Mechanics and Foundation Engineering, Japanese Society of Soil Mechanics and Foundation Engineering, Tokyo.

59. Tajimi, H. (1969), "Dynamic Analysis of a Structure Embedded in an Elastic Stratum", Proceedings, Fourth World Conference on Earthquake Engineering, Santiago, Chile.

60. Tajimi, H. (1970), "Dynamic Earth Pressure on Basement Walls in the Elastic Ground", Proceedings, Third Japanese Earthquake Engineering Symposium, Tokyo, November.

61. Tajimi, H. (1973), "Dynamic Earth Pressures on Basement Wall", Proceedings, Fifth World Conference on Earthquake Engineering, Rome, Italy.

62. Teng, W.C. (1962), Foundation Design, Prentice Hall Inc., Englewood Cliffs, New Jersey.

63. Trifunac, M.D., Lee, V. (1973), "Routine Computer Processing of Strong Motion Accelerograms", Report EERL 73-03, California Institute of Technology, Earthquake Engineering Research Laboratory.

64. Wang, C.K., Salmon, C.G. (1973), Reinforced Concrete Design, Second Edition, Intext Educational Publishers, New York.

65. Winterkorn, H.F., Fang, H.Y. (1975), Foundation Engineering Handbook, Van Nostrand Reinhold, New York.

66. Whitman, R.V. (1979), "Dynamic Behavior of Soil and its Application to Civil Engineering Projects", Proceedings, Sixth Pan-American Conference on Soil Mechanics and Foundation Engineering, Lima, Peru.

67. Wood, J.H. (1973), "Earthquake Induced Soil Pressures on Structures", Report No. EERL 73-05, Earthquake Engineering Research Laboratory California Institute of Technology, Pasadena, California.

68. Wood, J.H. (1975), "Earthquake Induced Pressures on a Rigid Wall Structure", Bulletin of the New Zealand Society for Earthquake Engineering, Vol. 8, No. 3, September.

69. Yanev, P.I., Editor (1978), "Reconnaissance Report, Miyagi-Ken-Oki Japan Earthquake, June 12, 1978", Earthquake Engineering Research Institute, Berkeley, California, December.

70. Yuxian, H. (1979), "Some Engineering Features of the 1976 Tangshan Earthquake", Visit of the Soil Dynamics Delegation of the American Society of Civil Engineers to the People's Republic of China, August 25-September 10, 1979.

APPENDIX A

SCALING RELATIONS   (Hoek [15])

Every quantity of physics and mechanics has a dimension which can be expressed as a function of the fundamental dimensions:

M – mass		F – force ($F = MLT^{-2}$)
L – length	or	L – length
T – time		T – time

If a formula is dimensionally correct, it is valid in all systems of units.

By the method of dimensional analysis ([3],[15]) relations between the equations governing the states of the model and prototype can be derived.

The stress and displacement at a point in the structure will depend upon the following factors:

1.) The geometry of the structure. The behavior of a point defined by the coordinates x, y, z can be described by a typical length dimension L and set of dimensionless ratios L_R relating all other lengths to L.

2.) Material properties: For example, for a linearly elastic isotropic material.

ρ = mass density of the material.

E = Young's modulus of the material.

ν = Poisson's ratio of the material (dimensionless).

Other material properties can be related to ρ and E by sets of dimensionless ratios ρ_R, E_R.

3.) Applied stress conditions:

P = externally applied load.

Q = externally applied stress.

u_0 = externally induced displacement.

σ_0 = internal stress.

g = acceleration of gravity.

a = externally applied acceleration.

Other stress conditions are related to P, Q, u_0, σ_0, a by sets of dimensionless ratios P_R, Q_R, U_{OR}, σ_{OR}, a_R.

The behavior of a point x,y,z in the structure at time t is defined by a resulting stress σ and a resulting displacement u and depend upon the abovementioned parameters and dimensionless ratios.

The quantities σ, u, x, y, z, t, L, ρ, E, ν, P, Q, σ_0, u_0, g, a are all derived from the three fundamental units of force F, length L, and time T. The Poisson's ratio ν is already dimensionless.

The dimensions of the listed parameters are given in Table A.1.

TABLE A.1

	σ	u	x	y	z	t	L	ρ	E	ν	P	Q	σ_o	u_o	g	a
F	1	0	0	0	0	0	0	1	1	0	1	1	1	0	0	0
L	-2	1	1	1	1	0	1	-4	-2	0	0	-2	-2	1	1	1
T	0	0	0	0	0	1	0	2	0	0	0	0	0	0	-2	-2

The table consists of a matrix of rank 3. According to Buckingham's first theorem, one may obtain 16-3 = 13 dimensionless independent groups of parameters from those listed. Hoek chooses the following:

$$\frac{\sigma L^2}{P},\ \frac{u}{L},\ \frac{x}{L},\ \frac{y}{L},\ \frac{z}{L},\ \frac{t^2 a}{L},\ \frac{E L^2}{P},\ \frac{\rho a L^3}{P},\ \nu,\ \frac{a}{g},\ \frac{Q L^2}{P},\ \frac{u_o}{L},\ \frac{\sigma_o L^2}{P}$$

It should be noted that other combinations than those listed above are possible. For this particular set, however, all other groups would be combinations of those listed.

Buckingham's second theorem (Buckingham's Π Theorem) states that a dimensionally homogeneous equation (one which does not depend on the units of measurement) can be reduced to a relationship between a complete set of dimensionless products.

From Buckingham's Π Theorem then the displacement u, and the stress σ at a point (x, y, z) can be expressed by the following dimensionless equations

$$\frac{u}{L} = F\left(\frac{x}{L}, \frac{y}{L}, \frac{z}{L}, \frac{t^2 a}{L}, \frac{EL^2}{P}, \frac{\rho a L^3}{P}, \nu, \frac{a}{g}, \frac{\sigma L^2}{P}, \right.$$

$$\left. \frac{u_o}{L}, \frac{\sigma_o L^2}{P}, L_R, E_R, P_R, Q_R, u_{OR}, \rho_R, \sigma_{OR}, a_R \right) \quad (A.1)$$

$$\frac{\sigma L^2}{P} = G\left(\frac{x}{L}, \frac{y}{L}, \ldots, a_R \right) \quad (A.2)$$

in which F and G are undetermined functions. The parameter t is the dynamic time scale.

For the two systems, model and prototype to by physically similar, the functions F and G must be the same for each. Therefore, the following conditions of similitude are established.

The subscripts m and p will refer to model and prototype parameters respectively.

1.) Model similitude related to natural properties: Since Poisson's ratio is dimensionless, the model and prototype must have the same Poisson's ratio:

$$\nu_m = \nu_p \quad (A.3)$$

Combining the remaining natural properties E and ρ by dimensionless grouping:

$$\frac{\rho a L^3}{P} \cdot \frac{g}{a} \cdot \frac{P}{EL^2} = \frac{\rho g L}{E} \quad (A.4)$$

Therefore:

$$\frac{\rho_m g_m L_m}{E_m} = \frac{\rho_p g_p L_p}{E_p} \qquad (A.5)$$

or

$$\frac{L_p}{L_m} = \frac{E_p}{E_m} \frac{\rho_p}{\rho_m} \frac{g_m}{g_p} \qquad (A.6)$$

If the model material is identical to the prototype material $(E_m = E_p;\ \rho_m = \rho_p;\ \nu_m = \nu_p)$ and the model is subjected to an artificial acceleration $N \cdot g$ (N is the scale factor) then:

$$\frac{L_p}{L_m} = \frac{g_m}{g_p} = \frac{Ng}{g} = N \qquad (A.7)$$

It can be thus seen that by use of the centrifuge, scale models manufactured of the prototype material are suitable.

2.) Model similitude in relation to applied stresses: Applied stresses are defined by the parameters P, Q, σ_o, u_o and a and appear in the dimensionless groups:

$$\frac{t^2 a}{L},\ \frac{EL^2}{P},\ \frac{\rho a L^3}{P},\ \frac{a}{g},\ \frac{QL^2}{P},\ \frac{u_o}{L},\ \frac{\sigma_o L^2}{P}$$

Taking the grouping:

$$\frac{Q}{E} = \frac{QL^2}{P} \cdot \frac{P}{EL^2} \qquad (A.8)$$

Therefore:

$$\frac{Q_m}{Q_p} = \frac{E_m}{E_p} \tag{A.9}$$

also:

$$\frac{P_m}{E_m L_m^2} = \frac{P_p}{E_p L_p^2} \qquad \text{or} \qquad \frac{P_m}{P_p} = \frac{E_m L_m^2}{E_p L_p^2} \tag{A.10}$$

From the grouping:

$$\frac{\sigma_o}{E} = \frac{\sigma_o L^2}{P} \cdot \frac{P}{EL^2} \tag{A.11}$$

Therefore:

$$\frac{\sigma_{om}}{\sigma_{op}} = \frac{E_m}{E_p} \tag{A.12}$$

Displacements are scaled directly by:

$$\frac{u_{om}}{u_{op}} = \frac{L_m}{L_p} \tag{A.13}$$

Inertia and gravity forces in the model and the prototype are characterized by the dimensionless groups $\frac{\rho a L^3}{P}$ and $\frac{a}{g}$ which were already used in deriving expression (A.4).

Finally, dynamic or inertial forces involve a time scale which can be derived from the grouping:

$$\frac{t^2 E}{L^2 \rho} = \frac{t^2 a}{L} \cdot \frac{P}{\rho a L^3} \cdot \frac{EL^2}{P} \tag{A.14}$$

Therefore:

$$\frac{t_m}{t_p} = \left(\frac{\rho_m}{\rho_p} \frac{E_p}{E_m}\right)^{1/2} \frac{L_m}{L_p} \qquad (A.15)$$

Using a centrifuge model made of the same material as the prototype ($E_m = E_p$; $\rho_m = \rho_p$; $\nu_m = \nu_p$) and subjecting it to the centrifuge artificial gravitational acceleration N · g (A.7).

(A.9) reduces to: $\qquad Q_m = Q_p \qquad (A.16)$

(A.10) reduces to: $\qquad \dfrac{P_m}{P_p} = \dfrac{1}{N^2} \qquad (A.17)$

(A.12) reduces to: $\qquad \sigma_{om} = \sigma_{op} \qquad (A.18)$

(A.13) reduces to: $\qquad \dfrac{u_{op}}{u_{om}} = N \qquad (A.19)$

(A.15) reduces to: $\qquad \dfrac{t_p}{t_m} = N \qquad (A.20)$

One can clearly see the convenience of centrifuge modelling. From (A.16), (A.18) and the fact that $E_p = E_m$ can also note that the strains in the model and prototype are identical. In the event that the soil behavior exhibits its usual nonlinearity, the same considerations hold, if prototype and model soils are the same.

In the experiments, it was necessary to model reinforced concrete walls by means of aluminum. The stiffness of the wall EI is modelled as follows. The dimensions of EI are FL (actually FL^2L^{-1}). It has been shown, by equation (A.17) that force scales as N^2, and length of course, scales as N, so that the EI of the

model must be equal to $1/N^3$ the EI of the prototype. For a given, but arbitrary design of a prototype reinforced concrete wall, the EI can be calculated. In the model, the E of the aluminum is known, and the wall thickness can therefore be selected to produce the appropriate, scaled value of EI.

The yield characteristics of the wall itself were not modelled. In the prototype, yield would be indicated by the creation of a plastic hinge at the point of maximum moment, i.e., at the base of the stem. In order to model this, a notch or groove would have to be cut along the base of the model to a point so that the stem would fail easily at that point and thus simulate the plastic hinge.

Consolidation time scale (Rowe [46]):

In the study of liquefaction, the time rate of flow of water from the soil is considered in comparison with the rate at which pore pressures are generated. The consolidation process thus requires consolidation time scaling.

The time factor T of consolidation is defined by:

$$T = \frac{C_v \, t_c}{(nH)^2} \tag{A.21}$$

where

c_v is the coefficient of consolidation

t_c is consolidation time

H is the height of the stratum to be drained

n is the number of drainage boundaries (1 or 2)

It is required that $T_m = T_p$. If the soil materials are identical then:

$$\frac{C_v \, t_c m}{n^2 \, H_m^{\,2}} = \frac{C_v \, t_c p}{n^2 \, H_P^{\,2}} \tag{A.22}$$

since

$$\frac{H_m}{H_p} = \frac{1}{N}$$

then

$$\frac{t_c m}{t_c p} = \frac{1}{N^2} \tag{A.23}$$

which establishes the consolidation time scale.

APPENDIX B

WALL PROGRAM LISTING

Following is a listing of the data processing program WALL described in Section 4.2. The following subroutines were developed:

MAIN(program)	DIGIT	PAPRNT
ALGEQN	INTEG	PRESS
APLOT	MAP	QUINT
BASCOR	MAXARR	SHEAR
BIGMAX	MOMENT	SPLINE
CRUNCH	PAGE	SUBU
DERIV	PAPLOT	YDISP

The following called subroutines are system subroutines of the IBM 370/3032 system at the Booth Computing Center of Caltech.

EQSOV   —   System of equations solving routine.

LSQUAR   —   Polynomial least-squares fitting routine.

SYSSYM* —   Symbol plotting routine.

VLABEL* —   Axis/axis label plotting routine.

XYPLOT* —   Line plotting routine.

XYPLT* —   Point Plotting routine.

*Calcomp plotter.

MAIN

```
        C      MAIN PROGRAM
        C      ***********
        C      PROGRAM TO DETERMINE PARAMETERS CF MODEL AND PROTOTYPE
        C      RETAINING STRUCTURES BASED CN CENTRIFUGE EXPERIMENTS
        C
CCC1           COMMON/RED/A(1502,12),T(1502),AX(112),BX(112),CALI(15,2),X(10),
              X          TCALI,ITM,NT,NA,NPOLY,NS2,NINT,R,EIM,HTM,AGS,GAMMAM,
              X          NTYPE,FIM,NC,XP(5)
CCC2           COMMON/GREEN/CMAX(2),CMIN(2),IFLTCD
CCC3           COMMON/BLACK/DIS(1502,3)
CCC4           COMMON/PINK/A1(1502),A2(1502)
CCC5           COMMON/ORANGE/TCPI,TCPF,BCTI,BLTF,NC
CCC6           COMMON/GRAY/TITLE1(18),TITLE2(18)
CCC7           DIMENSION DIS1(2,3)
        C
CCC8           READ 101,TITLE1,TITLE2
CCC9           READ 102,OMECA,SC,EIM,HTM,FIM,GAMMA,NPOLY,NSR4,NINT,NTYPE
CC10           NS2=NSR4+1
CC11           READ 103,(X(I),I=2,NS2)
CC12           READ 104,NC
CC13           NPR=NC+1
CC14           IF(NPR.EQ.1)NPR=2
CC15           READ 103,(XP(I),I=2,NPR)
        C
        C      OMEGA  = RPM AT WHICH CENTRIFUGE CPERATES
        C      SC     = DISTANCE FROM AXIS CF CENTRIFUGE FOTATION TO TOP OF MODEL
        C               WALL (IN)
        C      EIM    = EI CF MCDEL WALL (LE-IN**2/IN)
        C      HTM    = HEIGHT CF MCDEL WALL (IN)
        C      FIM    = FUNDAMENTAL FREQUENCY CF MODEL WALL (HZ)
        C      GAMMA  = UNIT WEIGHT CF PROTOTYPE (AND MCDEL) SOIL AT 1G (PCF)
        C      NPOLY  = CRDER OF POLYNOMIAL DESIRED FOR LEAST-SQUARES FIT CF DATA
        C               MUST BE GE.3 AND LE.(NSR4+1)
        C      NSR4   = NUMBER CF STRAIN CAGE LCCATIONS AT THE CENTER CF MODEL
        C               WALL (VERTICAL AXIS)
        C      NINT   = NUMBER CF DESIRED INTERVALS FOR WHICH RESULTS ARE WANTED
        C               ALCNG THE WALL
        C      NTYPE  = TYPE CF WALL
        C               NTYPE=0  CANTILEVER WALL
        C               NTYPE=1  SHEET PILE WALL
        C      X(I)   = LCCATIONS CF STRAIN CACES FROM TCP TC BCTTCM
        C      NC     = NUMBER CF PRESSURE TRANSDUCERS
        C      XP(I)  = LCCATIONS CF PRESSURE TRANSDUCERS FROM TCP TC BCTTCM
        C
CC16           NS2=NS2+1
CC17           X(1)=0.0
CC18           X(NS2)=HTM
CC19           NSR4A=NS2
CC20           NPR=NPR+1
CC21           XP(1)=0.0
CC22           XP(NPR)=HTM
        C
        C      DETERMINE GRAVITATIONAL ACCELERATION (AGS)
        C
CC23           R=SC+(HTM/2.0)
CC24           AGS=0.00002&354*R*(OMEGA**2)
```

```
        C
CC25          ANINT=FLCAT(NINT)
CC26          F=HTM/ANINT
CC27          ANINT=ANINT+1.0
CC28          NINT=NINT+1+3
CC29          AX(1)=C.0
CC30          CC 10 I=2,NINT
CC31       10 AX(I)=AX(I-1)+F
CC32         .CO 11 I=1,NINT
CC33       11 EX(I)=-AX(I)/HTM
CC34          EI=EIM*AGS**3
CC35          FT=HTM*AGS
CC36          F1=FIM/AGS
CC37          GAMMAN=GAMMA*AGS
CC38          GAMMA=GAMMA/1728.0
CC39          GAMMAN=GAMMAN/1728.0
        C
CC40          CALL CIGIT
        C
CC41          NINTT=NINT-3
CC42          GAMMA1=GAMMAN*1728.0
CC43          GAMMA2=GAMMA*1728.0
CC44          PRINT 200
CC45          PRINT 201,TITLE1,TITLE2
CC46          PRINT 202,CMEGA,SC,R,AGS,HTM,HT,EIM,EI,FIM,F1,GAMMA1,GAMMA2,
             XNPCLY,NINTT,NA,NSR4,NQ
CC47          PRINT 214,ITM
        C
CC48          IF(NA.EC.0)GC TC 21
CC49          DC 20 I=1,ITM
CC50          CC 20 J=1,NA
CC51       20 A(I,J)=-A(I,J)*386.22
        C
CC52       21 DC 22 I=1,NS2
CC53       22 X(I)=X(I)/HTM
CC54          IF(NA.EC.C)GC TC 24
CC55          PRINT 203
CC56          CC 23 I=1,NA
CC57       23 PRINT 204,I,(CALI(I,J),J=1,2)
CC58       24 PRINT 205
CC59          CC 25 I=1,NSR4
CC60          K=I+NA
CC61          L=I+1
CC62       25 PRINT 206,I,(CALI(K,J),J=1,2),X(L)
CC63          CC 26 I=1,NSR4A
CC64       26 X(I)=X(I)*HTM
        C
CC65          IF(NG.NE.0)GC TC 61
CC66       27 IF(NC.EC.0)GC TC 29
CC67          PRINT 207
CC68          CC 28 I=1,NC
CC69          K=NT+I+NC
CC70       28 PRINT 204,I,(CALI(K,J),J=1,2)
CC71       29 PRINT 208,TCALI
        C
        C    CMIN(I),CMAX(I) / I=1 LCCATICN   I=2 TIME
```

```
                              MAIN

     C      IFLTCD = TIME PLCT CCDE
     C      IFLTCD = C FIRST 20% CF TIME PLCT IS AMPLIFIED
     C      IFLTCD = 1 REGULAR LINEAR TIME PLCT
     C
0072          READ 105,CMIN(1),CMAX(1),CMIN(2),CMAX(2),IFLTCD
     C
     C      CALL MCMENT
0073          IF(NC.NE.0)GC TC 70
0074          CALL SHEAR
0075          CALL PRESS
     C
0076     30  IF(NA.EC.0)GC TC 37
     C
     C      FIND CISPLACEMENTS BY INTEGRATING ACCELERCMETER RECCRDS
     C      THERE IS A BASELINE CCRRECTICN CF THE ACCELERCGRAPHS
     C
0077          CISI(1,1)=TCFI
0078          CISI(2,1)=TCFF
0079          CISI(1,2)=BCII
0080          CISI(2,2)=BCIF
0081          CISI(1,3)=0.0
0082          CISI(2,3)=C.C
0083          DC 31 J=1,NA
0084     31  CALL BASCCR(J)
0085          DC 34 J=1,NA
0086          DC 32 I=1,ITM
0087     32  A1(I)=A(I,J)
0088          CALL INTEG(ITM,T,A1,A2,0)
0089          CALL INTEG(ITM,T,A2,A1,C)
0090          CCCC=(CISI(2,J)-CISI(1,J)+A1(I)-A1(ITM))/(T(ITM)-T(1))
0091          CCCD=CISI(1,J)-A1(1)-CCCC*T(1)
0092          DC 33 I=1,ITM
0093     33  CIS(I,J)=A1(I)+CCCC*T(I)+CCCD
0094     34  CCNTINUE
     C
0095          IF(NA.NE.1)GC TC 36
0096          DC 35 J=2,3
0097          DC 35 I=1,ITM
0098     35  CIS(I,J)=C.C
0099     36  CCNTINUE
     C
0100     37  CALL NDISP
     C
0101          IF(NA.EC.0)GC TC 39
0102          DC 38 I=1,ITM
0103          DC 38 J=1,NA
0104          A(I,J)=A(I,J)/(AGS*386.22)
0105     38  CIS(I,J)=DIS(I,J)/FTM
0106     39  DC 40 I=1,ITM
0107     40  T(I)=T(I)*F1M
     C
     C      PLCT AND PRINT CUT ACCELERCGRAPH AND CISPLACEMENT RECCRDS
     C
0108          IF(NA.EC.0)GC TC 47
0109          CALL APLCT
0110          DC 46 N=1,30
```

MAIN

```
C111              PRINT 200
C112              PRINT 210
C113              L=N*50
C114              DC 45 J=1,5C
C115              I=(L-50)+J
C116              IF(I.GT.ITM)GC TO 47
C117              IF(NA.EC.1)GC TO 44
C118              IF(NA.EC.2)GC TO 43
C119              PRINT 211,I,T(I),A(I,1),CIS(I,1),A(I,2),CIS(I,2),A(I,3),CIS(I,3)
C120              GC TC 45
C121           43 PRINT 212,I,T(I),A(I,1),CIS(I,1),A(I,2),CIS(I,2)
C122              GC TC 45
C123           44 PRINT 213,I,T(I),A(I,1),CIS(I,1)
C124           45 CCNTINUE
C125           46 CCNTINUE
C126           47 CCNTINUE
C127              CC TC 77
       C
C128           61 DC 64 I=1,NFF
C129           64 XF(I)=XF(I)/FTM
C130              PRINT 205
C131              DC 66 I=1,NC
C132              K=I+NT
C133              L=I+1
C134           66 PRINT 206,I,(CALI(K,J),J=1,2),XP(L)
C135              DC 67 I=1,NFF
C136           67 XP(I)=XF(I)*FTM
C137              GC TC 27
       C
C138           70 CALL FRESS
C139              CALL SFEAR
C140              CALL MCMENT
C141              CC TC 30
       C
C142           77 CCNTINUE
       C
C143          101 FCRMAT(18A4/18A4)
C144          102 FCRMAT(6F10.0,4I5)
C145          103 FCRMAT(8F10.C)
C146          104 FCRMAT(I5)
C147          105 FCRMAT(4F10.0,I5)
       C
C148          200 FCRMAT(1H1)
C149          201 FCRMAT( 5X,18A4,/,5X,18A4,/,5X,'*************************************
                 X*****************************************')
C150          202 FCRMAT(///,1X,'CENTRIFUCE RPM=',31X,F8.2,
                 X/,1X,'CISTANCE FRCM CENTRIFUCE AXIS TC TCP CF WALL=',F9.2,1X,
                 X'INCFES',
                 X/,1X,'CISTANCE FRCM CENTRIFUCE AXIS TC MIDCLE CF WALL=',F6.2,1X,
                 X'INCFES',
                 X/,1X,'CRAVITATICNAL ACCELERATICN AT MIDCLE OF WALL=',F9.2,1X,
                 X'G-S',//,
                 X/,1X,'MCCEL WALL FEIGFT=',F19.2,1X,'INCFES',15X,'FRCTCTYPE WALL HE
                 XIGFT=',F19.2,1X,'INCFES',
                 X/,1X,'MCCEL WALL EI=',F23.2,1X,'LE-IN**2/IN',10X,'PRCTCTYPE WALL E
                 XI=',F23.2,1X,'LB-IN**2/IN',
```

MAIN

```
              X/,1X,'MCDEL FUNDAMENTAL FRECUENCY=',F9.2,1X,'HERTZ',16X,'PRCTCTYPE
              X FUNCAMENTAL FREQUENCY=',F9.2,1X,'HERTZ',
              )/,1X,'CENSITY CF MCCEL SCIL=',F15.2,1X,'FCF',18X, 'DENSITY CF PRCT
              XCTYPE SCIL=',F15.2,1X,'PCF',//,
              )/,1X,'CRCLR CF PCLYNCMIAL IN LEAST-SCUARES FIT=',15X,I2,
              X/,1X,'NUMBER OF PCINTS AT WHICH CATA EVALUATICN TAKES PLACE=',I4,
              X///,1X,'NUMBER CF ACCELERCMETERS=',I3,
              X/,1X,'NUMBER CF STRAIN GACES=',I5,
              X/,1X,'NUMBER CF PRESSURE GACES=',I3)
0151      203 FCFMAT(//,1X,'CALIERATICN FACTCRS CF TRANSCUCERS',
              X/,1X,'*******************************',/,
              X/,1X,'ACCELERCMETER',11X,'SLCPE',5X,'Y-INTERCEPT',
              X/,1X,'-------------',11X,'-----',9X,'-----------')
0152      204 FCFMAT(6X,I2,2X,2E20.3)
0153      205 FCFMAT(/,1X,'STRAIN CAGE',13X,'SLCPE',5X,'Y-INTERCEPT',
              X12X,'LCCATICN',
              X           /,1X,'-----------',13X,'-----',9X,'-----------',
              X12X,'--------')
0154      206 FCFMAT(6X,I2,2X,3E20.3)
0155      207 FCFMAT(/,1X,' CELTA EEAM',13X,'SLCPE',5X,'Y-INTERCEPT',
              X           /,1X,' ----------',13X,'-----',9X,'-----------')
0156      208 FCFMAT(/,1X,'TIME CALIERATICN SCALE=',E10.3)
0157      209 FCFMAT(/,1X,'PRESSURE CAGE',11X,'SLCPE',5X,'Y-INTERCEPT',
              X12X,'LCCATICN',
              X           /,1X,'-------------',11X,'-----',9X,'-----------',
              X12X,'--------')
0158      210 FCFMAT(    21X,'ACCELERCMETER NC.1 (TCP CF WALL)',
              X             5X,'ACCELERCMETER NC.2 (BASE CF WALL)',
              X             7X,'ACCELERCMETER NC.3 (FREE FIELC)',/,
              X            21X,'*****************************',
              X             5X,'*****************************',
              X             7X,'*****************************',/,
              X1X,'TIME',    ' CIMENSICNLESS',3X,'CIMENSICNLESS',6X,'CIMENSICNLESS'
              X          ,6X,'CIMENSICNLESS',6X,'CIMENSICNLESS',6X,'CIMENSICNLESS'
              X          ,6X,'CIMENSICNLESS',/,1X,'STEF',1X,'TIME (T*F1)',
              X2X,'ACCELERATICN (A/G) CISFLACEMENT (Y/H)',
              X1X,'ACCELERATICN (A/C) CISFLACEMENT (Y/H)',
              X1X,'ACCELERATICN (A/C) CISFLACEMENT (Y/H)',/,
              X1X,'---- ------------ -------------------- -------------------- ------
              X------------',1X,      '-------------------- -------------------- ------
              X------------')
0159      211 FCFMAT(1X,I4,E13.3,6E15.3)
0160      212 FCFMAT(1X,I4,E13.3,4E15.3)
0161      213 FCFMAT(1X,I4,E13.3,2E15.3)
0162      214 FCFMAT(1X,'NUMBER CF TIME STEFS=',I7,/)
          C
0163          STCP
0164          ENC
```

ALGEGN

```
CCC1          SUBROUTINE ALGEGN(N,A,E,Y)
         C
         C    SUBROUTINE CALLED IN SPLINE
         C
CCC2          DIMENSION A(1500,3),U(1500,3),D(1500,3),E(1),Y(1)
         C
CCC3          U(1,2)=A(1,2)
CCC4          U(1,3)=A(1,3)
CCC5          Y(1)=E(1)
CCC6          DO 23 I=2,N
CCC7          I1=I-1
CCC8          D(I,2)=1.0
CCC9          U(I,3)=A(I,3)
CC10          D(I,1)=A(I,1)/U(I1,2)
CC11          U(I,2)=A(I,2)-D(I,1)*U(I1,3)
CC12          IF(ABS(U(I,2)).LT.1.0E-09)GO TO 35
CC13       23 CONTINUE
CC14       23 Y(I)=E(I)-D(I,1)*Y(I1)
CC15          Y(N)=Y(N)/U(N,2)
CC16          I=N
CC17       25 I1=I-1
CC18          Y(I1)=(Y(I1)-U(I1,3)*Y(I))/U(I1,2)
CC19          I=I-1
CC20          IF(I.EQ.1)GO TO 31
CC21          GO TO 25
CC22       31 RETURN
CC23       35 PRINT 107
         C
CC24      107 FORMAT(//5X,' IS A MATRIX WHICH REQUIRE PIVOTING OR IS SINGULAR')
         C
CC25          RETURN
CC26          END
```

APLOT

```
CCC1          SUBROUTINE APLOT
         C
         C      SUBROUTINE TO PLOT ACCELEROGRAPHS AND CORRESPONDING DISPLACEMENTS
         C
CCC2          COMMON/RED/A(1502,12),T(1502),AX(112),BX(112),CALI(15,2),X(10),
        X            TCALI,ITM,NT,NA,NPCLY,NS2,NINT,F,EIM,HTM,AGS,GAMMAM,
        X            NTYPE,FIM,NC,XF(5)
CCC3          COMMON/BLACK/DIS(1502,3)
CCC4          COMMON/PINK/A1(1502),A2(1502)
CCC5          COMMON/GRAY/TITLE1(18),TITLE2(18)
CCC6          DIMENSION AA(2),FB(2),CCC(3),AMXX(3),DMXX(3),MAXX(3),MDXX(3),
        X            AAA(1),BBB(1)
         C
         C      AMIN=-AMAX
         C      YMIN=-YMAX
         C
CCC7          READ 270,TMIN,TMAX,AMIN,AMAX,YMIN,YMAX
         C
CCC8          DO 105 J=1,NA
CCC9          DO 104 I=1,ITM
CC10          A1(I)=A(I,J)
CC11      104 A2(I)=DIS(I,J)
CC12          CALL BIGMAX(A1,ITM,AMXX(J),MAXX(J))
CC13      105 CALL BIGMAX(A2,ITM,DMXX(J),MDXX(J))
         C
CC14          CINTT=(ABS(TMAX-TMIN))/8.0
CC15          CINTA=(ABS(AMAX-AMIN))/2.5
CC16          CINTY=(ABS(YMAX-YMIN))/2.5
CC17          TMN=-1.75*CINTT
CC18          TMX=13.25*CINTT
CC19          AMN=-6.25*CINTA
CC20          AMX= 3.75*CINTA
CC21          YMN=-2.75*CINTY
CC22          YMX= 7.25*CINTY
         C
CC23          DO 125 I=1,3
CC24      125 CCC(I)=0.0
         C
CC25          K=10
CC26          DO 160 I=1,NA
CC27          CALL VLABEL(1.75,1.5,TMIN,TMAX,8.0,K,'TIME   (T*F1)',12,0,'(F4.1)',
        X4)
CC28          CALL SYSSYM(2.75,4.275,0.1,TITLE1,72,0.0)
CC29          CALL SYSSYM(2.75,4.125,0.1,TITLE2,72,0.0)
CC30          IF(I.NE.1)GO TO 131
CC31          CALL VLABEL(1.75,5.0,TMIN,TMAX,8.0,K,'ACCELEROMETER NC.1   (TOP OF
        XWALL)',33,0,'(F4.1)',4)
CC32      131 CONTINUE
CC33          IF(I.NE.2)GO TO 132
CC34          CALL VLABEL(1.75,5.0,TMIN,TMAX,8.0,K,'ACCELEROMETER NC.2   (BOTTOM
        XOF WALL)',36,0,'(F4.1)',4)
CC35      132 CONTINUE
CC36          IF(I.NE.3)GO TO 133
CC37          CALL VLABEL(1.75,5.0,TMIN,TMAX,8.0,K,'ACCELEROMETER NC.3   (FREE FI
        XELD)',32,0,'(F4.1)',4)
CC38      133 CONTINUE
```

AFLCT

```
UC39          CALL VLABEL(1.75,1.5,YMIN,YMAX,2.5,2,'DISP  (Y/H)',11,1,
             X'(F5.2)',5)
CC40          CALL VLABEL(1.75,5.C,AMIN,AMAX,2.5,4,'ACCEL  (A/C)',12,1,
             X'(F4.1)',4)
       C
CC41          CALL PAGE
CC42          LAB=0
CC43          AA(1)=1.75
UC44          AA(2)=9.75
CC45          EE(1)=2.75
CC4C          EE(2)=2.75
UC47          CALL XYPLCT(2,AA,EE,0.C,15.0,0.0,10.0,CCC,LAB)
CC48          EE(1)=4.C
CC49          EE(2)=4.C
CC50          CALL XYPLCT(2,AA,EE,0.C,15.0,0.0,10.0,CCC,LAB)
CC51          EE(1)=6.25
CC52          EE(2)=6.25
CC53          CALL XYPLCT(2,AA,EE,C.C,15.C,0.0,10.0,CCC,LAB)
CC54          EE(1)=7.5
CC55          EE(2)=7.5
CC56          CALL XYPLCT(2,AA,EE,0.C,15.0,0.0,10.0,CCC,LAB)
CC57          AA(1)=9.75
CC58          EE(1)=1.5
CC59          EE(2)=4.C
CC60          CALL XYPLCT(2,AA,EE,C.C,15.0,0.0,10.0,CCC,LAB)
CC61          EE(1)=5.0
CC62          EE(2)=7.5
CC63          CALL XYPLCT(2,AA,EE,C.C,15.0,0.0,10.0,CCC,LAB)
       C
CC64          DO 130 J=1,ITM
CC65          A1(J)=A(J,I)
CC66    130   A2(J)=DIS(J,I)
CC67          AAA(1)=AMXX(I)
CC68          EEE(1)=T(MAXX(I))
CC69          CALL XYPLT(1,EEE,AAA,TMN,TMX,AMN,AMX,CCC,LAB,1)
CC70          AAA(1)=DMXX(I)
CC71          EEE(1)=T(MDXX(I))
CC72          CALL XYPLT(1,EEE,AAA,TMN,TMX,YMN,YMX,CCC,LAB,1)
CC73          CALL XYPLCT(ITM,T,A1,TMN,TMX,AMN,AMX,CCC,LAB)
CC74          LAB=-1
CC75          CALL XYPLCT(ITM,T,A2,TMN,TMX,YMN,YMX,CCC,LAB)
CC76    160   CONTINUE
       C
CC77    270   FORMAT(EF10.C)
       C
CC78          RETURN
CC79          END
```

EASCCR

```
CCC1            SLBRCUTINE EASCCR(J)
        C
        C       SUBRCUTINE TC CCRRECT ACCELERCGRAPHS WITH RESPECT TC THE BASELINE
        C
CCC2            CCMMCN/REC/A(1502,12),T(1502),AX(112),EX(112),CALI(15,2),X(10),
        X             TCALI,ITM,NT,NA,NPCLY,NS2,NINT,F,EIM,HTM,AGS,GAMMAM,
        X             NTYPE,FIM,NG,XP(9)
CCC3            CCMMCN/BLACK/CIS(1502,3)
CCC4            REAL*E STCR(2,7)
CCC5            CIMENSICN CATA(3,1502),C(2)
CCC6            ECUIVALENCE (CIS,CATA)
        C
CCC7            IF(J.GT.1)GC TC 440
CCC8            CC 436 I=1,ITM
CCC9        436 CATA(3,I)=1.C
CC10        44J CC 444 I=1,ITM
CC11            CATA(1,I)=T(I)
CC12        444 CATA(2,I)=A(I,J)
CC13            CFISC=0.0
        C
CC14            CALL LSCCAR(CATA,ITM,2,C,CFISC,STCR)
        C
CC15            CC 446 I=1,ITM
CC16        446 A(I,J)=A(I,J)-(C(1)+C(2)*T(I))
        C
CC17            RETURN
CC18            ENC
```

BIGMAX

```
CCC1          SUBROUTINE BIGMAX(A,K,AMAX,KMAX)
        C
        C     SUBROUTINE TO PICK OUT LARGEST VALUE OF A ONE DIMENSIONAL ARRAY A(K)
        C
CC02          DIMENSION A(1)
        C
CCC3          AMAX=C.C
CCC4          DO 770 I=1,K
CCC5          IF(ABS(A(I)).GT.ABS(AMAX))GO TO 765
CCC6          GO TO 770
CCC7      765 AMAX=A(I)
CCC8          KMAX=I
CCC9      770 CONTINUE
        C
CC10          RETURN
CC11          END
```

CRUNCH

```
CCC1          SUBROUTINE CRUNCH
        C
        C     SUBROUTINE TO SORT OUT PARAMETERS FROM TIME-SPACE ARRAY XX FOR
        C     PLOTTING AND OUTPUT
        C     PARAMETERS CHOSEN ARE STATIC,MAXIMUM DYNAMIC,AND FINAL STATIC
        C
CCC2          COMMON/RED/A(1502,12),T(1502),AX(112),EX(112),CALI(15,2),X(10),
        X            TCALI,ITM,NT,NA,NPOLY,NS2,NINT,F,EIM,FTM,AGS,GAMMA,
        X            NTYPE,FIM,NG,XF(5)
CCC3         COMMON/ELLE/X1(112),X2(112),X3(112),TT(1502),XX(1502,112),XM(1),
        X            YM(1),TM(1),ITMA,IXMAX
        C
        C     FIND MAXIMUM PARAMETER AND CORRESPONDING TIME AND LOCATION
        C
CCC4          NINTT=NINT-3
CCC5          CALL MAXARR(XX,ITM,NINTT,XXMAX,ITMAX,IXMAX)
        C
CCC6          DO 140 I=1,NINT
CCC7          X1(I)=XX(1,I)
CCC8          X2(I)=XX(ITMAX,I)
CCC9      140 X3(I)=XX(ITM,I)
CC10          XM(1)=XXMAX
CC11          YM(1)=-AX(IXMAX)/FTM
CC12          TM(1)=T(ITMA)*FIM
CC13          DO 141 I=1,ITM
CC14      141 TT(I)=XX(I,IXMAX)
        C
CC15          RETURN
CC16          END
```

DERIV

```
0001          SUBROUTINE DERIV(N,H,Y,DY)
      C
      C       SUBROUTINE TO NUMERICALLY DIFFERENTIATE A SET OF N POINTS (X,Y)
      C       USING A 4TH ORDER FINITE DIFFERENCE SCHEME
      C
0002          DIMENSION Y(1),DY(1)
      C
0003          N=N-2
0004          DO 2 I=1,2
0005        2 DY(I)=(-50.0*Y(I)+96.0*Y(I+1)-72.0*Y(I+2)+32.0*Y(I+3)-6.0*Y(I+4))/
             X(24.0*H)
0006          DO 4 I=3,N
0007        4 DY(I)=(Y(I-2)-8.0*Y(I-1)+8.0*Y(I+1)-Y(I+2))/(12.0*H)
0008          N=N+2
0009          M=N-1
0010          DO 6 I=M,N
0011        6 DY(I)=(50.0*Y(I)-96.0*Y(I-1)+72.0*Y(I-2)-32.0*Y(I-3)+6.0*Y(I-4))/
             X(24.0*H)
      C
0012          RETURN
0013          END
```

DIGIT

```
0001          SUBROUTINE DIGIT
        C
        C      SUBROUTINE TO READ AND SCALE VALUES FROM THE DIGITIZER (FORMAT(10I8))
        C
0002          COMMON/RED/A(1502,12),T(1502),AX(112),BX(112),CALI(15,2),X(10),
             X          TCALI,ITM,NT,NA,NPOLY,NS2,NINT,F,EIM,HTM,AGS,GAMMAN,
             X          NTYPE,FIM,NC,XP(5)
0003          COMMON/ELLE/X1(112),X2(112),X3(112),TT(1502),XX(1502,112),XM(1),
             X          YM(1),TM(1),ITMAX,IXMAX
0004          COMMON/FINK/A1(1502),A2(1502)
0005          COMMON/CRANCE/TCPI,TCPF,PCTI,PCTF,NC
0006          REAL*8 STCR(2,7)
0007          DIMENSION IA(1502,12),IT(1502),IXBASE(21),IYBASE(21),XBASE(21),
             X          YBASE(21),DATA(3,21),C(2),IMAX(12),ITMM(12),ICHECK(12)
0008          EQUIVALENCE (IA,A),(IT,T),(IXBASE,XBASE),(IYBASE,YBASE)
        C
        C      NA=NUMBER OF ACCELEROMETERS (UP TO 3)
        C      NC=NUMBER OF CANTILEVER DISPLACEMENT TRANSDUCERS (UP TO 2)
        C      NP=NUMBER OF PRESSURE TRANSDUCERS
        C      NT=NUMBER OF TRACES DIGITIZED (UP TO 12)=ACCELEROMETERS + STRAIN GAGES
        C                                        + PRESSURE TRANSDUCERS
        C      CALI(I,J)=CALIBRATION FACTORS FOR EACH TRACE
        C               CALI(I,1)=SLOPE OF CALIBRATION
        C               CALI(I,2)=Y-INTERCEPT OF CALIBRATION
        C               Y=CALI(I,1)*X+CALI(I,2)
        C      A(I,J) IS THE ARRAY OF DIGITIZED POINTS
        C      TCALI=TIME CALIBRATION SCALE
        C
0009          READ 501,NA,NS,NP,NC
0010          NT=NA+NS+NP
0011          N=NT+NC
0012          READ 502,((CALI(I,J),J=1,2),I=1,N),TCALI
        C
        C      SET UP DIGITIZER COORDINATES WITH FIXED TRACE
        C
0013          DO 305 J=1,5
0014          I1=(5*J)-4
0015          I2=I1+4
0016          READ 503,((IXBASE(I),IYBASE(I)),I=I1,I2)
0017          DO 302 K=I1,I2
0018          IF(IXBASE(K).EQ.999999)GO TO 306
0019          XBASE(K)=FLOAT(IXBASE(K))
0020      302 YBASE(K)=FLOAT(IYBASE(K))
0021      305 CONTINUE
0022      306 KK=K-1
0023          DO 307 I=1,KK
0024          DATA(1,I)=XBASE(I)
0025          DATA(2,I)=YBASE(I)
0026      307 DATA(3,I)=1.0
0027          CHISQ=0.0
        C
0028          CALL LSQUAR(DATA,KK,2,CHISQ,STCR)
        C
0029          AC=XBASE(1)
0030          BC=C(1)+(XBASE(1)*C(2))
0031          CC=XBASE(KK)
```

DIDIT

```
0032              CC=C(1)+(XEASE(KK)*C(2))
0033              HYPC=((CC-AC)**2)+((CC-EC)**2)
0034              HYPC=SCRT(HYPO)
0035              SINW=(CC-EC)/HYPC
0036              CCSW=((CC-AC)/HYPC
        C
        C         READ IN DICITIZED TRACES
        C
0037              DC 380 J=1,NT
0038              DC 311 K=1,200
0039              I1=(5*K)-4
0040              I2=I1+4
0041              READ 503,((IT(I),IA(I,J)),I=I1,I2)
0042              DC 310 L=I1,I2
0043              IF(IT(L).EC.999999)GC TO 312
0044              XX(L,J)=FLCAT(IT(L))
0045        310   A(L,J)=FLCAT(IA(L,J))
0046        311 CONTINUE
0047        312 ITM=L-1
        C
        C         EASELINE CCRRECTION
        C
0048              DC 315 I=1,ITM
0049              XC=XX(I,J)
0050              YC=A(I,J)
0051              XX(I,J)=((XC-AC)*CCSW)+((YC-BC)*SINW)
0052        315   A(I,J)=-((XC-AC)*SINW)+((YC-EC)*CCSW)
        C
        C         THE XX(I,J) ARRAY STCRES TIME VALUES TEMPORARILY
        C
        C         * * * * * * * * * * * * * * * * * * * * * * * * * * * * * *
        C         * A(1,J) WILL BE THE SET CF TRACES AT CNE G (STATIC)       *
        C         * A(2,J) WILL BE THE SET CF TRACES AT MULTIPLE G (STATIC)  *
        C         * FROM A(3,J) CN, THE TRACES WILL BE FRCM THE DYNAMIC PORTION *
        C         * * * * * * * * * * * * * * * * * * * * * * * * * * * * * *
        C
0053              ICHECK(J)=0
0054              XX(1,J)=0.0
0055              XX(2,J)=0.0
0056              IF(ITM.LE.2) GC TO 349
0057              DC 340 I=4,ITM
0058        340   XX(I,J)=XX(I,J)-XX(3,J)
0059              XX(3,J)=0.0
0060              DC 348 I=4,ITM
0061              IF(XX(I,J).LE.XX(I-1,J))GC TO 343
0062              GC TO 343
0063        343 ICHECK(J)=ICHECK(J)+1
0064              PRINT 600,J,ICHECK(J),I,XX(I-1,J),XX(I,J)
0065        348 CONTINUE
0066        349 CONTINUE
        C
0067              IF(J.GT.NA)GC TO 354
0068              DC 350 I=3,ITM
0069        350 A(I,J)=A(I,J)-A(2,J)
0070              A(1,J)=0.0
0071              A(2,J)=0.0
```

DIGIT

```
0072            GC TC 357
0073        354 CCNTINLE
0074            CC 355 I=2,ITM
0075        355 A(I,J)=A(I,J)-A(1,J)
0076            A(1,J)=C.0
0077        357 CCNTINUE
            C
            C      SCALE RECCRDS
            C
0078            DC 360 I=1,ITM
0079            XX(I,J)=TCALI*XX(I,J)
0080        360 A(I,J)=A(I,J)*CALI(J,1)+CALI(J,2)
            C
            C      MCCEL PARAMETERS HAVE NOW BEEN SCALED
            C
0081            IF(NA.EC.0)GC TC 370
0082            ITM1=ITM-2
0083            CC 365 I=1,ITM1
0084            XX(I,J)=XX(I+2,J)
0085        365 A(I,J)=A(I+2,J)
0086            ITM=ITM1
0087            GC TO 375
            C
0088        370 ITM=1
0089            A(1,J)=A(2,J)
0090        375 CCNTINUE
0091            TMAX(J)=XX(ITM,J)
0092            ITMM(J)=ITM
0093        380 CCNTINUE
            C
0094            CC 381 I=1,NT
0095            IF(ICFECK(I).NE.0)STCP
0096        381 CCNTINLE
            C
0097            CALL BICMAX(TMAX,NT,TMX,ICUM)
0098            TMX=TMX*FIM
0099            IF(TMX.GE.3.0)GC TO 383
0100            ITM=(TMX*150.0)+1.0
0101            ITM=ITM+1
0102            T(1)=0.0
0103            CC 382 I=2,ITM
0104        382 T(I)=(FLCAT(I-1)/150.0)/FIM
0105            CC TC 386
0106        383 ITM=((TMX-3.0)*75.0)+451.0
0107            ITM=ITM+1
0108            T(1)=0.0
0109            CC 384 I=2,450
0110        384 T(I)=(FLCAT(I-1)/150.0)/FIM
0111            CC 385 I=451,ITM
0112        385 T(I)=(FLCAT(I-226)/75.0)/FIM
0113            IF(ITM.LE.1500)GC TC 388
0114            PRINT 601,ITM
0115            ITM=1500
            C
            C      SMCCTH CUT DATA WITH CUBIC SPLINE
            C
```

DIDIT

```
C116        388 DO 357 J=1,NT
C117            ITS=ITMM(J)
U118            DO 395 I=1,ITS
C119            A1(I)=XX(I,J)
0120        395 A2(I)=A(I,J)
C121            CALL SPLINE(ITS,A1,A2,ITM,T,TT)
0122            DO 396 I=1,ITM
U123        396 A(I,J)=TT(I)
C124        397 CONTINUE
        C
        C       READ IN INITIAL AND FINAL DIGITIZED DISPLACEMENT VALUES
        C       AT TOP AND BOTTOM OF WALL
        C
0125            READ 503,ITOPI,ITOPF,IBOTI,IBOTF
C126            TOPI=FLOAT(ITOPI)
C127            TOPF=FLOAT(ITOPF)
0128            BOTI=FLOAT(IBOTI)
0129            BOTF=FLOAT(IBOTF)
0130            M1=NT+1
C131            M2=NT+2
C132            IF(NC.EQ.0)GO TO 399
U133            TOPI=TOPI*CALI(M1,1)+CALI(M1,2)
C134            TOPF=TOPF*CALI(M1,1)+CALI(M1,2)
C135            IF(NC.EQ.1)GO TO 399
0136            BOTI=BOTI*CALI(M2,1)+CALI(M2,2)
0137            BOTF=BOTF*CALI(M2,1)+CALI(M2,2)
C138        399 CONTINUE
0139            NT=NA+NS
        C
C140        501 FORMAT(4I5)
C141        502 FORMAT(8F10.0)
C142        503 FORMAT(10I8)
        C
C143        600 FORMAT(1X,'***ERROR*** - TRACE J=',I3,' ICHECK(J)=',I3,' I=',I4,
                X' XX(I-1,J)=',F10.2,' XX(I,J)=',F10.2)
0144        601 FORMAT(1H1,1X,'ACTUAL NUMBER OF TIME STEPS WAS ',I4,/,1X,
                X'ONLY FIRST 1500 TIME STEPS COULD BE USED DUE TO STORAGE LIMITS')
        C
0145            RETURN
C146            END
```

INTEG

```
0001          SUBROUTINE INTEG(N,X,Y,SY,K)
       C
       C      SUBROUTINE TO NUMERICALLY INTEGRATE A SET OF N DATA POINTS (X,Y)
       C      OVER A PRESCRIBED INTERVAL USING THE TRAPEZOIDAL RULE
       C      THE INTEGRAL BETWEEN X(1) AND X(I) WILL BE EVALUATED AT EACH STEP I
       C      K=0    ORDER OF INTEGRATION MAINTAINED
       C      K=1    ORDER OF INTEGRATION REVERSED
       C
0002          DIMENSION Y(1),SY(1),X(1)
       C
0003          IF(K.EQ.1)GO TO 5
0004          NN=N
0005          SY(1)=0.0
0006          DO 1 I=2,NN
0007        1 SY(I)=SY(I-1)+((X(I)-X(I-1))/2.0)*(Y(I)+Y(I-1))
0008          GO TO 9
       C
0009        5 NN=N-1
0010          SY(N)=0.0
0011          DO 6 J=1,NN
0012          I=N-J
0013        6 SY(I)=SY(I+1)+((X(I+1)-X(I))/2.0)*(Y(I)+Y(I+1))
0014        9 CONTINUE
       C
0015          RETURN
0016          END
```

MAF

```
CC01          SUBROUTINE MAP(X,Y,Z,XMAX,XMIN,YMAX,YMIN,ZMAX,ZMIN,NXX,NYY,NCTR)
C
C         SUBROUTINE TO MAKE CONTOUR PLOTS OF A RECTANGULAR GRID CONTAINING
C         COORDINATES (X,Y) AND CORRESPONDING FUNCTION Z(X,Y)
C
CC02          DIMENSION X(1),Y(1),CCC(3),CTR(81),XX(4),YY(4),ZZ(4),XC(4),YC(4),
     X          XC(1),YC(1),Z(1502,1)
C
CC03          DO 2 I=1,3
CC04        2 CCC(I)=0.0
C
C         SET UP CONTOURS
C
CC05          NCTRS=NCTR-1
CC06          THS=FLOAT(NCTRS)
CC07          CZ=(ZMAX-ZMIN)/THS
CC08          CTR(1)=ZMIN
CC09          DO 3 I=2,NCTR
CC10        3 CTR(I)=CTR(I-1)+CZ
C
CC11          LAB=0
CC12          ICHK=-1
CC13          NX=NXX-6
CC14          NY=NYY-2
CC15          DO 50 I=1,NX,6
CC16          XX(1)=X(I)
CC17          XX(2)=X(I+6)
CC18          XX(3)=X(I+6)
CC19          XX(4)=X(I)
CC20          DO 50 J=1,NY,2
CC21          YY(1)=Y(J)
CC22          YY(2)=Y(J)
CC23          YY(3)=Y(J+2)
CC24          YY(4)=Y(J+2)
CC25          ZZ(1)=Z(I,J)
CC26          ZZ(2)=Z(I+6,J)
CC27          ZZ(3)=Z(I+6,J+2)
CC28          ZZ(4)=Z(I,J+2)
CC29          DO 50 K=1,NCTR
C
C         INTERPOLATE
C
CC30        5 L=0
CC31          DO 17 II=1,4
CC32          JJ=MOD(II,4)+1
CC33          IF(CTR(K).GT.ZZ(II))GO TO 7
CC34          IF(CTR(K).GT.ZZ(JJ))GO TO 10
CC35          GO TO 17
CC36        7 IF(CTR(K).LE.ZZ(JJ))GO TO 10
CC37          GO TO 17
CC38       10 L=L+1
CC39          IF(ZZ(II).EQ.ZZ(JJ))GO TO 12
CC40          ZSL=(CTR(K)-ZZ(II))/(ZZ(JJ)-ZZ(II))
CC41          XC(L)=XX(II)+(XX(JJ)-XX(II))*ZSL
CC42          YC(L)=YY(II)+(YY(JJ)-YY(II))*ZSL
CC43          GO TO 17
```

MAF

```
0044            12 XC(L)=XX(II)
0045               YC(L)=YY(II)
0046            17 CONTINUE
         C
         C      PLOTTING
         C
0047               IF(L.EQ.0)GO TO 50
0048               IF(L.GT.2)GO TO 40
0049               CALL XYPLOT(L,XC,YC,XMIN,XMAX,YMIN,YMAX,DCC,LAB)
0050            40 CONTINUE
0051            50 CONTINUE
         C
0052               RETURN
0053               END
```

MAXABR

```
CCC1          SUBROUTINE MAXABR(A,KX,KY,AMAX,KXMAX,KYMAX)
         C
         C    SUBROUTINE TO PICK OUT THE LARGEST ABSOLUTE VALUE OF A
         C    TWO-DIMENSIONAL ARRAY A(KX,KY)
         C
CCC2          DIMENSION A(1502,1)
         C
CCC3          AMAX=0.0
CCC4          DO 770 I=1,KX
CCC5          DO 770 J=1,KY
CCC6          IF(ABS(A(I,J)).GT.ABS(AMAX))GO TO 765
CCC7          GO TO 770
CCC8      765 AMAX=A(I,J)
CCC9          KXMAX=I
CC1C          KYMAX=J
CC11      770 CONTINUE
         C
CC12          RETURN
CC13          END
```

MOMENT

```
CCC1          SUBROUTINE MOMENT
       C
       C      SUBROUTINE TO FIND MOMENTS ALONG THE WALL FOR ALL TIME
       C      A LEAST-SQUARES POLYNOMIAL FIT WILL BE MADE ON THE STRAIN GAGE DATA
       C      WHICH WILL GENERATE BOUNDARY CONDITIONS AT THE BOTTOM OF THE WALL
       C      SO THAT A QUINTIC SPLINE FIT CAN BE MADE
       C
CCC2          COMMON/RED/A(1502,12),T(1502),AX(112),BX(112),CALI(15,2),X(10),
             X        TCALI,ITM,NT,NA,NPOLY,NS2,NINT,H,EIH,HTM,AGS,GAMMAM,
             X        NTYPE,F1M,NC,XP(5)
CC03          COMMON/GREEN/CMAX(2),CMIN(2),IPLTCD
CCC4          COMMON/BLUE/X1(112),X2(112),X3(112),TT(1502),XX(1502,112),XM(1),
             X        YM(1),TM(1),ITMAX,IXMAX
CCC5          COMMON/YELLOW/TF(112),TS(112)
CCC6          REAL*8 STCR(11,25)
CCC7          DIMENSION AM(10),BM(10),DATA(3,10),C(11),EC(6),S1(2),S2(2),LS(2),
             X        CC(3)
CCCc          DATA S1/'M(ME','NT'/,S2/'M*H/','EI'/,LS/6,6/
       C
CCC9          READ 701,CMIN,CMAX
       C
CC10          MF=NPOLY+1
CC11          NS1=NS2-1
       C      GO TO 650
CC12          IF(NTYPE.NE.1)GO TO 602
CC13          NPT=NS2
CC14          AM(NS2)=0.0
CC15          GO TO 604
CC16      602 NPT=NS1
CC17      604 AM(1)=0.0
CC18          DO 605 I=1,NPT
CC19      605 DATA(3,I)=1.0
CC20          CHISC=0.0
CC21          DO 606 I=1,3
CC22      606 EC(I)=0.0
       C
CC23          DO 650 I=1,ITM
CC24          DO 6509 J=1,NINT
CC25      6509 TF(J)=XX(I,J)
CC26          CALL INTEG(NINT,AX,TF,TS,0)
CC27          AM(2)=TS(26)
CC28          AM(3)=TS(47)
CC29          AM(4)=TS(59)
CC30          AM(5)=TS(69)
       C      DO 607 J=2,NS1
       C  607 AM(J)=A(I,J+NA-1)
CC31          DO 610 J=2,NPT
CC32          DATA(1,J-1)=X(J)
CC33      610 DATA(2,J-1)=AM(J)
CC34          NPT=NPT-1
       C
CC35          CALL LSQUAR(DATA,NPT,MF,C,CHISC,STCR)
       C
CC36          NPT=NPT+1
CC37          DO 616 J=4,6
CC38      616 EC(J)=0.0
```

MOMENT

```
0039            DO 617 J=1,NS2
0040        617 AM(J)=0.0
0041            DO 618 J=2,NS2
0042            DO 618 K=1,NF
0043        618 AM(J)=AM(J)+C(K)*X(J)**(K-1)
0044            IF(NTYPE.EC.1)AM(NS2)=0.0
      C
      C         CALCULATE BOUNDARY CONDITIONS AT BOTTOM OF THE WALL
      C
0045            DO 620 J=1,NF
0046            BC(4)=BC(4)+C(J)*X(NS2)**(J-1)
0047            BC(5)=BC(5)+FLOAT(J-1)*C(J)*X(NS2)**(J-2)
0048        620 BC(6)=BC(6)+FLOAT(J-2)*FLOAT(J-1)*C(J)*X(NS2)**(J-3)
0049            IF(NTYPE.NE.1)GO TO 624
0050            BC(4)=0.0
      C
      C         CALCULATE MOMENTS WITH CUBIC SPLINE
      C
0051        624 CALL CLINT(NS2,X,AM,NINT,AX,TS,BC)
      C
0052            DO 625 J=1,NINT
0053        625 XX(1,J)=TS(J)*2.0
0054        625 CONTINUE
      C6500 DO 6025 I=1,ITM CCCCCCCCCCCC
      C         DO 6005 J=1,NINT          C
      C6005 TF(J)=XX(I,J)                 C
      C         CALL INTEG(NINT,AX,TF,TS,0)C
      C         DO 6020 J=1,NINT           C
      C6020 XX(I,J)=TS(J)                  C
      C6025 CONTINUE CCCCCCCCCCCCCCCCCCCCC
      C
0055            WRITE(21)XX
0056            ENDFILE 21
0057            REWIND 21
0058            CALL CRUNCH
      C
0059            DO 652 I=1,ITM
0060            DO 652 J=1,NINT
0061        652 XX(I,J)=XX(I,J)*HTM/EIM
0062            DO 655 I=1,NINT
0063            X1(I)=X1(I)*HTM/EIM
0064            X2(I)=X2(I)*HTM/EIM
0065        655 X3(I)=X3(I)*HTM/EIM
0066            XM(I)=XM(I)*HTM/EIM
0067            DO 656 I=1,ITM
0068        656 TT(I)=TT(I)*HTM/EIM
      C
0069            NSO=NS1-1
0070            DO 658 I=1,NSO
0071        658 EM(I)=-X(I+1)/HTM
0072            DO 660 I=1,3
0073        660 CCC(I)=0.0
0074            LAE=0
0075            CINTX=(ABS(CMAX(1)-CMIN(1)))/2.5
0076            CINTC=(ABS(CMAX-CMIN))/2.5
0077            YMIN=-4.0*CINTX
```

FCRENT

```
0078          YMAX= 6.0*CINTX
0079          XMIN=-7.5*CINTD+DMIN
0080          XMAX= 7.5*CINTD+DMIN
      C       DO 670 J=1,3
      C       GO TO (661,663,665),J
      C 661   DO 662 I=1,NSO
      C 662   AM(I)=2.0*A(1,I+NA)*FTM/EIM
      C       GO TO 667
      C 663   DO 664 I=1,NSO
      C 664   AM(I)=2.0*A(ITMAX,I+NA)*FTM/EIM
      C       GO TO 667
      C 665   DO 666 I=1,NSO
      C 666   AM(I)=2.0*A(ITM,I+NA)*FTM/EIM
      C 667   CALL XYPLT(NSO,AM,EM,XMIN,XMAX,YMIN,YMAX,CCC,LAB,2)
      C 670   CONTINUE
      C
0081          DO 670 J=1,3
0082          GO TO (661,663,665),J
0083      661 AM(1)=X1(26)
0084          AM(2)=X1(47)
0085          AM(3)=X1(55)
0086          AM(4)=X1(66)
0087          GO TO 667
0088      663 AM(1)=X2(26)
0089          AM(2)=X2(47)
0090          AM(3)=X2(55)
0091          AM(4)=X2(66)
0092          GO TO 667
0093      665 AM(1)=X3(26)
0094          AM(2)=X3(47)
0095          AM(3)=X3(55)
0096          AM(4)=X3(66)
0097      667 CALL XYPLT(NSO,AM,EM,XMIN,XMAX,YMIN,YMAX,CCC,LAB,2)
0098      670 CONTINUE
      C
0099          CALL PAPRNT(1)
0100          CALL PAPLOT(S1,S2,LS,DMIN,DMAX)
      C
0101          DO 680 I=1,ITM
0102          DO 680 J=1,NINT
0103      680 XX(I,J)=XX(I,J)*EIM/FTM
      C
0104      701 FORMAT(2F10.0)
      C
0105          RETURN
0106          END
```

PAGE

```
0001          SUBROUTINE PAGE
       C
       C      SUBROUTINE TO SET UP PLOTTING ON AN 8-1/2 X 11 INCH AREA
       C
0002          DIMENSION A(2),B(2),DCC(3)
       C
0003          DO 120 I=1,3
0004      120 DCC(I)=0.0
0005          LAB=0
0006          A(1)=0.0
0007          A(2)=11.0
0008          B(1)=0.0
0009          B(2)=0.0
0010          CALL XYPLOT(2,A,B,0.0,15.0,0.0,10.0,DCC,LAB)
0011          A(1)=11.0
0012          B(2)=8.5
0013          CALL XYPLOT(2,A,B,0.0,15.0,0.0,10.0,DCC,LAB)
0014          A(1)=0.0
0015          A(2)=0.0
0016          CALL XYPLOT(2,A,B,0.0,15.0,0.0,10.0,DCC,LAB)
0017          A(2)=11.0
0018          B(1)=8.5
0019          CALL XYPLOT(2,A,B,0.0,15.0,0.0,10.0,DCC,LAB)
       C
0020          RETURN
0021          END
```

PAPLOT

```
0001          SUBROUTINE PAPLOT(S1,S2,LS,DMIN,DMAX)
       C
       C      SUBROUTINE TO PLCT OUT,CN A SINGLE 8-1/2 X 11 PAGE A CONTOUR MAP CF
       C      A PARAMETER ALCNG WITH PLOTS OF STATIC INITIAL AND FINAL VALUES AS
       C      WELL AS MAXIMUM DYNAMIC VALUES
       C
0002          COMMON/RED/A(1502,12),T(1502),AX(112),BX(112),CALI(15,2),X(10),
       X             TCALI,ITM,NT,NA,NPOLY,NS2,NINT,H,EIM,HTM,AGS,GAMMAM,
       X             NTYPE,FIM,NC,XP(9)
0003          COMMON/BLUE/X1(112),X2(112),X3(112),TT(1502),XX(1502,112),XM(1),
       X             YM(1),TM(1),ITMAX,IXMAX
0004          COMMON/GREEN/CMAX(2),CMIN(2),IPLTCD
0005          COMMON/GRAY/TITLE1(18),TITLE2(18)
0006          DIMENSION S1(1),S2(1),LS(1),DOC(3),AA(2),BB(2),T1(4),T2(3),T3(1),
       X             LT(4),CX(10),CY(10),CZ(10),PX(1),PY(1),TD(1)
0007          DATA T1/'LOCA','TICN','  (X','/H)'/,T2/'TIME','  (T','*F1)'/,
       X        T3/'X/H'/,T4/'T*F1'/,LT/15,12,3,4/,TD/'    '/
       C
0008          DC 701 I=1,3
0009     701  DCC(I)=0.0
0010          DC 702 I=1,ITM
0011     702  T(I)=T(I)*F1M
0012          NINT=NINT-3
       C
0013          CALL PAGE
0014          LAB=0
0015          CALL VLABEL(1.5,2.0,CMAX(1),CMIN(1),5.0,5,T1,LT(1),1,'(F3.1)',3)
0016          CALL VLABEL(7.5,1.5,CMAX(1),CMIN(1),2.5,2,T3,LT(3),1,'(F3.1)',3)
0017          CALL VLABEL(7.5,1.5,CMIN,DMAX,2.5,2,S2,LS(2),0,'(F5.2)',5)
0018          CALL VLABEL(7.5,5.0,DMIN,DMAX,2.5,2,S2,LS(2),1,'(F5.2)',5)
0019          START=1.5+((5.0-(FLOAT(LS(1))*5.0/12.0))/2.0)
0020          CALL SYSSYM(START,7.25,0.5,S1,LS(1),0.0)
0021          CALL SYSSYM(1.0,1.15,0.1,TITLE1,72,0.0)
0022          CALL SYSSYM(1.0,1.0,0.1,TITLE2,72,0.0)
0023          IF(IPLTCD.EC.0)GC TO 703
0024          CALL VLABEL(1.5,2.0,CMIN(2),CMAX(2),5.0,5,T2,LT(2),0,'(F4.1)',4)
0025          CALL VLABEL(7.5,5.0,CMIN(2),CMAX(2),2.5,2,T4,LT(4),0,'(F4.1)',4)
0026          GC TO 704
0027     703  CALL VLABEL(7.5,5.0,CMIN(2),CMAX(2),2.5,1,T4,LT(4),0,'(F4.1)',4)
0028          CALL VLABEL(1.5,2.0,CMIN(2),CMAX(2),5.0,1,T2,LT(2),0,'(F4.1)',4)
0029          CC=CMAX(2)-CMIN(2)
0030          PA=0.2*CC+CMIN(2)
0031          PB=0.8*CC+CMIN(2)
0032          PC=0.05*CC+CMIN(2)
0033          PD=0.15*CC+CMIN(2)
0034          PE=0.1*CC+CMIN(2)
0035          PF=0.6*CC+CMIN(2)
0036          CALL VLABEL(4.0,2.0,PA,PB,1.875,3,TD,4,0,'(F4.1)',4)
0037          CALL VLABEL(2.125,2.0,PC,PD,1.25,2,TD,4,0,'(F4.1)',4)
0038          CALL VLABEL(8.125,5.0,PE,PF,1.25,1,TD,4,0,'(F4.1)',4)
0039          CALL VLABEL(8.75,5.0,PA,PF,0.625,1,TD,4,0,'(F4.1)',4)
       C
0040     704  AA(1)=1.5
0041          AA(2)=6.5
0042          BB(1)=7.0
0043          BB(2)=7.0
```

PAPLOT

```
0044              CALL XYPLOT(2,AA,BB,0.0,15.0,0.0,10.0,DOC,LAB)
0045              AA(1)=6.5
0046              BB(1)=2.0
0047              CALL XYPLOT(2,AA,BB,0.0,15.0,0.0,10.0,DOC,LAB)
0048              AA(1)=7.5
0049              BB(1)=4.0
0050              AA(2)=10.0
0051              BB(2)=4.0
0052              CALL XYPLOT(2,AA,BB,0.0,15.0,0.0,10.0,DOC,LAB)
0053              AA(1)=10.0
0054              BB(1)=1.5
0055              CALL XYPLOT(2,AA,BB,0.0,15.0,0.0,10.0,DOC,LAB)
0056              AA(1)=7.5
0057              BB(1)=7.5
0058              AA(2)=10.0
0059              BB(2)=7.5
0060              CALL XYPLOT(2,AA,BB,C.0,15.0,0.0,10.0,DOC,LAB)
0061              AA(1)=10.0
0062              BB(1)=5.0
0063              CALL XYPLOT(2,AA,BB,0.0,15.0,0.0,10.0,DOC,LAB)
         C
0064              IF(IPLTCD.NE.0)GC TC 712
0065              CA=CC/(2.0*(PA-CMIN(2)))
0066              CB=(1.0-CA)*CMIN(2)
0067              DA=CC/(2.0*(CMAX(2)-PA))
0068              DB=((CMAX(2)+CMIN(2))/2.0)-(DA*PA)
0069              DC 710 I=1,ITM
0070              IF(T(I).LT.PA)GO TC 708
0071              T(I)=(T(I)*DA)+DB
0072              GC TC 710
0073          708 T(I)=(T(I)*CA)+CB
0074          710 CCNTINUE
         C
0075          712 NB=NT-NA
0076              DC 714 I=1,NB
0077              CX(I)=-X(I+1)/HTM
0078          714 CY(I)=0.0
0079              IF(NC.EC.0)GC TO 718
0080              DC 717 I=1,NC
0081          717 CZ(I)=-XP(I+1)/HTM
         C
         C        SCALE PARAMETERS FOR CONTOUR PLOTTING
         C
0082          718 CINT=(ABS(CMAX(1)-CMIN(1)))/5.0
0083              XMIN=-7.0*CINT
0084              XMAX= 3.0*CINT
0085              CINT=(ABS(CMAX(2)-CMIN(2)))/5.0
0086              TMIN=-1.5*CINT
0087              TMAX=13.5*CINT
         C
         C        PLCT CONTOURS
         C
0088              IF(NC.EQ.0)GC TO 720
0089              CALL XYPLT(NC,CY,CZ,TMIN,TMAX,XMIN,XMAX,CCC,LAB,4)
0090          720 CALL XYPLT(NB,CY,CX,TMIN,TMAX,XMIN,XMAX,DOC,LAB,3)
0091              AA(1)=CMIN(2)
```

PAPLOT

```
0092            BB(1)=BX(IXMAX)
0093            AA(2)=CMAX(2)
0094            BB(2)=BX(IXMAX)
0095            CALL XYPLOT(2,AA,BB,TMIN,TMAX,XMIN,XMAX,DOC,LAB)
0096            AA(1)=T(ITMAX)
0097            BB(1)=-CMIN(1)
0098            AA(2)=T(ITMAX)
0099            BB(2)=-CMAX(1)
0100            CALL XYPLCT(2,AA,BB,TMIN,TMAX,XMIN,XMAX,DOC,LAB)
0101            PX(1)=T(ITMAX)
0102            PY(1)=BX(IXMAX)
0103            CALL XYPLT(1,PX,PY,TMIN,TMAX,XMIN,XMAX,DOC,LAB,1)
0104            CALL MAP(T,BX,XX,TMAX,TMIN,XMAX,XMIN,DMAX,DMIN,ITM,NINT,21)
     C
     C          PLOT INITIAL AND FINAL STATIC PARAMETERS AS WELL AS MAXIMUM DYNAMIC ONES
     C
0105            CINTX=(ABS(CMAX(1)-CMIN(1)))/2.5
0106            CINTT=(ABS(CMAX(2)-CMIN(2)))/2.5
0107            CINTD=(ABS(DMAX-DMIN))/2.5
0108            YMIN=-4.0*CINTX
0109            YMAX= 6.0*CINTX
0110            XMIN=-7.5*CINTD+DMIN
0111            XMAX= 7.5*CINTD+DMIN
0112            CALL XYPLT(1,XM,YM,XMIN,XMAX,YMIN,YMAX,DOC,LAB,1)
0113            IF(NC.EQ.0)GC TO 722
0114            CALL XYPLT(NC,CY,CZ,XMIN,XMAX,YMIN,YMAX,DOC,LAB,4)
0115        722 CALL XYPLT(NB,CY,CX,XMIN,XMAX,YMIN,YMAX,DCC,LAB,3)
0116            AA(1)=0.0
0117            AA(2)=0.0
0118            BB(1)=-CMAX(1)
0119            BB(2)=-CMIN(1)
0120            CALL XYPLCT(2,AA,BB,XMIN,XMAX,YMIN,YMAX,DOC,LAB)
0121            CALL XYPLCT(NINT,X1,BX,XMIN,XMAX,YMIN,YMAX,DCC,LAB)
0122            CALL XYPLCT(NINT,X2,BX,XMIN,XMAX,YMIN,YMAX,DOC,LAB)
0123            CALL XYPLCT(NINT,X3,BX,XMIN,XMAX,YMIN,YMAX,DCC,LAB)
0124            YMIN=-5.0*CINTD+DMIN
0125            YMAX= 5.0*CINTD+CMIN
0126            XMIN=-7.5*CINTT
0127            XMAX= 7.5*CINTT
0128            IF(IPLTCD.NE.0)GC TO 726
0129            IF(TM(1).LT.PA)GC TO 725
0130            TM(1)=(TM(1)*DA)+CB
0131            GC TC 726
0132        725 TM(1)=(TM(1)*CA)+CB
0133        726 CALL XYPLT(1,TM,XM,XMIN,XMAX,YMIN,YMAX,DOC,LAB,1)
0134            BB(1)=0.0
0135            BB(2)=0.0
0136            AA(1)=CMIN(2)
0137            AA(2)=CMAX(2)
0138            CALL XYPLCT(2,AA,BB,XMIN,XMAX,YMIN,YMAX,DOC,LAB)
0139            LAB=-1
0140            CALL XYPLCT(ITM,T,TT,XMIN,XMAX,YMIN,YMAX,COC,LAB)
     C
0141            IF(IPLTCD.NE.0)GC TC 734
0142            PG=(CMAX(2)+CMIN(2))/2.0
0143            DC 729 I=1,ITM
```

PAPLCT

```
0144          IF(T(I).LT.PG)GO TO 728
0145          T(I)=(T(I)-CB)/DA
0146          GC TO 729
0147      728 T(I)=(T(I)-CB)/CA
0148      729 CCNTINUE
0149          IF(TM(1).LT.PG)GC TO 732
0150          TM(1)=(TM(1)-CB)/DA
0151          GC TC 734
0152      732 TM(1)=(TM(1)-CB)/CA
      C
0153      734 DC 735 I=1,ITM
0154      735 T(I)=T(I)/F1M
0155          NINT=NINT+3
      C
0156          RETURN
0157          END
```

PAPRNT

```
0001        SUBROUTINE PAPRNT(IPARM)
        C
        C     SUBROUTINE TO PRINT OUT PARAMETERS
        C
0002        COMMON/RED/A(1502,12),T(1502),AX(112),BX(112),CALI(15,2),X(10),
            X          TCALI,ITM,NT,NA,NPOLY,NS2,NINT,H,EIM,HTM,AGS,GAMMAM,
            X          NTYPE,F1M,NG,XP(9)
0003        COMMON/BLUE/X1(112),X2(112),X3(112),TT(1502),XX(1502,112),XM(1),
            X          YM(1),TM(1),ITMAX,IXMAX
        C
0004        NINT=NINT-3
0005        TA=T(1)*F1M
0006        TB=T(ITMAX)*F1M
0007        TC=T(ITM)*F1M
0008        DO 61 N=1,3
0009        PRINT 200
0010        GO TO(51,52,53,54),IPARM
0011     51 PRINT 201
0012        GO TO 57
0013     52 PRINT 202
0014        GO TO 57
0015     53 PRINT 203
0016        GO TO 57
0017     54 PRINT 204
0018     57 PRINT 220,TA,TB,TC
0019        L=N*50
0020        DO 60 J=1,50
0021        I=(L-50)+J
0022        IF(I.GT.NINT)GO TO 62
0023        TX=-BX(I)
0024     60 PRINT 221,I,X1(I),X2(I),X3(I),TX
0025     61 CONTINUE
0026     62 CONTINUE
        C
0027        DO 81 N=1,15
0028        PRINT 200
0029        GO TO(71,72,73,74),IPARM
0030     71 PRINT 201
0031        GO TO 77
0032     72 PRINT 202
0033        GO TO 77
0034     73 PRINT 203
0035        GO TO 77
0036     74 PRINT 204
0037     77 TX=-BX(IXMAX)
0038        PRINT 222,TX,TX
0039        L=N*50
0040        DO 80 J=1,50
0041        I=(L-50)+J
0042        K=I+(N-1)*50
0043        KK=K+50
0044        IF(KK.GT.ITM)GO TO 82
0045        TY=T(K)*F1M
0046        TZ=T(KK)*F1M
0047     80 PRINT 223,K,TT(K),TY,KK,TT(KK),TZ
0048     81 CONTINUE
```

PAPRNT

```
0049          82 CONTINUE
0050             NS=(2*N-1)*50
0051             IF(K.EQ.NS)GO TO 86
0052             DO 85 I=K,NS
0053             TY=T(I)*F1M
0054             IF(I.GT.ITM)GO TO 86
0055          85 PRINT 224,I,TT(I),TY
0056          86 CONTINUE
0057             NINT=NINT+3
       C
0058         200 FORMAT(1H1)
0059         201 FORMAT(31X,'* * * * * * * * *',
                X      /,31X,'* MOMENT (M*H/EI) *',
                X      /,31X,'* * * * * * * * * *')
0060         202 FORMAT(25X,'* * * * * * * * * * * * * * * *',
                X      /,25X,'* SHEAR (Q/(0.5*RO*G*(H**2))) *'
                X      /,25X,'* * * * * * * * * * * * * * * *')
0061         203 FORMAT(25X,'* * * * * * * * * * * * * * * * *',
                X      /,25X,'* EARTH PRESSURE (P/(RO*G*H)) *',
                X      /,25X,'* * * * * * * * * * * * * * * * *')
0062         204 FORMAT(29X,'* * * * * * * * * * *',
                X      /,29X,'* DISPLACEMENT  (Y/H) *',
                X      /,29X,'* * * * * * * * * * *')
0063         220 FORMAT(17X,'STATIC',10X,'MAXIMUM DYNAMIC',6X,'FINAL STATIC',6X,
                X'LOCATION',/,12X,'(T*F1)=',E10.3,3X,'(T*F1)=',E10.3,3X,'(T*F1)=',
                XE10.3,5X,'(X/H)',/,12X,'_____    _____   __
                X_____    _____')
0064         221 FORMAT(6X,I4,E19.3,2E20.3,F10.3)
0065         222 FORMAT(10X,'MAXIMUM DYNAMIC',8X,'TIME',14X,'MAXIMUM DYNAMIC',8X,
                X'TIME',/,12X,'(X/H)=',F5.3,9X,'(T*F1)',15X,'(X/H)=',F5.3,9X,
                X'(T*F1)',/,10X,'_____    _____    _____
                X_____    _____')
0066         223 FORMAT(6X,I4,2E15.3,7X,I4,2E15.3)
0067         224 FORMAT(6X,I4,2E15.3)
       C
0068             RETURN
0069             END
```

PRESS

```
0001          SUBROUTINE PRESS
          C
          C   SUBROUTINE TO DERIVE EARTH PRESSURES BY SHEAR DIFFERENTIATION
          C   OR BY QUINTIC SPLINE FITS CF PRESSURE TRANSDUCER DATA AS DONE
          C   IN SUBROUTINE MOMENT
          C
0002          COMMON/RED/A(1502,12),T(1502),AX(112),BX(112),CALI(15,2),X(10),
          X       TCALI,ITM,NT,NA,NPOLY,NS2,NINT,H,EIM,HTM,AGS,GAMMAM,
          X       NTYPE,F1M,NC,XP(9)
0003         -COMMON/BLUE/X1(112),X2(112),X3(112),TT(1502),XX(1502,112),XM(1),
          X       YM(1),TM(1),ITMAX,IXMAX
0004          COMMON/GREEN/CMAX(2),CMIN(2),IPLTCD
0005          COMMON/YELLOW/TR(112),TS(112)
0006          REAL*8 STCR(11,25)
0007          DIMENSION S1(2),S2(3),LS(2),RE(1502),DOC(3),AA(1),BB(1),AM(10),
          X       BM(10),DATA(3,10),C(11),XP1(10),AM1(10)
0008          DATA S1/'PRES','SURF'/,S2/'P/(R','O*G*','H)'/,LS/8,10/
          C
0009          READ 991,DMIN,DMAX
          C
0010          NI=NINT-4
0011          IF(NC.NE.0)GO TO 900
0012          DO 825 I=1,ITM
0013          DO 809 J=1,NINT
0014      809 TR(J)=XX(I,J)
0015          CALL DERIV(NINT,H,TR,TS)
          C
          C   FIND LOCATION CF PRESSURE RESULTANT (RE(I))
          C
0016          AR=0.0
0017          YA=0.0
0018          DO 815 J=1,NI
0019          DA=0.5*(AX(J+1)-AX(J))*(TS(J+1)+TS(J))
0020          Y=(AX(J+1)+AX(J))/2.0
0021          AR=AR+DA
0022      815 YA=YA+Y*DA
0023          RE(I)=YA/AR
0024          DO 820 J=1,NINT
0025      820 XX(I,J)=TS(J)
0026      825 CONTINUE
          C
0027      827 CALL CRUNCH
          C
0028          DO 830 I=1,ITM
0029          DO 830 J=1,NINT
0030      830 XX(I,J)=XX(I,J)/(GAMMAM*HTM)
0031          DO 835 I=1,NINT
0032          X1(I)=X1(I)/(GAMMAM*HTM)
0033          X2(I)=X2(I)/(GAMMAM*HTM)
0034      835 X3(I)=X3(I)/(GAMMAM*HTM)
0035          XM(1)=XM(1)/(GAMMAM*HTM)
0036          DO 836 I=1,ITM
0037          RE(I)=-(RE(I)/HTM)
0038      836 TT(I)=TT(I)/(GAMMAM*HTM)
          C
0039          DO 840 I=1,3
```

PRESS

```
0040            840 DCC(I)=0.0
0041                LAB=0
0042                CINTX=(ABS(CMAX(1)-CMIN(1)))/2.5
0043                CINTD=(ABS(DMAX-DMIN))/2.5
0044                YMIN=-4.0*CINTX
0045                YMAX= 6.0*CINTX
0046                XMIN=-7.5*CINTD+DMIN
0047                XMAX= 7.5*CINTD+DMIN
0048                AA(1)=0.0
0049                BB(1)=RE(1)
0050                CALL XYPLT(1,AA,BB,XMIN,XMAX,YMIN,YMAX,DOC,LAB,1)
0051                BB(1)=RE(ITMAX)
0052                CALL XYPLT(1,AA,BB,XMIN,XMAX,YMIN,YMAX,DOC,LAB,0)
0053                BB(1)=RE(ITM)
0054                CALL XYPLT(1,AA,BB,XMIN,XMAX,YMIN,YMAX,DOC,LAB,5)
     C
0055                IF(NC.EQ.0)GO TO 940
0056                NSO=NW-2
0057                DO 858 I=1,NSO
0058            858 BM(I)=-XP(I+1)/HTM
0059                DC 860 I=1,3
0060            860 CCC(I)=0.0
0061                LAB=0
0062                CINTX=(ABS(CMAX(1)-CMIN(1)))/2.5
0063                CINTD=(ABS(DMAX-DMIN))/2.5
0064                YMIN=-4.0*CINTX
0065                YMAX= 6.0*CINTX
0066                XMIN=-7.5*CINTD+DMIN
0067                XMAX= 7.5*CINTD+DMIN
0068                DC 870 J=1,3
0069                GC TO (861,863,865),J
0070            861 DC 862 I=1,NSO
0071            862 AM(I)=A(1,I+NT)/(GAMMAM*HTM)
0072                GC TC 867
0073            863 DC 864 I=1,NSO
0074            864 AM(I)=A(ITMAX,I+NT)/(GAMMAM*HTM)
0075                GC TC 867
0076            865 DC 866 I=1,NSO
0077            866 AM(I)=A(ITM,I+NT)/(GAMMAM*HTM)
0078            867 CALL XYPLT(NSO,AM,BM,XMIN,XMAX,YMIN,YMAX,DOC,LAB,2)
0079            870 CONTINUE
0080                GC TC 940
     C
0081            900 NPP=NPOLY+1
0082                NPT=NC+1
0083                NW=NPT+1
0084                AM(1)=0.0
0085                DC 905 I=1,NPT
0086            905 DATA(3,I)=1.0
0087                CHISQ=0.0
     C
0088                DC 930 I=1,ITM
0089                DO 907 J=2,NPT
0090            907 AM(J)=A(I,J+NT-1)
0091                DC 910 J=2,NPT
0092                DATA(1,J-1)=XP(J)
```

PRESS

```
0093        910 DATA(2,J-1)=AM(J)
0094            NPT=NPT-1
          C
0095            CALL LSQUAR(DATA,NPT,NPP,C,CHISQ,STOR)
          C
0096            NPT=NPT+1
0097            DO 917 J=1,NW
0098        917 AM(J)=0.0
0099            DO 918 J=2,NW
0100            DO 918 K=1,NPP
0101        918 AM(J)=AM(J)+C(K)*XP(J)**(K-1)
0102            NW1=NW-1
0103            DO 922 J=1,NW1
0104            XP1(J)=XP(J)
0105        922 AM1(J)=AM(J)
          C
          C   CALCULATE PRESSURES WITH CUBIC SPLINE
          C
0106            CALL SPLINE(NW1,XP1,AM1,NINT,AX,TS)
          C
          C   FIND LOCATION OF PRESSURE RESULTANT (RE(I))
          C
0107            AR=0.0
0108            YA=0.0
0109            DO 925 J=1,NI
0110            DA=0.5*(AX(J+1)-AX(J))*(TS(J+1)+TS(J))
0111            Y=(AX(J+1)+AX(J))/2.0
0112            AR=AR+DA
0113        925 YA=YA+Y*DA
0114            RE(I)=YA/AR
0115            DO 927 J=1,NINT
0116        927 XX(I,J)=TS(J)
0117        930 CONTINUE
0118            GO TO 827
          C
0119        940 CALL PAPRNT(3)
0120            CALL PAPLOT(S1,S2,LS,DMIN,DMAX)
          C
0121            DO 943 I=1,ITM
0122            DO 943 J=1,NINT
0123        943 XX(I,J)=XX(I,J)*(GAMMAM*HTM)
          C
0124        991 FORMAT(2F10.0)
          C
0125            RETURN
0126            END
```

QUINT

```
0001            SUBROUTINE CUINT(NN,X,Y,M,S,T,BC)
        C
        C ....SLBROUTINE TO FIT A CUINTIC SPLINE TC A SET CF DATA PCINTS (X,Y)
        C     BC ARE BOUNDARY CONDITIONS
        C     BC(1)=Y(1);BC(2)=Y'(1);BC(3)=Y''(1);
        C     BC(4)=Y(NN);BC(5)=Y'(NN);BC(6)=Y''(NN)
        C
0002            DIMENSICN BC(6)
0003            DIMENSION X(1),Y(1),S(1),T(1),H(500),A(50,50),B(50),U(6,6),C(6,7)
0004            CCMMON/PURPLE/JWANT,FIR(500),SEC(500)
        C
0005            IF(NN.GT.501)GO TO 9S
0006            N=NN-1
0007            NM1=N-1
0008            DC 5 I=1,N
0009            H(I)=X(I+1)-X(I)
0010          5 CCNTINUE
0011            N6=N*6
0012            DC 15 I=1,N6
0013            B(I)=0
0014            DC 15 J=1,N6
0015         15 A(J,I)=0.0
0016            DC 25 I=1,3
0017         25 A(I,I)=1.0
        C
0018            B(1)=BC(1)
0019            B(2)=BC(2)
0020            B(3)=BC(3)
0021            B(N6-2)=BC(4)
0022            B(N6-1)=BC(5)
0023            B(N6)=BC(6)
        C
0024            DC 40 I=1,NM1
0025            B(4+(I-1)*6)=Y(I+1)
0026            IR=4+(I-1)*6
0027            IC=6*I+1
0028            A(IR,IC)=1.0
0029            IC=IC-1
0030            DC 35 J=1,5
0031         35 A(IR+J,IC+J)=-1.0
0032            ARG=H(I)
0033            IR=3+(I-1)*6
0034            IC=(I-1)*6
0035            CALL SUBU(ARG,U)
0036            DC 37 JC=1,6
0037            DC 37 JR=1,6
0038         37 A(IR+JR,IC+JC)=U(JR,JC)
0039         40 CCNTINUE
        C
0040            CALL SUBU(H(N),U)
0041            IR=N6-3
0042            IC=N6-6
0043            DC 50 JC=1,6
0044            DO 50 JR=1,6
0045         50 A(IR+JR,IC+JC)=U(JR+1,JC)
        C
```

CUINT

```
      C ....ECSOV IS A SYSTEM SUBROUTINE
      C
0046        CALL ECSOV(N6,A,B,10,1.0E-4,C,IT,0)
0047        DO 60 I=1,M
0048        IF(S(I).LT.X(1)) GO TO 53
0049        DO 52 J=1,N
0050        IF(S(I).LE.X(J+1)) GO TO 55
0051     52 CONTINUE
      CCCCCCCCCCCCCCCCCCCCC
0052        GO TO 55
      CCCCCCCCCCCCCCCCCCCCCCC
0053     53 PRINT 106,I
0054        GO TO 60
0055     55 CONTINUE
0056        SX=S(I)-X(J)
0057        T(I)=C(1,J)+SX*(C(2,J)+(SX/2.)*(C(3,J)+(SX/3.)*(C(4,J)+(SX/4.)*
           X(C(5,J)+(SX/5.)*C(6,J))))
0058        IF(JWANT.EQ.0) GO TO 60
0059        SEC(I)=C(3,J)+SX*(C(4,J)+(SX/2.)*(C(5,J)+(SX/3.)*C(6,J)))
0060     60 CONTINUE
0061        RETURN
      C
0062     99 PRINT 107
      C
0063    106 FORMAT(/,' THE',I5,'TH ELEMENT OF THE ARRAY S IS OUT OF RANGE',/,
           X' ERROR MESSAGE FROM CUINT',/)
0064    107 FORMAT(/,' N IS LARGER THAN 501',/,
           X' ERROR MESSAGE FROM CUINT',/)
      C
0065        RETURN
0066        END
```

SHEAR

```
0001          SUBROUTINE SHEAR
       C
       C      SUBROUTINE TO DERIVE SHEARS BY MOMENT DIFFERENTIATION OR
       C      PRESSURE DISTRIBUTION INTEGRATION
       C
0002          COMMON/RED/A(1502,12),T(1502),AX(112),BX(112),CALI(15,2),X(10),
              X          TCALI,ITM,NT,NA,NPOLY,NS2,NINT,H,EIM,HTM,AGS,GAMMAM,
              X          NTYPE,F1M,NC,XP(9)
0003          COMMON/BLUE/X1(112),X2(112),X3(112),TT(1502),XX(1502,112),XM(1),
              X          YM(1),TM(1),ITMAX,IXMAX
0004          COMMON/YELLOW/TR(112),TS(112)
0005          DIMENSION S1(2),S2(3),LS(2)
0006          DATA S1/'SHEA','R'/,S2/'C/(P','AE/K','AE)'/,LS/5,11/
       C
0007          READ 801,DMIN,DMAX
       C
0008          DO 725 I=1,ITM
0009          DO 709 J=1,NINT
0010      709 TR(J)=XX(I,J)
0011          IF(NC.NE.0)GO TO 712
0012          CALL DERIV(NINT,H,TR,TS)
0013          GO TO 714
0014      712 CALL INTEG(NINT,AX,TR,TS,0)
0015      714 DO 720 J=1,NINT
0016      720 XX(I,J)=TS(J)
0017      725 CONTINUE
       C
0018          CALL CRUNCH
       C
       C      PAE/KAE=0.5*RO*G*(H**2) - FROM M-O ANALYSIS
       C
0019          DO 727 I=1,ITM
0020          DO 727 J=1,NINT
0021      727 XX(I,J)=XX(I,J)/(0.5*GAMMAM*(HTM**2))
0022          DO 735 I=1,NINT
0023          X1(I)=X1(I)/(0.5*GAMMAM*(HTM**2))
0024          X2(I)=X2(I)/(0.5*GAMMAM*(HTM**2))
0025      735 X3(I)=X3(I)/(0.5*GAMMAM*(HTM**2))
0026          XM(1)=XM(1)/(0.5*GAMMAM*(HTM**2))
0027          DO 736 I=1,ITM
0028      736 TT(I)=TT(I)/(0.5*GAMMAM*(HTM**2))
       C
0029          CALL PAPRNT(2)
0030          CALL PAPLOT(S1,S2,LS,DMIN,DMAX)
       C
0031          DO 744 I=1,ITM
0032          DO 744 J=1,NINT
0033      744 XX(I,J)=XX(I,J)*(0.5*GAMMAM*(HTM**2))
       C
0034      801 FORMAT(2F10.0)
       C
0035          RETURN
0036          END
```

```
                                SPLINE
0001              SUBROUTINE SPLINE(NN,X,Y,M,S,T)
         C
         C        SUBROUTINE TO FIT A CUBIC SPLINE TO A SET OF NN POINTS (X,Y)
         C
0002              CCMMCN/WHITE/IWANT,DER(1500)
0003              DIMENSICN X(1),Y(1),S(1),T(1),A(1500,3),B(1500),P(1500),H(1500)
         C
0004              IF(NN.GT.1501)GC TC 90
0005              N=NN-1
0006              NM1=N-1
0007              DC 5 I=1,N
0008            5 H(I)=X(I+1)-X(I)
0009              DC 15 I=1,NM1
0010              A(I,1)=H(I)/H(I+1)
0011              A(I,2)=2.0*(H(I+1)+H(I))/H(I+1)
0012              A(I,3)=1.0
0013           15 B(I)=6.0*((Y(I+2)-Y(I+1))/H(I+1)-(Y(I+1)-Y(I))/H(I))/H(I+1)
0014              A(1,1)=0
0015              A(NM1,3)=0
0016              CALL ALGECN(NM1,A,B,P)
0017              DC 45 I=1,M
0018              IF(S(I).LT.X(1))GC TC 26
0019              DC 25 J=1,N
0020              IF(S(I).LE.X(J+1))GC TC 28
0021           25 CCNTINUE
         C        CCCCCCCC
0022              GC TC 28
         C        CCCCCCCC
0023           26 PRINT 106,I
0024              GC TC 45
0025           28 IF(J.EQ.1)GO TC 30
0026              IF(J.EC.N)GO TC 40
0027              T(I)=(P(J-1)*(X(J+1)-S(I))**3+
                 XP(J)*(S(I)-X(J))**3+(6.0*Y(J+1)-H(J)**2*P(J))*(S(I)-X(J))+
                 X(6.0*Y(J)-H(J)**2*P(J-1))*(X(J+1)-S(I)))/(6.0*H(J))
0028              GC TC 45
0029           30 T(I)=(P(J)*(S(I)-X(J))**3+(6.0*Y(J+1)-H(J)**2*P(J))*(S(I)-X(J))+
                 X6.0*Y(J)*(X(J+1)-S(I)))/(6.0*H(J))
0030              GC TC 45
0031           40 T(I)=(P(J-1)*(X(J+1)-S(I))**3+6.0*Y(J+1)*(S(I)-X(J))+
                 X(6.0*Y(J)-H(J)**2*P(J-1))*(X(J+1)-S(I)))/(6.0*H(J))
0032           45 CCNTINUE
0033              IF(IWANT.EC.0)RETURN
0034              DC 80 I=1,M
0035              IF(S(I).LT.X(1))GC TC 52
0036              DC 50 J=1,N
0037              IF(S(I).LE.X(J+1))GO TC 54
0038           50 CCNTINUE
0039           52 PRINT 106,I
0040              GC TC 80
0041           54 IF(J.EQ.1)GO TC 60
0042              IF(J.EQ.N)GO TC 70
0043              DER(I)=(3.0*P(J)*(S(I)-X(J))**2-P(J-1)*(X(J+1)-S(I))**2)+
                 X6.0*(Y(J+1)-Y(J))-H(J)**2*(P(J)-P(J-1)))/(6.0*H(J))
0044              GC TC 80
0045           60 DER(I)=(3.0*P(J)*(S(I)-X(J))**2+6.0*(Y(J+1)-Y(J))-H(J)**2*P(J))/
```

SPLINE

```
          X(6.0*H(J))
0046          GC TC 80
0047      70 DER(I)=(-3.0*P(J-1)*(X(J+1)-S(I))**2+6.0*(Y(J+1)-Y(J))+
          XH(J)**2*P(J-1))/(6.0*H(J))
0048      80 CONTINUE
0049         RETURN
0050      90 PRINT 107
C
0051     106 FCRMAT('0    THE ',I5,'TH ELEMENT OF ARRAY S IS OUT OF RANGE -----
          .XERROR MESSAGE FROM SPLINE')
0052     107 FCRMAT ('0  N IS LARGER THAN 1501, SCRRY')
C
0053         RETURN
0054         END
```

```
0001              SUBROUTINE SUBU(X,U)
          C
          C ....SUBROUTINE CALLED IN CUINT
          C
0002              DIMENSION U(6,6)
0003              DO 5 I=1,6
0004              DO 5 J=1,6
0005            5 U(I,J)=0.0
0006              DO 15 I=2,6
0007           15 U(I,I)=X
0008              DO 25 I=1,5
0009           25 U(I+1,I)=1.0
0010              U(2,3)=0.5*X*X
0011              U(3,4)=U(2,3)
0012              U(4,5)=U(2,3)
0013              U(5,6)=U(2,3)
0014              U(2,4)=U(2,3)*X/3.0
0015              U(3,5)=U(2,4)
0016              U(4,6)=U(2,4)
0017              U(2,5)=U(2,4)*X/4.0
0018              U(3,6)=U(2,5)
0019              U(2,6)=U(2,5)*X/5.0
          C
0020              RETURN
0021              END
```

YDISP

```
0001          SUBROUTINE YDISP
       C
       C      SUBROUTINE TO DETERMINE DISPLACEMENTS BY DOUBLE INTEGRATION OF MOMENTS
       C
0002          COMMON/RED/A(1502,12),T(1502),AX(112),BX(112),CALI(15,2),X(10),
              X           TCALI,ITM,NT,NA,NPOLY,NS2,NINT,H,EIM,HTM,AGS,GAMMAM,
              X           NTYPE,FIM,NC,XP(9)
0003          COMMON/BLUE/X1(112),X2(112),X3(112),TT(1502),XX(1502,112),XM(1),
              X           YM(1),TM(1),ITMAX,IXMAX
0004          COMMON/YELLOW/TR(112),TS(112)
0005          COMMON/BLACK/DIS(1502,3)
0006          DIMENSION S1(3),S2(1),LS(2)
0007          DATA S1/'DISP','LACE','MENT'/,S2/'Y/H'/,LS/12,3/
       C
0008          READ(21)XX
0009          READ 381,DMIN,DMAX
0010          DO 201 I=1,ITM
0011          DO 201 J=1,2
0012      201 DIS(I,J)=DIS(I,J)*EIM
       C
       C      DETERMINE DISPLACEMENTS
       C
0013          DO 250 I=1,ITM
0014          DO 212 J=1,NINT
0015      212 TR(J)=XX(I,J)
0016          CALL INTEG(NINT,AX,TR,TS,1)
0017          CALL INTEG(NINT,AX,TS,TR,1)
0018          EE=(TR(1)-TR(NINT)+DIS(I,2)-DIS(I,1))/(AX(NINT)-AX(1))
0019          FF=DIS(I,1)-(EE*AX(1))-TR(1)
0020          DO 237 J=1,NINT
0021      237 XX(I,J)=(TR(J)+(EE*AX(J))+FF)/EIM
0022      250 CONTINUE
       C
0023          CALL CRUNCH
       C
0024          DO 274 I=1,ITM
0025          DO 274 J=1,NINT
0026      274 XX(I,J)=XX(I,J)/HTM
0027          DO 277 I=1,NINT
0028          X1(I)=X1(I)/HTM
0029          X2(I)=X2(I)/HTM
0030      277 X3(I)=X3(I)/HTM
0031          XM(1)=XM(1)/HTM
0032          DO 278 I=1,ITM
0033      278 TT(I)=TT(I)/HTM
       C
0034          CALL PAPRNT(4)
0035          CALL PAPLOT(S1,S2,LS,DMIN,DMAX)
       C
0036          DO 280 I=1,ITM
0037          DO 280 J=1,NINT
0038      280 XX(I,J)=XX(I,J)*HTM
0039          DO 288 I=1,ITM
0040          DO 288 J=1,2
0041      288 DIS(I,J)=DIS(I,J)/EIM
       C
```

YDISP

```
0042          381 FORMAT(2F10.0)
          C
0043              RETURN
0044              END
```

BLK DATA

```
0001          BLOCK DATA
0002          COMMON/WHITE/IWANT,DER(1500)
0003          COMMON/PURPLE/JWANT,FIR(500),SEC(500)
0004          DATA IWANT/0/,JWANT/0/
0005          END
```

APPENDIX C

LIST OF SYMBOLS

Symbols are defined where they first appear in the text. A summary of the symbols employed and their dimensions is given in this appendix.

LOWER CASE SYMBOLS

Symbol	Definition	Dimensions
a	externally applied acceleration	LT^{-2}
a_R	set of dimensionless external acceleration ratios	–
d	thickness	L
du	digitizer unit	–
e	void ratio	–
f_a	elastic strength of aluminum	FL^{-2}
$f_m f_p$	frequency of vibration of model, prototype	T^{-1}
f_1	fundamental frequency	T^{-1}
g	gravitational acceleration	LT^{-2}
$g_m g_p$	gravitational acceleration of model, prototype	LT^{-2}
h	height	L
i	angle of backfill slope	o
k	number of dimensionless groups	–
l	length of beam	L

Symbol	Definition	Dimensions
n	number of drainage boundaries	–
n	number of parameters	–
t	time	T
t_c	consolidation time	T
$t_{cm} t_{cp}$	consolidation time of model, prototype	T
$t_m t_p$	model, prototype time	T
u_o	externally induced displacement	L
$u_{om} u_{op}$	externally induced displacement of model, prototype	L
u_{oR}	set of dimensionless externally induced displacement ratios	L
v	lateral velocity	LT^{-1}
x, y, z	length and distance in coordinate directions	L
y	wall displacement	L

UPPER CASE SYMBOLS

Symbol	Definition	Dimensions
A	constant of integration	-
B	constant of integration	L
C_a	expression dependent on Mononobe-Okabe parameters	-
C_v	coefficient of consolidation	$L^2 T^{-1}$
E	Young's modulus	FL^{-2}
E_A	Young's modulus of aluminum	FL^{-2}
$E_m E_p$	Young's modulus of model, prototype	FL^{-2}
E_R	set of dimensionless Young's modulus ratios	-
EI	stiffness per unit width of wall	$FL^2 L^{-1}$
F	typical force dimension	F
F()	function of	-
F.S.	factor of safety	-
G	shear modulus	FL^{-2}
$G_m G_p$	shear modulus of model, prototype	FL^{-2}
G()	function of	-
G.S.	Ground surface	-
H	height	L
H_A	height at which resultant force acts	L
H_f	depth of frost cover in front of wall	L
$H_m H_p$	height of model, prototype	L
I	moment of inertia per unit width of wall	$L^4 L^{-1}$

Symbol	Definition	Dimensions
K_A	coefficient of static active lateral earth pressure	--
K_{AE}	coefficient of total active lateral earth pressure	--
K_{PE}	coefficient of total passive lateral earth pressure	--
L	typical length dimension	L
$L_m L_p$	length scale of model, prototype	L
L_R	set of dimensionless length ratios	--
M	typical mass dimension	M
M	moment	FLL^{-1}
M_A	active static moment	FLL^{-1}
M_{AE}	active total (static + dynamic) moment	FLL^{-1}
M_D	design moment	FLL^{-1}
M_o	overturning moment	FLL^{-1}
M_R	resisting moment	FLL^{-1}
MMI	Modified Mercalli Intensity	--
N	centrifuge gravitational acceleration scale factor	--
N	ratio of prototype to model length scales	--
P	pressure	FL^{-2}
P	externally applied load	F
P_A	active static resultant wall force	FL^{-1}
$P_m P_p$	externally applied load of model, prototype	F
P_{AE}	total (static + dynamic) active wall force	FL^{-1}

Symbol	Definition	Dimensions
P_{PE}	total (static + dynamic) passive wall force	FL^{-1}
P_R	set of dimensionless external load ratios	–
Q	shear force	FL^{-1}
Q	externally applied stress	FL^{-2}
$Q_m Q_p$	externally applied stress of model, prototype	FL^{-2}
Q_R	set of dimensionless externally applied stress ratios	–
R_A	maximum static active pressure	FL^{-2}
R_{AE}	maximum total (static + dynamic) active pressure	FL^{-2}
RW1	Retaining Wall #1	–
RW2	Retaining Wall #2	–
S	unit section modulus of cross section	$L^3 L^{-1}$
T	typical time dimension	T
T	time factor of consolidation	–
$T_m T_p$	time factor of consolidation of model, prototype	–
W	weight of soil wedge behind wall	FL^{-1}
W	weight of backfill	FL^{-1}

GREEK SYMBOLS

Symbol	Definition	Dimensions
β	angle of wall back slope	$^{\circ}$
γ	unit weight of soil	FL^{-3}
δ	angle of wall-soil friction	$^{\circ}$
θ	$\tan^{-1}[k_h/(1-k_v)]$	
ν	Poisson's ratio	–
$\nu_m\nu_p$	Poisson's ratio of model, prototype	–
ρ	mass density	ML^{-3}
$\rho_m\rho_p$	mass density of model, prototype	ML^{-3}
σ_c	internal stress	FL^{-2}
$\sigma_{om}\sigma_{op}$	internal stress of model, prototype	FL^{-2}
σ_{oR}	set of dimensionless internal stress ratios	–
ϕ	angle of internal friction of soil	$^{\circ}$
ΔP_{AE}	active wall force increment due to earthquake load	FL^{-1}

APPENDIX D

FINITE ELEMENT COMPARISON

For an analytical comparison, it was decided to perform a finite element analysis on the wall-soil system of test 1CN0002 using the linearly elastic structural analysis program SAPIV (Bathe, et. al. [1]).

The finite element grid was first drawn up as shown in Figure D.1 with the retaining wall (shown with speckles) embedded in the soil. Prototype dimensions were used (i.e., wall height was 18 ft) and the boundaries were determined to be those existing in a postulated prototype centrifuge bucket (i.e., 50 times larger than their actual size). The wall illustrated is much thicker than that which would be the prototype (1 ft thick vs. 3.15" thick if it were aluminum), but its Young's Modulus was chosen much less so that the stiffnesses EI would be the same. This was done in order to get a more suitable aspect ratio for the elements which form the wall and base. Incompatible modes were used in the wall and base quads in order to have better bending behavior in these elements, especially since the wall was modelled with only one layer of elements.

Unfortunately, the soil elements had to be attached to the beam (wall) elements as there was no provision in the code to have sliding between elements. This would have been more desirable.
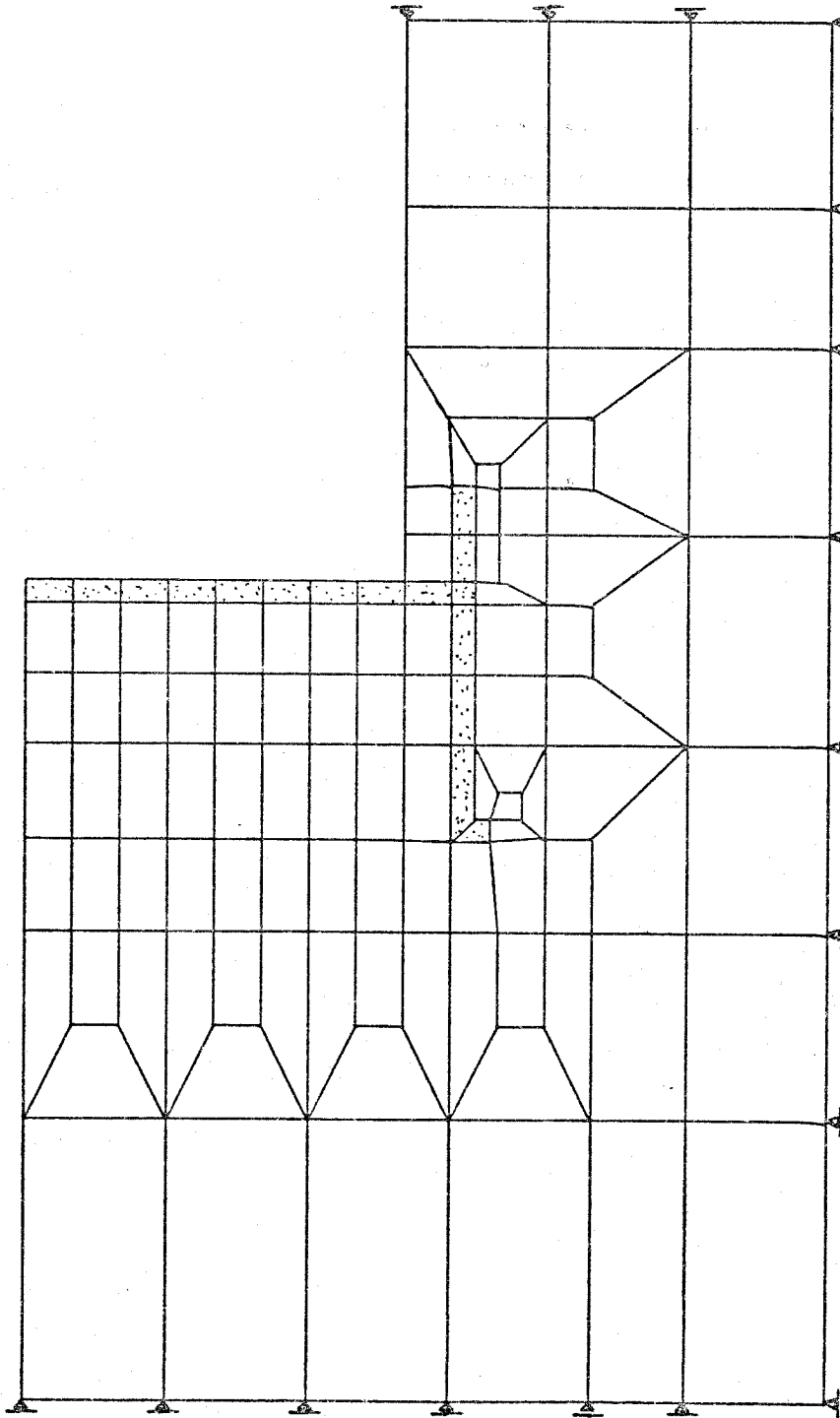
FIGURE D.I – FINITE ELEMENT GRID (SCALE 7.8 FT. PER IN.)

The soil shear moduli were determined from the relationship given by Seed and Idriss [54] between the shear modulus and the confining pressure:

$$G = 1000K_2(\sigma'_m)^{1/2} \tag{D.1}$$

in which

G = shear modulus of soil

σ'_m = mean principal effective stress.

K_2 = a parameter which is primarily a function of void ratio and strain amplitude

Because of the high strain range involved in a retaining wall problem, K_2 was chosen from the extreme right of Figure D.2 to be 4. The soil moduli were then calculated from equation (D.1) for the various depths, making some adjustments for the soil in the vicinity of the toe of the wall for the fact that the soil level in front of the wall is lower than that in back.

First of all, the problem was run for a static gravity body load in the negative vertical direction. The problem was then run dynamically as a forced response problem using modal superposition and the free-field acceleration record (prototype) of test 1CN0002 (Figure 5.5a) in the horizontal direction. The damping used was assumed 10% of critical. The total dynamic response was then obtained by superposition of the static response and the lateral dynamic one.
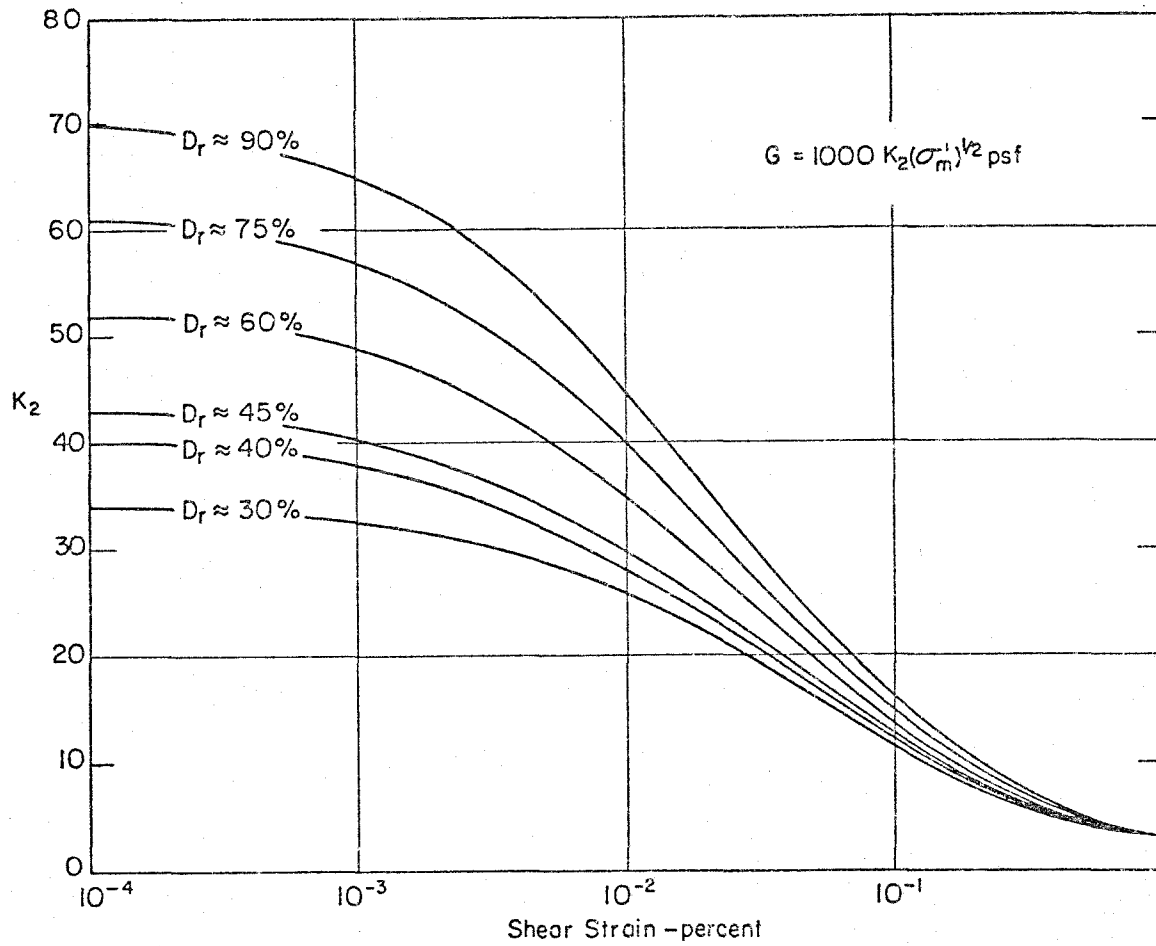
SHEAR MODULI OF SANDS AT DIFFERENT RELATIVE DENSITIES.

FIGURE D.2 – FROM (54)

The first six natural frequencies of the finite element system
were found to be 1.188 Hz, 1.388 Hz, 1.45 Hz, 1.987 Hz, 2.449 Hz, and
2.536 Hz. Only the 6th frequency of 2.536 Hz even resembled the actual
fundamental frequency of 2.57 Hz and its mode shape is most likely very
different.

Figures D.3, D.4, and D.5 illustrate the static and maximum
dynamic displacement, pressure, and moment distributions along the wall
for both the centrifuge model test and the finite element problem. As
can be seen from these figures there is virtually no correlation between
the two in any of the cases.

From this illustration one can see the perils in using elastic
theories (which are the basis for the finite element program used) in
trying to model the retaining wall problem which after all is the
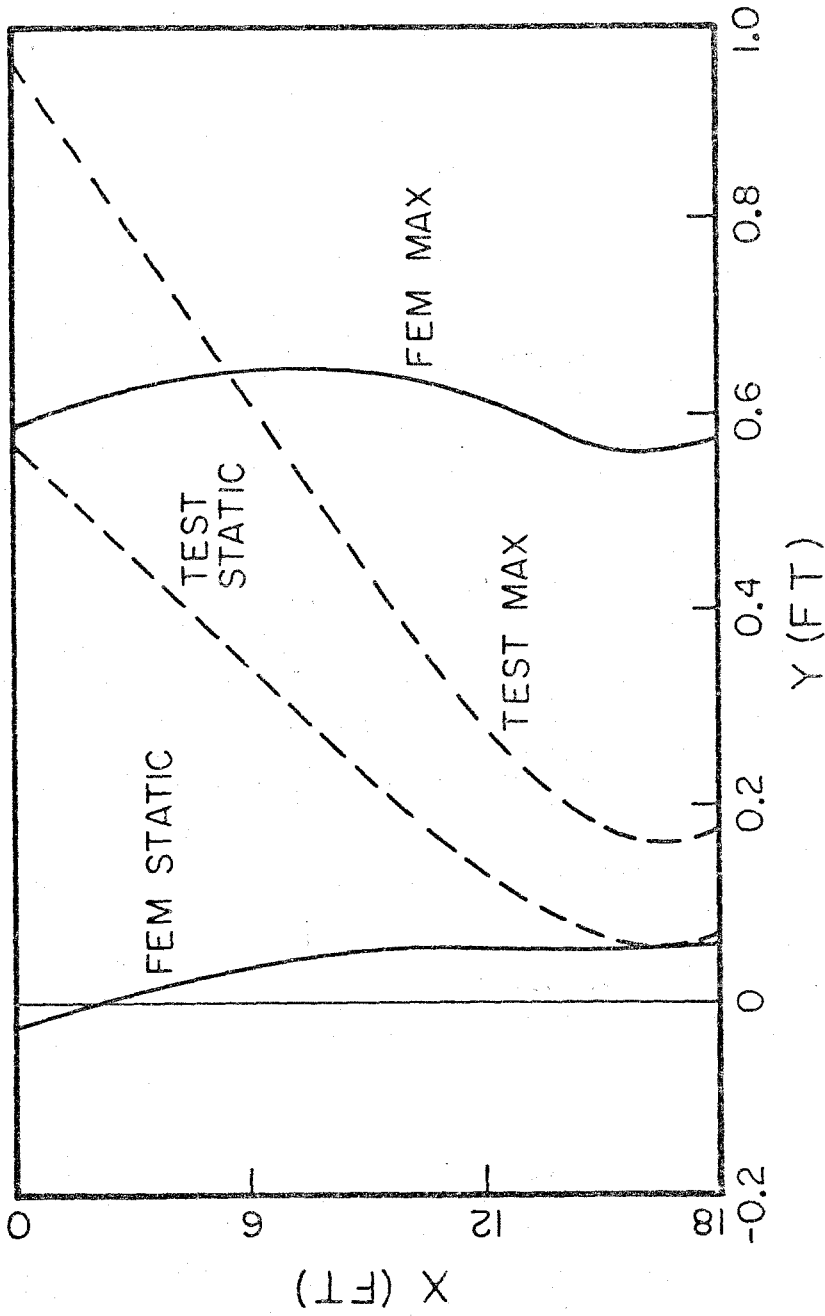classic most simple plasticity example. Elastic solutions for retaining
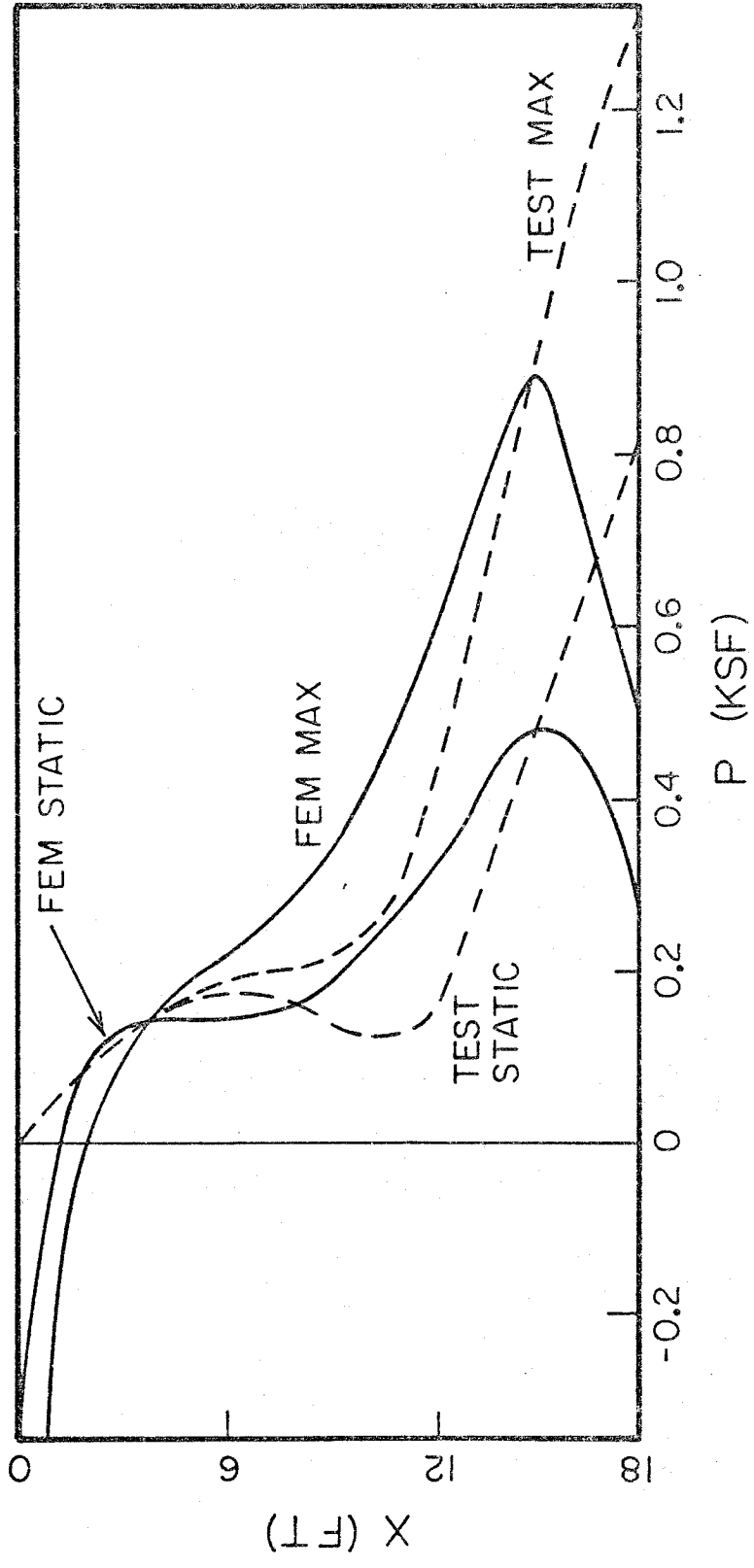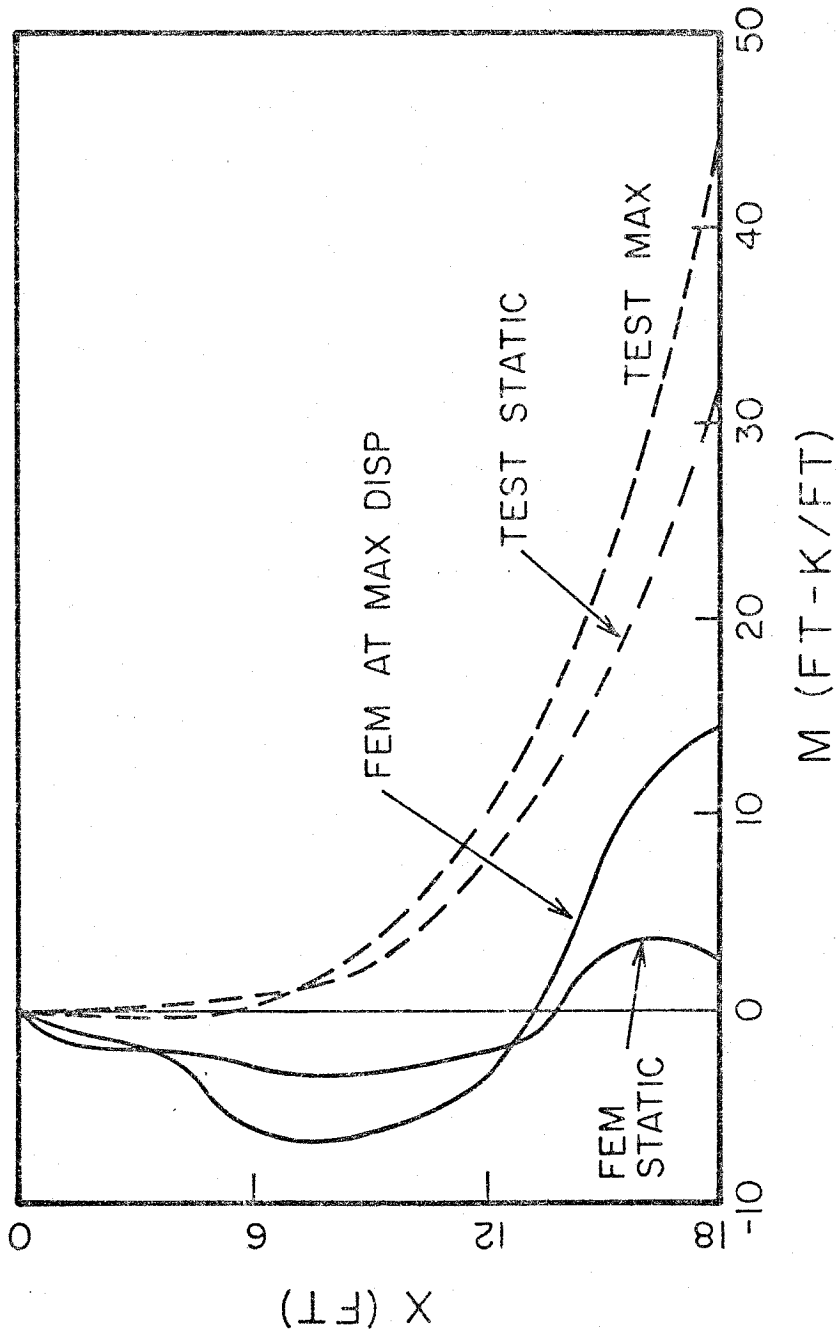wall problems should be avoided.

FIGURE D.3

FIGURE D.4

FIGURE D.5